

# The Petrology of the Muav Formation, Tonto Group, Grand Canyon, Arizona

Andrew A. Snelling, Answers in Genesis, PO Box 510, Hebron, Kentucky 41048.

## Abstract

Investigation of the nature of the folding of the Cambrian Tonto Group strata in Grand Canyon necessitates first investigating the petrology of those strata. The Cambrian Muav Formation is a 42–252 m (136–827 ft) thick cliff-forming unit that outcrops towards the top of the Tonto Group along ~500 km of the walls of Grand Canyon and beyond. Erosion of the underlying Precambrian basement rocks produced the Great Unconformity on which the Tonto Group was deposited as part of the fining upwards Sauk megasequence that blankets North America and other continents. The Muav Formation consists of dominant thick and thin beds and laminae of limestones, sometimes with alternating siltstone partings, with minor dolostone beds and laminae and some extensive intraformational flat-pebble conglomerate layers. A few trilobites, brachiopods, and other invertebrates, as well as small shell fragments are found fossilized in the Muav Formation, along with traces and burrows left by worms and other invertebrates. U-Pb dated detrital zircon grains from the underlying Tapeats Sandstone coupled with biostratigraphic trilobite faunal zones correlated globally have constrained the conventional age of the Muav Formation to 499–502 Ma. Detrital zircon U-Pb ages from the underlying Bright Angel Formation identify the primary source of the silicate grains within the Muav limestones as the locally underlying Precambrian crystalline basement. Uniformitarian interpreted depositional environments for the Muav Formation are shallow marine to subtidal, intertidal, and tidal flats environments, yet it has been described as “one of the most dramatic global marine transgressions in Earth history.” Calcite is dominant with subordinate dolomite, while quartz and K-feldspar contents range from 2.7% to 55.9% and 0.9% to 26.3%, respectively. Illite is present, indicative of the detrital muscovite flakes that are wedged between the other grains. The limestones are fine-grained and generally poorly sorted, with angular to sub-rounded, medium silt to fine sand-sized quartz and K-feldspar grains scattered through the tiny-grained calcite matrix (micrite), all cemented by recrystallized calcite. The dominant thickening, thinning, and pinching out of laminae, occasional current ripples, megaripples and cross-laminations, and some extensive intraformational flat-pebble conglomerate layers are consistent with rapid transport and deposition by high-energy storm-like surges, with spontaneous stratification of the heterogranular sediment mixture and of lime mud floccules. There is no evidence, macroscopic or microscopic, of any metamorphic changes to the detrital mineral grains or textures. Instead, the mineralogical content, textural features, sedimentary structures, continental-scale deposition, and even the tracks and traces of transitory invertebrates, all indicate rapid burial. Furthermore, all are consistent with the catastrophic erosion of the Great Unconformity near the initiation of the global Genesis Flood cataclysm only about 4,350 years ago, and the subsequent hurricane- and tsunami-driven rapid short-distance transport and deposition of the sediments that form the Muav Formation, likely in the first few days or weeks of that year-long event.

**Keywords:** Muav Formation, Cambrian, Tonto Group, Grand Canyon, stratigraphy, fossils, sedimentary structures, conventional zircon U-Pb ages, provenance, depositional environments, limestone, calcite, dolomite, quartz, K-feldspar, detrital muscovite, global Flood cataclysm.

## Introduction

The Cambrian Muav Formation is the 42–252 m (136–827 ft) thick formation that outcrops in generally prominent cliffs near the top of the Tonto Group, overlying the thick recessive slope-forming Bright Angel Formation and the prominent cliffs of Tapeats Sandstone. Together, these Tonto Group formations are at the base of the Paleozoic sequence of flat-lying sedimentary layers making up the walls of Grand Canyon for ~500 km through the Canyon and beyond. It consists primarily of thick and thin beds and laminae of limestones, sometimes with alternating siltstone partings, with minor dolostone beds and laminae and some extensive intraformational flat-

pebble conglomerate layers. The Muav Formation was deposited as part of the fining upwards Sauk megasequence that blankets North America and has been traced across other continents (Clarey 2020).

Many structures in sedimentary rock layers result from the primary depositional processes, such as graded bedding and cross-bedding (Boggs 1995). On the other hand, soft-sediment deformation or penecontemporaneous structures are so called because they develop at the time of deposition or shortly thereafter, during the early stages of the sediment's consolidation and before full lithification. This is because the sediments need to be unconsolidated or “liquid-like” for such deformation to occur (Boggs 1995).

However, other structures in sedimentary rocks are caused by deformation long after lithification and diagenesis have occurred. Rocks buried deep in the earth may be under sufficient prolonged confining pressures or stress and temperatures to deform plastically. In other words, incremental strain over a long period. This also is believed to be able to fold rock layers. These types of behavior are called ductile deformation. It is the ability of a rock to accumulate strain (folding) on a mesoscopic scale. Under the confining pressures and accompanying elevated temperatures, the rock grains may recrystallize and/or the minerals undergo metamorphism, some new minerals such as micas growing perpendicular to the stress to accommodate it. Hand and thin section analysis should be able to determine if rocks have experienced ductile deformation. The Paleozoic rocks, including the Muav Formation of Grand Canyon most likely were not buried deep enough to experience ductile deformation as they were well above the brittle-ductile transition zone. Incremental strain over sustained periods of time is harder to differentiate. As noted above, it can also result in ductile deformation.

On the other hand, under some near surface conditions, rock layers may remain coherent because the grains and/or layers within them can facilitate the folding. This type of deformation is most common in near surface rocks and is a type of brittle deformation. Most near surface rock layers undergo brittle fracturing and faulting, leaving the rock's grains fractured. Some coherent units may slide past one another along bedding planes as the rocks are folded. This helps accommodate folding through flexural slip. Tell-tale signs of this should be thus clearly evident in outcrops and from microscope examination of the rock fabric and the sediment grains.

There are several prominent locations in Grand Canyon where the Paleozoic sedimentary rock layers are folded, sometimes in conjunction with faulting. And where apparently, unresolved questions as to whether the folding represents soft-sediment deformation folding or later tectonic folding (ductile or brittle) after the whole strata sequence was deposited. In most instances the folding is usually claimed to be the result of ductile (plastic) behavior of the lithified sedimentary rocks under prolonged stress due to Late Mesozoic-Early Cenozoic deformation during the Laramide Orogeny, hundreds of millions of years after the whole Paleozoic strata sequence was deposited (Huntoon 2003; Karlstrom and Timmins 2012). However, the macroscopic fabric of the Cambrian Tonto Group sedimentary rock layers involved in these folds should be able to determine if the folding was instead due to soft-sediment deformation. Any soft-sediment deformation should have occurred

soon after deposition of these sedimentary units in the Cambrian (499–508Ma) (Karlstrom et al. 2020), and well before the tectonic activity of the Laramide Orogeny in the terminal Mesozoic and earliest Cenozoic (60–70Ma). This poses an apparent dilemma that obviously needs resolving, and thus a focused study was designed to determine the timing and nature of this folding, beginning with a thorough investigation of the petrology of each of these rock units, and subsequent detailed examination of these rock units in the folds.

One of the folds in question is the deformation of the Cambrian Tapeats Sandstone upwards into, and against the Butte Fault at the synclinal hinge of the East Kaibab Monocline in eastern Grand Canyon during the Laramide Orogeny (Huntoon 2003; Karlstrom and Timmins 2012). The best exposed fold along this system is in Carbon Canyon at river mile 65 (figs. 1 and 2). Hill and Moshier (2009) claim that evidence from field studies and rock deformation experiments demonstrate that these solid rocks behaved in a ductile manner as the sandstone strata were deformed slowly under great stress, and that the strata thus were “bent” by microscopic reorientations of mineral grains and by changes in bedding thickness along the fold. They then reference Huntoon (2003) to state that these tight folds in beds of the Tapeats Sandstone in Carbon Canyon can be explained by mechanical crowding at the synclinal hinge of the East Kaibab Monocline during slow deformation under stress of the solid sandstone in a ductile manner.

However, Hill and Moshier (2009) offer no supporting evidence of these claims. They provide no documentation of the quoted rock deformation studies, nor any evidence from any thin section examination of the Tapeats Sandstone from these folds of the claimed microscopic reorientations of mineral grains. And the only documentation they provide of any field studies is a single photograph of the vertical beds of the Tapeats Sandstone at the Carbon Canyon location, but not of the folded beds showing the mechanical crowding. For that they refer to Huntoon (2003), but his field photograph, while showing the bent beds of the Tapeats Sandstone at the location in question, is incorrectly labeled as the south wall of Chuar Canyon, when it is in fact the south wall of Carbon Canyon. Furthermore, Huntoon (2003) did not provide any thin section evidence for any reorientation of mineral grains.

Subsequently, Tapp and Wolgemuth (2016) similarly discussed the Carbon Canyon fold. They showed a photo of the fold (their fig. 12–13, 125), describing it as compressional folding in the Tapeats Sandstone. On an overlay they traced some of the sandstone beds through the fold, some of the

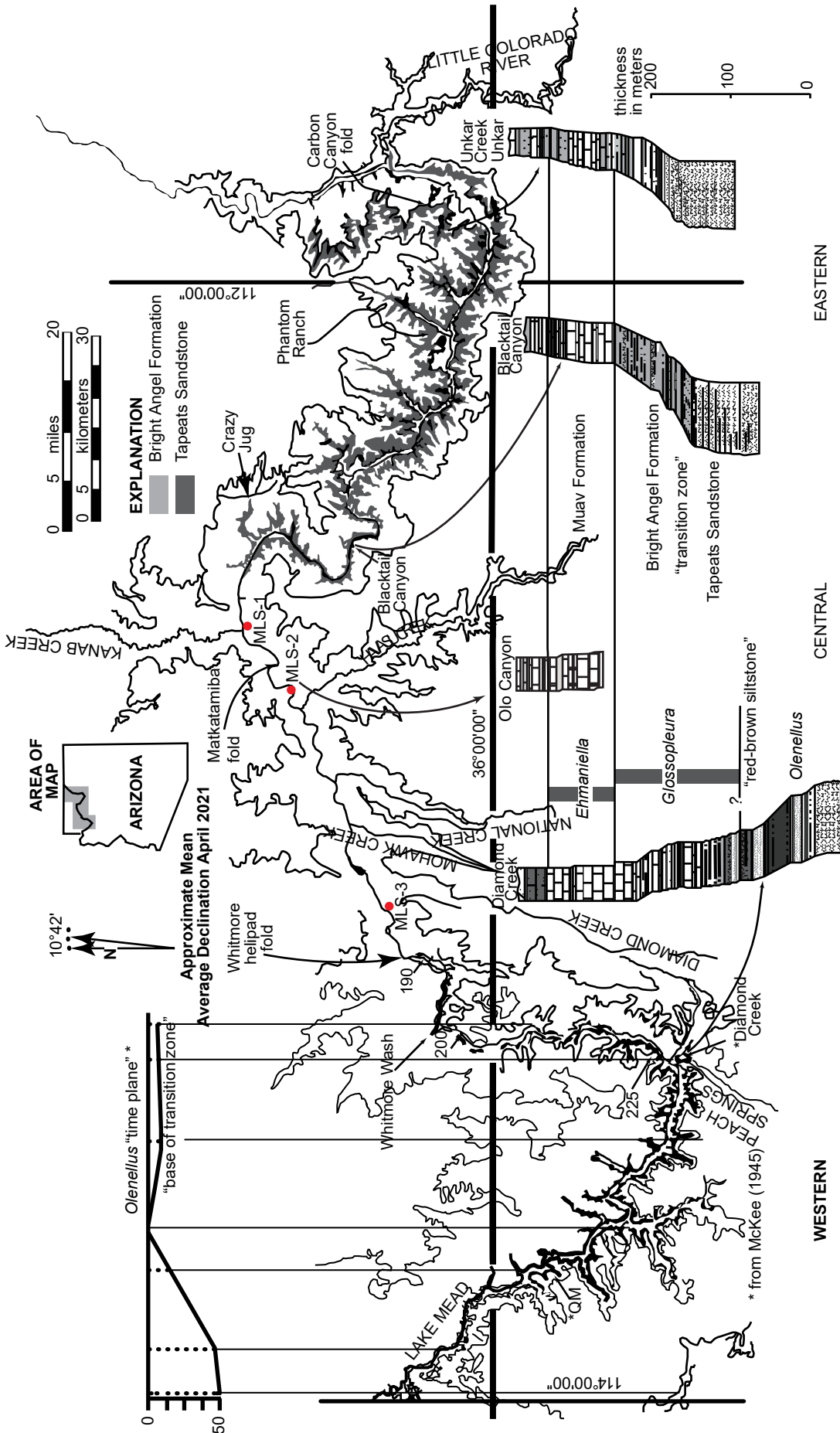


**Fig. 1.** Map of Grand Canyon showing the extent of exposure of the siliciclastic components of the Tonto Group, the Tapeats Sandstone and the overlying Bright Angel Formation (after Rose 2006, 225, fig. 1). The Muav Formation is exposed through the full length of Grand Canyon, below from river mile 35 in Marble Canyon to the Grand Wash Cliffs. Below the map are four representative stratigraphic sections shown in stylized profile of geomorphic expression. These four sections are provided in detail in Appendix A (Unkar), B (Blacktail Canyon), C (Olo Canyon) and D (Diamond Creek), available online in the Supplementary materials. The inset in the upper left is the basis for the time-transgressive model proposed by McKee (1945). The datum was compiled from the reported height (in meters) at which McKee reported collecting *Olenellus* fossils from seven sites above the base of the "base of the transition zone" in western Grand Canyon.



**Fig. 2.** The Carbon Canyon fold in which beds of the Tapeats Sandstone have been folded (bent) through 90° adjacent to the Butte Fault. Carbon Canyon is a side canyon to the Colorado River corridor at river mile 65 and the fold is exposed best in the southern wall of the canyon about 2 km (~1.2 mi) from the river. The man who is ~1.8 m (6 ft) tall standing on the fold provides the scale.

fractures, and the apparent changing direction of the fold noses, which they claimed to be due to flexural slippage. They claimed that the bending resulted in numerous fractures in each sandstone bed that did not heal (reseal). They then illustrated what flexural slippage would look like in two hypothetical folds (in their fig. 12–14, 125), describing how flexural slippage creates gaps in the fold noses that may be filled in later with weathered material or weaker rock units may deform into the spaces. Either way, the layering in the fold hinges would likely be thickened relative to the widths of the sandstone beds along the fold limbs. They claimed that neither of these features would be present if this fold had occurred due to soft-sediment deformation. However, their photo of the fold shows no such thickening of the sandstone beds in the fold noses, and they fail to discuss alternate explanations for the fractures, such as horizontal contraction within the beds during dewatering and lithification. Additionally, there is no evidence of thickening of shale-rich beds in the Bright Angel Formation where they are folded, as would be expected.

There is another location in Grand Canyon where there is similar folding, but in exposed Muav Formation at river mile 148.8, known as the Matkatamiba fold (figs. 1 and 3). The fold is river right in the cliff above the Colorado River, clearly visible, and thus easily accessible from the ledges at river level from where climbing is possible up to the fold. It is an open fold with very broad flexure of the constituent limestone and dolostone beds at the boundary between the Gateway Canyon and Havasu Members of the Muav Formation. Again, the folding is claimed to have occurred during the Laramide Orogeny (Karlstrom and Timmins 2012), a very long time after the Cambrian deposition of the Muav Formation, yet the character of the limestone and dolostone beds also appear to be consistent with soft-sediment deformation soon after deposition. Neither Hill and Moshier (2009) nor Tapp and Wolgemuth (2016) make any mention of the Matkatamiba fold.

It has been extensively documented that lithified rocks which have suffered ductile deformation will exhibit outcrop evidence of bedding plane slip and



**Fig. 3.** The Matkatamiba fold in which beds of the Muav Formation have been folded (bent). The fold is on river right about 100 ft (~33 m) above the river at river mile 148.8. The light colored (lower) unit is the Gateway Canyon Member while the overlying reddish (iron-oxide-stained) unit is the Havasus Member. The sharp and smooth boundary between the two members of the Muav Formation is clearly evident, but indicated for clarity. The man who is ~1.8 m (6 ft) tall standing just below the boundary at the upper left provides the scale. The locations are marked at which various samples were collected from either side of the boundary between the two members.

attenuation, such as flexural slippage (Ramsay 1967). However, field examination of these specific folds is insufficient to determine whether they were due to ductile behavior of the lithified rocks under much later prolonged stress or due to soft-sediment deformation soon after deposition. Detailed microscopic examination is thus absolutely necessary to document the character of the limestone and dolostone, specifically, the textural relationships between the constituent grains and the timing of the formation of the cement (lithification). Tell-tale microscopic textures would be evident, such as grain-boundary sliding, preferred orientation and recrystallization of the original detrital grains, as well as deformation lamellae and undulose extinction in those grains. And the original sedimentary cement between the grains would be absent or metamorphosed. Such textural features should be absent if the folding was due to soft-sediment deformation, as the original detrital grains and the cement binding them together in the sandstone, limestone, and dolostone in the folds would be essentially identical to those in the same rock units distant from the folds.

It appears that none of these earlier investigators have done any thin section investigations of the limestone and dolostone beds in the Muav Formation to substantiate their claims of their ductile deformation in such folds. Obviously, more detailed field and laboratory studies (especially intensive microscope examination) are needed to resolve the questions of what condition the limestone and dolostone beds were in when they were deformed into this fold, and thus how soon after their deposition the deformation occurred, before or after lithification of the limestone and dolostone. Any field and laboratory study of the Muav Formation in the Matkatamiba fold should thus also include a field and laboratory study of the Muav Formation in other locations distant from this fold. This would enable observations and conclusions at the one location to be confirmed in the studies at the other locations. The evidence seen in thin section examination of the limestone and dolostone beds in this fold should be different from that in the unfolded distant Muav Formation limestone and dolostone samples if the folding was due to ductile behavior under the stress of deformation of the lithified limestone and dolostone, whereas the microscope

evidence should be nearly identical in all samples if the folding was due to soft-sediment deformation.

Therefore, on a research and sampling trip through Grand Canyon with National Park Service approval, some 15 samples of the Muav Formation were collected, 12 samples from the Matkatamiba fold, and three samples from similar stratigraphic positions within the formation at sufficient distances away from this fold so as to provide comparative control samples for the subsequent detailed thin section examination (figs. 1 and 3). Thus, the purpose of this paper is to review extensively what is already known about the petrology of the Muav Formation as the context for then reporting the detailed microscope observations made on the collected samples. From the mineralogy and textures of these samples, inferences can then be drawn about the sediment source, its transport and deposition, and the formation's subsequent history, providing the documentation that can be referred to and built on in a subsequent paper focused on the timing of lithification (cementation) of the Muav Formation in the Matkatamiba fold before or after the folding occurred, that is, soft-sediment deformation or ductile deformation, respectively.

### Past Investigations of the Tonto Group

The earliest conventional scientific explanations for deposition of the Lower Paleozoic strata of the Grand Canyon region were offered by some of the most prominent North American geologists. Indeed, the Cambrian of Grand Canyon is regarded as one of the classic sedimentary rock sequences exposed in North America. These strata crop out in the lower cliff sections of Grand Canyon, along a prominent, essentially horizontal surface known as the Tonto Platform in the central part of the canyon, and near the banks of the Colorado River in western areas of the Canyon (figs. 1 and 4). The surface of the Tonto Platform roughly coincides with the top of the lowermost Cambrian unit, the Tapeats Sandstone. Above the Tapeats, a series of small cliffs are separated by thicker intervals of slopes composed of alternating beds of finer-grained deposits of shale, siltstone, and sandstone of the Bright Angel Formation. These, in turn, are overlain by cliffs of resistant carbonates of the Muav Formation and then the Frenchman Mountain Dolostone (formerly the "unclassified dolomites"), the topmost units of the Tonto Group.

The Tonto Group forms the base of the kilometers-thick succession of generally flat-lying sedimentary strata that makes up the Colorado Plateau. As described above, it straddles the conspicuous slope in the classic Grand Canyon cliff-slope profile known as the Tonto Platform (fig. 4). This geomorphic profile is consistent throughout the eastern exposures of Grand

Canyon, which are much more visited, photographed, and familiar to most people. However, there is a great gap in exposed outcrops which separates the distinct eastern and western exposures of the Tonto Group (fig. 1). Only the uppermost cliff-forming carbonates of the Muav Formation are continuously traceable across the ~50km (31mi) gap between these exposures, and the stratigraphy of the less familiar western exposures differs in important ways from that of the eastern exposures. For one, the quality of Tonto Group exposure is poorer in the western canyon in that several faults complicate the traceability of marker beds. Secondly, it is covered by lava or rubble across several tens of kilometers. Lastly, the inaccessible sheer cliffs impede close inspection.

The Tonto Group was first defined by Gilbert (1875, his fig. 82) and Powell (1876, 60) and then recognized to be Cambrian by Walcott (1895, 317). The conventional model of shelf deposition for the Tonto Group on a passive continental margin can be traced from Powell (1891) through Gilbert (1875), Walcott (1910) and Noble (1914; 1922), to McKee (1945). It is now a textbook example of a marine transgressive sequence to which Sloss (1963) applied the term "Sauk sequence."

McKee (1945) provided the most comprehensive account of Tonto Group deposition. He proposed a time-transgressive, "deepening seas" model which in the decades since has endured as a classic model of passive margin sedimentation and a landward advance of a wave-worn shoreline. His "deepening seas model" described the threefold division of the Tonto Group as:

- (1) a nearshore, high-energy regime represented by the Tapeats Sandstone,
- (2) an offshore, low-energy regime represented by the Bright Angel Shale (now the Bright Angel Formation), and
- (3) an even more distal low-energy carbonate buildup as "a chemical precipitate," represented by the Muav Limestone (now the Muav Formation).

Unlike his predecessors, McKee (1945) claimed that all three units, including the Tapeats Sandstone, were deposited below wave base. That conclusion was necessitated by the presence of the phyllosilicate glauconite in the upper portion of the Tapeats Sandstone and in shales of the Bright Angel Formation. Glauconite has long been accepted as a necessary indicator of low oxygen conditions in a deep marine setting, but this is no longer the case (McRae 1972). Other facies characteristics that are contrary to deep marine deposition were only minimally discussed by McKee (1945) in general terms of minor regressions or other temporarily exceptional conditions. This simple and elegant explanation for the intact layer-cake stratigraphy of the Grand

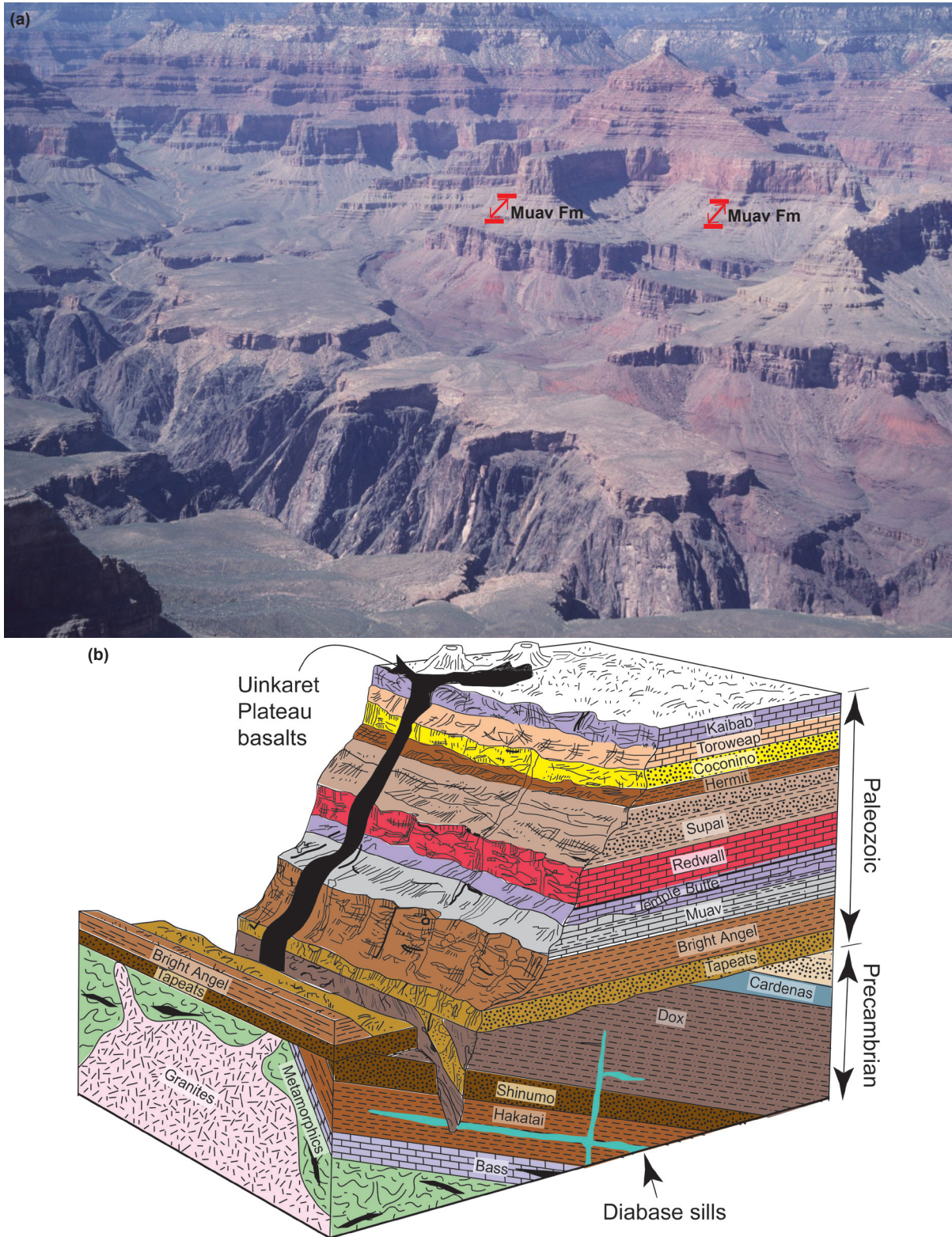


**Fig. 4.** The strata of the Grand Canyon. (a) The view of Grand Canyon from the South Rim overlooks. From the skyline looking down are the horizontal sedimentary layers making up the walls of the Canyon. The small “capping” on the cliff near the foreground, below which is the inner gorge consisting of schists intruded by granites, is the Tapeats Sandstone. The extensive wide almost flat areas above the Tapeats Sandstone in the middle foreground is the Tonto Platform. Above the Tapeats Sandstone in the slope is the overlying Bright Angel Formation, which is overlain by small cliffs of the harder limestones and dolostones of the Muav Formation (arrowed). (b) A block diagram of Grand Canyon strata corresponding to the vista seen in (a), except for the basalts that are found in the western Canyon (after Austin 1994, 13, fig.2.5).

Canyon's Tonto Group was thus settled on early and generally has not been revisited.

An important consideration in the development of the "deepening seas" model of time-transgressive shoreline retreat is that McKee (1945) worked his way eastward from the thicker basin-ward exposures of western Grand Canyon, starting at Grand Wash Cliffs, to the region of central Grand Canyon reported previously by Noble (1914; 1922). Comparatively little early stratigraphic work was done on the eastern exposures, so McKee (1945) depended on the single generalized measured section of Wheeler and Kerr (1936) to characterize the stratigraphy of the eastern exposures. In so doing, he applied Noble's solely lithologic facies criteria for subdividing the Tonto Group to the western exposures and as a result placed the Bright Angel Formation–Muav Formation contact some 150 m (492 ft) below what it would be if lithologic contacts were followed instead (see Huntoon 1989). This quirk in nomenclature provided an artificial view that the Muav and Bright Angel Formations crossed time boundaries with reference to biostratigraphically defined "time planes" (fig. 5).

Conventional chronostratigraphic control within the Tonto Group is provided by sparse and poorly preserved trilobite fragments and rare articulated trilobites but is complicated by numerous misidentifications by Resser (1945), subsequent taxonomic revisions (for example, Sundberg 1999), and the probability of mixed samples among poorly recorded collection sites. Nevertheless, McKee (1945) portrayed the biostratigraphy as thorough and precise, indicating uniform convergence of "thin fossil zones" with definite lithologic boundaries lower in the section as they are traced from west to east (fig. 5).

The classic work of McKee (1945) and Resser (1945) has endured as the most comprehensive study of the Cambrian system in Grand Canyon. These Cambrian strata occur throughout the Rocky Mountains and have since become the classic (textbook) example of a transgressive fining-upwards sequence of sandstone, mudstone, and limestone that accumulated on the slowly subsiding Cordilleran miogeocline and adjacent craton (Lochman-Balk 1970; 1971; Stewart 1972; Stewart and Suczek 1977). It is thus postulated that during the early and middle Cambrian, a north-south trending strandline migrated progressively eastward across the craton. This shoreline was characterized by numerous embayments and offshore islands that affected sedimentation in nearshore areas. Shoreline migration was mostly eastward, resulting in deposition of coarse clastics in shallow water areas to the east and finer clastics and carbonates in the more offshore areas to the west. Numerous regressive phases apparently interrupted this overall eastward transgression resulting in complicated facies interactions.

However, the subsequent limited research on these strata has not kept pace with conventional developments in the last 50 years of the dynamics of today's nearshore and shelf depositional systems (for example, Nummedal 1991), failing to apply them to the uniformitarian explanation for the deposition of these rock units. Only a few studies have attempted to carefully document the lateral and vertical facies associations, including the Muav Formation (Blakey and Middleton 2012; Elston 1989; Hagadorn et al. 2011; Hereford 1977, Martin 1985; Martin, Middleton, and Elliott 1986; Middleton 1989; Middleton and Elliott 2003; Rose, Middleton and Elliott 1998; Rose 2003; 2006; 2011; Wanless 1973a). Wanless (1973a, b; 1975; 1981) presented the first challenge to the "deepening seas" model in demonstrating the petrographic similarity between modern intertidal carbonates and the Muav Formation facies that McKee (1945) interpreted as the most distal and deepest of the Tonto Group deposits. Wanless (1973a, b; 1981) further suggested that the whole of the Tonto Group deposition was in extremely shallow water. On the basis of detailed stratigraphic, sedimentologic, and paleontologic studies of measured sections of the Bright Angel Formation in eastern Grand Canyon, Martin (1985) and Martin, Middleton, and Elliott (1986) maintained that deposition of the transgressive succession was in a subtidal marine environment influenced by tidal and meteorologic currents, including those due to storms.

Elston (1989) built on the "classic work" of McKee (1945) by taking his measured sections, and those of Noble (1922) and Wheeler and Kerr (1936) and recompiling them carefully with the same lithologies but adding some measured sections of his own in eastern Grand Canyon. His correlations and his revised nomenclature are depicted in fig. 6. His proposed correlations indicated that following deposition of the massive sandstone member of the Tapeats Sandstone in western Grand Canyon, an eastward transgression of the epicontinental sea across the central and eastern Grand Canyon occurred at or near the *Olenellus* horizon, which lies a few feet above the top of the massive sandstone member. The overlying red brown sandstone member in the west traces into the upper part of the Tapeats Sandstone in the central and eastern Grand Canyon, and the underlying shaly interval in the west passes into parallel-bedded, cross-laminated sandstone eastwards into the central Canyon. Correlations above the Tapeats Sandstone indicated that a series of marker beds, identified as members of the Bright Angel Formation, record facies changes reflecting slight shifts in environments of marine deposition rather than major transgressions and regressions of the epeiric sea as concluded by McKee (1945).

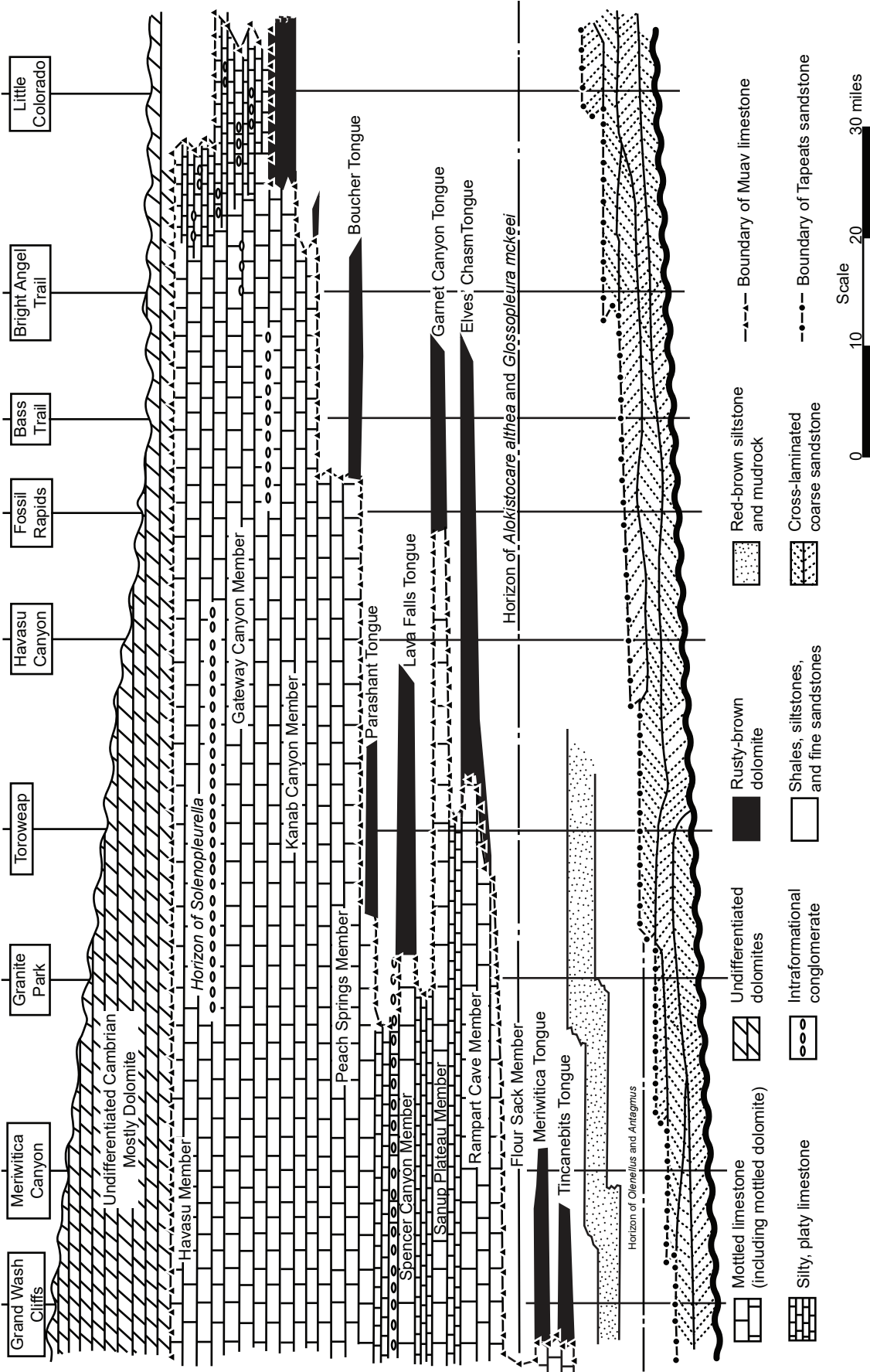
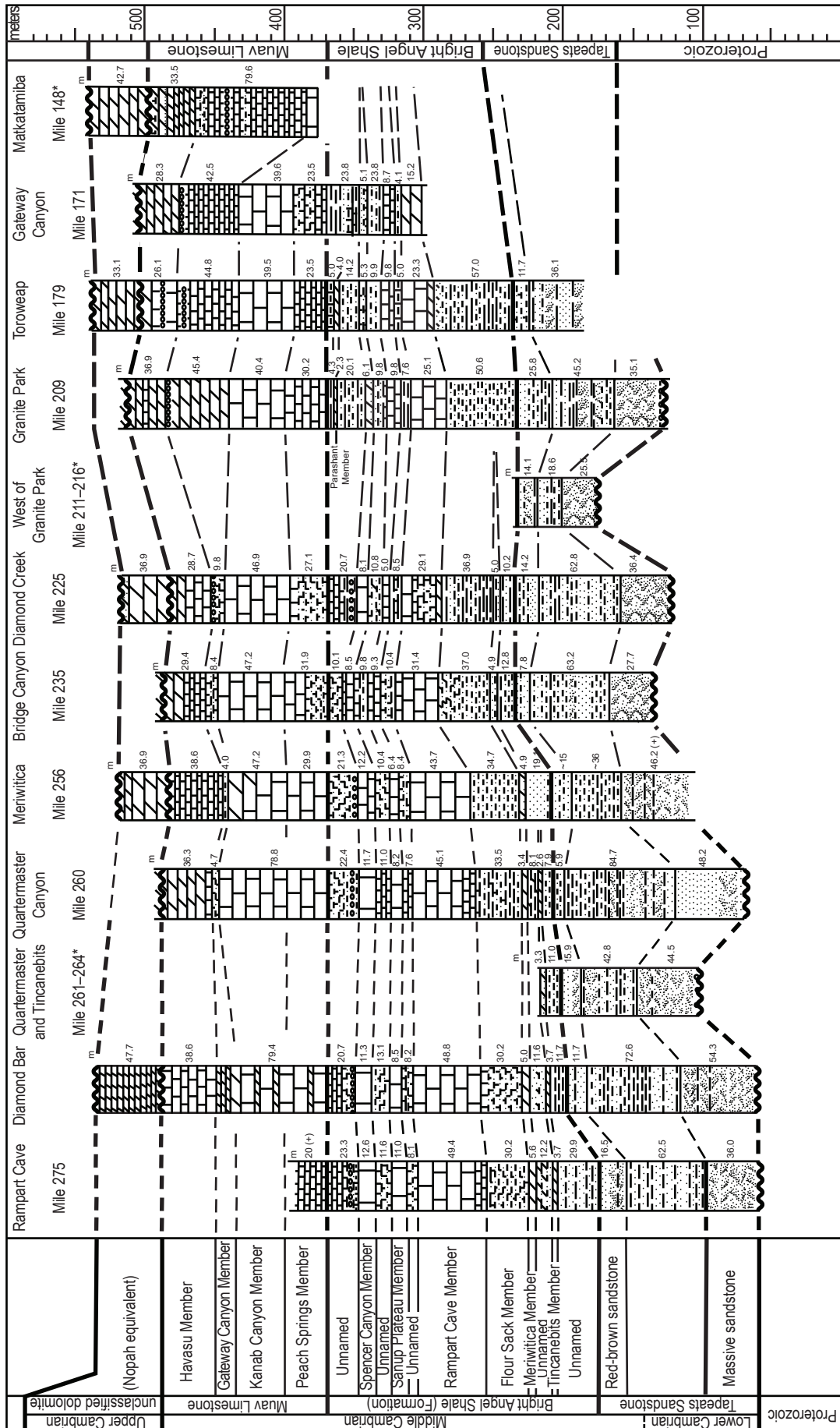
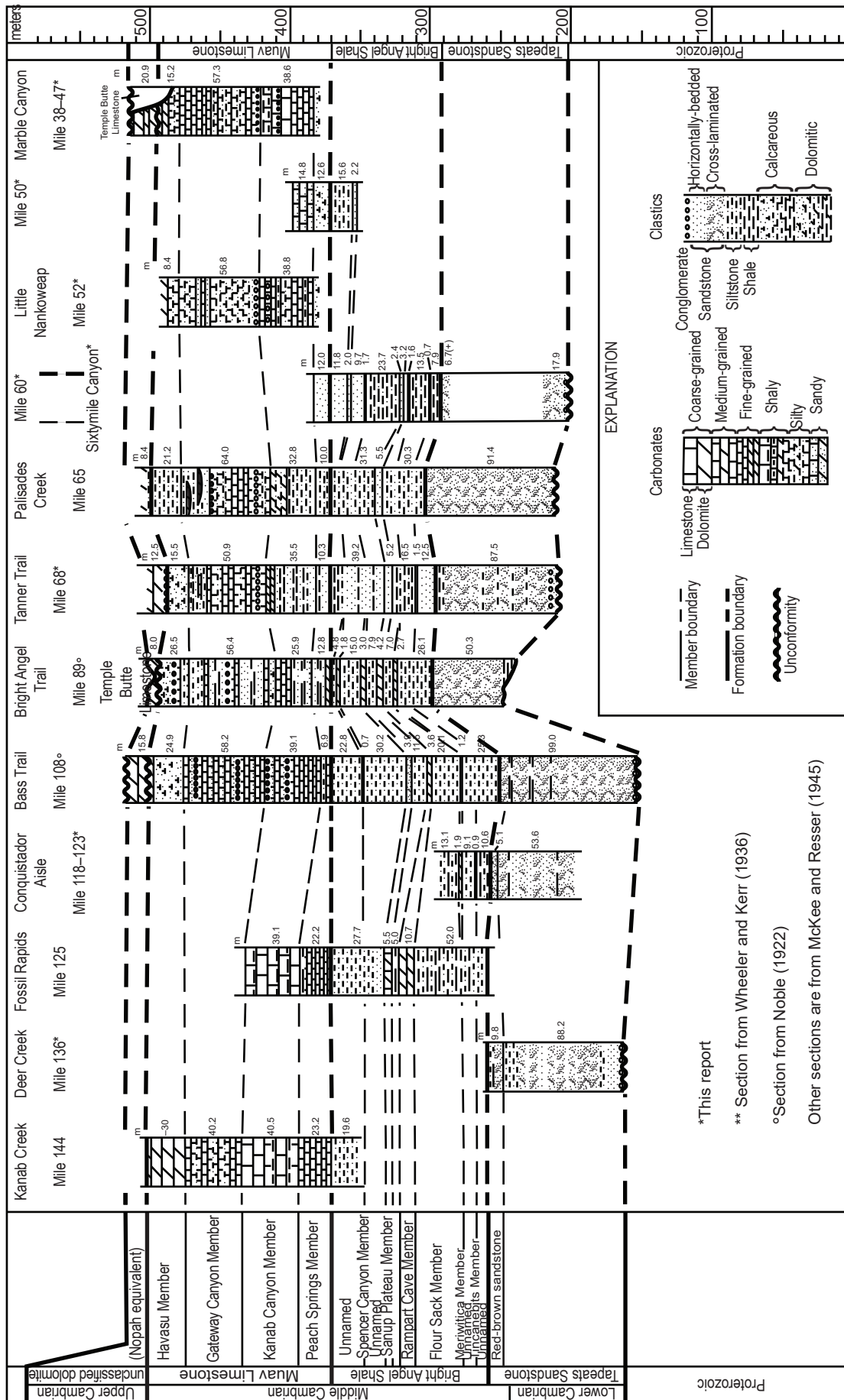


Fig. 5. The diagrammatic section of McKee (1945, 14, fig.1) of the Cambrian deposits in Grand Canyon, showing stages in transgression and regression and distribution of facies from east to west. His time planes are horizontal, and the actual thickness varies from 1,500 ft (about 460 m) in the west to 800 ft (about 245 m) in the east.





**Fig. 6 (pages 148 and 149).** The diagrammatic sections of Elston (1989, 134–135, figs. 15a,b) showing the correlation of the Cambrian Tonto Group deposits in the Grand Canyon and the facies changes based on McKee (1945), Noble (1922) and Wheeler and Kerr (1936) but with his revised nomenclature. (a) The western half of the Grand Canyon, Rampart Cave (river mile 275.8) to Matkatamiba Canyon (river mile 148.5). (b) The eastern half of the Grand Canyon, Kanab Creek (river mile 1.44) to Marble Canyon (river miles 38–47).

Subsequently, Middleton and Elliott (2003) summarized the then newest data to describe the depositional systems of the Tonto group presumed to have existed during the Cambrian history of northern Arizona, using both sedimentologic and ichnologic data. Rose (2003; 2006; 2011) provided new stratigraphic data and sedimentologic evidence from his 29 measured complete and partial sections to support Wanless' (1973a, b) claim and detailed the depositional, geochemical, and biological characterization of his proposed extensive, pervasively shallow paleoenvironment responsible for the Tonto Group. He also proposed that his (Rose 2003) measured section at Blacktail Canyon (river mile 120.5) as a suitable formal type section (figs. 1 and 7, and Appendix B in the Supplementary material), because it is accessible from the Colorado River, and because it is between two long straight stretches of the river, which provides a clear view in both directions of the continuity of marker beds and the cliff-slope profile that help define unit boundaries. Finally, Blakey and Middleton (2012) briefly reviewed the interpreted paleogeography and geologic history of the Cambrian system's record in Grand Canyon within the overall tectonic setting of southwestern North America.

Most recently, Karlstrom et al. (2018; 2020) have redefined the Tonto Group and Sauk megasequence

in Grand Canyon region. They concluded that the Sixtymile Formation is Cambrian and therefore locally the base of the Tonto Group, conformably overlain by the Tapeats Sandstone and the Bright Angel Formation. Similarly, they concluded the Frenchman Mountain Dolostone is conformable above the Muav Formation. It extends across Grand Canyon as the Undifferentiated Dolomite (McKee 1945) whose name it now replaces and is thus the topmost part of the Tonto Group and the Sauk megasequence transgression.

### Regional Stratigraphic Relationships of the Tonto Group

As now proposed, the Tonto Group in the Grand Canyon region comprises five formations that are, in ascending order, the Sixtymile Formation, Tapeats Sandstone, Bright Angel Formation (primarily shale), Muav Formation (primarily limestone), and the Frenchman Mountain Dolostone (Karlstrom et al. 2020). The term "Tonto Group" was first used by Gilbert (1874; 1875) to describe the Tapeats-Bright Angel-Muav fining-upwards sandstone-shale-limestone sequence, although he considered these rock units to be Silurian. Subsequent stratigraphic and paleontologic work by Walcott (1890; 1895) established that the Tonto Group is Cambrian, and Noble (1914) introduced these three formation names



**Fig. 7.** The full profile of the entire Tonto Group just above Blacktail Canyon and looking towards it around river mile 120.5, central Grand Canyon (indicated), which Rose (2011) has proposed as the type section for the Tonto Group. The three main formations making up the Tonto Group (as labeled) are easily distinguished by their profiles in the cliff face (see also the matching graphic stratigraphic log in Appendix B of the Supplementary materials).

during his mapping of the Shinumo Quadrangle in the Grand Canyon.

Strata of the Tonto Group also crop out along the Grand Wash Cliffs in western Arizona and further west at Frenchman Mountain just outside Las Vegas, Nevada, where the Muav Formation is overlain conformably by the Frenchman Mountain Dolostone. To the east, the Tonto Group also crops out in the Juniper Mountains and Black Hills in west-central Arizona (Middleton and Elliott 2003). In those areas the Tapeats Sandstone is overlain disconformably by the Devonian Martin Formation, or the Chino Valley Formation of uncertain age designation (Hereford 1975). It is presumed that the Bright Angel and Muav Formations were removed by extensive pre-Devonian erosion (Middleton and Elliott 2003). In central Arizona scattered outcrops of the Tapeats Sandstone occur along the East Verde River and in the Sierra Ancha Range north of Young, Arizona. Tonto Group equivalents in southeastern Arizona include the Bolsa Quartzite and part of the overlying Abrigo Formation (Hayes and Cone 1975; Middleton 1989).

These Cambrian strata overlie a variety of Precambrian lithologies throughout Grand Canyon. In the eastern Canyon and in some central areas, the Tonto Group rests on tilted beds of the Precambrian Grand Canyon Supergroup, which consists of the Unkar and Chuar groups, whereas in the western areas and other central places the Tonto Group nonconformably overlies various older Precambrian granite plutons that intrude schists of the Granite Gorge Metamorphic Suite (Karlstrom et al. 2003) (figs. 4 and 8). This major unconformity between the Precambrian and Tonto Group strata, which has been long recognized, is called the Great Unconformity due to its visual prominence and continental (and global) extent (Peters and Gaines 2012). Traditionally, it has been thought to represent either a considerable period of time during which there were episodes of slow mountain-building and extensive weathering and erosion, or a very short and intense period of catastrophic uplift and erosion. Walcott (1910) applied the name “Lipalian interval” to the period of uniformitarian time represented by this unconformity. Since the Tonto Group is Cambrian (~500Ma) where it sits on the crystalline basement granites and metamorphic schists (fig. 8b) that are generally dated at 1.6–1.7 Ga (Karlstrom et al. 2003) the time interval at the Great Unconformity is about 1.1 Ga. In contrast, where the Tonto Group sits on the tilted Grand Canyon Supergroup sedimentary strata (fig. 8a) it has been harder to date those sedimentary rocks, so their ages have been variously estimated based on the 1.1 Ga Rb-Sr age for the Cardenas Basalt lavas that are sandwiched between the Unkar Group and Chuar Group sedimentary strata

(Elston and McKee 1982; Larson, Patterson, and Mutschler 1994). Thus the time interval at the Great Unconformity with the Grand Canyon Supergroup sedimentary strata is <500Ma.

However, recent radiometric dating results have further constrained the time interval represented by the Great Unconformity. A U-Pb age of 742Ma was obtained for zircons within a thin tuff bed at the top of the Walcott Member of the Kwagunt Formation (Chuar Group) just below the Great Unconformity (Karlstrom et al. 2000). Subsequently, an Ar-Ar age of 764Ma was obtained for authigenic K-feldspar within early diagenetic marcasite nodules in the underlying Awatubi Member of the Kwagunt Formation (Dehler et al. 2017), and a U-Pb age of 729Ma was obtained for zircons in the same thin tuff bed at the top of the overlying Walcott member (Rooney et al. 2018), both in the upper Chuar Group of the uppermost Grand Canyon Supergroup in eastern Grand Canyon. Furthermore, in eastern Grand Canyon a small wedge of sedimentary strata known as the Sixtymile Formation is sandwiched between the Grand Canyon Supergroup and the Tonto Group. Hithertofore, they have been regarded as Precambrian and thus below the Great Unconformity. However, Karlstrom et al. (2018; 2020) have convincingly demonstrated that the Sixtymile Formation contains detrital zircons with the youngest U-Pb ages of 505–527Ma and is thus Cambrian. It is therefore now regarded as being above the Great Unconformity, and thus represents the onset of the transgression that deposited the overlying Tonto Group. So, the time interval at the Great Unconformity could be about 200Ma when the Sixtymile Formation is present.

The surface on which the Tonto Group accumulated was fairly irregular, though it is also flat at many locations. Where irregular it was characterized by a rolling topography of resistant bedrock “hills” (often Unkar Group Shinumo Quartzite) and “lowlands.” The Precambrian bedrock appears to have been extensively weathered in places and eroded during the claimed prolonged period of subaerial exposure. Walcott (1880) and Noble (1914) were first to recognize that the Precambrian surface represented an apparent paleotopography and that Tonto Group sedimentation patterns were influenced by the relief and lithologies of those “hills.” Others likewise documented the influence of the Precambrian topography on Cambrian sedimentation in other areas of the Rocky Mountains and in the midcontinent (Middleton and Elliott 2003). There are numerous places in the Canyon where the Tapeats Sandstone thins across or pinches out against those Precambrian highs. Where the Tapeats Sandstone pinches out, the Bright Angel Formation directly overlies the Precambrian surface.

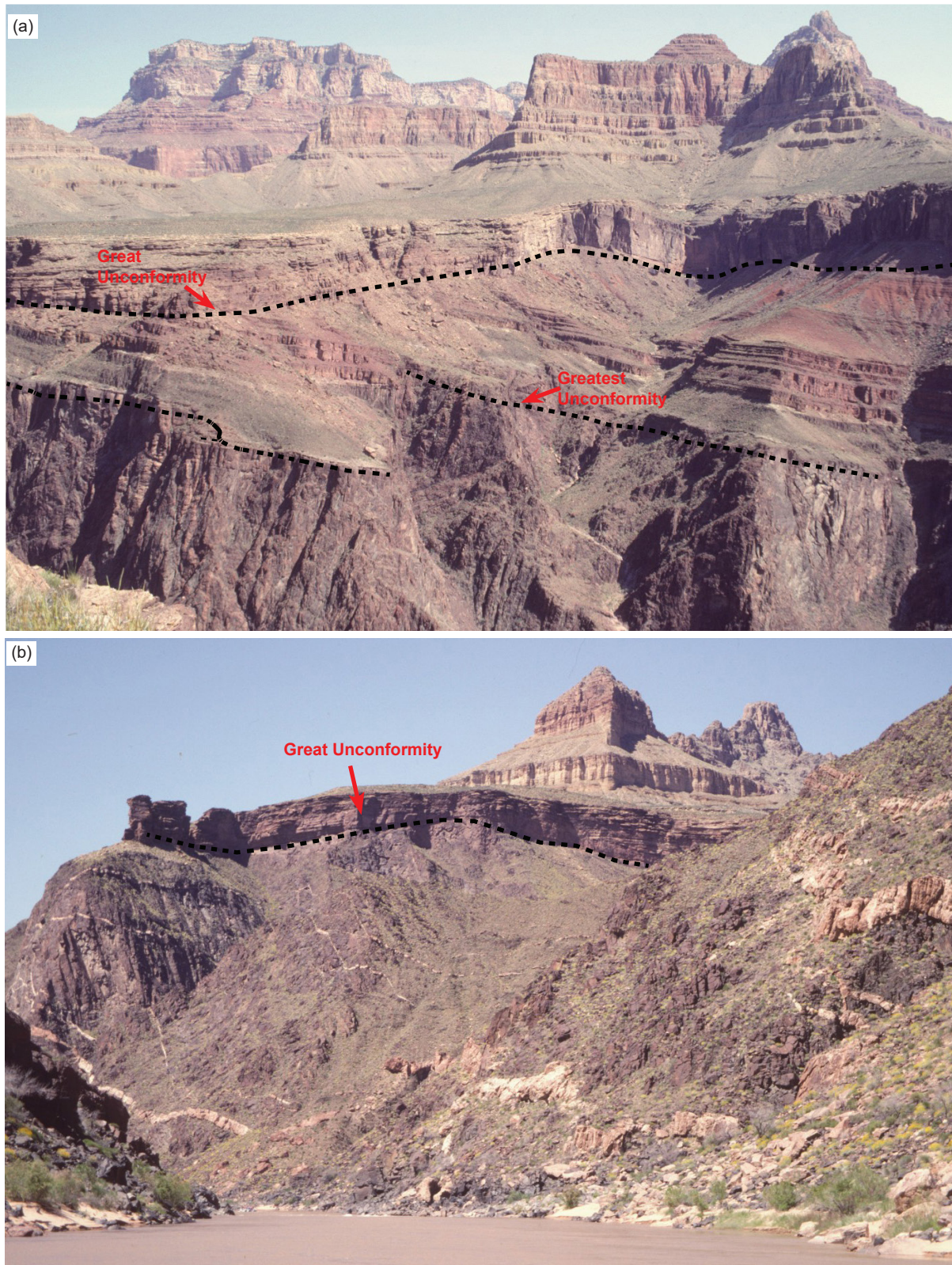


**Fig. 8.** The Great Unconformity as exposed throughout the Grand Canyon. (a) View from the edge of Horseshoe Mesa of the tilted Precambrian Unkar Group sedimentary strata with the Grand Canyon Supergroup eroded across at the Great Unconformity with the Tapeats Sandstone deposited on it, overlain by the Bright Angel and Muav Formations. (b) The Great Unconformity is just below the cliff of Tapeats Sandstone on the near horizon and consists of the eroded surface of the Ruby Pluton (a hornblende-biotite granodiorite intruded by later large granitic veins) at about river mile 105. The Bright Angel Formation is barely visible in the slope overlying the Tapeats Sandstone, but the cliff formed by the Muav Formation is clearly evident.

A claimed apparently highly weathered horizon occurs on top of the Precambrian surface in several places in the Canyon. The only effort to understand the genesis of that claimed horizon is that of Sharp (1940). His study suggested that extensive chemical weathering of Precambrian rocks occurred prior to deposition of Cambrian sediments. In places that apparently highly weathered surface or potential regolith is up to 15.3m (50ft) thick, but elsewhere is generally less than 3.1m (10ft) thick. Sharp (1940) speculated that where the Tapeats Sandstone sits on unaltered Precambrian basement, that regolith was probably removed by the wave erosion associated with the initial Cambrian transgression. Sharp (1940) and McKee (1945) suggested that the presence of such a thick, apparently weathered horizon indicated that dominantly humid conditions existed during the earliest Paleozoic prior to deposition of the Tonto Group. However, there have been no petrologic and geochemical studies that could substantiate that hypothesis. Furthermore, from a uniformitarian perspective during the ~200 million years or more represented at the Great Unconformity, the climate could have changed numerous times prior to deposition of the Tonto Group, and in the presumed absence of terrestrial vegetation weathering processes in soils would have been different (Basu 1981), so a humid climate interpretation is quite tenuous.

At the continental scale, Sloss (1963) recognized that the Great Unconformity and the overlying Tonto Group could be correlated across North America, the latter representing the first of six major sequences of rock-stratigraphic units which he named the Sauk megasequence. Peters and Gaines (2012) further documented that the Great Unconformity is a well-recognized, globally-occurring stratigraphic surface, which in most regions across the globe separates continental crystalline basement rocks from much younger Cambrian shallow marine sedimentary deposits, that is, the Sauk megasequence (Tapeats, Bright Angel, and Muav). Using stratigraphic and lithologic data for 21,521 rock units from 830 geographic locations in North America they demonstrated that, for example, the Tapeats Sandstone correlates with very similar basal Sauk sandstones right across North America (fig. 9), such as the Flathead Sandstone in Wind River Canyon, Wyoming, the Mt. Simon Sandstone in a drill-hole in northern Illinois, and the Sawatch Formation near Manitou Springs, Colorado. Similarly, Clarey and Werner (2018) constructed over 1,500 local stratigraphic columns across North America, South America, Africa, and the Middle East recording the detailed lithologic information and the Sloss megasequence boundaries at each site. From these

data they created a detailed 3-D lithology model for each continent using the local columns, and also constructed maps of the basal lithology for each megasequence. They thus demonstrated the continuity of the basal Sauk sandstone layer (the Tapeats Sandstone), as well as the Bright Angel and Muav Formations and their equivalents) across the North American continent, across North Africa and the Middle East, and across South America where the Sauk is only found within portions of Peru, Bolivia, and northern Argentina. Furthermore, in many locations the basal Sauk megasequence is also coincident with the Great Unconformity.

### The Stratigraphy of the Muav Formation

The Muav Formation was originally deemed the youngest formation of the Tonto Group, until the overlying Frenchman Mountain Dolostone was recently added to the Tonto Group. The Muav Formation forms resistant cliffs above the Bright Angel Formation throughout Grand Canyon. Noble (1914) named the formation from exposures in Muav Canyon and recognized four subdivisions because these have persistent lithological features and topographic expressions. Contact with the Bright Angel Formation is gradational and characterized by complex intertonguing of the two formations (fig. 10). The observation that the Muav limestones contains a far greater percentage of clastics in the Bright Angel section of the Canyon than farther west at Noble's type locality led Schuchert (1918) to conclude that it should be referred to as the Muav Formation, just as Noble (1914) had recognized.

As a result of his detailed mapping through Grand Canyon west of Fossil Rapids (river mile 125.5), McKee (1945) reported that the thickness of the Muav Formation as he defined it varies from 136ft (~41.5m) near the Little Colorado River (river mile 61.8) at the eastern end of Grand Canyon to 827ft (~252.1m) along the Grand Wash Cliffs (river mile 279) at the western end. At Toroweap (~river mile 178.5) about midway through the Canyon the thickness is 439ft (133.8m). McKee (1945) added to his measured sections those sections measured by Noble (1922) and Wheeler and Kerr (1936) and defined seven members within the Muav Formation—from bottom to top stratigraphically, the Rampart Cave, Sanup Plateau, Spencer Canyon, Peach Springs, Kanab Canyon, Gateway Canyon, and Havasu Members (fig. 5). He differentiated these members on the basis of key marker horizons defined by fossil faunas, intraformational conglomerates, or persistent beds of shale and/or thin-bedded limestone. The upper three members can be correlated throughout the entire canyon, whereas the lower four members are confined to areas west of Fossil Rapids (fig. 5).

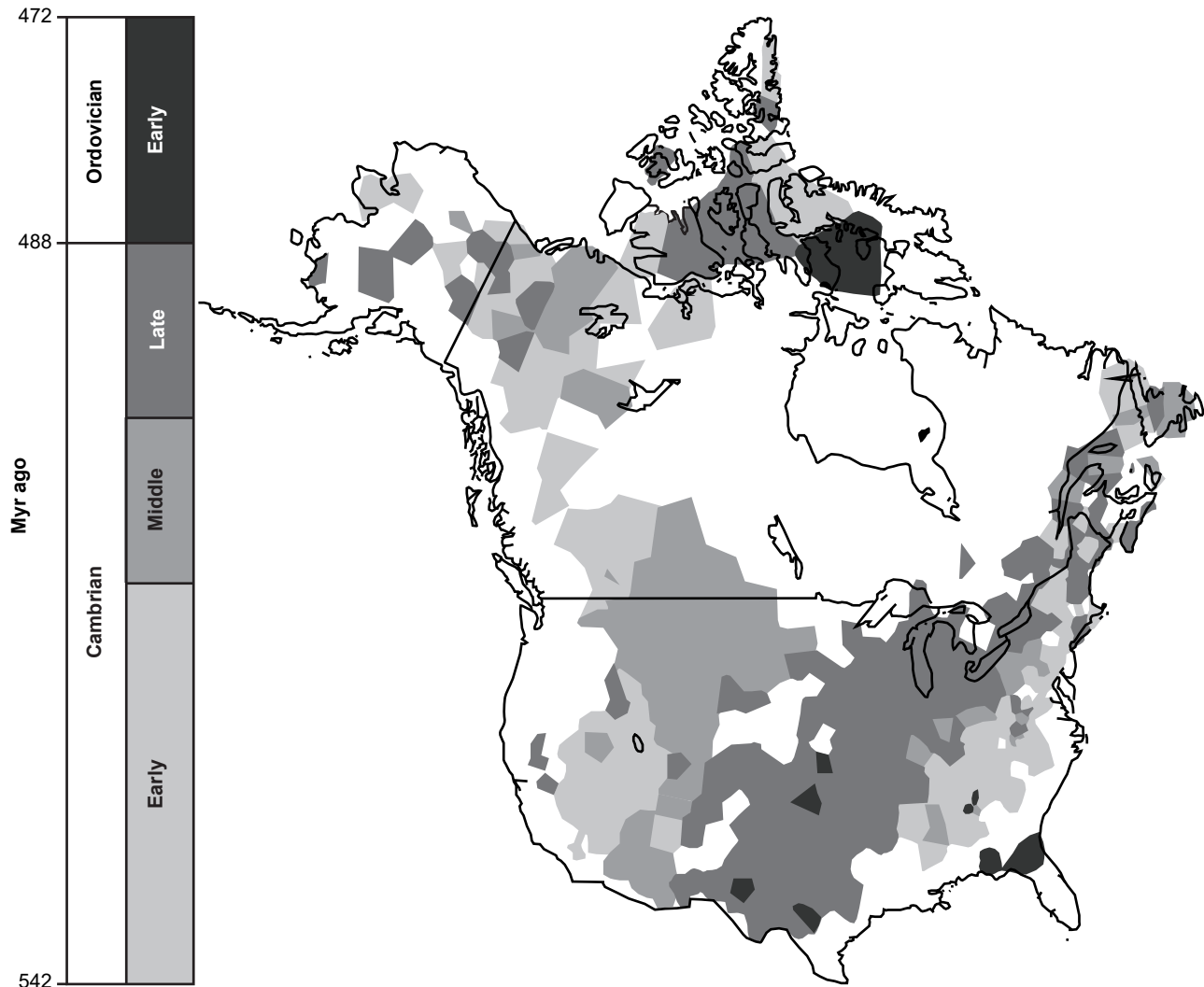


**Fig. 9.** The distribution and age of the Sauk megasequence, the oldest Phanerozoic sedimentary rocks of North America (after Peters and Gaines 2012, 363, fig.1). Not only were the basal Tapeats Sandstone and its equivalents, as well as the overlying Bright Angel and Muav Formations, deposited continent-wide, but the Great Unconformity beneath it was also eroded continent-wide and beyond (globally).

As summarized by Middleton and Elliott (2003), the Muav Formation consists of thin- to thick-bedded, commonly mottled, dolomitic and calcareous mudstone and packstone, as well as beds of intraformational and flat-pebble conglomerate. Thin beds of micaceous shale and siltstone, minor amounts of fine-grained sandstone, and silty limestone occur at numerous horizons in the formation, where they form small recesses and/or benches in the otherwise cliff-forming carbonates. The amount of siliciclastics increases toward the east, concomitant with a decrease in carbonates. Bedding thickness, in general, increases toward the west.

#### **The Stratigraphy Mapped by McKee (1945)**

As a result of the intertonguing relationships between the Muav and the Bright Angel Formations, thickness trends within the Muav Formation are variable (fig. 5). The unit thickens to the west.

McKee (1945) determined that the Muav Formation is 827ft (~252.1m) thick in the Grand Wash Cliffs (river mile 279) near Lake Mead, 439ft (133.8m) thick at Toroweap (~river mile 178.5) in the central Grand Canyon, and only 136ft (~41.5m) thick at the confluence of the Little Colorado River with the Colorado River (~river mile 61.8) at the eastern end of the Grand Canyon. McKee (1945) defined seven members of the Muav Formation (fig. 11).

#### *Rampart Cave Member*

The Rampart Cave Member is the basal subdivision throughout western Grand Canyon. It forms the lowest massive cliff of a series that largely controls the topographic expression of the lower Canyon from Grand Wash (~river mile 287) eastward to Meriwitica (a branch of Spencer Canyon at river mile 246.5), then appears as a prominent wall as far east as Toroweap (~river mile 178.5). Thus, it does not

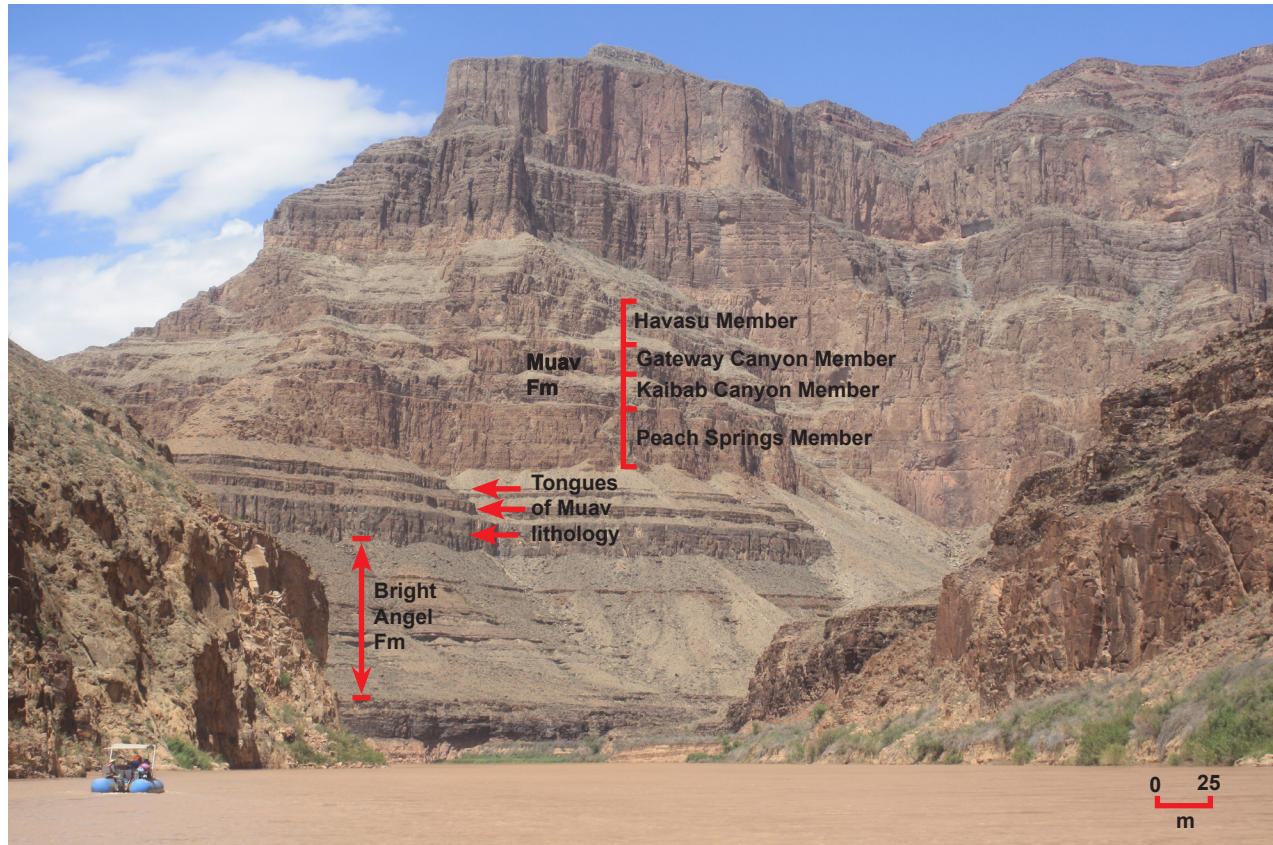


**Fig. 10.** Apparent complex intertonguing relationships in the western Grand Canyon (river mile 257.5) between the Bright Angel Formation (in the slope above the first small “cliff” at river level in the distance) and the overlying Muav Formation (the prominent cliffs above the slope). At the top of that slope are three small, stepped cliffs representing hard carbonate beds compared to the softer shale beds between them that have more easily eroded. Those three small cliff-forming carbonate beds were initially mapped as tongues of Muav lithology within the Bright Angel Formation (fig. 5, McKee 1945), but are now included in the Bright Angel Formation (Elston 1989; Rose 2003). The Members within the Muav Formation are denoted, though in this section it is difficult to find the boundary between the Kanab Canyon and Gateway Canyon Members. Scale as indicated.

have a uniform thickness, but diminishes eastwards from 160 ft (~49 m) thick in the Grand Wash Cliffs (river mile 279) to 76.5 ft (~23 m) thick at Toroweap. McKee (1945) described its lithology as remarkably uniform, consisting almost entirely of gray or dark gray, aphanitic limestone with a small amount of light-brown or tan, silty mottling. However, he argued that the eastward decrease in the member’s thickness may be partly explained by a progressive lateral transition from limestone to shale facies in the basal beds, although much of the thickness change had resulted from the amount of sedimentation progressively decreasing eastwards. Otherwise, in the most southern outcrops at Diamond Creek and Peach Springs (river mile 226) algal (*Girvanella*) limestones form much of the basal and upper beds of this member and argillaceous limestones and dolostones of a “rusty-brown” type make up its middle beds. At the eastern end of the member at Toroweap only the upper part is limestone, the lower beds being typical rusty-brown dolostone. Further east all the beds are the massive, rusty-brown crystalline dolostone that

form a cliff which is an excellent horizon marker called the *Elves Chasm Tongue* throughout most of the central Canyon (fig. 5). At Gateway Canyon (river mile 171.5) this tongue is 50 ft (~15 m) thick, at Fossil Rapids (river mile 125.5) it is 35 ft (~10.6 m) thick, and at Bass Canyon (river mile 108.5) it is only 12 ft (~3.6 m) thick, but Noble (1922) traced it eastwards from Bass Canyon to and beyond Hermit Canyon (river mile 95.5).

#### *Sanup Plateau Member*

The overlying Sanup Plateau Member as defined by McKee (1945) crops out as the lower of two thin but persistent cliff-forming units that extend through the western two-thirds of Grand Canyon between slope-forming tongues of shales and siltstones (fig. 11). In its Meriwitica Canyon (river mile 246.5) section it is composed of thick-bedded, dark-gray, aphanitic limestone with prominent bands of siltstone that weather red-brown. Farther west at Quartermaster Canyon (river mile 260.2) and Rampart Cave (river mile 275) this lithology prevails, but eastward and

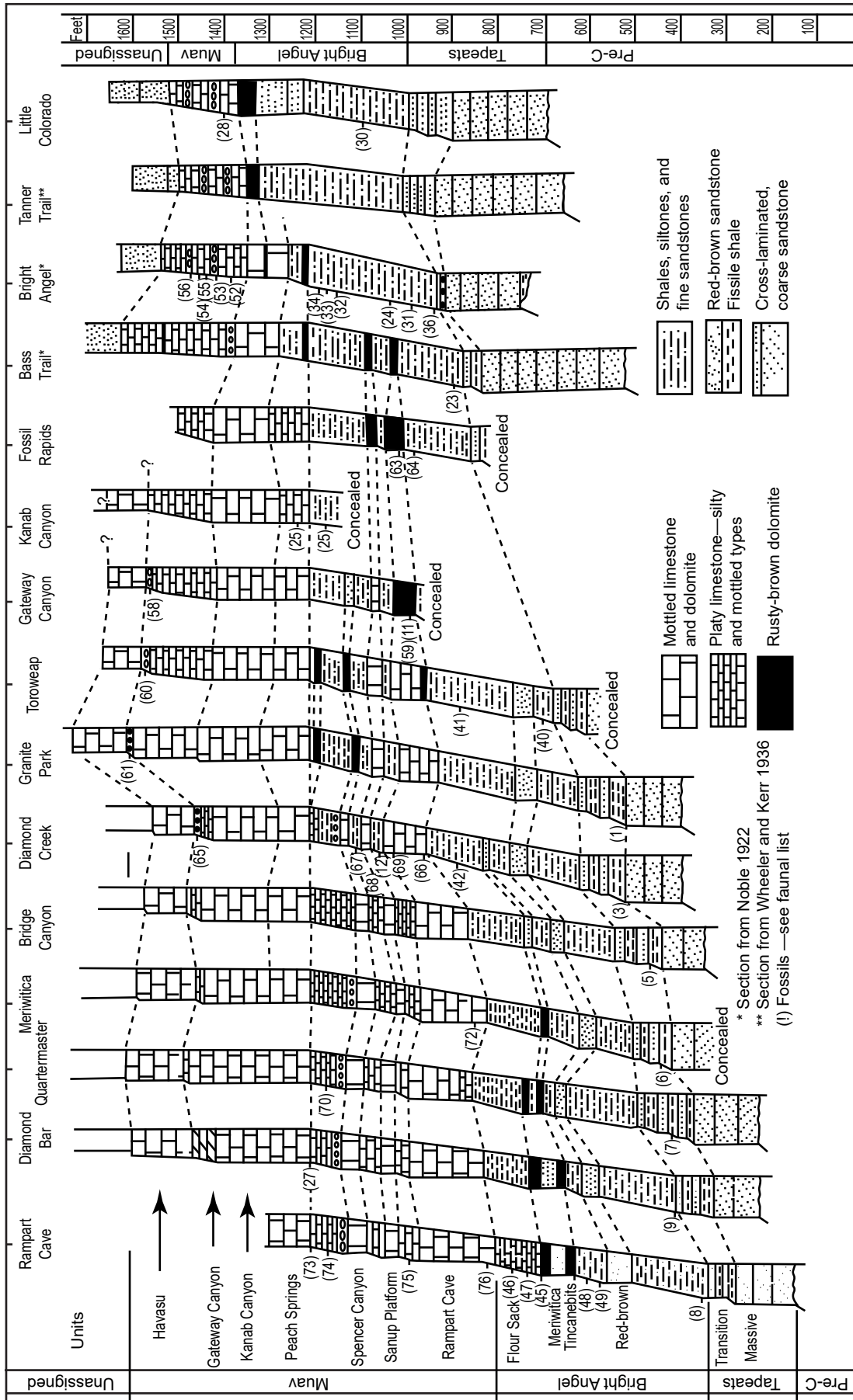


Fig. 11. The McKee (1945, 19, fig. 2b) correlation of the Tonto Group units and formations based on lithologies (after Elston 1989, 132, fig. 15.1).

southward it changes to algal limestone containing small spheres of *Girvanella* frequently filled with red-brown dolomite grains, the algal structures being most conspicuous at Toroweap (~ river mile 178.5) and Fossil Rapids (river mile 125.5), and in Peach Springs Wash (river mile 226). The thickness of this member as measured by McKee (1945) averages 25–30ft (7.6–9.1m) but varies approximately from 36ft (~11m) thick at Rampart Cave through 21ft (6.4m) at Meriwitica and 32ft (~9.7m) at Granite Park (river mile 209) to 28.5ft (8.7m) at Gateway Canyon (river mile 171.5) and only 18ft (5.5m) at Fossil Rapids. The eastward extension of this member beyond Fossil Rapids is another rusty-brown dolostone called the *Garnet Canyon Tongue* which is a conspicuous feature as far east as Hermit Canyon (river mile 95.5) (fig. 5). Its average thickness is about 12ft (~3.6m). Noble (1922) described this tongue in Garnet Canyon (river mile 115) as consisting of beds of “snuff-brown” dolostone ranging in thickness from a few inches (~0.1m) to 8ft (~2.4m) with associated beds of green, magenta and brown cross-bedded sandstone. Some dolostone beds contain no visible impurities, but others contain scattered grains of glauconite and tiny rounded quartz grains and exhibit cross-bedding. Many beds contain broken shells of brachiopods.

#### *Spencer Canyon Member*

Stratigraphically above is the Spencer Canyon Member (McKee 1945). It extends eastward from the Grand Wash Cliffs (river mile 279) to Diamond Creek (river mile 226), with an average thickness of 40ft (12.2m) decreasing to 26.6ft (8m) thick at Diamond Creek (figs. 5 and 9). McKee (1945) described it as composed of medium- to dark-gray, aphanitic limestone, mottled with red-brown siltstone. He found it relatively uniform in composition throughout but could be subdivided into three parts on the basis of bed thickness. The beds comprising the basal 20ft (6.1m) are thick and massive, forming a persistent cliff. The next 10ft (3.05m) is thin-bedded and frequently weathers into a slope, while the uppermost 10ft (3.05m) resemble the bottom part and also forms a cliff. In this same stratigraphic position from Diamond Creek eastward is another thin “rusty-brown” dolostone unit known as the *Lava Falls Tongue* that forms a resistant cliff. At Granite Park (river mile 209) it is 20ft (6.1m) thick, but further east at Toroweap (~ river mile 178.5) it is 17.5ft (5.3m) thick and at Gateway Canyon (river mile 171.5) 16.5ft (5m) thick. This tongue is similarly divisible into three units—a basal ledge-forming dolostone which weathers rusty brown, a middle slope-forming unit of green shale and brown siltstone, and an upper cliff-forming carbonate unit.

Between and above each of these three members of the Muav Formation and their corresponding tongues are tongues of Bright Angel Formation lithologies (figs. 10 and 11), which together constitute the complex intertonguing between the Bright Angel and Muav Formations as mapped by McKee (1945) (fig. 5). They are typically composed of weak, thin-bedded sediments that persistently weather to slopes or benches.

#### *Bright Angel Tongues*

The Bright Angel tongue above the Rampart Cave Member throughout most of its extent is 20–30ft (6.1–9.1m) thick (McKee 1945). At Bass Canyon (river mile 108.5) it consists principally of green shales and buff, platy siltstones with some thin beds of glauconite. Whereas to the west as far as Gateway Canyon (river mile 171.5) and southwest to Diamond Creek (river mile 226) shales are still common in this tongue, silty, platy limestones are dominant having largely taken the place of the siltstones in its eastern end. Even further west and north mottled aphanitic limestones similar to the Muav members above and below, except for being thin-bedded, are common, while in the extreme western Canyon these limestones constitute most of this tongue.

The Bright Angel tongue above the Sanup Plateau Member averages 35ft (~10.7m) thick (McKee 1945). Eastward from Grand Wash Cliffs (river mile 279) to and beyond Meriwitica Canyon (river mile 246.5) it consists chiefly of thin-bedded, platy, silty limestone, but includes some glauconitic siltstones and mottled limestones. Farther east, from Diamond Creek (river mile 226) to near Toroweap (~ river mile 178.5), clastic sediments dominate over the platy limestone with silty partings, having graded into platy siltstones, which are very easy to recognize as the slope-forming beds between two massive cliffs. Indeed, between Gateway Canyon (river mile 171.5) and Toroweap this tongue is readily divisible into a lower-slope-forming unit about 10ft (~3.05m) thick of platy siltstone that changes eastward into green shale, overlain by a resistant cliff of ferruginous glauconitic siltstone and dolomite averaging 3ft (~0.9m), and by a 20ft (6.1m) thick upper slope-forming unit of green shale. Still farther east, between Toroweap and Fossil Rapids (river mile 125.5), this tongue consists of thin green shales and some ferruginous-glauconitic sandstones. And eastwards beyond Fossil Rapids the green shale cannot be readily distinguished from similar other units higher in the Bright Angel Formation. Thus, there is a transition from Muav lithologies eastwards to Bright Angel lithologies.

And finally, the Bright Angel tongue above the Spencer Canyon Member averages about 70ft (21.3m) thick (McKee 1945). It can be recognized as a unit of

shales, siltstones and thin, silty limestones forming a transitional series from the Grand Wash Cliffs (river mile 279) eastwards to Gateway Canyon (river mile 171.5), beyond which it merges into the main body of the Bright Angel Formation. It persistently forms a slope of thin beds, which contrasts with the resistant cliffs of the hard, massive rock above and below. At Gateway Canyon, Toroweap (~river mile 178.5) and Granite Park (river mile 209) this Bright Angel tongue is composed of thin green shales, platy brown siltstones, and ferruginous-glaucconitic sandstones. Further west at Meriwitica and Quartermaster Canyons (river miles 246.5 and 260.2 respectively) this tongue consists of platy limestones that weather to brown silty surfaces and very thin-bedded, mottled aphanitic limestones. The percentage of the latter limestone increases westward and grades upwards into the similar but thick-bedded and more massive limestone of the overlying Peach Springs Member of the Muav Formation.

Near the base of this Bright Angel tongue above the Spencer Canyon Member of the Muav Formation is a zone of intraformational flat-pebble conglomerates (McKee 1945, pl. 12a, b) that extends from Diamond Creek (river mile 226) westward to the end of Grand Canyon (fig. 5). It forms a marker horizon consisting of one or two pebble beds and separate glauconite-rich silty, platy limestone lenses and beds that very commonly contains small-scale interference ripple marks.

The upper four members of the Muav Formation are jointly contiguous through Grand Canyon, thickening westwards from where first exposed in Marble Canyon through to the western end of Grand Canyon (figs. 5, 7 and 10–13).

#### *Peach Springs Member*

The lowermost of these is the Peach Springs Member, which consists of a mottled, aphanitic limestone and extends from Fossil Rapids (river mile 125.5) westwards to the end of Grand Canyon (McKee 1945). This member's type locality is in Peach Springs Wash (near Diamond Creek at river mile 226) where it consists of thin-bedded gray limestone, some of which is aphanitic and some fine-grained, but much mottled with brown siltstone which in places has developed a reticulate surface pattern or forms irregular bands. In its eastern section, in the central Grand Canyon between Fossil Rapids and Toroweap (~river mile 178.5), this limestone is a uniform 72–77 ft (21.9–23.5 m) thickness, thin-bedded, and weathers into a weak cliff or steep slope (fig. 13). However, west of Toroweap it thickens to about 98 ft (~29.9 m) at Meriwitica Canyon (river mile 246.5) and its beds are thicker and more massive, forming a prominent cliff (fig. 10). No evident marker beds

serve as time planes within the member, but its top and basal contacts are likely time planes across the area, as indicated by the uniformity in type and amount of the limestone between them. Eastward of Fossil Rapids, at Garnet Canyon (river mile 115), Bass Canyon (river mile 108.5) and beyond, beds in the same stratigraphic position progressively thin and consist chiefly of dolostone and siltstone that Noble (1922) considered to be the top unit of the Bright Angel Formation (fig. 12). However, because the base on the unit is marked by a persistent and conspicuous rusty-brown dolostone that can be traced further eastward as far as Cottonwood Creek (river mile 81.2) where it is still 52 ft (~15.8 m) thick, McKee (1945) called it the *Boucher Tongue* and recognized it as a time plane (fig. 5).

#### *Kanab Canyon Member*

The overlying Kanab Canyon Member is the lowermost member of the Muav Formation throughout the eastern Grand Canyon (McKee 1945). At its type locality at the mouth of Kanab Canyon (river mile 144) it is the lowest massive cliff-forming unit some 143 ft (~43.6 m) thick not far above the level of the Colorado River. Walcott (1880) described it as a massive, gray and drab, thin-bedded, mottled limestone. The Kanab Canyon Member's thickness is much the same at 130–133 ft (39.6–40.5 m) westward (fig. 13) and northward of its type locality as far as Granite Park (river mile 209). Beyond there its lithology is so similar to that of the overlying Gateway Canyon Member from which it is not separated by any shale or other distinctive beds that the two members can no longer be distinguished from one another (fig. 10). In contrast, as well as decreasing in thickness to 128 ft (39 m) at Fossil Rapids (river mile 125.5), 97 ft (29.5 m) at Bass Canyon (river mile 108.5) and only 62 ft (18.9 m) at Cottonwood Creek (river mile 81.2), the latter two sections measured by Noble (1922), its lithology changes considerably eastwards from Kanab Canyon. Whereas at its type locality it consists of a single massive cliff of uniform mottled limestone, only 25 mi (~40 km) away to the southeast in Bass Canyon it includes a 10 ft (3.05 m) thick basal sandy shale unit. And 8 mi (12.9 km) further away it is divisible into two lithological units of about equal thickness, the upper half being the similar mottled limestone, but the lower half containing impure limestone with many partings of gray sandstone and greenish shale. These two divisions are then recognizable eastward for about 20 mi (32.2 km) to at least Cottonwood Creek, where limestone is nearly absent from the lower unit and is relatively impure in the upper. Then a further 10 mi (16.1 km) east along the Tanner trail in the eastern Grand Canyon, the upper unit of the member is

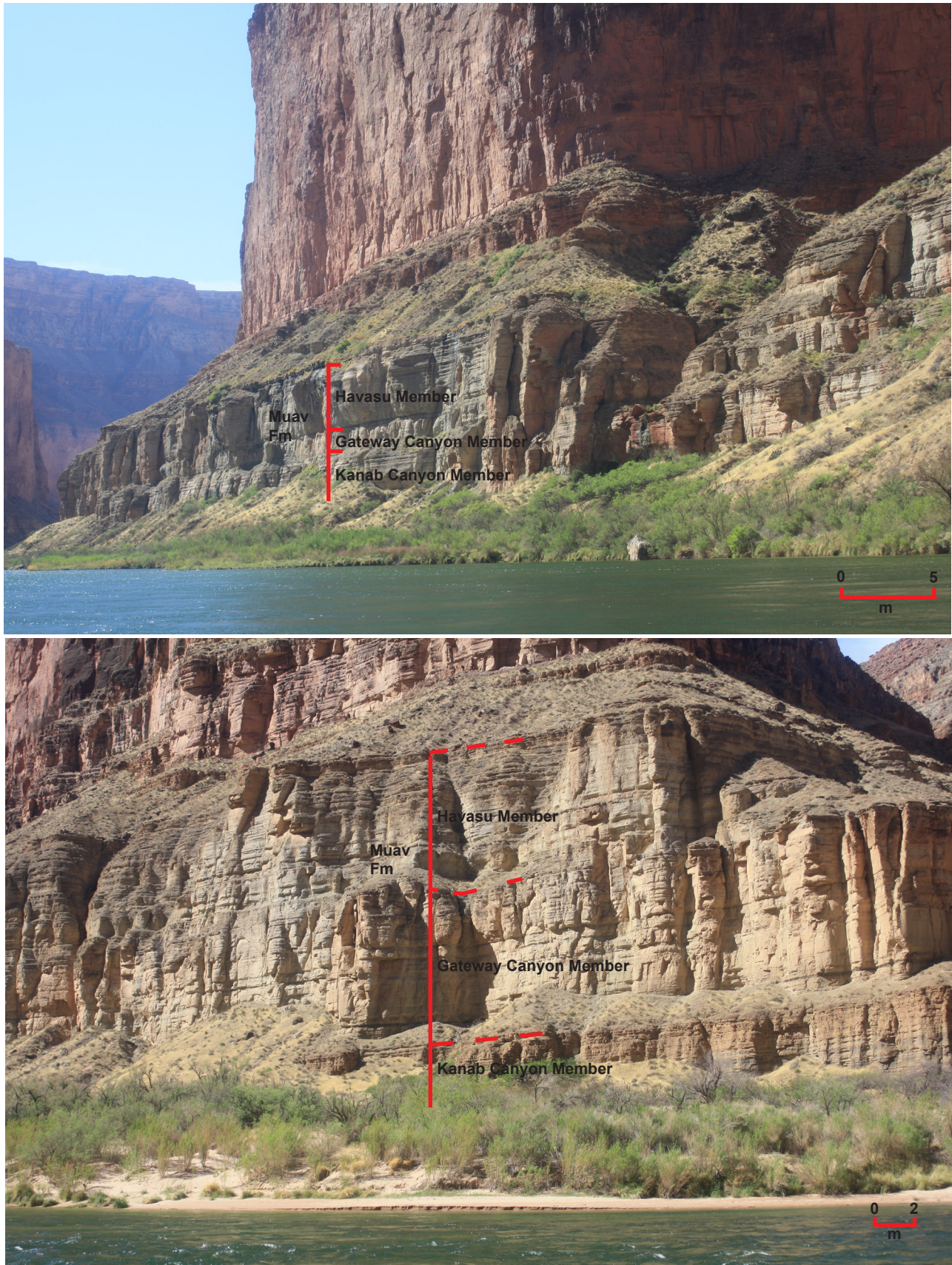


**Fig. 12.** The Kanab Canyon, Gateway Canyon and Havasu Members of the Muav Formation exposed in the cliffs just along the Colorado River in Marble Canyon. The boundaries are marked by distinctive breaks between them. (a) At river mile 49.5, river right. (b) At river mile 50, river right.



**Fig. 13.** The four members of the Muav Formation exposed in the cliff looking downstream from National Canyon (river mile 167.2), in ascending order—Peach Springs, Kanab Canyon, Gateway Canyon and Havasu.

only 19ft (5.8m) thick (as measured by Wheeler and Kerr 1936) and consists of rusty-brown dolostone, whereas the lower unit consists of glauconitic and ferruginous sandstone and shale similar to those in the underlying the Bright Angel Formation (fig. 11).

#### *Gateway Canyon Member*

The Gateway Canyon Member is the second member from the base of the Muav Formation in the eastern Grand Canyon, overlying the Kanab Canyon Member (McKee 1945) (figs. 5 and 11). To the west at Toroweap (~river mile 178.5) and Granite Park (river mile 209) it is the third member from the base owing to the Peach Springs Member underlying the Kanab Canyon Member. Further west from Diamond Creek (river mile 226) the Gateway Canyon Member merges with the Kanab Canyon Member and loses its identity, while between Meriwitica and Quartermaster Canyons (river miles 246.5 and 260.2 respectively) the underlying Peach Springs Member also becomes indistinguishable from the merged Gateway Canyon and Kanab Canyon Members (fig. 10). The combined thickness of these members, however, decreases appreciably toward the west, being 372ft (113.4m) at Granite Park and 258ft (78.6m) at Grand Wash Cliffs (river mile 279). Gradations from east to west in the thickness of bedding and in the lithology of the

Gateway Canyon Member are responsible for changes in its topographic expression. Whereas, throughout eastern Grand Canyon it forms a slope which contrasts with the resistant cliff of the underlying Kanab Canyon Member, from Garnet Canyon (river mile 115) to Toroweap it normally weathers into a much steeper slope or even cliff. Further west it forms a massive, sheer wall, much like those formed by the members above and below it.

The type locality of the Gateway Canyon Member is at the mouth of Gateway Canyon (river mile 171.5), now known as Mohawk Canyon, where it is 137ft (41.8m) thick and consists of thin beds (1–4in or ~2–10cm thick) of mottled, aphanitic limestone separated by parting planes of yellow-brown siltstone, which are responsible for its breaking down into a steep, step-like slope. Its base is determined by a weak zone that forms a bench at the top of the Kanab Canyon Member, while a continuous conglomerate bed at this horizon from Hermit Canyon (river mile 95.5) to Garnet Canyon (river mile 115) could be considered a “time plane.” Its upper limit is marked by a fossil-bearing flat-pebble conglomerate zone at the base of the overlying cliff, while a continuous prominent red-brown sandstone bed at the same horizon from Elves Chasm (river mile 117.2) to Bass Canyon (river

mile 108.5) also forms the division line. Westward to and beyond Granite Park (river mile 209) it is fairly constant in total thickness and character, although the internal beds become thicker (1–2ft or 0.3–0.6m at Toroweap, and 2–4ft or 0.6–1.2m at Granite Park) and the siltstone partings less numerous so that it forms a massive cliff (fig. 13). The basal weak zone and topmost conglomeratic zone are also present. However, from Diamond Creek (river mile 226) westward the defining basal marker beds are absent. Eastward from Gateway Canyon this member is progressively less massive, contains more clastic materials, and is thinner-bedded. At Bass Canyon (river mile 108.5) and further east the normal, mottled gray, aphanitic limestone beds are mostly less 2in (2cm) thick and alternate with thin beds of intraformational conglomerate and with micaceous gray, platy limestone.

#### *Havasus Member*

The overlying Havasu Member is the topmost member of the Muav Formation and also consists of beds of mottled aphanitic limestone (McKee 1945). At its type locality near the mouth of Havasu Canyon (river mile 157.3) it forms a sheer cliff overlying the narrow bench that is marked by the fossil-bearing flat-pebble conglomerate zone. The same relationships occur further west (fig. 13) at Gateway Canyon (river mile 171.5), Toroweap (~river mile 178.5), Granite Park (river mile 209) and Diamond Creek (river mile 226). Farther west between Bridge Canyon (river mile 235.3) and Grand Wash Cliffs (river mile 279) both the conglomerate and fossil beds are absent at the base, but the cliff unit and underlying bench are readily traceable across the area (fig. 10). However, eastward from the type locality at Havasu Canyon the exact equivalent of the Havasu Member has not been determined because of lack of critical data between Havasu Canyon (river mile 157.3) and Bass Canyon (river mile 108.5) where Noble (1922) made detailed studies. There it may be equal to the upper half of a thin-bedded limestone unit (Noble's subdivision C), to the overlying clastic deposits, or to both. Difficulties in correlation result from pronounced changes in lithology and thus topographic expression across the areas east of Havasu Canyon, and also the absence of the marker beds which indicate the base of the member from Havasu Canyon westward. However, the presence of the same fossils at 112ft (~34m) above the base of the Gateway Canyon Member near Bright Angel trail (river mile 89.5), and the correspondence in thickness between the lower half of Noble's subdivision C and the Gateway Canyon Member to the west indicate that the base of the Havasu Member is within Noble's subdivision C in the eastern Grand Canyon.

The thickness of the Havasu Member throughout most of Grand Canyon is about 100ft (~30.5m), but in the extreme western Canyon it averages closer to 120ft (~37.6m). The Havasu Member also varies in lithology, consisting of mottled aphanitic limestone in places, and mottled fine-grained dolostone elsewhere. Generally, the limestone forms the lower beds of the member and the dolostone the upper beds, but the relative positions and amounts of each are not constant, suggesting to McKee (1945) that the dolostone beds represent replacement of limestone. Much of the dolostone is red or pink, mottled with tan. Glauconite-rich beds are found near the top of this member at Toroweap (~river mile 178.5) and Granite Park (river mile 209), and the member's upper limit is marked by a group of thin carbonate beds which are found as a narrow bench or a recess in most places.

#### **Subsequent Mapping of the Stratigraphy**

The focus of the investigation of Wanless (1973a) was to reevaluate the depositional environment of the Grand Canyon's Cambrian strata sequence, but he also provided some stratigraphic observations. Wanless (1973b) reported that the Muav Formation consists of 1–8m (~3.3–26.2ft) thick units of dolomitized eocrinoidal biocalcarene and algal-ball limestone, flat-pebble intraclast beds, and what he claimed were a few stromatolites. Wanless (1975) included a measured stratigraphic section at the same Diamond Bar Ranch location in the Grand Wash Cliffs (river mile 279) south of the Grand Canyon measured by McKee (1945). He then focused on a 20m (~66ft) thick sequence composed dominantly of very thinly laminated, soft-pellet dolomicrites (or dololaminites) that interrupted the top section of the characteristic burrowed, thin-bedded nodular limestone (pelmicrite) of the ~234m (~768ft) thick Muav Formation (fig. 14).

Wanless (1975) found this dolomicrites unit persisted east-west across the depositional strike for almost 15km (~9.3mi). He described the laminites as composed of aphanocrystalline dolomite and soft-pellet aphanocrystalline dolomite containing 2–15% angular quartz and feldspar silt and ovoid pellets 120–200µm in long diameter and provided two photomicrographs of them. The laminations are 1mm or less in thickness. They are either as stacks of thin, single mud laminae that are continuous with even thickness, or couplets of a thin, continuous mud lamina, and then a discontinuous pellet-sand lamina. Furthermore, the continuous mud laminae have uniform thickness and drape irregularities and are commonly over-steepened, whereas the discontinuous pellet-sand laminae are quite well-sorted, form thin starved ripples and depression fillings, and do not drape.

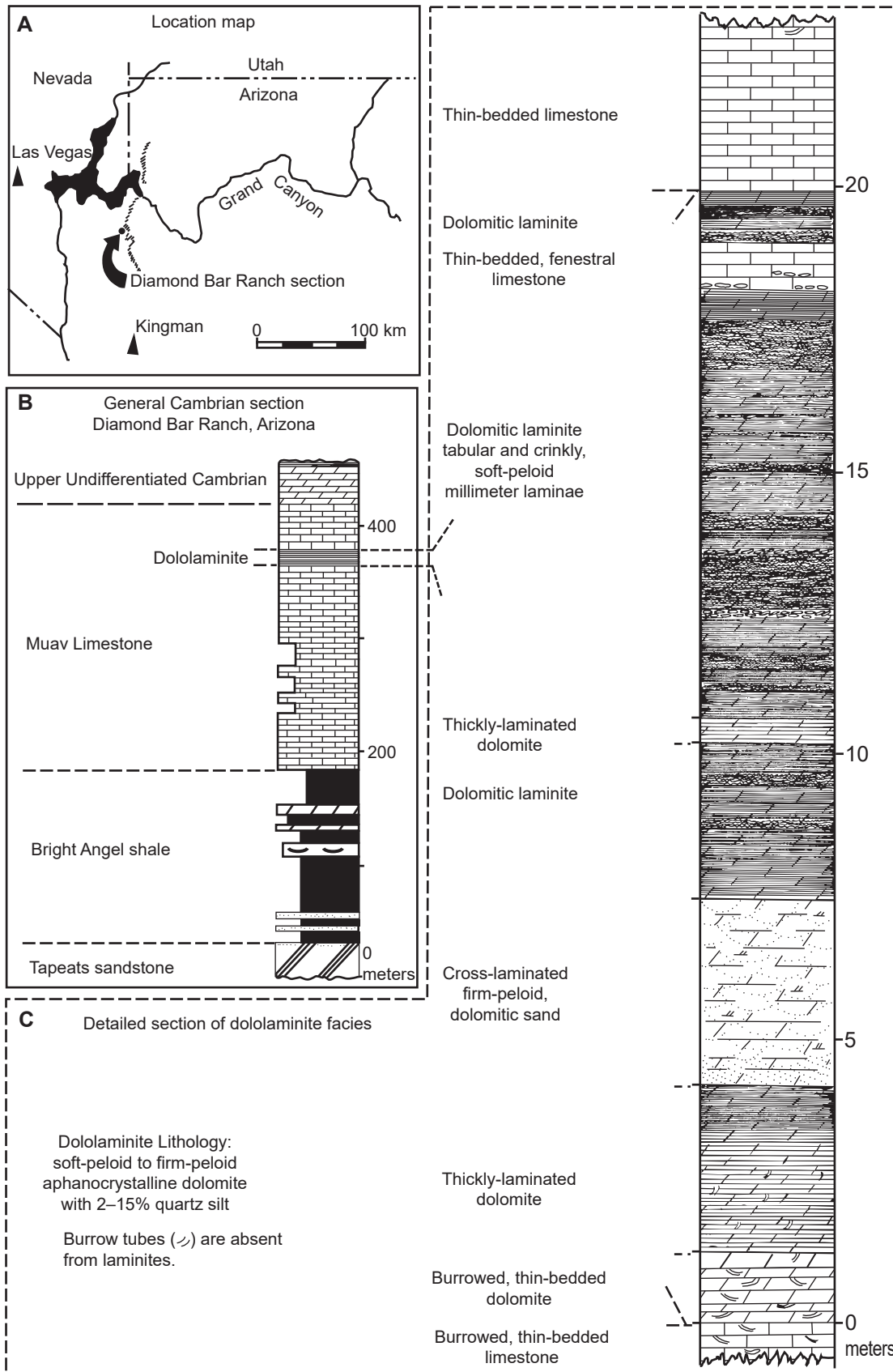


**Fig. 14.** The dololaminites in the upper Muav Formation in the Diamond Bar Ranch area, after Wanless (1975) (a) Location map of the Diamond Bar Ranch area at the western end of Grand Canyon where the Cambrian section was measured. (b) The general Cambrian section. (c) Detailed section of the dololaminite facies.

Wanless (1975) also described beds of three lithologies associated with the dololaminites. First, thickly-laminated dolomite consisting of continuous layers 1–15 mm (~0.04–0.6 in) thick with minor scour pockets and small vertical burrows grade upward into dololaminites. Second, cross-laminated, dolomitized, firm pellet sand, consisting of dominantly small (<3 cm or 1.2 in thick) trough cross-laminations, no burrows, and also planar high-angle and low-angle cross-laminations in the upper part of the sequence. And third, thin-bedded, fenestral limestone consisting of very thin-bedded, firm pellet microsparite with the bedding disrupted, numerous planar discontinuous fenestrae zones, no burrowing, and flat-pebble limestone intraclasts filling small scour depressions.

Subsequently, Huntoon (1989) raised the mapping nightmare of McKee's (1945) designation of all the shale units in the Cambrian section of the western Grand Canyon as members of the Bright Angel Shale because the upper shale units intertongue there with the limestone units he defined as members of the lower Muav Limestone (fig. 10). Yet this intertonguing is absent from eastern Grand Canyon, so McKee's (1945) stratigraphic boundaries for the Muav had resulted in a discontinuity between the geologic maps of the western and eastern Grand Canyon.

Elston (1989) and several of his associates measured five stratigraphic sections of the Tonto Group throughout Grand Canyon intermediate to those measured and compiled by McKee (1945), but also added four more stratigraphic sections of the far eastern exposures beyond Palisades Creek (river mile 66) as far as Marble Canyon (river miles 38–47), also adding the stratigraphic sections of Noble (1922) and Wheeler and Kerr (1936). Having recompiled carefully all available stratigraphic sections with the same lithologies, Elston (1989) redefined the stratigraphic boundary between the Bright Angel and Muav Formations. He retained the Peach Springs, Kanab Canyon, Gateway Canyon, and Havasu as members of the Muav Formation but used the base of the Peach Springs Member as the datum for the base of the Muav to make correlations with his revised nomenclature as depicted in fig. 6. He noted that the north-to-south facies change from carbonate to sandstone is observed in Marble Canyon and easternmost Grand Canyon. Marker carbonate beds persist into the dominantly sandstone sections of the Little Colorado River to Palisades Creek section (river miles 62–66) measured by McKee (1945) and Tanner Trail section (river mile 69) measured by Wheeler and Kerr (1936). Elston (1989) found that the four members of the Muav Formation remain fairly constant in lithologic character following the transition from sandstone to sandy carbonate

to carbonate westward from easternmost Grand Canyon. The Peach Springs Member most commonly is represented by a single relatively uniform depositional unit, and its contact with the overlying Kanab Canyon Member is marked in many places by a thin ash-fall tuff bed (including further west at Frenchman Mountain, Nevada). The Kanab Canyon Member commonly crops out as two resistant cliff-forming ledges, whereas the overlying Gateway Canyon Member is thinner bedded, tends to be less resistant and commonly is characterized by a steep slope/cliff/slope profile rather than by a steep cliff. Elston (1989) also noted that the Gateway Canyon Member is abnormally 80 m (~262.5 ft) thick at Matkatamiba Canyon (river mile 148.4). Otherwise, the Havasu member at the top of the Muav Formation is cliff-forming and characteristically consists of a lower unit of limestone overlain by a unit of dolostone.

Middleton (1989) mostly summarized the description of the Muav Formation by McKee (1945). Because of its gradational and complex intertonguing with the underlying Bright Angel Formation the Muav Formation thins to the east, varying from 827 ft (~252.1 m) thick in the Grand Wash Cliffs, to 439 ft (133.8 m) thick at Toroweap (~ river mile 178.5), and to only 136 ft (~41.5 m) thick at the Little Colorado River (~river mile 61.8). It also appears to become younger to the east, being above the *Alokistocare-Glossopleura* zone (Middle Cambrian) in the western Canyon but to the east the upper Muav contains the *Bathyriscus-Elrathina* zone (late Middle Cambrian). The Muav Formation forms resistant cliffs throughout Grand Canyon because it consists of thin to thick beds of nodular limestone and dolomitic packstone and mudstone. Persistent beds of intraformational limestone conglomerate were used by McKee (1945) to subdivide the Muav into seven members, which have already been described in detail. Thus Middleton (1989), who may not have been aware of Elston's (1989) work, did not adopt Elston's (1989) redefining of the Muav Formation as just McKee's (1945) top four members. Yet Billingsley, Hendricks, and Lucchitta (1987) had documented an erosional unconformity between McKee's basal Rampart Cave Member of the Muav and his Flour Sack member of the Bright Angel Formation in western Grand Canyon, whereas that contact appears gradational in other areas. Otherwise, Middleton (1989) noted that thin beds of micaceous and dolomitic mudstone and minor sandstone occur at several horizons where they form minor recesses in the Muav Formation cliffs.

Rowland, Osborn, and Graber (1995) measured the ~141 m (~462.6 ft) thick stratigraphic section of the Muav Formation exposed in Fern Glen Canyon (river mile 168.5) (see fig. 13). It includes the uppermost

portion of the Peach Springs Member, which they described as several meters of green, glauconitic sandstone. This is consistent with McKee's (1945) report of Peach Springs siliciclastic lithologies in central Grand Canyon. However, such a thick interval of relatively coarse-grained siliclastics here is surprising given McKee's descriptions implying such facies occur only east of Fossil Rapids (river mile 125.5). Nevertheless, this glauconitic sandstone facies in the upper part of the Peach Springs Member here is evidently quite restricted in distribution as it is absent in the Tuckup Canyon section (river mile 165) only about 5 km (3.5 river miles) to the east (Billingsley 1970).

Rowland, Osborn, and Graber (1995) measured the Kanab Canyon Member as ~44 m (~144.4 ft) thick and consisting of cliff-forming, medium gray limestone. This measured thickness in Fern Glen Canyon (river mile 168.5) agrees closely with Billingsley's (1970) measurement of 39 m (~128 ft) in Tuckup Canyon (river mile 165) to the east and with McKee's (1945) measurements of 40 m (~131.2 ft) at Gateway Canyon to the west and of 44 m (~144.4 ft) in Kanab Canyon (river mile 144) further east. Whereas the base on the member is the sharp contact between the limestone and the underlying glauconitic sandstone, its upper contact with the overlying Gateway Canyon member is gradational. There is no conspicuous change in lithology, but there is a fairly abrupt change in resistance to erosion from the cliff-forming Kanab Canyon Member to the slope-forming Gateway Canyon Member above. As elsewhere, the Kanab Canyon Member in Fern Glen Canyon can be divided into two parts of about equal thickness based on topographic expression. The lower half consists of a 13 m (~42.7 ft) slope-forming interval which becomes more resistant upward and culminates in a 7 m (~23 ft) high cliff. The upper half begins with a 4 m (~13 ft) slope, followed above by a 9 m (~29.5 ft) high cliff and capped by an 11 m (~36 ft) slope. A slight recess in about the middle of the Kanab Canyon Member cliff due to the abundance of glauconite in the limestone separates the two portions.

The Gateway Canyon Member was measured by McKee (1945) at 42 m (~137.8 ft) thick in the Gateway Canyon (river mile 171.5) type section, whereas Rowland, Osborn, and Graber (1995) measured it at 56 m (~183.7 ft) thick in Fern Glen Canyon (river mile 168.5) and Billingsley (1970) reported 42 m (~137.8 ft) thick in Tuckup Canyon (river mile 165). Elston (1989) measured it at an abnormally 80 m (~262.5 ft) thick in Matkatamiba Canyon (river mile 148.4). This variation in its thickness may at least be partly due to uncertainty in determining the position of this member's lower contact. In Fern Glen Canyon Rowland, Osborn, and Graber (1995) found

this member consists of 52 m (~170.6 ft) of thinly bedded, ledge-forming, burrow-mottled limestone capped by a 4 m (~13 ft) interval of green calcareous shale and minor glauconitic quartz sandstone. The base of the member is gradational. McKee (1945) described the top of the member as being indicated by a flat-pebble conglomerate zone of wide regional extent at the bottom of the overlying cliff. Rowland, Osborn and Graber (1995) did not observe that flat-pebble conglomerate zone in Fern Glen Canyon but identified the top of the member as above the recessive shale and sandstone interval due to the cliff above it. The burrow-mottled limestone, the member's main lithology, occurs in decimeter-thick beds that form ledges, producing a staircase-like topography. This limestone becomes increasingly resistant up section so that its lower half forms a slope, while the upper half forms a cliff. Its burrow mottling is due to ichnofabric indices from moderately to intensely burrowed.

Rowland, Osborn, and Graber (1995) reported that the Havasu Member in Fern Glen Canyon (river mile 168.5) is ~35 m (~114.8 ft) thick, which compares with a thickness of "about 100 ft" (~30.5 m) that characterizes this member throughout most of Grand Canyon (McKee 1945) and of 32 m (~105 ft) in Tuckup Canyon (river mile 165) measured by Billingsley (1970). In Fern Glen Canyon Rowland, Osborn, and Graber (1995) found it consists of a lower 12 m (~39.4 ft) interval of limestone and an upper 23 m (~75.5 ft) interval of dolomite, whereas in Tuckup Canyon Billingsley (1970) reported just a few thin layers of thin-bedded pinkish dolomite interbedded with limestone in the extreme upper portion of the member. Rowland, Osborn, and Graber (1995) described the lower limestone interval as the same medium gray, burrow-mottled lithology that characterizes the bulk of the underlying Gateway Canyon Member. The upper dolomitic interval is darker and more resistant to erosion than the underlying limestone. It is purple and gray-green burrow-mottled dolomite that Rowland, Osborn, and Graber (1995) concluded is presumably a dolomitized variation of the underlying limestone, even though the contact between the two lithologies is sharp and parallel to the bedding. However, because of this pervasive dolomitization they found it difficult to determine the member's upper contact with the overlying unclassified dolomites (now known as the Frenchman Mountain Dolostone), which they placed at the base of a prominent 2.5 m (~8.2 ft) thick bed of very light gray dolomite, due to it being lighter in color, thicker and more resistant to erosion than the underlying Havasu Member beds.

Rose (2003) collected stratigraphic data from 29 representative full and partial measured sections at sites throughout western, central, and eastern

Grand Canyon. He recognized the same problem that Elston (1989) did with McKee's (1945) placement of the boundary between the Bright Angel Formation and Muav Formations in western Grand Canyon. Furthermore, Rose (2006, 2011) remarked that no type section yet exists for the Tonto Group or any of its constituent units, even though the section described by Noble (1922) along the Bass Trail has served as a de facto type section. Thus, Rose (2003) proposed his measured section at Blacktail Canyon (river mile 120.5) as a suitable formal type section (figs. 1 and 7, and Appendix B in the Supplementary material), because it is accessible from the Colorado River, and because it is between two long straight stretches of the river, which provides a clear view in both directions of the continuity of actual outcrop for tracing marker beds and for finding diagnostic fossils, as well as the cliff-slope profile that help define unit boundaries (Rose 2011).

Rose (2003), like those before him, found it difficult to distinguish in the field between limestone and dolostone in the Muav Formation, but adopted the same common field practice that lighter-colored carbonates are dolostone and the darkest-colored carbonates are limestone. He assumed that in general the siltier carbonates had been more porous and thus more susceptible to dolomitization through porewater infiltration. Rose (2003) identified the major lithologies which make up the Muav Formation similarly to McKee (1945)—rusty brown dolomite, *Girvanella* limestone, thin-bedded limestone, mottled limestone and dolostone, flat-bed conglomerate, platy siltstone and silty limestone, and dolomitic siltstone and dolosilt.

The rusty-brown dolomite (RBD) is a dark gray to medium orangish gray, fine to coarse crystalline, sugary textured, sideritic dolostone, confirmed by chemical analysis by Noble (1922), that weathers to a distinctive rust orange color. Individual dolomite rhombs are visible on fresh surfaces. RBDs are conspicuous resistant cliff-forming marker horizons in central and western Grand Canyon and are commonly paired.

The *Girvanella* limestone is characterized by mottling due to concentric spheres of rusty-brown to pale orange dolomitic silt and finely crystalline medium gray to slightly translucent brownish gray micrite generally 3–15 mm (~0.1–0.6 in) in diameter but sometimes consistently up to 17 mm (~0.67 in). Estimated concentrations are 20–50%, and these spheres are surrounded by a matrix of silty pale purplish gray to yellowish gray micrite in blocky beds 3–7 cm (~1.2–2.8 in) thick. Such beds are stratigraphically constrained to sets of up to 2 m (~6.6 ft) thick, but commonly overlie similarly bedded mottled limestone in which the mottles grade from

irregular to spherical shapes within a few tens of centimeters (~1–2 ft) vertical distance. McKee (1945) compared this oncoidal texture to those reported by Seward (1931, 105, fig. 41c) at Girvan, Scotland, that were associated with microscopic filamentous structures of the alga *Girvanella*. Yet neither he nor anyone else has checked the Muav Formation's *Girvanella* limestone to confirm whether *Girvanella* filaments are present with the spherical structures. And similar-looking small oncolites have been reported with other enigmatic filamentous structures of various designations (Demico and Hardie 1994), so the name *Girvanella* limestone only applies to a lithology.

The thin-bedded limestone is the most common lithology in the Muav Formation, comprising the greatest thickness and is reasonably consistent in internal composition, texture and bedding style (fig. 15). It is very finely crystalline and ranges in color from steel gray to very pale cement gray. Beds are crinkly to nodular and 1–7 cm (~0.4–2.8 in) thick with pale to dark green fissile shale or crumbly siltstone partings, or more commonly, pale yellow to pale orange dolomitic siltstone partings sub millimeter to several centimeters thick. Burrow mottling is common with burrows infilled with pale orange silt identical to that in the silty partings. The thin-bedded limestone interfingers with thicker decimeter-scale blocky horizons of mottled limestone and dolostone and is generally resistant and cliff-forming, both commonly in the upper parts of cliff-forming carbonate sequences.

The mottled limestone and dolostone differs from the thin-bedded limestone and dolostone by being decimeters rather than centimeters thick. The mottling is compositionally similar to the interbeds and partings within the thin-bedded limestone, with pale orange variously silicified or calcified dolomitic silt infillings, ranging from low- to high-index mottling (after Droser and Bottjer 1986), with medium mottling most common.

Rose (2003) reported that the flat-pebble conglomerates are interbedded with the thin-bedded limestones in varying concentrations, but commonly in 5–25 cm (~2.0–9.8 in) thick horizons spaced several decimeters to several meters (~1–10 ft or so) apart. The intraclasts are blade-like to irregular rounded polygonal dish-shaped as observed in rare bedding-plane exposures. Otherwise, most exposures are cross-sections that reveal predominant horizontal or sub-horizontal orientations of the clasts, which are finely crystalline limestone or dolostone of medium steel gray color. The matrix is silty and dolomitic, varying in color from medium and light gray to pale yellow or orange. Contacts between the flat-pebble conglomerates and the associated thin-bedded



**Fig. 15.** Typical thin-bedded limestone of the Gateway Canyon Member, the most common lithology in the Muav Formation just downstream from President Harding Rapid (river mile 44.5, river right). Scales are indicated.

limestones are sharp and commonly scoured at the base, with lens-shaped lumps or channels up to a meter (~3.3ft) thick and 3m (~10ft) wide.

There are also transitional variations between these flat-pebble conglomerates and the platy siltstone and silty limestone described by McKee (1945) and Rose (2003). A mostly pale olive-green silty mudstone with calcareous light gray to pale tan micritic intraclasts in extreme eastern Grand Canyon is comparable to the dololaminite described by Wanless (1973a; 1975) in extreme western Grand Canyon, both in the upper Muav Formation. This intraclastic mudstone is thinly-laminated (at mm-cm scale) and grades upwards over several meters (~10ft or so) to the calcareous flat-pebble conglomerate. The micritic intraclasts in this dololaminite appear in long horizons to be curled into odd-shaped tubes or cones similar to “jell-roll” structures described by Demicco and Hardie (1994).

Other variants include rare rudstones, packstones, and pisolitic grainstones (Rose 2003). A 5–7cm (~2–3in) thick rudstone in Marble Canyon contains tube-shaped or arcuate allochems composed of silty dolostone that appear shelly, and the horizon has yielded trilobite remains. It is draped over or scoured into pisolitic grainstone that occurs in the same horizon and which is cross-bedded at low angles and sometimes ripple-laminated or herringbone cross-laminated. Similar thinner horizons of a few meters lateral extent are associated with flat-pebble conglomerates at several other localities.

McKee (1945) described flat-pebble conglomerates that clustered locally as lenses and those in thin beds or sets of beds that extended many miles. The latter are “key” beds used to establish the time plane separating the Gateway Canyon and Havasu Members (figs. 5 and 6) in the absence of any fossil fauna. However, Rose (2003) found that even though these flat-pebble conglomerates and their variants were easily recognizable by contrast with the surrounding thin-bedded limestones in which they commonly occur, they are not as traceable laterally as individual beds or zones of beds over several miles as McKee (1945) claimed due to the terrain and scree cover, so he rejected them as reliable marker beds beyond the outcrop scale.

Rose (2003) also determined that the platy siltstone and silty limestone lithologies in the Muav Formation as described by Noble (1922) and McKee (1945) are equivalent to the variously micaceous and calcareous siltstone and green mudstone partings and inter-laminae associated with the thin-bedded limestones. These lithologies characterize the transition from the siliclastics of the Bright Angel Formation to the carbonates of the Muav Formation but are also present within higher parts of the Muav Formation.

Thick sections of well-indurated greenish-gray or purplish-brown micaceous mudstone with minimal interbedding of siltstone occur in thicknesses of a few meters (~10–12ft) to over 20m (>66ft) subjacent to the lowest massive cliff of the Kanab Canyon Member in central and eastern Grand Canyon. These lithologies also seem comparable to the dololaminates documented by Wanless (1973a; 1975) and are distinguishable from the green fissile shales on the basis of trace fossils and degree of induration.

Finally, Rose (2003) recognized a dolomitic siltstone or dolosilt lithology within the mottled limestones and as partings within the thin-bedded limestones. In central and western Grand Canyon these silty interbeds may reach decimeter (~30ft) scale and are commonly wavy-laminated at millimeter scale and may also exhibit herringbone cross-lamination. Colors range from pale orange to very pale yellowish gray with a dull gray to finely crystalline luster and porcelain texture. Throughout Grand Canyon beds of dolomitic siltstone and dolosilt 1–3m (~3.3–9.8ft) thick and exhibiting this pale yellowish gray color are interspersed at lower stratigraphic positions within the Muav Formation.

Furthermore, Rose (2003) maintained that the tongues of Muav Limestone named by McKee (1945) that extend eastward into the Bright Angel Formation are in fact parasequences capped by carbonates, especially the distinctively-colored rusty-brown dolostone (RBD) (fig. 11). Because these carbonates capped underlying siltstones, sandstones and green fissile shales equivalent to Bright Angel Formation lithologies, Rose (2003) reassigned McKee’s (1945) tongues to the Bright Angel Formation and thus placed its upper boundary with the Muav Formation at the base of the Peach Springs Member (fig. 10). Nevertheless, he delineated massive carbonate sequences within the massive cliff-forming carbonates comprising the Muav Formation (fig. 16). He equated these larger carbonate sequences with his carbonate capped parasequences and found they coincided with the named members of the Muav Formation. The carbonates are primarily thin-bedded, mottled, finely-crystalline limestones and dolostones variously interbedded with pale yellowish to red-brown dolomitic siltstone. The uppermost meter or more of each carbonate section is also typically recrystallized with a darker-colored, sucrosic texture which from a distance is a distinctive rust-colored band at the top of a massive cliff or within a larger cliff.

In these massive carbonate sequences (fig. 16) the transition from interbedded siltstone and mudstone to carbonate may be sharp or gradational, with the carbonate cement increasing in the more porous siltstone layers up-section. Rose (2003) found that the siltstone layers appear the most directly transitional

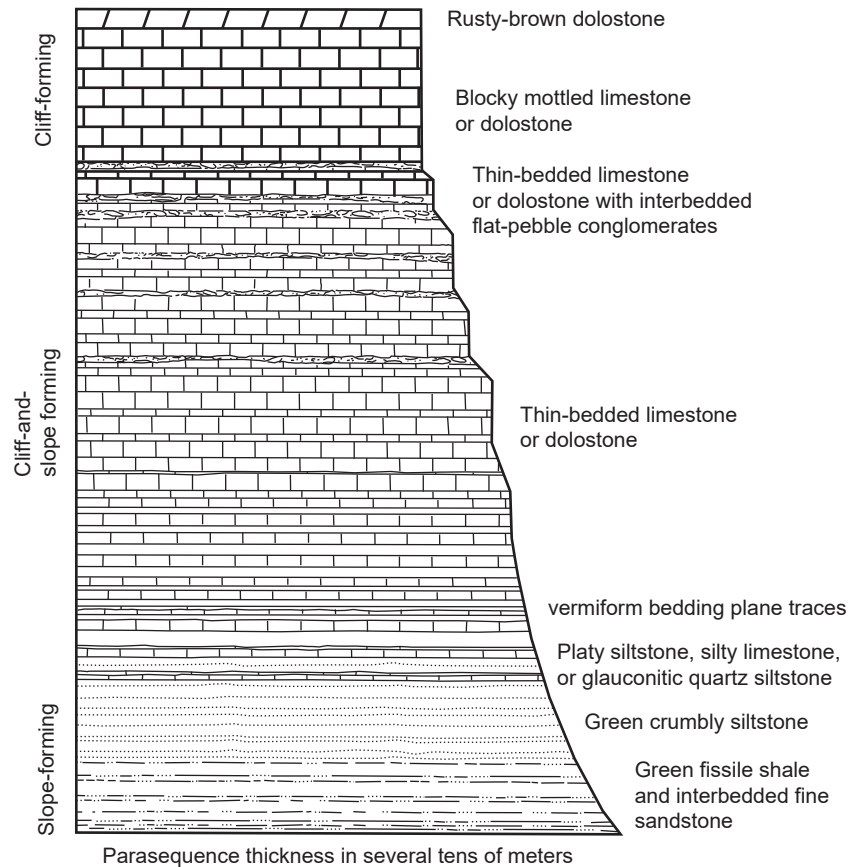


**Fig. 16.** Massive carbonate sequence that Rose (2003, 89, fig. 59) identified as comprising the Muav Formation.

to the fine-grained carbonate of the thin-bedded limestones, while the mudstone layers become siltier and dolomitic up-section. He interpreted the sandy substrates as originally looser and being susceptible to mat-ground stabilization (Schieber 1999), subsequent calcification, and dissolution of silica (Fein 2000). Furthermore, any additional silt in the depositional system could have been easily mixed with the comparatively more mobile fine-grained muds and clays (Kelling and Mullin 1975). He argued that such depositional segregation may be subtle initially but become accentuated through “diagenetic unmixing” (Ricken and Eder 1991). That process would have allowed carbonate crystallization to proceed in some laminae from dissolution of the carbonate content in neighboring laminae (Bathurst 1991).

The apparent lateral variations and relationships between Rose’s (2003) claimed parasequences is best exemplified by the cross-canyon lateral changes in the Rampart Cave Member. In western Grand Canyon it is a massive carbonate sequence that exceeds 50m (~164ft) in thickness and was mapped originally as the lowest member of the Muav Limestone (Huntoon 1989; McKee 1945). Yet in central Grand Canyon it thins and becomes the laterally-equivalent Elves Chasm Tongue (fig. 5), a resistant RBD of a carbonate-

capped sequence, while further east it becomes increasingly obscured among a host of similar beds within the Bright Angel Formation. Thus Rose (2003) interpreted these apparently lateral equivalent stacking patterns as due to differences in the nature and degree of surface deflation (weathering) and alteration during the slow-and-gradual course of sequential deposition of the sediments. That led him to follow Elston (1989) in redefining the boundary between the Muav Formation and the Bright Angel Formation, into which McKee’s (1945) lower Muav members and tongues were placed, as at the base of the Peach Springs Member (figs. 6 and 7).

Rose (2006; 2011) merely summarized briefly the details provided above from Rose (2003). He emphasized the gradual rather than sharp siliclastic-to-carbonate transition at the base of the Peach Springs Member, in contrast with its top being a sharp and laterally persistent pair of partings in a ~1m (~3.3ft) interval of fissile green shale or glauconitic siltstone containing specimens of the fossil trilobite *Glyphaspis* of the *Ehmaniella* Zone. The overlying massive cliff-forming Kanab Canyon Member is composed of dominantly thin-bedded pale-gray limestone which is variously mottled and nodular with partings 1–5cm (~0.4–2in) apart and pale orange dolomitic siltstone between the partings

and as mottle filling. The upper 1–3 m (~3.3–9.8 ft) of its massive carbonate cliffs consist of the distinctive rusty-brown dolomite (RBD). Then the overlying Gateway Canyon Member is a generally steep-slope-forming unit of thin-bedded mottled limestone with abundant flat-pebble conglomerates. Those irregular flat-pebble horizons exhibit local thickening from 5 cm (~2 in) to 15 cm (~6 in) as lens-shaped channel cross-sections with internally imbricated flat pebbles. In the western end of Grand Canyon the Gateway Canyon Member's mottled limestones grade into orangish silty thin-bedded dolostone or dolosilt in mm- to cm-scale laminae Wanless (1973a; 1975) called dololaminites, while at the eastern end these lithologies transition back and forth at varying stratigraphic intervals over lateral spans of ~200–300 m (~650–1,000 ft). Rose (2011) was inclined to place the Peach Springs Member also within the Bright Angel Formation and the uppermost Havasu Member into the overlying Unclassified Dolomites due to the preponderance of dolostone within it.

Finally, Karlstrom et al. (2018; 2020) redefined the Tonto Group to include the Sixtymile Formation, which locally underlies the Tapeats Sandstone, and the Unclassified Dolomites renamed as the Frenchman Mountain Dolostone, which regionally overlies the Muav Formation. However, they retained McKee's (1945) seven members of the Muav Formation and their intertonguing with the Bright Angel Formation, even though they cited Rose's (2003; 2006; 2011) work. They also ignored Elston's (1989) redefining of the boundary of the Muav Formation as the base of the Peach Springs Member (fig. 6) and his inclusion of just McKee's (1945) upper four members as the Muav Formation.

### Paleontology of the Muav Formation

Since the early work by McKee (1945) and Resser (1945) there has been virtually no work done on the taxonomy and biostratigraphy of Cambrian strata in the Grand Canyon (Middleton and Elliott 2003). Thus, the systematics of the invertebrate fauna remain the same. Except for trace fossils, which in places are quite common, body fossils are rare in the Tapeats Sandstone (Snelling 2021a) and only occur within the beds of the transition zone to the overlying Bright Angel Formation and Muav Formation. They are more common in the Bright Angel Formation (Snelling 2021b) but are also found in the Muav Formation.

Despite the paucity of well-preserved invertebrate fossils, analysis of the fauna has provided information on the biostratigraphic zonation of the Tonto Group (Middleton and Elliott 2003). Trilobites and brachiopods are the most abundant fossils reported from the Tonto Group (McKee 1945; Resser

1945; Snelling 2021a, b), though most specimens are poorly preserved. McKee (1945) mentioned that in the platy siltstone and silty limestone many trilobite and brachiopod fossils are preserved on flat bed surfaces. Fragments of sponges, "primitive" mollusks, echinoderms, and algae also occur in the Bright Angel Formation and Muav Formation, but these fossils are not very abundant. Indeed, there has been no further systematic work done on the fossils in the Muav Formation since McKee (1945) and Resser (1945).

Most trilobites in the Tonto Group are poorly preserved and some occur in the Muav Formation. McKee (1945) and Resser (1945) listed the following trilobites in three of the seven members McKee named and assigned to the Muav Formation:

**Rampart Cave Member**—*Alokistocare* sp., *Glossopleura* sp., *Glossopleura tuta*, *Kootenia* sp., *Kootenia schenki*, *Kootenia tetraspinosa*, *Zacanthoides* sp., *Anoria* sp., *Elrathia* sp.

**Peach Springs Member**—*Clavaspindella kanabensis*, *Kochina angustata*, *Kootenia mckeei*, *Parehmania nitida*, *Ptarmigahia* sp., *Solenopleurella diligens*, *Solenopleurella* sp.

**Gateway Canyon Member**—*Bolaspis aemula*, *Bolaspis* sp., *Glyphaspis* sp., *Glyphaspis tecta*, *Solenopleurella erosa*, *Clavaspindella* sp., *Glossopleura* sp., *Kootenia* sp., *Kootenia mckeei*, *Anoria* sp., *Solenopleurella porcata*

McKee (1945) mentioned that in some localities, quantities of spines and fragments of trilobite carapaces are scattered through the *Girvanella* limestone in the Rampart Cave Member and parts of trilobite spines or carapaces, some up to 7 mm (~0.3 in) in length, serve as nuclei in many nodules. McKee (1945) also reported numerous trilobite fossils being obtained from very thin aphanitic limestones at the base of the Peach Springs Member, also citing Walcott (1880) collecting some trilobite fossils from the Peach Springs Member at the mouth of Kanab Canyon. And in central Grand Canyon a thin but persistent zone of considerable stratigraphic importance contains trilobite *Solenopleurella porcata* remains in great abundance at the top of the Gateway Canyon Member. Otherwise, while determinable fossils are difficult to find in the Gateway Canyon Member generally, trilobite fossils were found at various other stratigraphic levels in eastern Grand Canyon.

Rose (2003) reported finding an exceptional rudstone horizon 5–7 cm (~2–3 in) thick in the upper Muav Formation (probably the Gateway Canyon Member) at river mile 45.5 in Marble Canyon that contains tube-shaped or arcuate allochems composed of silty dolostone that appear shelly, and the horizon yielded pygidia and cranidia of *Glyphaspis* sp.

Furthermore, Rose (2003) collected two pygidia and one glabella from a micaceous shale parting marking the boundary between the Peach Springs and Kanab Canyon Members at Cheops Pyramid (near Phantom Ranch) that were identified as *Glyphaspis kwaguntensis*.

Brachiopods occur in some of the mixed siliciclastic-carbonate facies of the Muav Formation. McKee (1945) and Resser (1945) listed the following brachiopods in the same three of the seven members McKee named and assigned to the Muav Formation: **Rampart Cave Member**—*Nisusia* cf. *obscura*, *Nisusia noblei*

**Peach Springs Member**—*Nisusia kanabensis*, *Lingulella kanabensis*, *Lingulella zetis*, *Paterina crenistria*

**Gateway Canyon Member**—*Nisusia noblei*

Resser (1945) reported sponge spicules from two sections of the Rampart Cave Member of the Muav Formation in western Grand Canyon. These consist of thick, six-rayed spicules that Resser suggested were similar to the purported sponge spicules of *Tholiastrella? bindei* that Walcott (1920) reported from the Cambrian of British Columbia.

Gastropods from the Muav Formation are represented by the one species, *Scenella hermitensis*, found in one location by Resser (1945) in the Gateway Canyon Member.

The clade Lophophorata is represented by several occurrences in the Rampart Cave, Peach Springs and Gateway Canyon Members of what Resser (1945) referred to as *Hyolithes* sp. because their preservation prevented more detailed identification. At the time Resser regarded them as gastropods, but they have more recently been assigned to their own clade (Meglitsch 1972).

Algal structures in the Muav Formation consist of convex-upward laminae of calcite and/or dolomite and also small nodules composed of concentric laminations that have been termed *Girvanella* (Resser 1945). As already noted, McKee (1945) compared this oncoidal texture to those reported by Seward (1931, 105, fig. 41c) at Girvan, Scotland, that were associated with the tangled mass of vermiform tubules or microscopic filamentous structures of the alga *Girvanella*. Yet, Resser, nor anyone else, has checked the Muav Formation's *Girvanella* limestone to confirm whether *Girvanella* filaments are present with these spherical structures.

Trace fossils, though not as abundant as in the Bright Angel Formation, are present in the Muav Formation throughout Grand Canyon. However, they are not as obvious as they are in the Bright Angel Formation. McKee (1945) mentioned trace fossils in some lithologies within some members of the Muav Formation but did not describe them in

detail. For example, he noted the fossilized burrows and trails and tabular borings of worm-like creatures being numerous throughout much of the thin-bedded mottled limestones within the Kanab Canyon Member, and the worm borings and fucoid-like casts (McKee 1932) common in thin-bedded limestones of the Gateway Canyon Member. Indeed, the origin of the blotches in the mottled limestones had been explained by Noble (1914) as due to fucoid-like markings and by Schuchert (1918) as the result of the work of worms, the latter saying that the beds are completely riddled with vertical and anastomosing worm burrows.

Wanless (1973a; 1975) described several horizons of burrowed, fine-grained carbonate which he had termed dololaminites. Similarly, Rose (2003) referred to the trace fossils in the same platy siltstone and silty limestone as being simple vermiform bedding plane traces composed mainly of arcuate grooves 1–4 mm (~0.04–0.16 in) in width with no other distinguishing features. Rose (2003) also mentioned the common burrow mottling in the thin-bedded limestones which comprise the greatest thickness within the Muav Formation, the burrows being infilled with pale orange silt identical to that found in the silty partings. Indeed, Rose (2003) highlighted the low to high mottling index in the mottled limestones using the mottling-by-ichnofacies index classification of Droser and Bottjer (1986). In this study, field observations made in National Canyon (river mile 167) documented worm trails fossilized on exposed bedding surfaces on a bench outcrop of the Peach Springs Member of the Muav Formation (fig. 17).

Yet there has been no attempt to provide systematic descriptions of these trace fossils. The only exception is Rose (2003) describing briefly his discovery in his Cheops Pyramid stratigraphic section (near Phantom Ranch) the preservation on the surface of a mega-ripple trough in a well-cemented pale yellow-gray dolosiltstone high in the Muav Formation of *Rusophycus* (a trilobite resting trace measuring 10 cm [~4 in] in length), *Treptichnus* (the result of burrowing priapulid worms [Vannier et al. 2010]) and *Planolites* (trails left by suspension feeders, such as either annelids [worms] or phoronids [sometimes called marine horseshoe worms] [Alpert 1974; McKee 1945]). Otherwise, horizontal burrows, which appear to be the most abundant variety in the Muav Formation, consist of relatively thin, sinuous traces, likely due to annelids (Middleton and Elliott 2003).

Finally, Wanless (1975) claimed he found small stromatolitic domes within what he described as crinkly, disrupted (micro-stromatolitic) dololaminite (fig. 14), though he provided no definitive evidence of these being due to stromatolitic algal mats.



**Fig. 17.** Fossilized worm trails exposed on bedding surfaces within the Peach Springs Member of the Muav Formation in National Canyon (river mile 167). (a) The benched outcrop. (b) Close view of fossilized worm trails. The diameter of the lens cap is 5 cm (2 in).

### Sedimentary Structures in the Muav Formation

Most of the Muav Formation is comprised of beds of horizontally laminated carbonates, principally limestone, sometimes thinly-bedded, that appear to be structureless and sometimes massive (McKee 1945; Middleton and Elliott 2003) (for example, fig. 15). However, McKee (1945, 108) in plate 9b showed current ripple marks on a stratification surface in thin-bedded Muav Formation limestone within the Gateway Canyon Member near Indian Garden (on the Bright Angel Trail above Pipe Creek Canyon), and in plate 12c he showed interference (“tadpole”) ripple marks on a stratification surface within the Gateway Canyon Member at Pipe Creek Canyon (river mile 89.5).

Otherwise, McKee (1945, 92) quoted Noble (1922) reporting broken and fragmentary brachiopod shells and cross-lamination within snuff-brown limestone associated with cross-bedded sandstone in the Garnet Canyon Tongue that is the lateral extension of the Rampart Cave Member of the Muav Formation. McKee (1945, 70) also reported that what he designated as platy siltstone and silty limestone, a common component of the Muav Formation, is often thin-bedded and commonly exhibits small-scale cross-lamination. The only other sedimentary structures within the Muav Formation McKee (1945, 65–70) commented on were those pertaining to the intraformational flat-pebble conglomerate beds because he considered them to be marker beds. He described the majority of the pebbles as being thin and flat, more or less rounded on their edges and relatively small, and definitely tending to be oriented in a horizontal attitude parallel to the bedding planes. Hence the reason he called them flat-pebble conglomerates. He also found many exceptions where the flat pebbles are resting on end or are steeply dipping at angles of 30° and 45° in a definite direction (often to the east), or even others that show no orientation at all.

Wanless (1975) reported numerous sedimentary structures, including fenestral fabrics and interpreted desiccation cracks. He documented the laminations in what he called a dololaminite in western Grand Canyon (fig. 14), which is likely within the lower section of the topmost Havasu Member of the Muav

Formation. The laminations are 1mm or less in thickness and occur either as stacks of thin, single mud laminae that are continuous with even thickness, or couplets of thin, continuous mud lamina and then, discontinuous pellet-sand lamina. Furthermore, the continuous mud laminae have uniform thickness and drape irregularities and are commonly oversteepened, whereas the discontinuous pellet-sand laminae are quite well-sorted, form thin starved ripples and depression fillings, and do not drape (fig. 18). He also reported tabular disrupted laminations consisting of stacks of continuous mud laminae disrupted by them, filled and unfilled supposed desiccation cracks that only penetrate one or two laminae, as well as irregularities and small scour pockets filled with pellet sand and small intraclast chips. Furthermore, there are crinkly disrupted laminations due to what he interpreted as small stromatolitic domes and also accentuated ripples, the over-steepened continuous mud laminae draping the domes and pellet-sand laminae discontinuous and pinching out on the domes, with thin irregular interpreted desiccation cracks separating the domes and penetrating 1 or 2cm.

Wanless (1975) also described associated thickly-laminated dolomite beds consisting of continuous layers 1–15mm (~0.04–0.6in) thick with minor scour pockets, and cross-laminated, dolomitized, firm pellet sand, consisting of dominantly small (<3cm or 1.2in thick) trough cross-laminations, and also planar high-angle and low-angle cross-laminations (fig. 19). Furthermore, the thin-bedded, fenestral limestone has its bedding disrupted, numerous planar discontinuous fenestrae zones, and flat-pebble limestone intraclasts filling small scour depressions.

Neither Middleton (1989) nor Rowland, Osborn, and Graber (1995) mention any sedimentary structures in the Muav Formation, but Middleton and Elliott (2003) noted that small-scale (less than 2in or 5cm thick) trough, planar tabular, and low-angle cross-stratification occurs at many localities.

Rose (2003), like those before him, commented on the thin-bedded limestone which comprises the greatest thickness within the Muav Formation as being crinkly to nodular, wavy-bedded and continuous, the beds being 1–7cm (~0.4–2.8in) thick

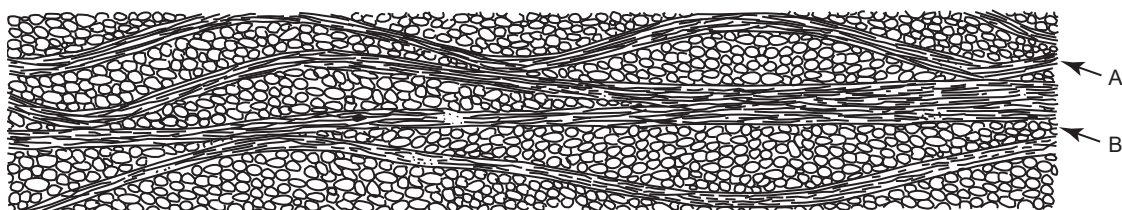


**Fig. 18.** Sketch of couplets of A—thin, continuous mud laminae, and B—thin, discontinuous pellet-sand laminae within the Cambrian section at Diamond Bar Ranch, after Wanless (1975).

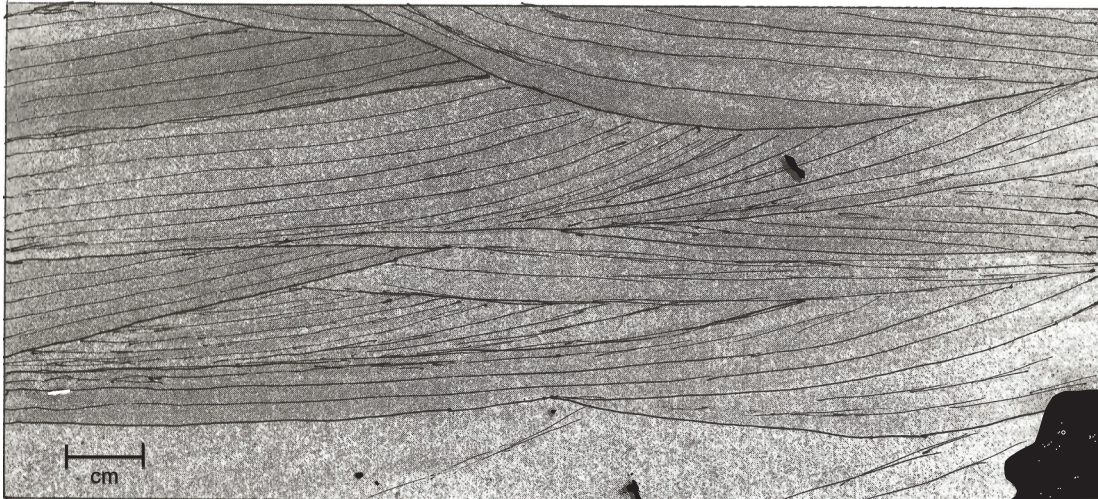


**Fig. 19.** Trough cross-laminated, dolomitized, firm-pellet sand within the Cambrian section at Diamond Bar Ranch, as depicted in negative print from peel, after Wanless (1975). The annotations have been added to make the cross-laminations more readily recognized.

with fissile shale or crumbly siltstone partings, or more commonly, dolomitic siltstone partings in thicknesses of sub-millimeter scale to (rarely) several centimeters (fig. 20). He also described the platy siltstone and silty limestone as laminar, crypto-microbially laminar and wavy laminar to stromatolitic, while the dolomitic siltstone and silty dolostone are commonly wavy-laminated at millimeter scale and exhibit herringbone cross-lamination. Both of these Rose (2003) regarded as parts of the dololaminites described by Wanless (1973a, 1975).

However, Rose (2003), like McKee (1945), mostly described the sedimentary structures associated with the flat-pebble conglomerates which he reported as interbedded with the thin-bedded limestone in varying concentrations, but commonly in 5–25 cm (~2.0–9.8 in) thick horizons spaced several decimeters to several meters (~1–10 ft or so) apart. Moreover, most exposures are cross-sectional views that thus reveal the orientations of the clasts as predominantly horizontal or sub-horizontal, though less commonly they are imbricated in bi-directional co-sets and are within herringbone cross-lamination patterns (Rose 2003, fig. 51B). Contacts between the flat-pebble conglomerates and associated thin-bedded limestones are sharp and commonly scoured at the base, with lens-shaped “lumps” or channels (Rose 2003, fig. 51-C) that in eastern Grand Canyon are up to a meter (~3.3 ft) in thickness and 3 m (~9.8 ft) in width.

Rose (2003) also reported other variants that include rare rudstones, packstones and pisolitic grainstones. A 5–7 cm (~2–3 in) thick rudstone in Marble Canyon composed of silty dolostone is draped over or scoured into pisolitic grainstone that occurs in the same horizon, and which is cross-bedded at low angles

and sometimes ripple-laminated or herringbone cross-laminated. Similar thinner horizons of a few meters lateral extent are associated with flat-pebble conglomerates at several other localities. In extreme eastern Grand Canyon, a silty mudstone in the upper Muav Formation with calcareous micritic intraclasts comparable to the dololaminite described by Wanless (1973a; 1975) is thinly-laminated (at mm-cm scale) and grades upwards over several meters (~10 ft or so) to the calcareous flat-pebble conglomerate. The micritic intraclasts in this dololaminite appear in long horizons to be curled into odd-shaped tubes or cones similar to “jell-roll” structures described by Demicco and Hardie (1994).

Rose (2006) repeated his description above of the thinly-laminated silty mudstone with calcareous micritic intraclasts that grades upwards and laterally into flat-pebble conglomerates and reiterated that these flat-pebble conglomerates abound in the Gateway Canyon Member of the Muav Formation, most commonly occurring as irregular thin beds of 5–15 cm (~2–6 in) thickness, but small channels and lenses are also common (Rose 2006, fig. 7, Little Colorado River area). Rose (2011) added that these lens-shaped channels of flat-pebble conglomerates have internally imbricated flat pebbles. Furthermore, these horizons splay and coalesce analogously to ferruginous sandstone (rusty brown dolomite) beds that are traceable individually no more than 100 m (~328 ft) and internally may display faint cross-bedding on weathered surfaces and contorted bedding from soft-sediment deformations in some western localities.

Observations of outcropping Muav Formation along the river corridor were made in this study. The dominant bedform within the Muav Formation throughout Grand Canyon is thinly-bedded laminated

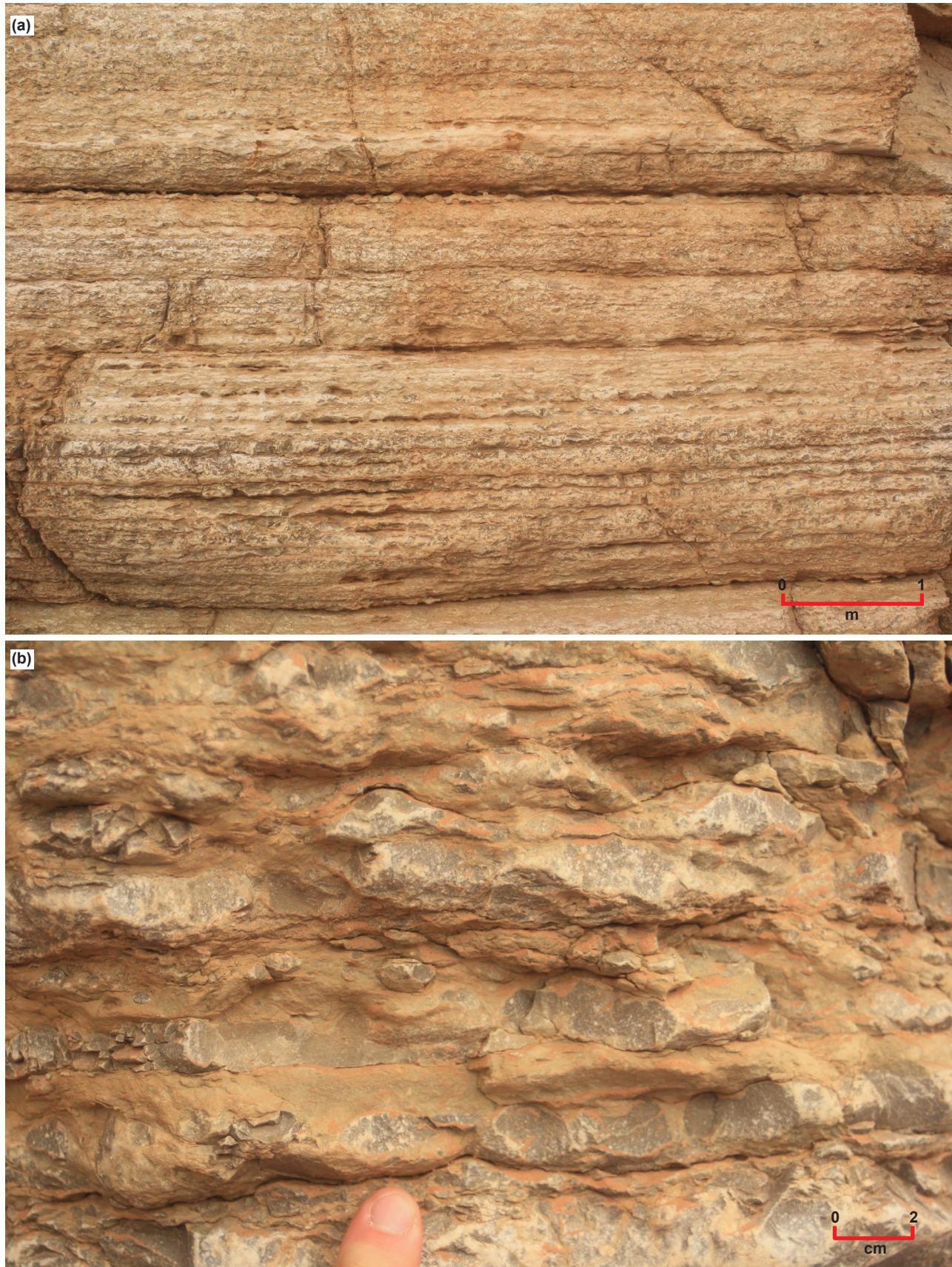


**Fig. 20.** (a) Typical thin-bedded limestone with thin crinkly to nodular, wavy-bedded beds with sub-millimeter thick siltstone partings in the Peach Springs Member, Fern Glen Canyon (river mile 168.5) (b) This closer view shows more clearly the nodular wavy beds of limestone with ultra-thin siltstone partings. The scales are indicated.

gray limestones (fig. 15). However, in many instances these laminated gray limestones are mottled due to partings of reddish-brown siltstone (fig. 20a). Closer inspection though reveals that the thin beds of harder gray limestone are not of uniform thickness, and in fact often have lower and upper bedding surfaces that are wavy, undulate and sometimes pinch out separated by the siltstone partings (fig. 20b). These bedform structures have to be a primary depositional feature. Elsewhere the laminae (thin beds) locally thicken and/or even increase locally in number (laterally over several meters) (fig. 21a). Additionally, there is possible intraformational soft-sediment deformation where the limestone laminae appear to have been folded, and/or there have been disruptions to the continuity of the thin beds so that the laminae then drape over those disrupted/terminated thin beds (fig. 22b).

At the Ledges Camp (river right at river mile 152) there are also other significant sedimentary structures. Exposed in cross-section in the benched outcrop of the Gateway Canyon Member (fig. 22a) are what appear to be megaripples (fig. 22b, d and g). [Similar features have been found in the lower Havasu Member (Whitmore 2022, pers. comm.)] The amplitude (height) of these megaripples is ~10cm (~4in.) and their wavelength is ~65cm (~26in or 2.13ft). Within the megaripples there appears to be crude cross-laminations (fig. 22b and c) and/or crude wavy rippled laminations (fig. 22d–h). These sedimentary structures appear to be only at the one stratigraphic level. The thin bed on whose upper surface these megaripples appear has a flat bottom surface parallel to the thin limestone beds beneath, while the overlying thin beds are draped over these megaripples, often thickened in the troughs between the crests of the underlying megaripples (fig. 22b, d, and g). There are hints that there may be rippled upper surfaces of other thin beds at other stratigraphic levels in the same cross-sectional bench exposure, but the amplitudes of the ripples are barely detectable.

### Conventional Age of the Muav Formation

In western Grand Canyon, the Muav Formation occurs above the *Alokistocare–Glossopleura* assemblage zone and has thus been biostratigraphically determined as Middle Cambrian in age (McKee 1945; Middleton and Elliott 2003). On the other hand, in eastern Grand Canyon, the upper part of the Muav Formation contains the *Bathyriscus–Elrathina* assemblage zone which biostratigraphically is late Middle Cambrian. This supposed decrease in age of the Muav Formation toward the east parallels the biostratigraphic age trends of the Tapeats Sandstone and the Bright

Angel Formation and reflects the west-to-east nature of the Cambrian transgression.

Naeser et al. (1989) fission-track dated a suite of fifteen zircon grains separated from a 2–3cm (~0.8–1.2in) thick green bentonite layer (a former volcanic ash or tuff bed) just above a ledge in thin-bedded limestone at the boundary between the Peach Springs and Kanab Canyon Members on river left just below Lower Lava Rapid at river mile 180.2 (Billingsley and Elston 1989). This thin ash-fall tuff bed marks this boundary in many places laterally (Elston 1989). Naeser et al. (1989) determined a fission-track age of  $535 \pm 48$ Ma [2 $\sigma$ ] (Lower Cambrian) for those 15 zircon grains from this prominent green tuff bed.

Snelling (2005b) collected two samples of the same green tuff layer between the Peach Springs and Kanab Canyon Members of the Muav Formation and had zircons grains separated from them for fission-track dating. Typical Muav tuff zircons and the fission tracks in them are shown in fig. 23. A variety of grain morphologies was present in both samples, from euhedral to rounded as well as intermediate forms. This is because when the lava cooled euhedral grains crystallized, but then when the lava was subsequently shattered by the volcanic eruption to produce ash some of the grains would have been abraded during their transport before deposition in the tuff bed.

Snelling (2005b) reported that the fission-track dating laboratory found that because the separated zircon grains showed a sufficiently large range of U contents, there were enough grains with spontaneous track densities suitable for track counting ( $10.31 \times 10^6$  tracks per  $\text{cm}^2$ ), and thus the reported fission-track age determinations were regarded as extremely reliable. The zircon grains from the two samples were characterized by central ages of  $139.0 \pm 24.5$ Ma and  $165.8 \pm 20.7$ Ma. However, the individual zircon grains had fission-track ages from  $34.9 \pm 7.2$ Ma to  $611.2 \pm 254.9$ Ma for the 20 grains in the first sample, and from  $68.4 \pm 8.3$ Ma to  $473.5 \pm 150.5$ Ma for the 23 grains in the second sample, so the numerical values of the central ages had no significance. A statistical analysis of the single grain fission-track ages in the first sample suggested the presence of three prominent populations characterized by ages of  $62 \pm 4$ Ma,  $200 \pm 15$ Ma, and  $432 \pm 66$ Ma (fig. 24a). The youngest group of fission-track ages that yielded the pooled age of  $62 \pm 4$ Ma was obtained from six euhedral grains. On the other hand, the youngest group of ages for five euhedral grains in the second sample collectively defined a pooled fission-track age of  $74.6 \pm 3.9$ Ma (fig. 24b). It was suggested that the discrepancy between these fission-track ages and that determined by Naeser et al. (1989) could be the differences in the etching conditions used in



**Fig. 21.** Thin-bedded, laminated gray limestones of the Gateway Canyon Member of the Muav Formation at about river mile 146.5 (river right), upstream from Matkatamiba Canyon. (a) Locally the thin laminae thicken and/or increase in number laterally over several meters. (b) Disruptions to the continuity of the thin laminae appear to be intraformational soft-sediment deformation, while some laminae appear to be terminated laterally. The scales are indicated.









**Fig. 22 (pages 177–180).** The benched outcrop of the Gateway Canyon Member of the Muav Formation at Ledges Camp (river right at river mile 152) with significant megaripples exposed in cross-section. (a) A general view of the ledges exposed with the megaripples evident in the middle of a small cliff (the scale is indicated). (b) A closer view of two of the megaripples with the immediately overlying laminae draped over them (the scale is indicated). (c) A close view of another similar megaripple showing some internal structure (the diameter of the lens cap is 5 cm or 2 in). (d) A close view of yet another similar megaripple with no clear internal structure evident (the scale is indicated). (e) The same two megaripples as in (c) and (d) showing the immediately overlying laminae draped over them (the scale is indicated). (f) A close view of yet another similar-sized megaripple but with clear evidence of internal cross-stratification (the scale is indicated). (g) The same megaripple as in (f) with another internally cross-stratified megaripple to its left with the same persistent crest height and wavelength between crests as also in (e) (the diameter of the lens cap is 5 cm or 2 in). (h) A close view of yet another similar megaripple along the same horizon in the benched outcrop, again with laminae draped over it but with no clear internal structure (the scale bar is marked in 1 cm intervals).

the respective laboratories. The laboratory used by Snelling (2005b) only using a short etching time, whereas Naeser et al. (1989) already knew the target age and etched their grains longer and chose only the fission-track ages that matched the target age.

Snelling (2005b) also reported U-Th-Pb radioisotope determinations on zircon grains from the second of the two Muav Formation tuff samples. Six grains were chemically abraded in order to eliminate any discordance caused by Pb loss, and isotopic analyses were performed by a thermal ionization mass spectrometer (TIMS) (Fig. 25). Only two grains (z4 and z6 in fig. 25b) yielded concordant ages of  $74.8 \pm 3.2$  Ma and  $169.0 \pm 0.5$  Ma ( $2\sigma$  errors) respectively (fig. 26). Otherwise, the individual grain model ages ranged from a  $^{206}\text{Pb}/^{238}\text{U}$  age of 68.2 Ma for grain z5 to a  $^{207}\text{Pb}/^{206}\text{Pb}$  age of 1621.2 Ma for grain z3. On a  $^{206}\text{Pb}/^{204}\text{Pb}$ - $^{207}\text{Pb}/^{204}\text{Pb}$  diagram the scatter of the data precluded the fitting of an isochron to them. However, when grain z6 was excluded an isochron fitted the five remaining data points with an MSWD value of 16 corresponding to a Pb-Pb isochron age

of  $1609 \pm 204$  Ma ( $2\sigma$  errors) (fig. 27). However, this MSWD value was too high for this to be an acceptable isochron, and grain z6 had been excluded, yet that grain had yielded the best concordant U-Pb age. Therefore, if grain z6 was included in the isochron analysis, then the data points for grains z1 and z3 had to be rejected to fit an isochron to the remaining data. But the resulting isochron justified this procedure, because those four data points yielded a Pb-Pb isochron with an excellent fit as the MSWD value is 0.61 and the probability 0.54 (fig. 27). The Pb-Pb isochron age thus derived is  $166 \pm 30$  Ma ( $2\sigma$  errors), which not surprisingly, is the same as the concordant U-Pb age of  $169.0 \pm 0.5$  Ma for grain z6. In contrast, the oldest model ages were consistent with zircon U-Pb ages of the granitic basement rocks in western Grand Canyon (Karlstrom et al. 2003), which suggests that this tuff has a very small component of contamination by older igneous material.

Matthews, Guest, and Madronich (2018) analyzed samples of the underlying Tapeats Sandstone from East Verde River, central Arizona and Frenchman

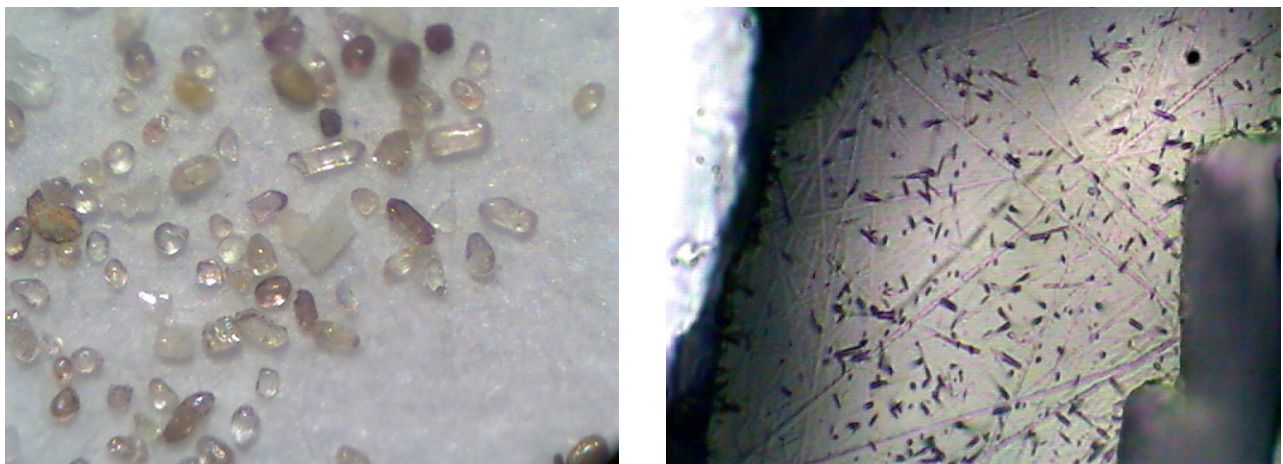


**Fig. 23.** (a) Some of the zircon grains recovered from tuff sample MT-3, collected from a thin tuff bed at the boundary between the Peach Springs and Kanab Canyon Members of the Muav Formation on river left just below Lower Lava Rapid at river mile 180.2 (Billingsley and Elston 1989). (b) The spontaneous fission tracks in the polished and etched surface of the mounted zircon grains from tuff sample MT-2, collected from the same thin tuff bed as sample MT-3. These photomicrographs were obtained courtesy of Pat Kelly, Operations Manager, Geotrack International (Snelling 2005b).

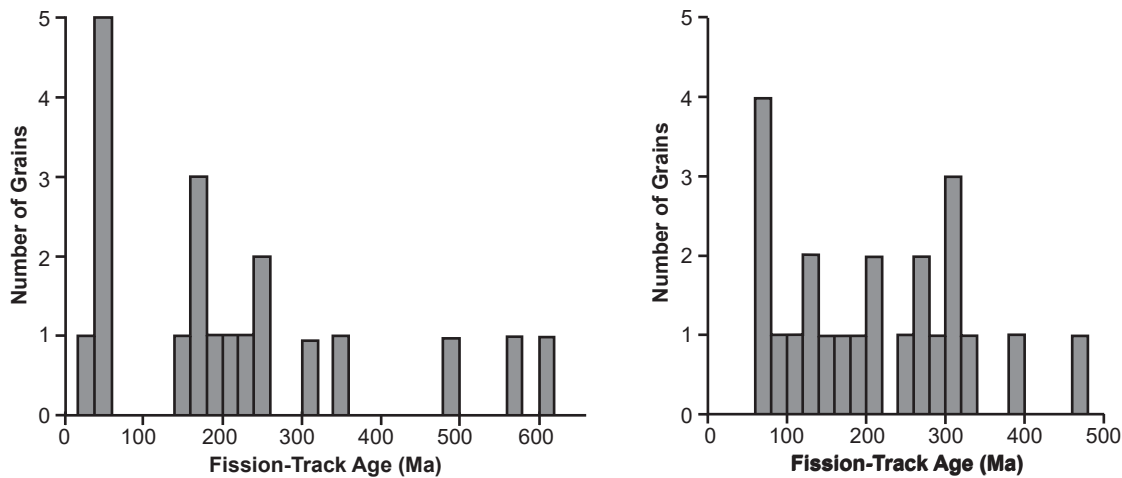


**Fig. 24.** Histograms of the individual zircon grain fission-track ages in the early Middle Cambrian Muav Formation tuff samples from river mile 180.2, river left, at the boundary between the Peach Springs and Kanab Canyon Members (a) MT-2, (b) MT-3 (Snelling 2005b).

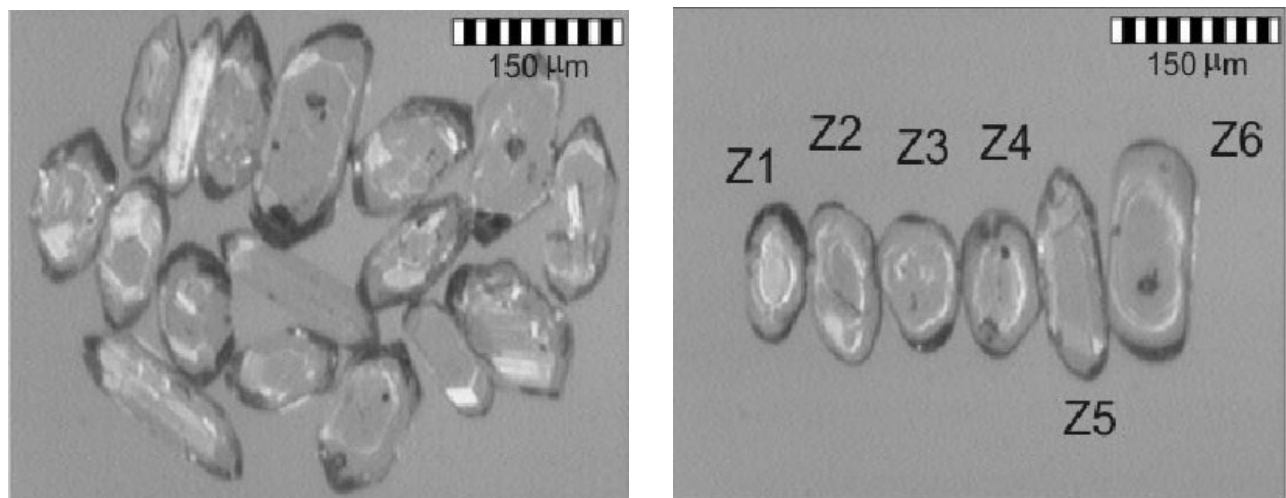


**Fig. 25.** Zircon grains from the Muav Formation tuff sample MT-3 collected from the thin bed between the Peach Springs and Kanab Canyon Members at river mile 180.2, river left. (a) Raw grains separated from the tuff. (b) The six selected grains after being air abraded to remove overgrowths, metamict zones, or portions of other minerals still clinging to their outer surfaces. Photomicrographs courtesy of Dr. Yakov Kapusta at Activation Laboratories, Ancaster, Ontario, Canada (Snelling 2005b)

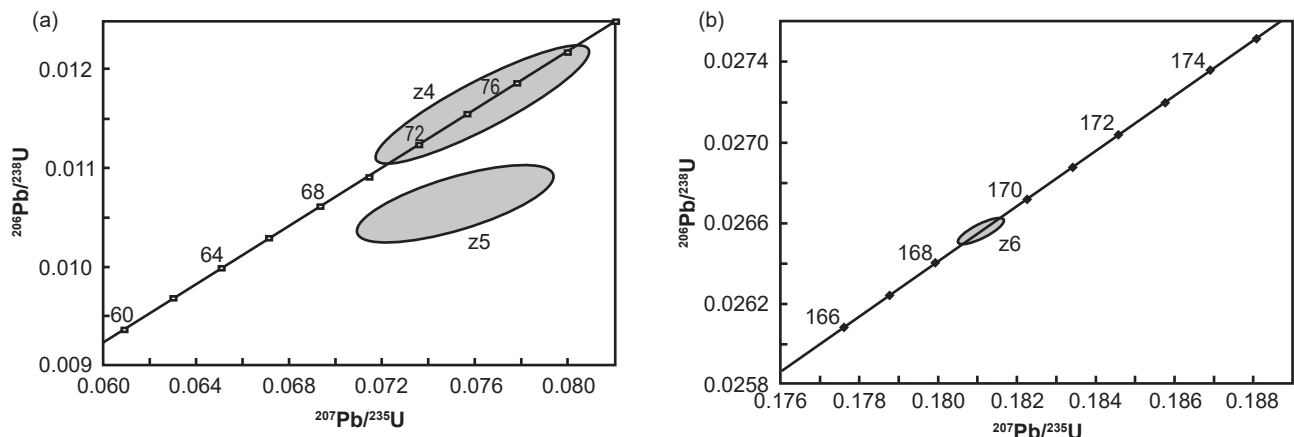


**Fig. 26.** Concordia plots of the U-Pb radioisotope data obtained from zircon grains from Muav Formation tuff sample MT-3 collected from the thin bed between the Peach Springs and Kanab Canyon Members at river mile 180.2, river left. Only two grains yielded concordant U-Pb ages: (a) z4 (74.8 Ma), and (b) z6 (169.0 Ma) (Snelling 2005b).

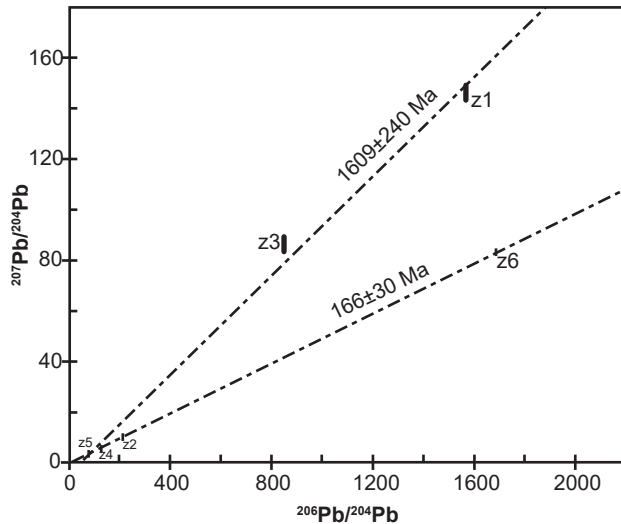


**Fig. 27.**  $^{206}\text{Pb}/^{204}\text{Pb}$  versus  $^{207}\text{Pb}/^{204}\text{Pb}$  isochrons fitted to the Pb radioisotope data obtained from the six zircon grains from Muav Formation tuff sample MT-3 collected from the thin bed between the Peach Springs and Kanab Canyon Members at river mile 180.2, river left. Five grains (z1, z2, z3, z4, z5) yielded an apparent isochron age of  $1609\pm 240$  Ma, but with an MSWD of 16 the fit is poor. However, four grains (z2, z4, z5, z6) yielded an isochron age of  $166\pm 30$  Ma, with a good MSWD of 0.61 and a probability of 0.54 (Snelling 2005b).

Mountain, southern Nevada and found they contained abundant middle Cambrian detrital zircons. Eight measurements from the central Arizona sample and seven measurements from the southern Nevada sample yielded concordant  $^{206}\text{Pb}/^{238}\text{U}$  ages of  $502.8\pm 8.1$  Ma and  $504.8\pm 8.2$  Ma, respectively (2 $\sigma$  including all sources of random and systematic uncertainty). Thus, these U-Pb dates for zircon grains within the underlying Tapeats Sandstone would seem to constrain the conventional age of the Muav Formation to probably <502 Ma.

Similarly, Karlstrom et al. (2018) U-Pb dated zircon grains from three Tapeats Sandstone samples, two of the three being from those same locations sampled by Matthews, Guest, and Madronich (2018). The youngest zircon grains in a coarse sandstone sample from 2 m (6.6 ft) above the base of the Tapeats Sandstone in Hermit Creek in Grand Canyon yielded a weighted mean LA-ICP-MS (laser-ablation-inductively coupled plasma-mass spectrometry) maximum age of  $505.4\pm 8.0$  Ma ( $n=12$ ). The youngest zircon grain population in a sample from the coarse-grained cross-bedded sandstone 30 m (98 ft) above the base of the unit in the westernmost limit of Tapeats exposures at Frenchman Mountain near Las Vegas, Nevada, yielded an age of  $504.7\pm 2.1$  Ma ( $n=28$ ). And the youngest grains in a sample from the coarse-grained, pebbly cross-bedded sandstone ~19 m (62 ft) above the unconformity with the granitic basement at the southeastern limit of Tapeats exposures along

the East Verde River in central Arizona yielded a weighted mean maximum depositional age of  $501.4\pm 3.8$  Ma ( $n=19$ ). Again, therefore, these further U-Pb dates for zircon grains within the underlying Tapeats Sandstone would seem to constrain the conventional age of the Muav Formation to probably <502 Ma.

In interpreting all these ages, Karlstrom et al. (2018) noted that the Tapeats Sandstone and Bright Angel Formation sections in western Grand Canyon that contain *Olenellus* Zone trilobites are thus probably older than 509 Ma (Peng, Babcock, and Cooper 2012). Yet these western Grand Canyon and Lake Mead region trilobites correspond to the upper half of Stage 4 of Cambrian Series 2 (Sundberg 2011), whereas *Glossopleura walcotti* Zone trilobites of the overlying Bright Angel Formation in eastern Grand Canyon (Foster 2011) correlate with Stage 5 of Cambrian Series 3, as do *Solenopleurella* trilobites from the uppermost Muav Formation. While a numerical age for the boundary between Cambrian Stages 4 and 5 has not yet been firmly established by the International Union of Geological Sciences, the International Commission on Stratigraphy (2022) has designated an age of ~509 Ma. Furthermore, the ages of fossils from these successions have been constrained by correlation of North American trilobite zones to trilobite provinces from other continents and by integrating recalibrated ages of Stages 3–5 ashes globally (Schmitz 2012) with revised fossil zonation (Sundberg et al. 2016) and chemostratigraphic and magnetostratigraphic correlation (Peng, Babcock, and Cooper 2012). Similarly, the *Peachella iddingsi* to *Bolbolenellus euparyia* Zone trilobites from upper Tapeats exposures near Las Vegas are probably 508.1–503.8 Ma. Thus, it can be concluded that conventionally the Tapeats Sandstone must have been deposited between 510 Ma and 500 Ma and the overlying Bright Angel and Muav Formations within the same timeframe or very soon thereafter, with younging of all formations from west to east.

Finally, Karlstrom et al. (2020) tandem U-Pb dated detrital zircons from the same samples of the Tapeats Sandstone and the locally underlying Sixtymile Formation (in eastern Grand Canyon) as used in the Karlstrom et al. (2018) study. That involved both LA-ICP-MS analyses followed by CA-ID-TIMS (chemical abrasion-isotope dilution-thermal ionization mass spectrometry) analyses of the youngest grains plucked from the LA-ICP-MS epoxy mounts in order to obtain precise maximum depositional ages for those two units based on the youngest zircon grains. For the Tapeats Sandstone the resultant depositional ages were  $\leq 508.19\pm 0.39$  Ma in eastern Grand Canyon,  $\leq 507.68\pm 0.36$  Ma in Nevada, and  $\leq 506.64\pm 0.32$  Ma in central Arizona.

And because the locally conformable underlying Sixtymile Formation had a similar maximum depositional age of  $\leq 508.6 \pm 0.8$  Ma they added it to the Tonto Group, as well as adding the Frenchman Mountain Dolostone, which conformably overlies the Muav Formation (fig. 28). They then combined these depositional ages with the biostratigraphy of trilobite biozones in the Tonto Group based on available precisely-dated regional and global sections (Schmitz 2012; Sundberg et al. 2016; 2020), tied to U-Pb zircon dated Cambrian marker beds elsewhere (Landing et al. 2015; Peng, Babcock, and Cooper 2012), to conclude that the Tapeats Sandstone is  $\sim 507$ – $508$  Ma.

Karlstrom et al. (2020) also confirmed that the long-proposed time transgressive nature of the Tonto Group is supported because the trilobite *Olenellus* is found in the western, but not eastern, Grand Canyon (fig. 28). They determined that the Bright Angel Formation which contains the *Olenellus*, *Glossopleura* and *Ehmaniella* biozones is  $\sim 502$ – $507$  Ma, the Muav Formation which contains the *Bolaspidella* and *Cedaria* biozones is  $\sim 502$ – $499$  Ma, and thus the conventional timeframe for deposition of the initial sheet Tapeats sands, then the Bright Angel muds, silts, and sands and the Muav lime muds and silts of the Tonto Group transgression likely took place in less than  $\sim 9$  Ma ( $\sim 499$ – $508$  Ma) rather than the 40–60 Ma proposed by McKee (1945) and Resser (1945).

### Provenance of the Muav Formation

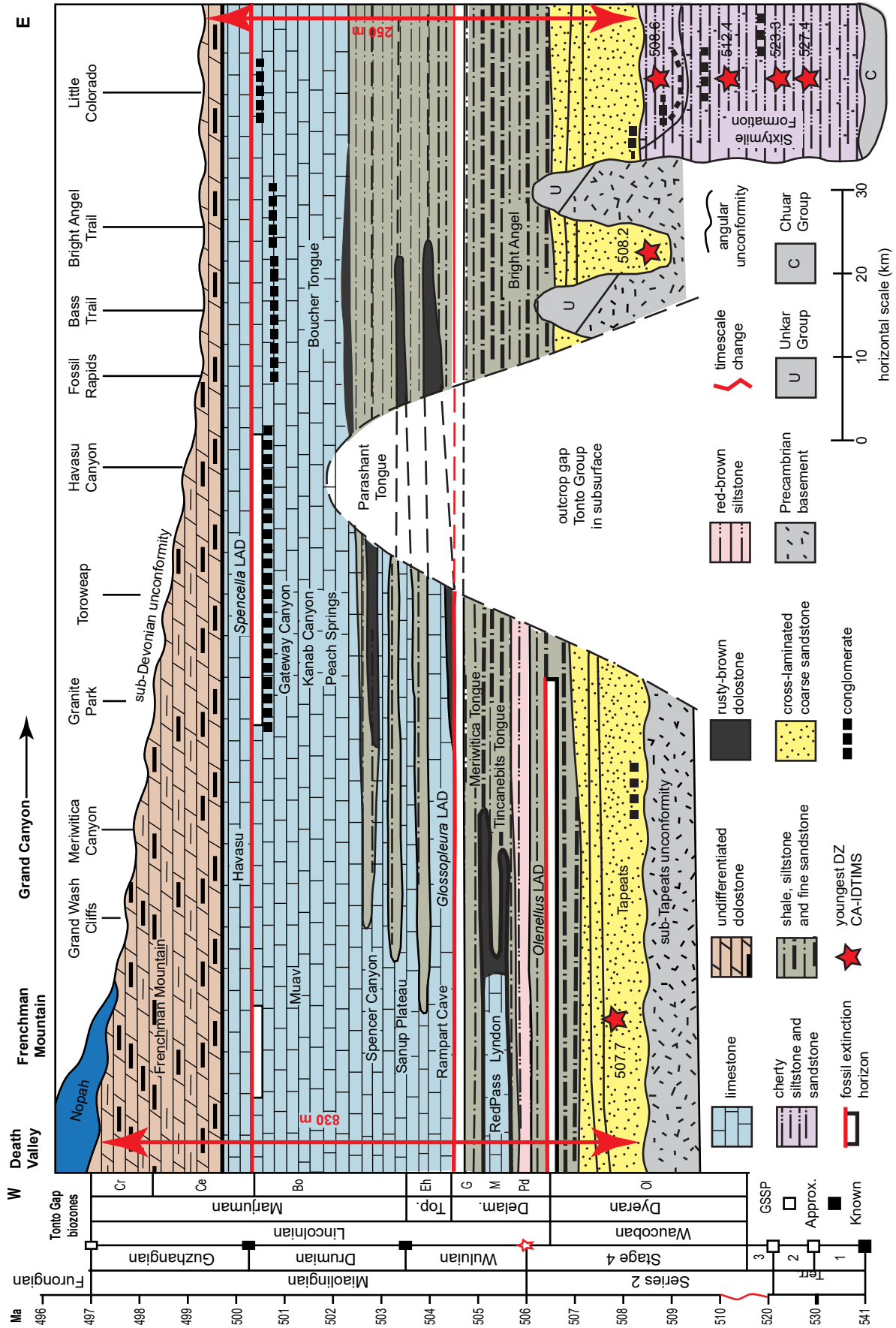
No detrital zircons have been recovered yet from the Muav Formation, but one study has U-Pb dated detrital zircons recovered from the underlying Bright Angel Formation to determine the provenance of its sediment. Gehrels et al. (2011) collected samples of fine-grained sandstone from three  $\sim 50$  cm (1.6 ft) thick horizons within the Bright Angel Formation that were representative in terms of grain size and composition. The three sandstone samples were from 1 m ( $\sim 3.3$  ft) above the base of the formation at about river mile 58.5 (near Malagosa Canyon), from

5 m ( $\sim 16.4$  ft) below the top of the formation at about river mile 51.5 (just above Little Nankowep Creek), and from 3 m ( $\sim 9.8$  ft) below the top of the formation at about river mile 49. Some of the separated zircon grains were selected for U-Pb dating analyses using laser ablation-multicollector-inductively coupled plasma-mass spectrometry (LA-MC-ICP-MS) after vetting for zonation using cathodoluminescence imaging to ensure only homogenous zones were spot analyzed—91, 105, and 86 grains, respectively.

Gehrels et al. (2011) found that the zircon grains within the samples were very small ( $< 100 \mu\text{m}$  in length), euhedral to only slightly rounded, and generally colorless to light pinkish. The ages obtained were plotted on U-Pb concordia diagrams and the Pb-Pb ages were listed as the “best ages.” The three samples yielded very similar age clusters, the main groups peaking around  $\sim 1.03$  Ga (very minor), 1.45 Ga (secondary), and 1.71 Ga (primary). With all three samples combined, the primary age peaks were at 1026 Ma ( $n=12$ ), 1457 Ma ( $n=63$ ), and 1712 Ma ( $n=113$ ). The statistical analysis used by Gehrels et al. (2011) confirmed that there was very good agreement between the three Bright Angel Formation samples of these age peaks.

These U-Pb ages for detrital zircon grains from the Bright Angel Formation are very similar to those they obtained for the underlying Tapeats Sandstone, with the statistical comparison confirming very good agreement. This was to be expected, as the Tapeats Sandstone and Bright Angel Formation were part of the same Sauk megasequence transgression that eroded and transported these sediments from the same source areas. Thus, the provenance interpretations are accordingly similar. Gehrels et al. (2011) concluded that most of the detritus deposited in the Bright Angel Formation was shed from the southwestern United States crystalline basement, with a much lesser contribution from the Grenville orogen to the south or far east. Of the crystalline basement contribution, much of that was likely local from the underlying Yavapai (1.70–1.80 Ga) and Mazatzal (1.62–1.70 Ga) provinces (Karlstrom et al.

**Fig. 28 (page 185).** Diagrammatic cross-section of the Tonto Group re-defining it across Arizona and through the Grand Canyon, from Karlstrom et al. (2020, 428, fig. 3) but modified from McKee (1945, 14, fig. 1). The vertical scale is time and the red scale bars show approximate thicknesses at each margin of the cross-section. The biochronology shown to the left is their working hypothesis, that could be refined with additional precise U-Pb detrital zircon (DZ) bracketing dates. The lower Tonto Group is in the subsurface in the central part of the transect, making correlations tentative. The sub-Tonto Group angular Great Unconformity has a variety of different-age Precambrian rocks beneath it, and hence a variable hiatus. Above the unconformity in the eastern part of the transect, islands (monadnocks) of tilted Unkar Group strata (resistant Shinumo Sandstone) created up to 200 m ( $\sim 656$  ft) of relief and were only covered by the Bright Angel Formation. Tonto Group biozones mentioned are: Ol—*Olenellus*; Pd—*Poliella denticulata*; M—*Mexicella mexicana*; G—*Glossopleura walcotti*; Eh—*Ehmaniella*; Bo—*Bolaspidella*; Ce—*Cedaria*; Cr—*Crepicephalus*. GSSP—global stratotype section and point; CA-IDTIMS—chemical abrasion–isotope dilution thermal ionization mass spectrometry; LAD—last appearance datum; Terr.—Terreneuvian; Delam.—Delamarian; and Top.—Topazan.



2003). Furthermore, they concluded that the slightly greater proportion of 1.62–1.70 Ga (Mazatzal) grains (35%) over 1.70–1.80 Ga (Yavapai) grains (65%) may reflect cratonward migration of the source regions during the Sauk transgression.

Since the Muav Formation was deposited as part of the same Sauk transgression, it would be logical to conclude that its lime and clastic detritus was likely sourced from the same area as the clastic detritus for the overlying Bright Angel Formation and Tapeats Sandstone. This is reasonable, given that petrographic examination of Muav Formation samples (see below) determined that the Muav Formation also includes identical but finer-grained clastic detritus to that in the Bright Angel and Tapeats, with detrital quartz and K-feldspar grains and detrital muscovite flakes making up significant proportions of the limestones, which as described above also include siltstone partings between their thin beds. It is also reasonable to thus assume that the lime detritus was probably produced from lime sediment on the ocean floor offshore further to the west. The ocean waters transgressing from the west with lime detritus entrained some fine-grained clastic debris as they swept over those Precambrian provinces. Furthermore, McKee (1945, 67) commented there is little doubt, judging from the nature of the pebbles in the intraformational flat-pebble conglomerates within the Muav Formation, that these were locally derived.

### Interpreted Depositional Setting of the Muav Formation

McKee (1945) interpreted much of the Muav Formation to have been deposited under uniformitarian conditions in distal offshore subtidal environments. He based this interpretation on faunal and textural characteristics within the Muav Formation. These include an open-marine fauna (for example, the trilobites), the very fine-grained nature of the mottled limestone and dolostone facies, and the observation that the Muav Formation grades eastward into an apparent shallow-water facies of the Bright Angel Formation. McKee (1945) also suggested that many of the flat-pebble conglomerates occurring throughout the formation were deposited in relatively deep water.

McKee (1945) considered the intraformational flat-pebble conglomerates to be extremely important beds within the Muav Formation. These beds, which are abundant from the Bass Trail eastward, consist of disc-like clasts of micrite and, occasionally, silt-size quartz and glauconite grains. The orientation of these clasts is variable. Some are oriented parallel with the bedding, some clasts are imbricated, and in some instances the clasts are vertical.

McKee (1945) described two associations of these conglomeratic beds. One variety consists of intraformational conglomerates that occur as scattered discontinuous lenses within thinly bedded limestones. The other variety consists of one to several thin conglomeratic beds that extend up to 45 mi (~73 km) (fig. 5). He considered that the great lateral persistence of these beds made them ideal stratigraphic markers, so he used them to correlate over great distances in Grand Canyon. He considered these widespread conglomerates to represent subtidal deposits formed under more energetic conditions during regressions.

The origin of the clasts obviously required early lithification by cementation and/or compaction because they are likely derived by erosion of the earlier-deposited sediments within the same depositional basin (Middleton and Elliott 2003). Where this lithification or induration took place is thus controversial because their provenance has not been conclusively investigated. Opinions range from rip-ups of carbonate muds exposed on tidal flats by storms and/or tidal channels to submarine lithification and subsequent erosion during storms.

Dew (1985) documented the occurrence of intraformational conglomerates similar to those in the Muav Formation in the Upper Cambrian DuNoir Limestone in Wyoming. Based on facies associations, that study showed that what was interpreted as intertidal and subtidal limestone conglomerates can occur over a short stratigraphic interval. Sepkoski (1982) demonstrated that storm-induced currents were mostly responsible for the widespread distribution of flat-pebble conglomerates in Montana's Cambrian strata. In that case the conglomerates are interbedded with shales that lack any evidence of subaerial exposure. Considering the stratigraphic importance that has been made of these conglomerates, Middleton and Elliott (2003) concluded it is clear that they represent a key lithofacies and that documentation of their mode of origin, whether subaerial or subtidal, needs to be determined.

Regardless of their mode of origin, Middleton and Elliott (2003) commented that it is particularly interesting that these intraformational flat-pebble conglomerates are only found within Cambrian and Ordovician strata. Sepkoski (1982) speculated that, because of the proliferation of organisms living within the sediments during and after their deposition, during and following the Ordovician the potential for early submarine cementation of subtidal carbonate shelf deposits was reduced substantially due to bioturbation processes. However, that hypothesis does not appear to have been since tested and, of course, assumes a subtidal origin for these beds.

Although many of the limestone and dolomite beds in the Muav Formation had been interpreted by McKee (1945) as subtidal, Wanless (1973a; 1975) reported what he considered to be intertidal and supratidal facies from dololaminite outcrops in western Grand Canyon (fig. 14). Many of the textures and structures he documented are similar to those found on modern tidal flats on Andros Island in the Bahamas. In particular, the laminated dolostones in the Muav Formation have many characteristics in common with laminated dolomites that occur on supratidal levees adjacent to tidal channels on Andros Island (Middleton and Elliott 2003; Wanless 1975). In those areas, fine-grained carbonate sediment is deposited during periods of overbank flooding following storms. Algae that inhabit the levees trap the sediment, resulting in the generation of continuous laminae of carbonate mud and pellets. Aitken (1967) referred to these laminated horizons as crypto-algal laminations because the evidence of algal binding had to be inferred. Discontinuous laminae also occur, produced by traction transport of pellets and other grains over the algal-bound sediment. Wanless (1975) reported that these dololaminite units are up to 66ft (20m) thick in the Muav Formation. This was interpreted as produced by prolonged periods of supratidal sedimentation far offshore from the apparent Cambrian strandline.

Middleton and Elliott (2003) concluded that it is clear the Muav Formation records interpreted episodes of both subtidal and peritidal deposition. They suggested that therefore a reasonable depositional model might be one of offshore shoals surrounded by deeper water areas, similar to the tidal flat model proposed by Pratt and James (1986) for Lower Ordovician shelf carbonates of Newfoundland. In their model, small localized carbonate islands occurred far offshore and were separated by subtidal areas. Middleton, Steidtmann, and DeBour (1980) documented similar facies distributions in Cambrian strata in Wyoming.

Rose (2003; 2006; 2011) adopted the predominantly tidal flat and carbonate shoal depositional environments model of Wanless (1973a). Three sedimentary features in particular he considered were diagnostic, namely, the 20m (~66ft) thick dololaminite sequence Wanless (1973a; 1975) claimed to be analogous to the modern storm-dominated tidal flats of the Bahamas, the claimed rare stromatolites in the Muav Formation of eastern Grand Canyon that would be indicative of peritidal sedimentation, and the intraformational flat-pebble conglomerate beds in western Grand Canyon that are indicative of strong bottom agitation and bedload transport of rounded limestone pebbles in medium quartz sand.

In particular, Rose (2003; 2006) highlighted his observation that the Muav's Gateway Canyon Member at river mile 45.5 in Marble Canyon is almost entirely composed of dololaminite. Then the exposure is continuous and traceable for several miles until its lithological content changes abruptly over a lateral distance of less than a kilometer so that at river mile 50 the full width of this member is the thin-bedded mottled limestone and interbedded flat-pebble conglomerate layers more typical of this member throughout the rest of the Canyon. He also pointed to the platy and nodular silty allochems within the siltier portions of this transition that resemble flat-pebble conglomerates and interpreted them as possible "jelly roll structures" (Demicco and Hardie 1994) that are supposedly indicative of extreme shallow environmental conditions. Supposed curling at the margins of these claimed allochems was interpreted as due to desiccation of the thin, possibly microbially stabilized sheets of carbonate mud. Rose (2003) also claimed there are a wide range of shapes and sizes of pelmicritic allochems also present in the upper Kanab Canyon Member underlying the Gateway Canyon Member's dololaminites. Some interpreted pelmicritic pisolites potentially show evidence of the activity of borers supposedly indicative of shallow water, while trilobite fragments mixed in with the allochems are suggestive of strong water currents.

Rose (2003) thus claimed that the supposed desiccation of carbonate mud veneers established a genetic link between the dololaminites and the flat-pebble conglomerates, even though the dololaminites of this type are not a common feature of the Muav Formation throughout Grand Canyon. However, silty horizons are common within centimeter-scale couplets of siltstone and finely-laminated silty limestone or dolostone, with the siltstone partings typically carbonate-cemented and reduced to millimeter-scale thickness, resulting in the cliff-forming succession of thin-bedded limestone or dolostone that is the predominant lithology of the Muav Formation. Yet, he still claimed that in superb surface exposures he could recognize a continuum linking burrow mottling to flat-pebble conglomerates, the borrowing activity in the micritic muds followed by desiccation supposedly having produced the flat micritic pebble clasts. He cited Kozub (1997) who proposed burrowing activity as one of three possible mechanisms for the release of flat pebble clasts, but who had assumed the original substrate had been a hardground, unlike what Rose (2003) was suggesting for these carbonate veneers within the Muav Formation. Yet Rose's suggestion of those flat pebble clasts being transported and deposited by high-energy storm events is consistent with a similar environmental model proposed by Kazmierczak and

Goldring (1978), Sepkoski, Bambach, and Dorser (1991), and Wu (1982).

McKee (1945) had relied on the traceability of these flat-pebble conglomerate horizons as time planes, but Rose (2003) found these horizons not to be traceable. He cited Owens (1985) as similarly documenting the discontinuity of flat-pebble horizons in an Upper Cambrian formation in Wisconsin and also criticizing the general assumption that flat-pebble conglomerates are traceable time planes representing regional storm events in shallow marine deposits. Thus, Rose (2003) insisted the association of the flat-pebble conglomerates with shallow-water dololaminites in the Muav Formation indicated that the transport and local concentration of the flat-pebble clasts likewise need not have been as dramatic and widespread as a storm but need only have reflected hydraulic conditions of higher advective energy than those conditions in which the clast material had initially formed. And since he envisaged much of the substrate during slow-and-gradual deposition of the Muav Formation were softgrounds or firmgrounds that were burrowed, then the continuum he perceived from blocky mottled limestones to thin-bedded limestones and flat-pebble conglomerates did not demand extreme basin-scale changes required of shelf-slope processes.

Therefore, Rose (2003) maintained that the poor lateral traceability of individual beds, local channelization and buildup, and unidirectional or herringbone imbrication of the flat pebbles more readily indicated localized advection in tidal channels than a dramatic basin-wide disturbance such as a storm. In support of his depositional model, Rose (2003, 2006) cited Cloyd, Demicco, and Spencer (1990) who had described just such a variety of juxtaposed facies types within a Middle-Upper Cambrian formation in Alberta purely in terms of storm enhancement of tidal currents in the development of eroded channels and transport of flat pebbles. They had concluded that such channels and associated mudstone laminites represented tidal channel migration and overbank deposits in river-like crevasse splays on a prograding peritidal carbonate flat rather than storm disruption at basin scale. Furthermore, Rose (2003, 2006) noted that contemporaneous carbonate units in the southern Great Basin immediately adjacent to Grand Canyon had been described by Adams and Grotzinger (1996), Lehmann et al. (1996), and Osleger et al. (1996) as largely peritidal, that is, ranging from subtidal to tidal flat environments.

In summary, Rose (2003) concluded that the Muav Formation represents a stage in Tonto Group development in which the depositional surface was capable of sustaining carbonate accumulation.

Clastic carbonates and siltstones, along with burrow mottling and interbedded calcareous mudstone, indicate highly variable substrate mobility and low overall clastic influx. Furthermore, the poor lateral traceability of laminar and thin-bedded structures, the interbedded siltstones, and the herringbone cross-bedding and flat-pebble conglomerates in the absence of reef-forming algal mounds together indicate deposition in a shallow, tidally-influenced depositional basin of very low relief. He added that early residual calcite cements are common in what he claimed are laterally extensive weathered horizons and thus may be an early diagenetic feature related to subaerial exposure and infiltration by meteoric porewater.

## Petrography of the Muav Formation

### Previous Studies

As petrographic methods were not routinely practiced on sedimentary rocks until later in the 1950s, McKee (1945) did not undertake a detailed petrographic investigation of the Muav Formation. Yet he did publish black and white photomicrographs of mottled, aphanitic limestone of the Kanab Creek Member at Diamond Creek (river mile 226) (plate 10d), of rubbly, aphanitic limestone from the top of the Kanab Canyon Member on the Bright Angel Trail (above river mile ~90) (plate 13b), and of *Girvanella* limestone of the Rampart Cave Member at Diamond Creek (river mile 226) (plate 13d). Additionally, he provided a black and white macroscopic photograph of limestone pebbles and glauconite on an eroded surface of aphanitic limestone from above the Spencer Canyon Member at Columbine (Emery) Falls (river mile 275.3) (plate 11b).

Even though Rose (2003) also completed a major stratigraphic mapping study, he likewise did not include much petrographic examination of the constituent rocks within the Muav Formation. He only published two black and white photomicrographs of the variety of allochems in the upper Kanab Canyon Member near river mile 45.5—a small ovate oolite (oncolite) and rounded peloid nearly 1 mm long in one image and the margin of a calcite allochem with a local concentration of glauconitic peloids and finely crystalline dolomite within a matrix of mixed fine-grained dolomite and calcite in the other image (Rose 2003, 206, fig. 107). He interpreted the micropeloidal concentration and organic pigmentation as possibly indicative of feeding by borers of the possibly original aragonite material. He also published three black and white photomicrographs of a sample of the thinly-bedded and mottled limestone which revealed a fine mosaic of dolomicrite in places replaced by drusy euhedral dolomite and with patches of calcite, some peloid concentrations and calcite “ghosts”

replaced by euhedral dolomite (Rose 2003, 219–220, fig. 116). Otherwise, Rose (2003) did not undertake any x-ray diffraction (XRD) analyses of any Muav Formation samples to study and quantify their mineral contents.

### Results of the Present Mineralogic Study

During an investigation of four folds in Grand Canyon, twelve samples of the Muav Formation were collected from the Matkatamiba fold (fig. 3), and three samples from outcrops along the Colorado River corridor distant from that fold (fig. 1). The purpose was to compare the samples from that fold with the distal samples to ascertain what effects (if any) the folding had on the limestone and dolostone beds of the Muav Formation and thus determine the conditions during, and the timing of, the folding relative to the conditions and timing of the deposition and subsequent lithification (cementation) of the Muav Formation. Details of the locations of these samples are provided in Appendix E (in the Supplementary material), in fig. 1 and table 1. The 15 samples were collected from several stratigraphic levels within the Muav Formation as indicated in table 1. One sample each was collected from the Peach Springs and Kanab Canyon Members, while seven came from the Gateway Canyon member and the remaining

six from the Havasu Member. Since the 12 samples along and through the Matkatamiba fold straddle the boundary between the Gateway Canyon Member and the overlying Havasu Member, the two sets of six samples from each unit in that outcrop come from the same two respective stratigraphic levels. All samples were sent to Calgary Rock and Materials Services, Inc. (Calgary, Canada) for thin sectioning and for x-ray diffraction (XRD) analyses.

### XRD Results

Calgary Rock and Materials Services, Inc., dried the samples overnight at 60°C, and selected 5–10 gm of each sample to grind for ten minutes in a pulverizing mill to obtain homogeneous powders. These powders were then packed in powder mounts against a glass surface before being mounted in the goniometer of a Rigaku Miniflex II x-ray diffractometer in which a copper source tube is used to provide the incident beam of monochromatic x-rays with a wavelength of 1.541874 Å. Samples were typically scanned from 4 to 60° 2θ (two theta) to obtain the XRD spectra. The raw data provided in a specific form by the x-ray computer were imported into the x-ray analysis software (Jade 2010), where peak positions, areas and heights are calculated. The software then provided the most likely matches

**Table 1.** Locations and stratigraphic details of all the Muav Formation samples examined in this study.

| Sample  | Location                             | Location Coordinates            | Stratigraphic Position                          | Notes   |
|---------|--------------------------------------|---------------------------------|---|---|
| MLS-01  | River mile 143.5                     | N 36° 23.543'<br>W 112° 37.581' | Kanab Canyon Member,<br>Muav Formation          | River left ledges just above Kanab Rapid                          |
| MLS-02  | River mile 153.6                     | N 36° 19.383'<br>W 112° 43.301' | Gateway Canyon Member,<br>Muav Formation        | River right just above Sinyella Rapid                             |
| MLS-03  | River Mile 180.2                     | N 36° 11.633'<br>W 113° 05.433' | Top of Peach Springs<br>Member, Muav Formation  | River left ledge just below Son of Lava Rapid                     |
| MFML-01 | Matkatamiba fold<br>River mile 148.8 | N 36° 23.553'<br>W 112° 37.558' | Top of Gateway Canyon<br>Member, Muav Formation | Upstream away from the hinge zones of the fold                    |
| MFML-02 | Matkatamiba fold<br>River mile 148.8 | N 36° 20.557'<br>W 112° 40.701' | Top of Gateway Canyon<br>Member, Muav Formation | 47.5 m along the bed downstream of MFML-01                        |
| MFML-03 | Matkatamiba fold<br>River mile 148.8 | N 36° 20.408'<br>W 112° 40.497' | Top of Gateway Canyon<br>Member, Muav Formation | 13.5 m along the bed downstream of MFML-02                        |
| MFML-04 | Matkatamiba fold<br>River mile 148.8 | N 36° 20.462'<br>W 112° 40.655' | Top of Gateway Canyon<br>Member, Muav Formation | 7.5 m along the bed downstream of MFML-03 in the lower hinge zone |
| MFML-05 | Matkatamiba fold<br>River mile 148.8 | N 36° 20.470'<br>W 112° 40.630' | Top of Gateway Canyon<br>Member, Muav Formation | 4 m along the bed downstream of MFML-04 in the lower hinge zone   |
| MFML-06 | Matkatamiba fold<br>River mile 148.8 | N 36° 20.368'<br>W 112° 40.643' | Top of Gateway Canyon<br>Member, Muav Formation | 6 m along the bed downstream of MFML-05 from the upper hinge zone |
| MFTB-01 | Matkatamiba fold<br>River mile 148.8 | N 36° 23.553'<br>W 112° 37.558' | Bottom of Havasu<br>Member, Muav Formation      | Above the boundary opposite MFML-01                               |
| MFTB-02 | Matkatamiba fold<br>River mile 148.8 | N 36° 20.557'<br>W 112° 40.701' | Bottom of Havasu<br>Member, Muav Formation      | 47.5 m along the bed downstream of MFTB-01                        |
| MFTB-03 | Matkatamiba fold<br>River mile 148.8 | N 36° 20.408'<br>W 112° 40.497' | Bottom of Havasu<br>Member, Muav Formation      | 13.5 m along the bed downstream of MFTB-02                        |
| MFTB-04 | Matkatamiba fold<br>River mile 148.8 | N 36° 20.462'<br>W 112° 40.655' | Bottom of Havasu<br>Member, Muav Formation      | 7.5 m along the bed downstream of MFTB-03 in the lower hinge zone |
| MFTB-05 | Matkatamiba fold<br>River mile 148.8 | N 36° 20.470'<br>W 112° 40.630' | Bottom of Havasu<br>Member, Muav Formation      | 4 m along the bed downstream of MFTB-04 in the lower hinge zone   |
| MFTB-06 | Matkatamiba fold<br>River mile 148.8 | N 36° 20.399'<br>W 112° 40.578' | Bottom of Havasu<br>Member, Muav Formation      | 6 m along the bed downstream of MFTB-05 from the upper hinge zone |

**Table 2.** Mineral compositions of the Muav Formation samples from x-ray diffraction (XRD) analyses, courtesy of Ray Strom, Calgary Rock and Materials Services, Inc., Canada.

| Sample  | Quartz | K-Feldspar | Plagioclase | Calcite | Dolomite | Siderite | Illite | Total  | Total Carbonates | Total Silicates |
|---------|--------|------------|-------------|---------|----------|----------|--------|--------|------------------|-----------------|
| MLS-01  | 3.0%   | 0.9%       | —           | 65.0%   | 31.1%    | —        | —      | 100.0% | 96.1%            | 3.9%            |
| MLS-02  | 10.2%  | 12.7%      | 1.9%        | 68.7%   | 2.2%     | —        | 4.3%   | 100.0% | 70.9%            | 29.1%           |
| MLS-03  | 8.1%   | 14.1%      | —           | 71.7%   | 3.3%     | —        | 2.8%   | 100.0% | 75.0%            | 25.0%           |
| MFML-01 | 25.6%  | 26.3%      | —           | 21.9%   | 19.8%    | —        | 6.4%   | 100.0% | 41.7%            | 58.3%           |
| MFML-02 | 28.2%  | 24.9%      | —           | 20.1%   | 26.8%    | —        | —      | 100.0% | 46.9%            | 53.1%           |
| MFML-03 | 39.3%  | 26.3%      | —           | 31.1%   | 2.8%     | —        | 0.5%   | 100.0% | 33.9%            | 66.1%           |
| MFML-04 | 12.2%  | 14.9%      | —           | 51.1%   | 17.0%    | —        | 4.8%   | 100.0% | 68.1%            | 31.9%           |
| MFML-05 | 34.8%  | 17.5%      | —           | 43.5%   | 3.6%     | —        | 0.6%   | 100.0% | 47.1%            | 52.9%           |
| MFML-06 | 7.2%   | 9.1%       | —           | 75.0%   | 7.6%     | —        | 1.1%   | 100.0% | 82.6%            | 17.4%           |
| MFTB-01 | 5.3%   | 6.0%       | —           | 71.4%   | 17.3%    | —        | —      | 100.0% | 88.7%            | 11.3%           |
| MFTB-02 | 55.8%  | 18.3%      | —           | 17.6%   | 3.8%     | —        | 4.5%   | 100.0% | 21.4%            | 78.6%           |
| MFTB-03 | 20.4%  | 15.6%      | —           | 60.5%   | 1.5%     | 0.8%     | 1.2%   | 100.0% | 62.8%            | 37.2%           |
| MFTB-04 | 22.5%  | 18.5%      | —           | 49.6%   | 2.7%     | —        | 6.7%   | 100.0% | 52.3%            | 47.7%           |
| MFTB-05 | 2.7%   | 4.5%       | —           | 92.8%   | —        | —        | —      | 100.0% | 92.8%            | 7.2%            |
| MFTB-06 | 4.9%   | 5.8%       | —           | 4.3%    | 81.9%    | —        | 3.1%   | 100.0% | 86.2%            | 13.8%           |

of minerals for each spectrum generated, from a database of over 100,000 compounds. The Rietveld Refinement Method was then used to determine the percentages of the minerals in the samples.

The results of the bulk rock XRD analyses are in table 2. Calcite is, of course, the dominant mineral in ten of the 15 Muav Formation samples, but still present in the other five samples, varying between 4.3% (MFTB-06) and 92.8% (MFTB-05). These two samples are immediately adjoining at the same stratigraphic level. Dolomite is present in all but one of the samples (MFTB-05 that is instead dominated by calcite), otherwise varying from 1.5% (MFTB-03) to 81.9% (MFTB-06), even though these two samples are likewise at the same stratigraphic level. The only other carbonate mineral present is siderite at 0.8% in one sample (MFTB-3). Surprisingly, quartz is present in all samples, even being the dominant mineral in four samples (MFML-01, 02, 03 and MFTB-02). Quartz contents range from 2.7% (MFTB-05) to 55.9% (MFTB-02). Similarly surprising, K-feldspar also features prominently in all samples, and ranges from 0.9% (MLS-01) to 26.3% in two samples (MFML-01 and 03). In fact, in eight samples K-feldspar quantities are slightly more dominant than quartz. For example, in MFML-01 K-feldspar is 26.3% and quartz is 25.6%. The biggest surprise is the presence in one sample (MLS-02) of 1.9% plagioclase. The final mineral constituent is the silicate illite, which is present in eleven of the samples and ranges from 0.5% (MFML-03) to 6.7% (MFTB-04). Given the microscopic examination of these samples (see below and

Appendix E), this illite in the XRD results is mostly muscovite. However, some of the illite is evident as green glauconite. Of potential significance is that the total silicates content (table 2, last column), that is, quartz, K-feldspar, plagioclase and illite (muscovite), is > 50% (that is, predominates) in five of the fifteen samples, and overall ranges from 3.9% (MLS-01) to 78.6% (MFTB-02).

The results of the clay fraction XRD analyses are in table 3. In these samples clay minerals do not occur in significant amounts. The clay mineral present in all samples is illite, varying from 42.4% (MLS-02) to

**Table 3.** Clay mineral fraction compositions of the Muav Formation samples from x-ray diffraction (XRD) analyses, courtesy of Ray Strom, Calgary Rock and Materials Services, Inc., Canada.

| Sample  | Illite | Illite/Smectite | Kaolinite | Chlorite | Total  |
|---------|--------|-----------------|-----------|----------|--------|
| MLS-01  | 52.2%  | 47.8%           | —         | —        | 100.0% |
| MLS-02  | 42.4%  | 46.4%           | 8.8%      | 2.4%     | 100.0% |
| MLS-03  | 93.3%  | 6.7%            | —         | —        | 100.0% |
| MFML-01 | 81.5%  | 18.5%           | —         | —        | 100.0% |
| MFML-02 | 74.7%  | 25.3%           | —         | —        | 100.0% |
| MFML-03 | 65.5%  | 34.5%           | —         | —        | 100.0% |
| MFML-04 | 86.5%  | 13.5%           | —         | —        | 100.0% |
| MFML-05 | 77.6%  | 22.4%           | —         | —        | 100.0% |
| MFML-06 | 100.0% | —               | —         | —        | 100.0% |
| MFTB-01 | 81.5%  | 18.5%           | —         | —        | 100.0% |
| MFTB-02 | 80.2%  | 19.8%           | —         | —        | 100.0% |
| MFTB-03 | 82.8%  | 17.2%           | —         | —        | 100.0% |
| MFTB-04 | 85.2%  | 14.8%           | —         | —        | 100.0% |
| MFTB-05 | 58.8%  | 41.2%           | —         | —        | 100.0% |
| MFTB-06 | 100.0% | —               | —         | —        | 100.0% |

100% (MFML-06 and MFTB-06), and dominates in all but one sample (MLS-02). As already noted, given the microscope examination of these samples (see below and Appendix E), this illite in the XRD results is mostly muscovite. Additionally, mixed-layered illite/smectite is present in all but two samples, ranging from 6.7% to 47.8%, and potentially is a measure of the glauconite content, which at best is trivial. Only one sample (MLS-02) contains other clay minerals, namely, kaolinite (8.8%) and chlorite (2.4%).

#### *Thin Section Examination*

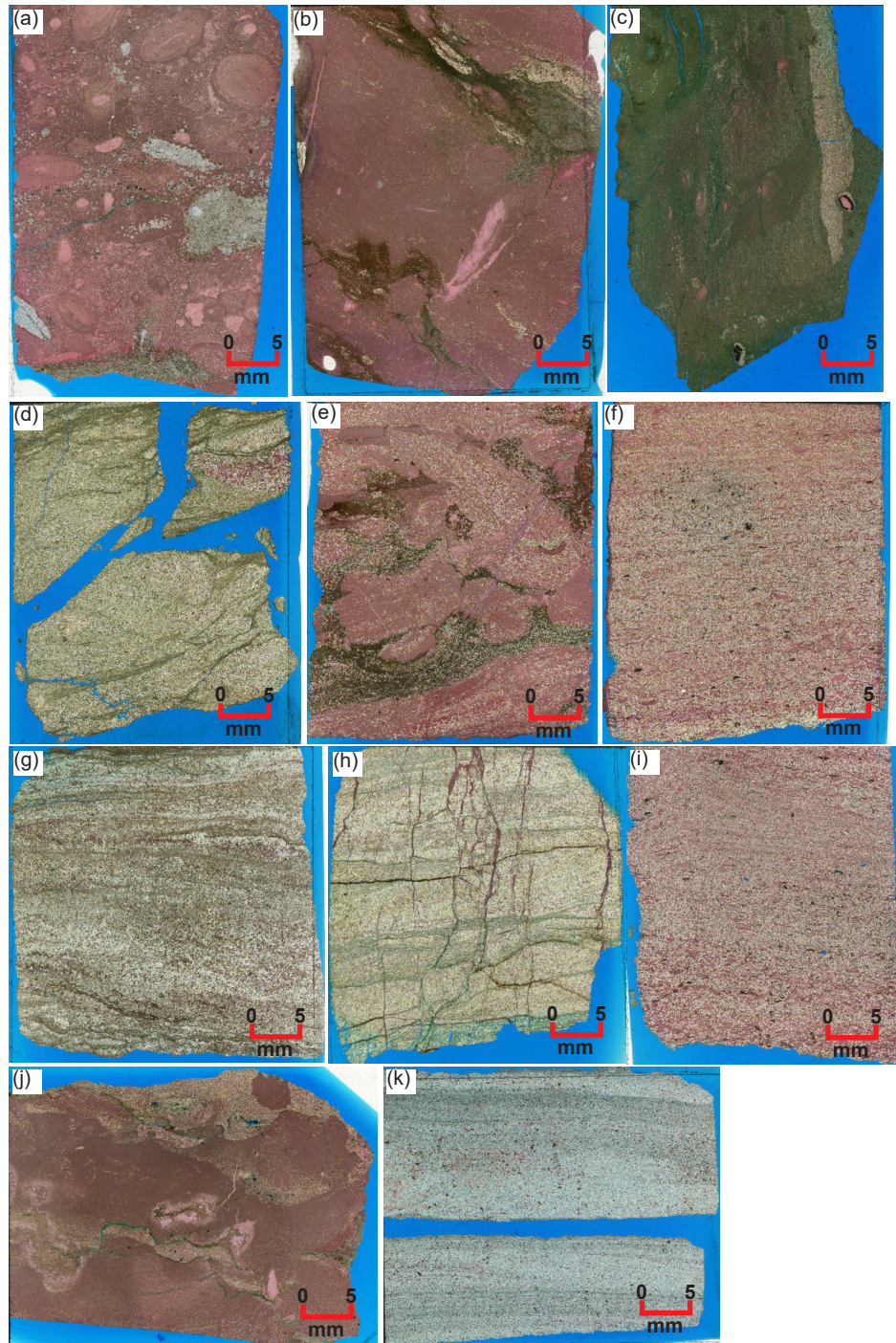
The thin sections for this study were all mounted on standard glass microscope slides. Before the slices were cut from the rock samples using a diamond saw, the rock samples were impregnated under confining pressure with epoxy resin that contained a blue dye. This ensured that grains did not get dislocated, or the rock fabrics get distorted during the sawing of the slices. However, this process left the thin sections with a blue dye staining as the surrounding background and in any holes or pores within the rock fabrics. Before cover slips were added, the thin sections were stained so as to make the K-feldspar and calcite in the rock fabrics more easily distinguished. Thus, the K-feldspar grains have a distinctive yellow color, and the calcite is pinkish in plane polarized light.

Petrographic descriptions of all 15 samples from extensive thin section examination are provided in Appendix E (in the Supplementary material), along with photographs of the whole thin sections (as in fig. 29) from which the descriptions were derived. The thin sections of all the samples are shown in fig. 29, while a representative set of photomicrographs in fig. 30 shows typical textures within each of the samples. It should be noted that in these thin sections there is occasionally a blue dye staining between the grains, and sometimes encroaching on the grain edges or even across grain surfaces or along fractures. This blue dye is associated with the epoxy that the samples were impregnated with prior to the preparation of the thin sections.

It should again be noted that the 15 samples were collected from several stratigraphic levels within the Muav Formation as indicated in table 1. One sample each was collected from the Peach Springs and Kanab Canyon Members, while seven came from the Gateway Canyon Member and the remaining six from the Havasu Member. Since the 12 samples along and through the Matkatamiba fold straddle the boundary between the Gateway Canyon Member and the overlying Havasu Member, the two sets of six samples from each unit in that outcrop come from the same two respective stratigraphic levels. Those six samples in each of those two sets are thus comparable to one another.

What is immediately evident is that whereas all 15 samples were described as limestones in outcrop, in thin section silicate mineral grains are visible in all of them. In fact, in five of the samples, silicates constitute >50% of their content (see the last column in table 2). Indeed, their silicate mineral contents (primarily quartz and K-feldspar grains) range from 3.9% to 78.6%. The quartz grains usually predominate in quantity over the K-feldspar grains, though in some samples their contents are about equal, while in a few samples K-feldspar is slightly more dominant than quartz. Furthermore, these silicate mineral grains mostly range in size from medium and coarse silt (regarded as mud) to very fine sand, though a few grains reach fine sand size, using the standard definitions and terminologies for size of Udden (1914), Wentworth (1922), and Folk (1980). These quartz and K-feldspar grains are also mostly sub-angular to sub-rounded, though some are angular, either irregular-shaped or even slivers, and a few are rounded, using the definitions and terminology for shape of Powers (1953) and Folk (1955). A few K-feldspar grains are even sub-euhedral former laths. And whether in the high silicate minerals content samples (>45%) where they are evenly scattered (for example, MFML-05 and MFTB-02 and -03, fig. 29h, f, and i, respectively) or in the lower silicate minerals content where they are unevenly scattered and sometimes clumped (for example, MLS-02 and MFML-06, fig. 29j and e, respectively), the quartz and K-feldspar grains are poorly sorted with the different sized angular and sub-rounded grains near one another, using the standard definition and terminology for sorting of Folk (1966, 1980) and Pettijohn, Potter, and Siever (1973). Where clumped together, the quartz grains sometimes meet at triple points.

The only other silicate minerals present in these limestones are plagioclase grains, muscovite flakes, and glauconite grains. The plagioclase grains are isolated and only present in a few samples, and then only evident due to their multiple twinning under crossed polars. The muscovite flakes are present in the thin sections of all samples but in varying quantities and always seen edge-on as cross-sections of books of thin sheets. They are associated with the quartz and K-feldspar grains between which they usually occur, are mostly subparallel to the bedding, and sometimes are bent around the quartz and K-feldspar grains with split or frayed ends. The glauconite grains are not universally present. In a few samples (for example, MFTB-04, fig. 29l and fig. 30p) they occur as rounded peloids, sometimes with the central "seed" grain present around which the peloid grew. In other samples the glauconite appears to be due to illite alteration of K-feldspar grains.



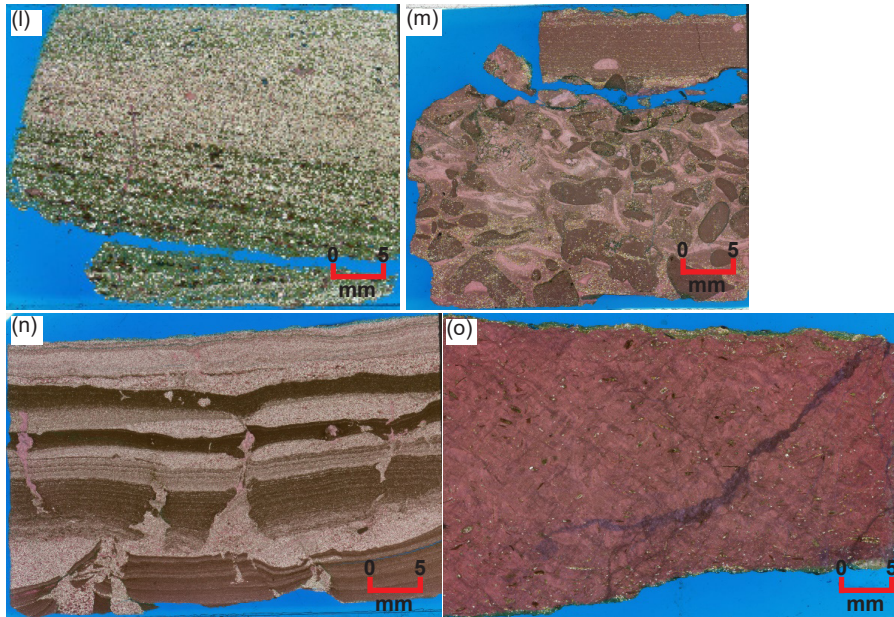


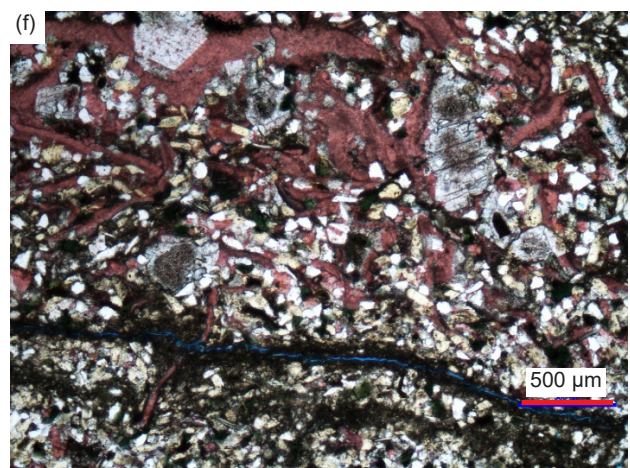
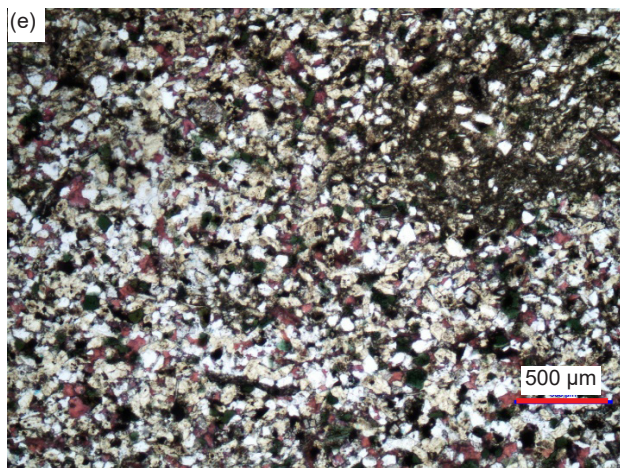
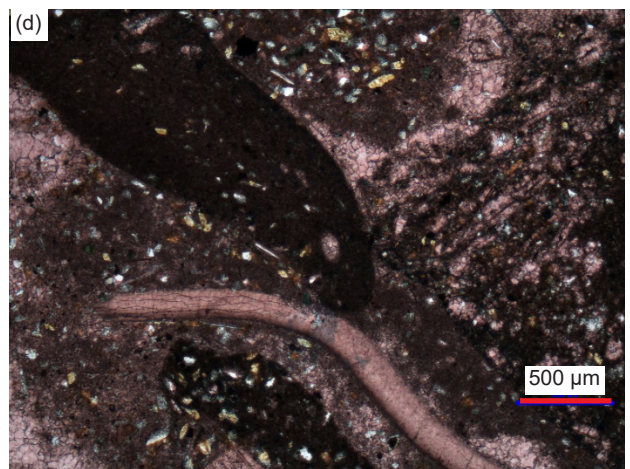
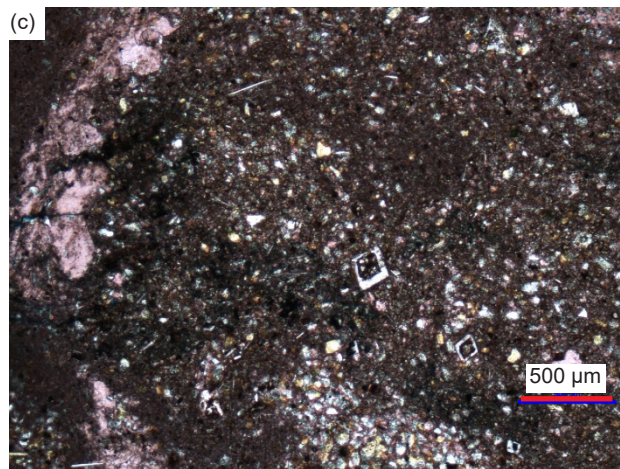
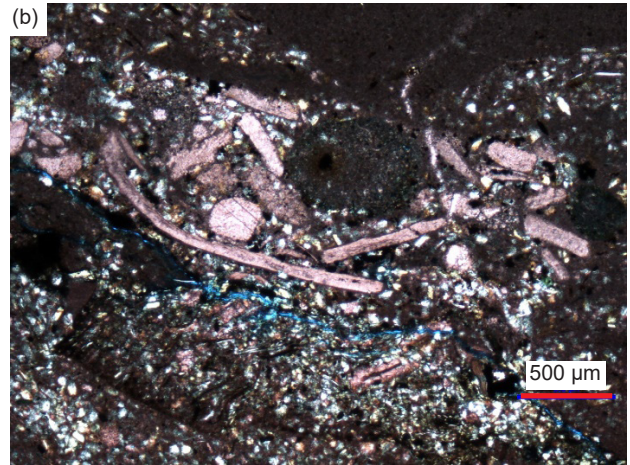
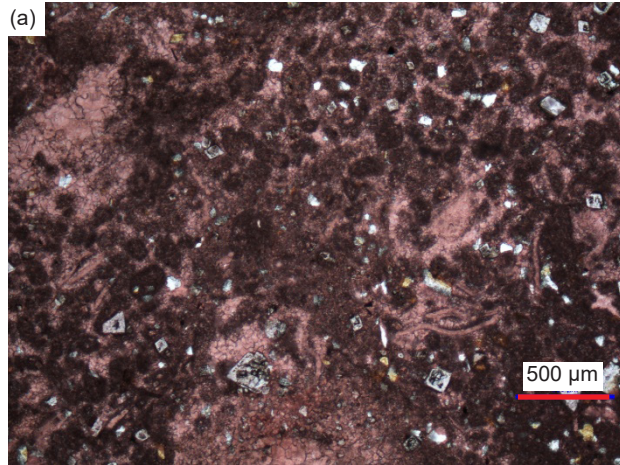
**Fig. 29 (pages 192 and 193).** The thin sections of all 15 Muav Formation samples at normal hand specimen scale (scale bars indicate ~5 mm), orientated so that the bedding is across the image and the upside is to the top. (a) MLS-01, (b) MFTB-01, (c) MFTB-06, (d) MFML-01, (e) MFML-06, (f) MFTB-02, (g) MFML-02, (h) MFML-05, (i) MFTB-03, (j) MLS-02, (k) MFML-03, (l) MFTB-04, (m) MLS-03, (n) MFML-04, and (o) MFTB-05.

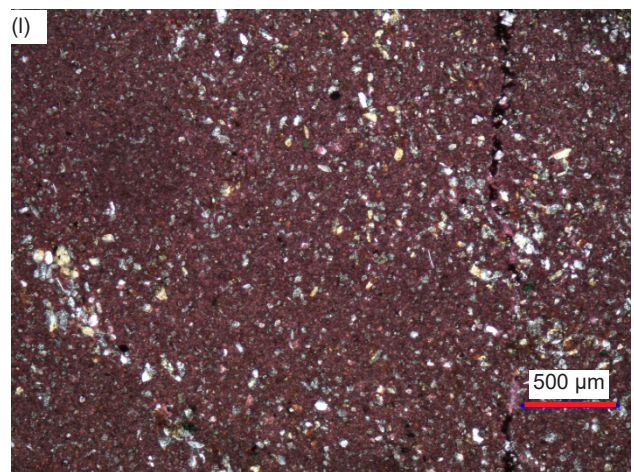
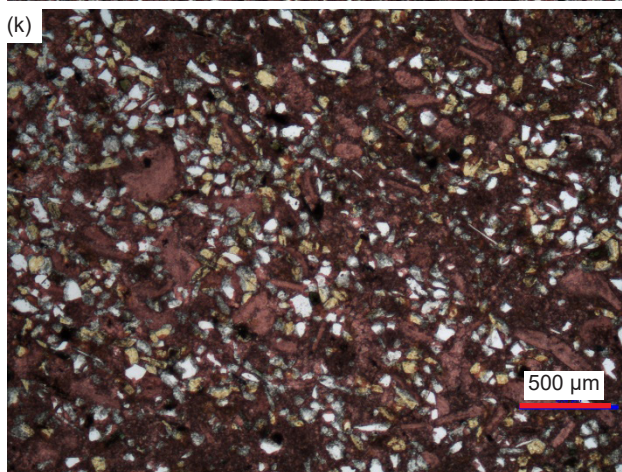
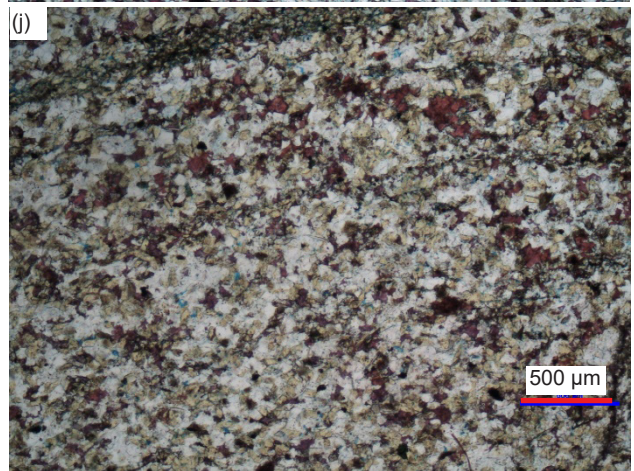
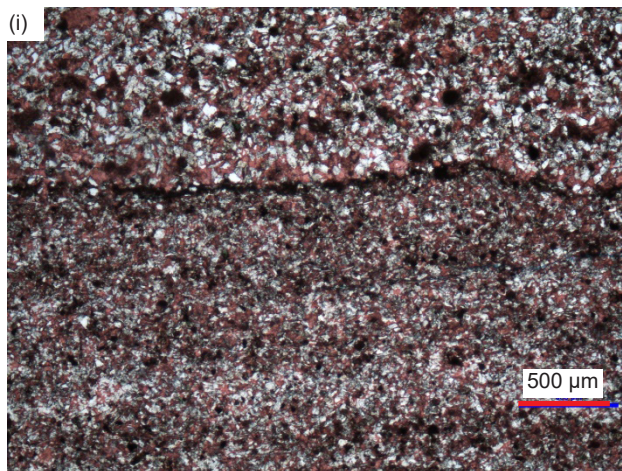
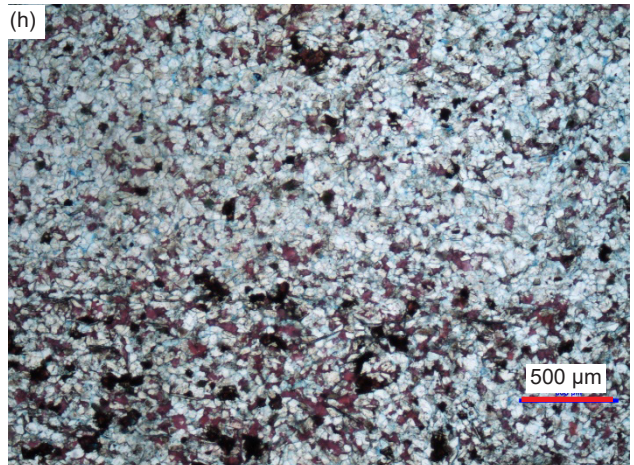
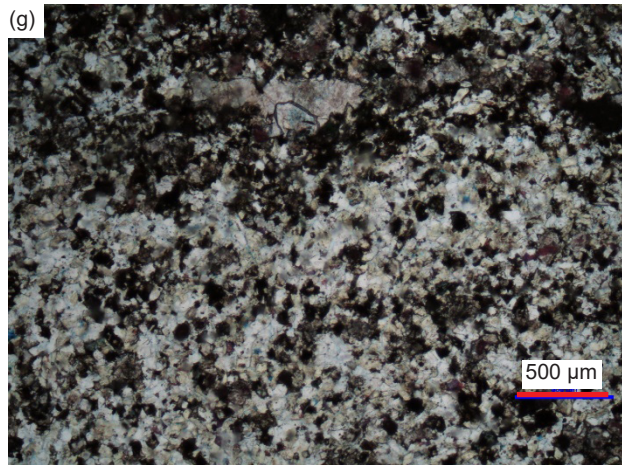
All these silicate grains and flakes are in most samples “floating” in a matrix of mud-sized calcite grains (micrite). The calcite content varies between 4.3% and 92.8%, these extremes being in adjacent samples only 6 m apart at the same stratigraphic level at the base of the Havasu Member (MFTB-05 and -06, fig. 29o and c, respectively). Some calcite has recrystallized into larger grains, while some later calcite fills cross-cutting veins. Also, often present is micro-crystalline calcite in cross-sections of fossil shell fragments of various sizes and shapes, most likely representing mostly brachiopods and lesser bivalves (fig. 30b, d, f, k, and o). Dolomite is present in all but one sample, otherwise ranging from 1.5% to 81.9%, and while usually being subordinate to calcite it is the dominant carbonate in two samples ((MFML-02 and MFTB-06, fig. 29g and c, respectively). The dolomite grains are generally mud to fine sand sized, but often there are larger rhombs with growth zones marked by linings of iron oxides. The dolomite would appear to have replaced calcite, as would the siderite present (0.8%) in one sample (table 2).

Even though there is such a wide variation in the contents of these samples, the total carbonates ranging from 21.4% to 96.1% (table 2), texturally they are very similar. Due to their silicate mineral contents as silt and fine sand sized clasts, these could be called silty limestones or carbonate siltstones. According to Folk (1959, 1962) these limestones would be classified based on transported and authigenic constituents as medium crystalline very fine to fine calcarenites,

or alternately as fossiliferous intramicrudites where the micro-crystalline matrix or allochems are >10% and the intraclasts are >25%, and as fossiliferous intraclast-bearing micrite, though these names do not take into account the occasional peloids or oolites. Less confusing classification terminology was adopted by Dunham (1962) and slightly revised by Wright (1992). Accordingly, these rocks are classified as mostly wackestones where the >10% silicate grains are calcite mud-supported, as calcareous mudstones where in a few samples the silicate grains are <10%, and as packstones in those few samples where the >50% silicate grains support the rock fabric. These are regarded as primarily depositional textural terms that likewise do not take into account the occasional peloids or oolites. Scholle and Ulmer-Scholle (2003) noted that the Dunham (1962) classification has the advantage of its worldwide use due to its partially quantifiable, descriptive (objective) terminology.

In most of the 12 samples collected from the topmost Gateway Canyon Member and the basal Havasu Member in the Matkatamiba fold closely-spaced fine and parallel laminations are clearly evident and even some cross-laminations, often marked by the alignment of the silicate mineral clasts (for example, MFML-02, -03 and MFTB-02, -03 and -04, fig. 29g, k, f, i, and l, respectively). In one instance (MFML-04, fig. 29n) these laminations are grouped into thin alternating beds, some of which are graded, of fine-grained calcareous siltstone and of micrite. Furthermore, it is apparent that soon after deposition





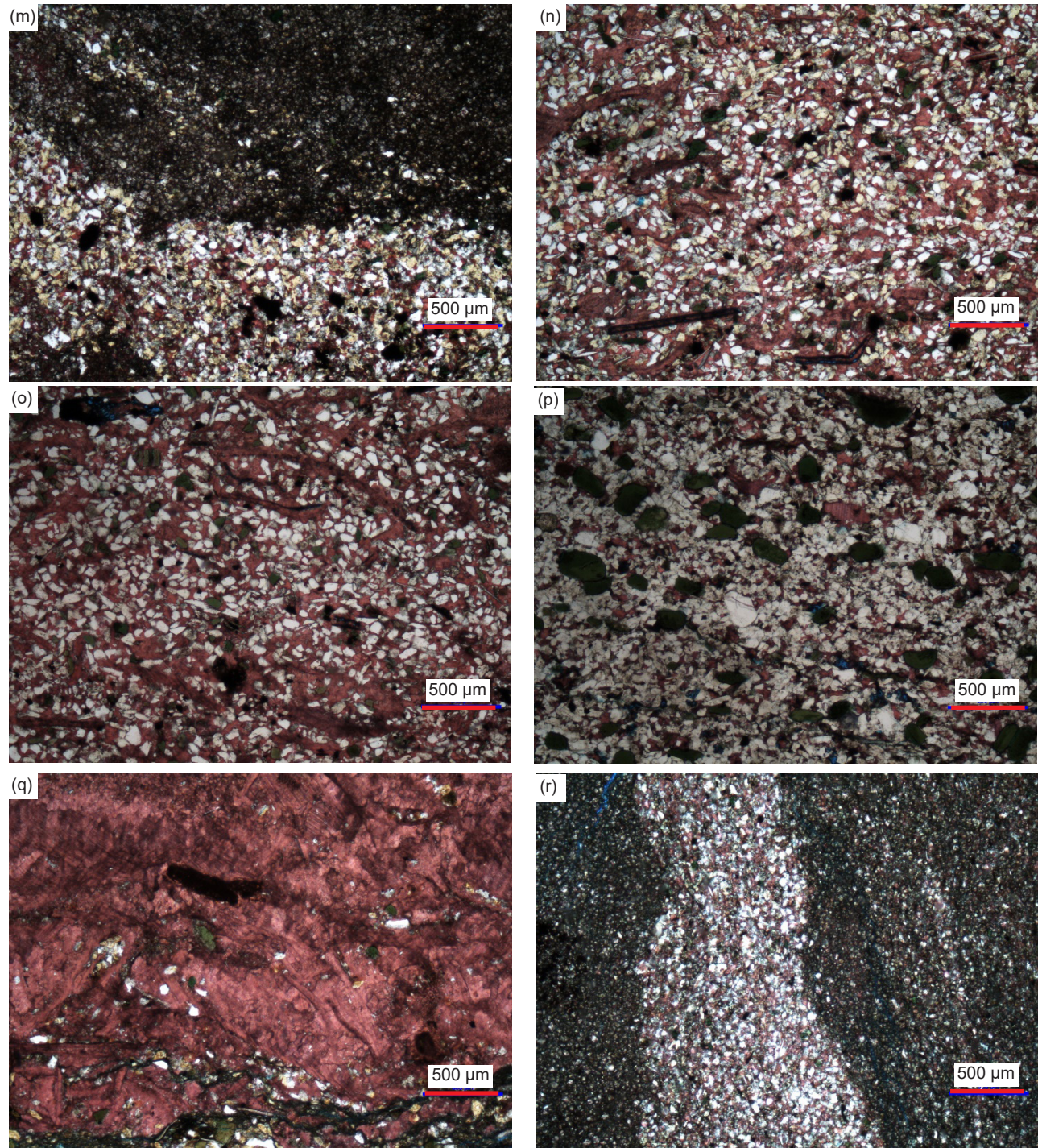


**Fig 30 (pages 194–196).** A representative set of photomicrographs at the same scale (as indicated) showing the variations in the textures in the samples from the Muav Formation. (a) MLS-01, (b), (c) MLS-02, (d) MLS-03, (e), (f) MFML-01, (g) MFML-02, (h) MFML-03, (i) MFML-04, (j) MFML-05, (k) MFML-06, (l), (m) MFTB-01, (n) MFTB-02, (o) MFTB-03, (p) MFTB-04, (q) MFTB-05, and (r) MFTB-06

while still soft these laminae were disturbed or deformed, as some of the fine-grained silt moved through breaks in the micrite laminae, intruding like diapirs and veins as “injectites.” In another instance (MFML-06, fig. 29e), the soft-sediment deformation completely disturbed the original layers, so they formed alternating “blobs” and “swirls.” And in other samples that are dominated (>50%) by quartz and K-feldspar grains (MFML-01 and -05, fig. 29d and h, respectively), post-depositional fracturing occurred perpendicular and obliquely to the laminations to slightly offset them, with the fractures filled by thin calcite veins.

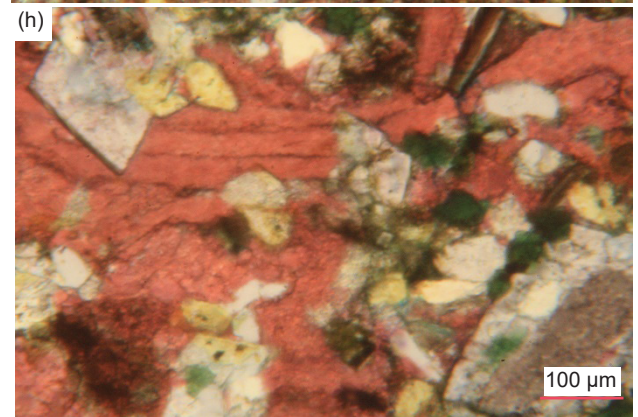
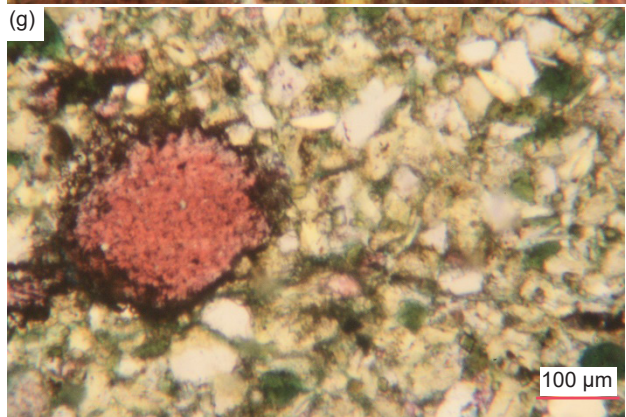
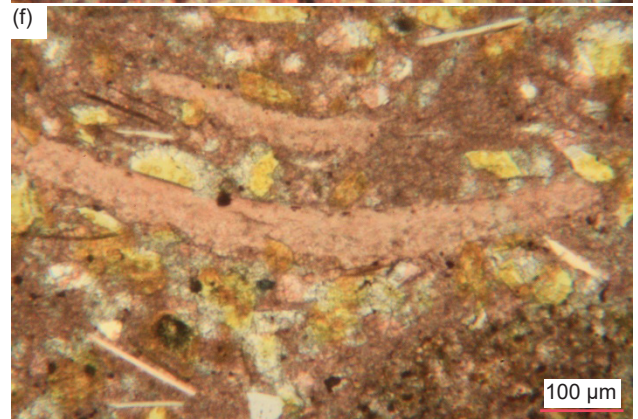
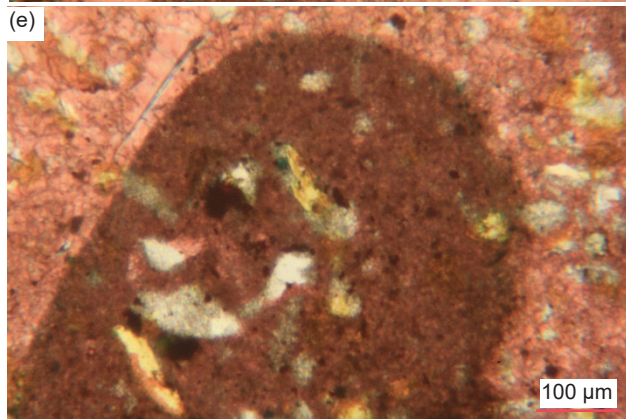
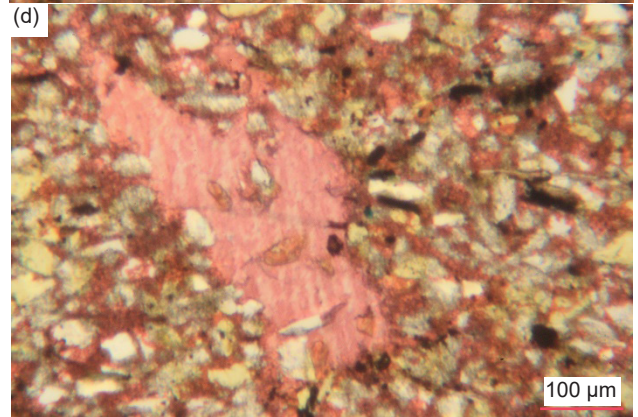
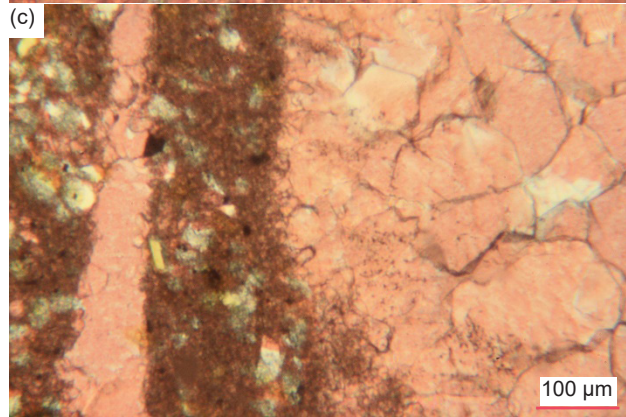
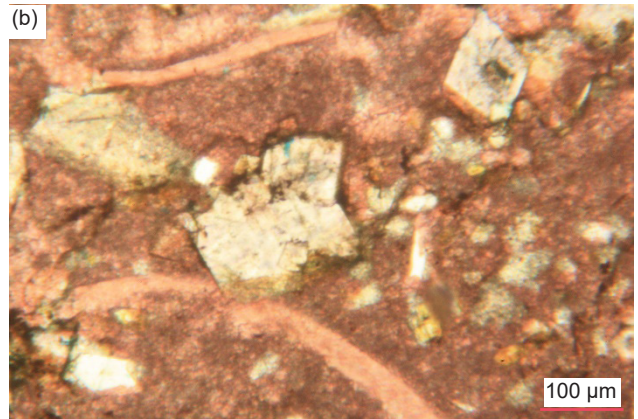
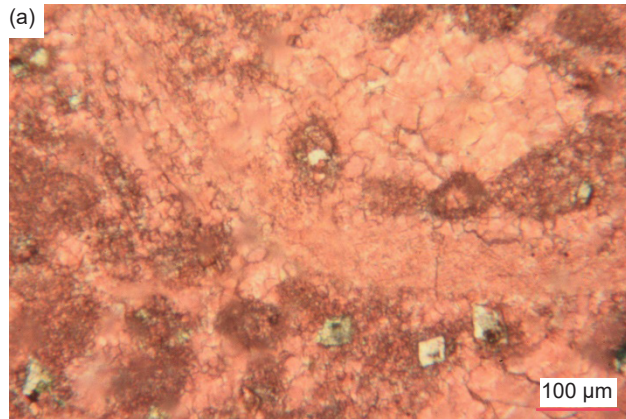
### Calcite

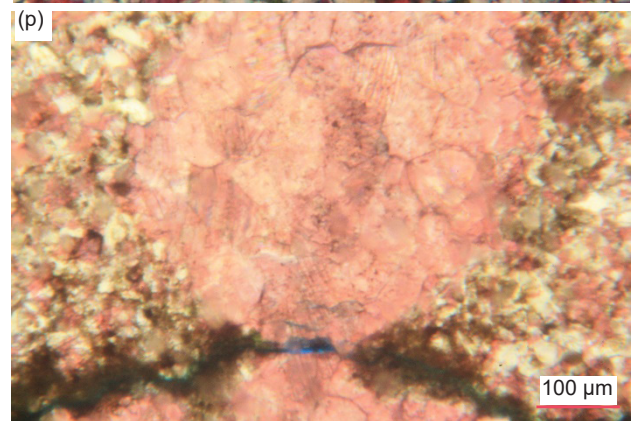
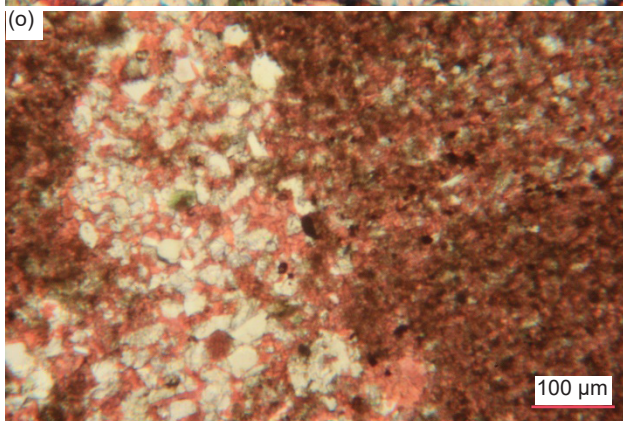
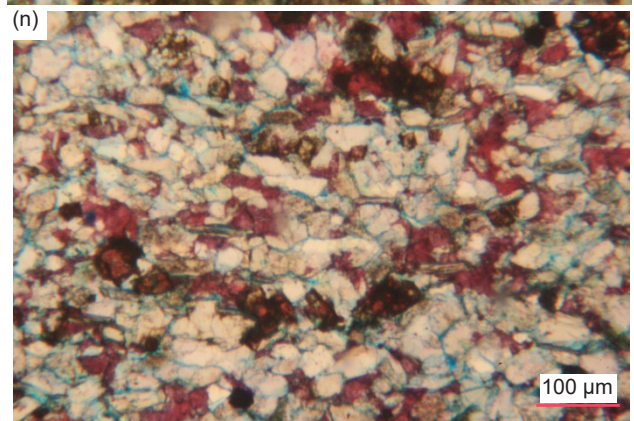
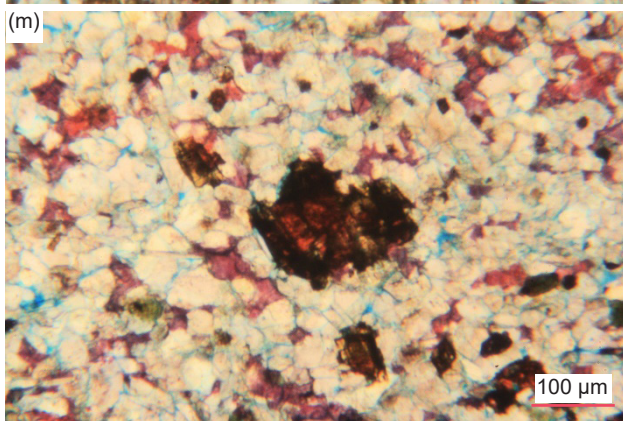
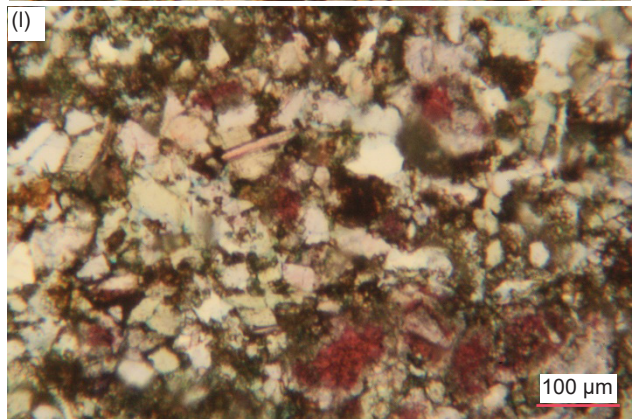
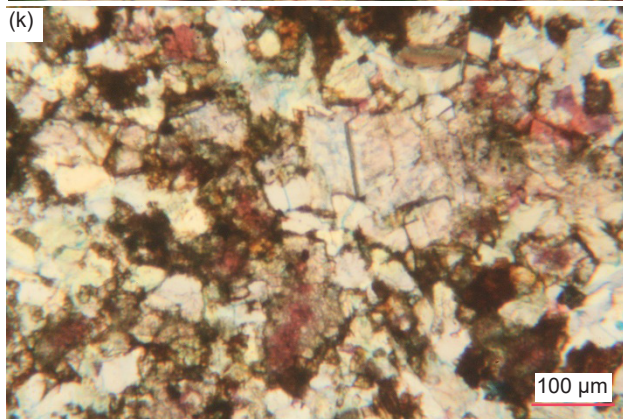
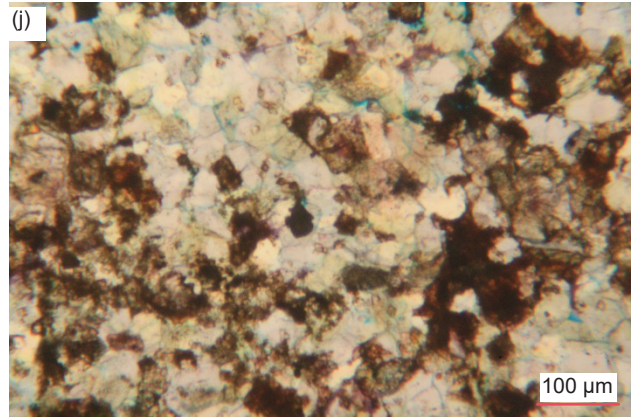
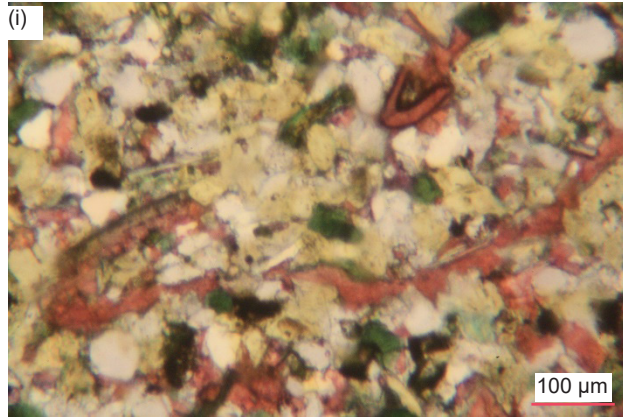
The dominant carbonate component of all but two of these 15 samples is calcite, varying overall from 4.3% to 92.8%. Most samples consist of either a dominant massive, densely-packed interlocking mosaic of very tiny or ultra-fine-grained (mud-sized) grains and rhombs (0.01–0.03mm,  $\phi=+6.72$  -  $+5.01$ ) of calcite (micrite) variably iron-oxides-stained as a speckled dusting or in small blotches and streaks (fig. 31). Sometimes the calcite matrix is mud to coarse silt and very fine sand-sized (0.02–0.12mm,  $\phi=+5.71$  -  $+3.06$ ). Where it is subordinate, the calcite matrix consists of very small (0.05–0.11mm,  $\phi=+4.23$  -  $+3.19$ ), small (0.13–0.17mm,  $\phi=+3.06$  -  $+2.57$ ) and small-medium (0.20–0.47mm,  $\phi=+2.33$  -  $+1.09$ ) crystals, many of which are due to recrystallization, particularly the larger crystals, and thus are set at different extinction angles, which are variably iron-oxides-stained, including along cleavage planes. In some samples, there are numerous scattered recrystallized tiny to very small (0.03–0.13mm,  $\phi=+5.01$  -  $+2.95$ ) and small-medium (0.16–0.30mm,  $\phi=+2.66$  -  $+1.75$ ) interstitial calcite grains and occasional rhombs, pink-stained and often iron-oxides-stained (sometimes heavily), usually isolated between other mosaic grains (quartz and K-feldspar) but sometimes connected to one another in small to very large patches (the latter with tiny quartz grains embedded in them), all acting as cement. The calcite cement grains sometimes have been recrystallized to form large and even huge (0.42–0.77mm,  $\phi=+1.25$  -  $+0.38$ ) platy crystals (with characteristic cleavage evident), or sometimes have formed large patches of recrystallized calcite, that in either instance engulf some of the mosaic quartz and K-feldspar grains. Alternately, these medium and large-huge sized patches (some elongated) of the calcite matrix have sometimes been recrystallized to very small to small (0.05–0.18mm,  $\phi=+4.23$  -  $+2.40$ ) and medium (0.36mm,  $\phi=+1.46$ ) platy calcite crystals at different extinction angles and sometimes with characteristic cleavage evident and which are lightly speckled

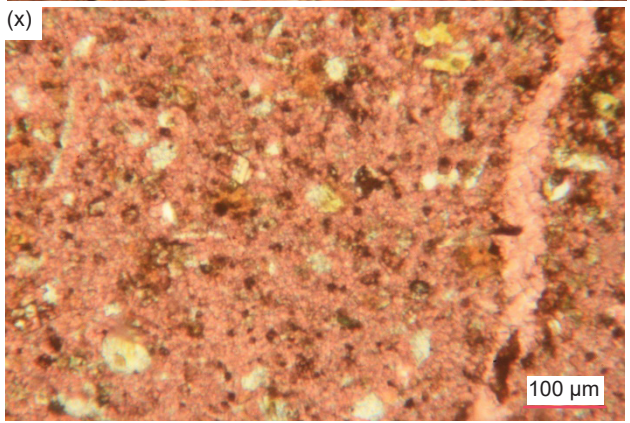
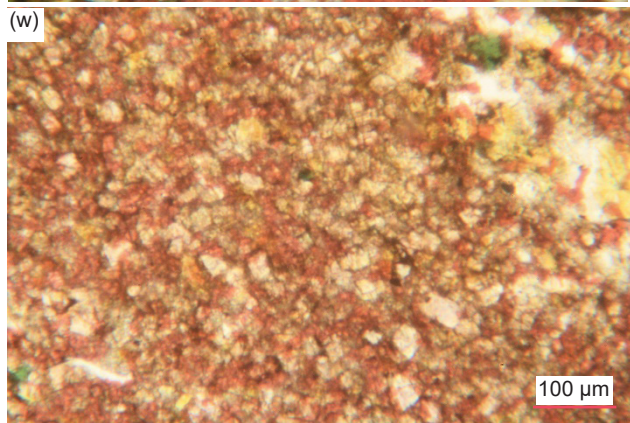
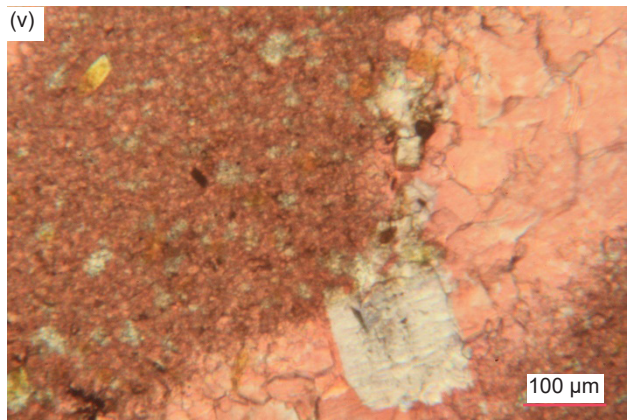
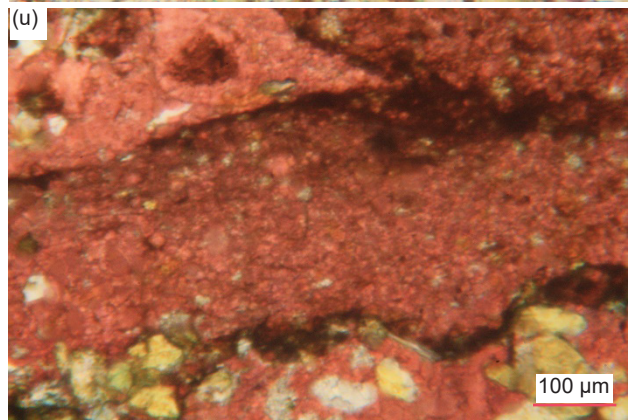
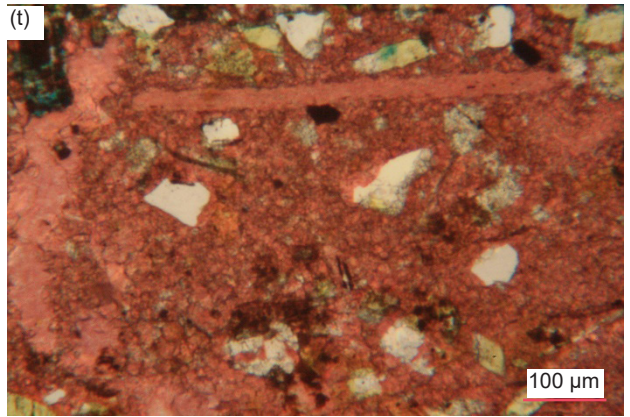
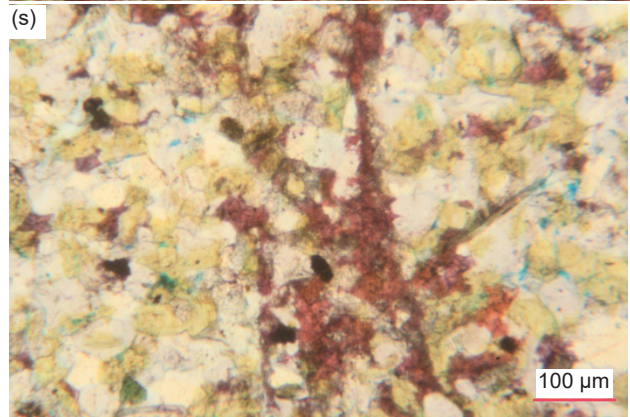
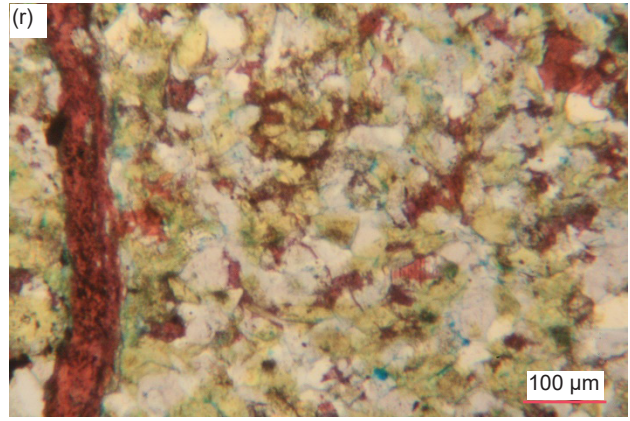
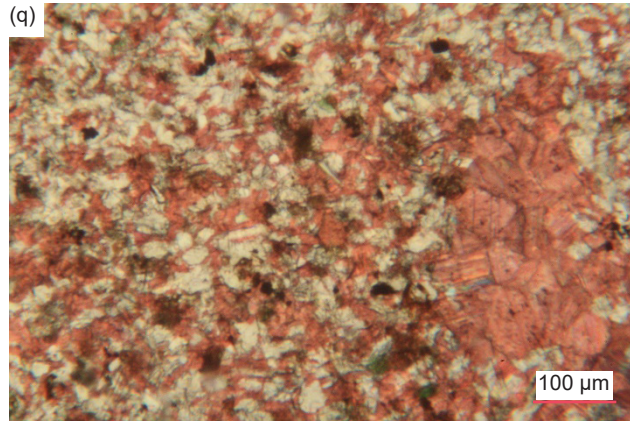
and stained with iron oxides (or sometimes heavily stained or with streaks of iron oxides).

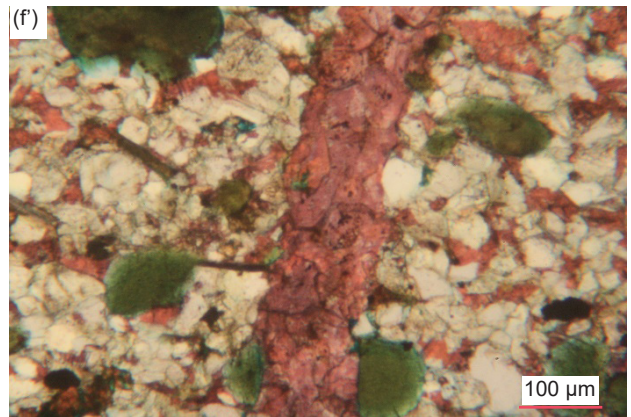
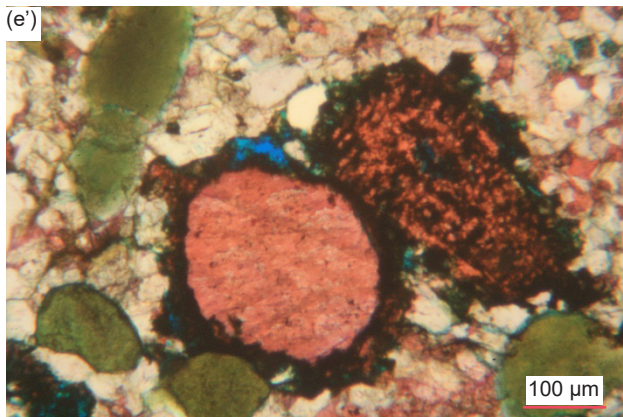
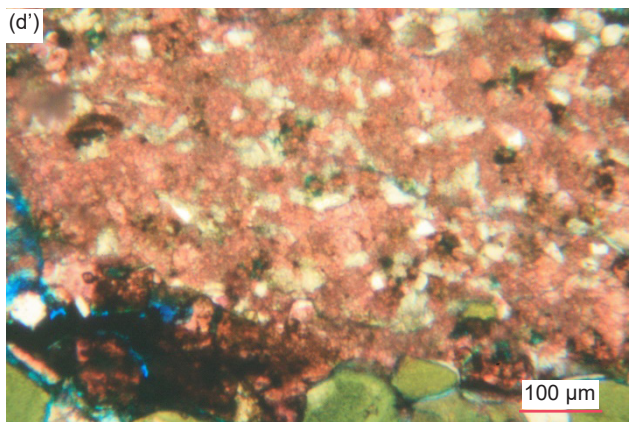
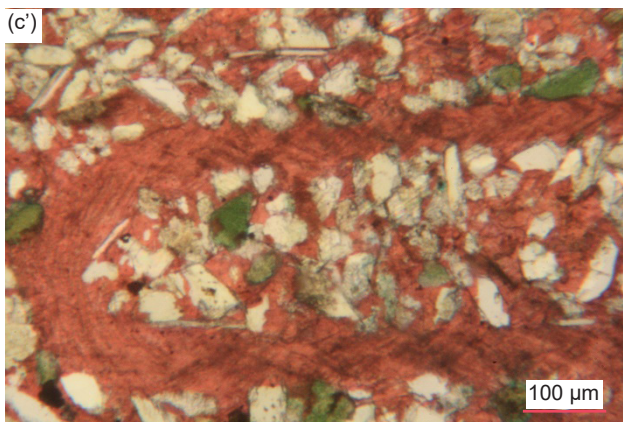
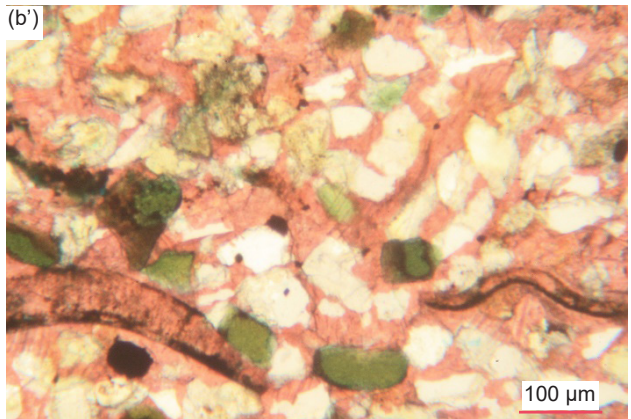
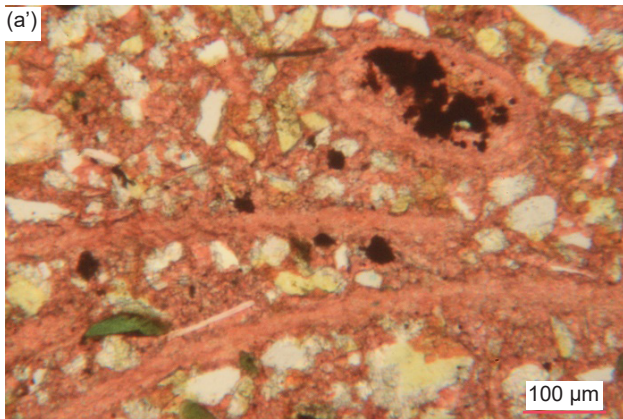
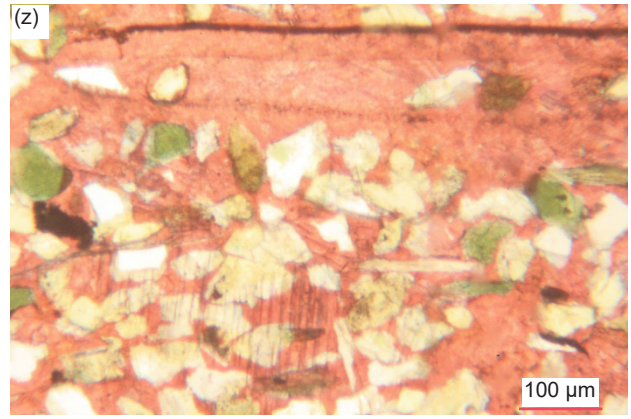
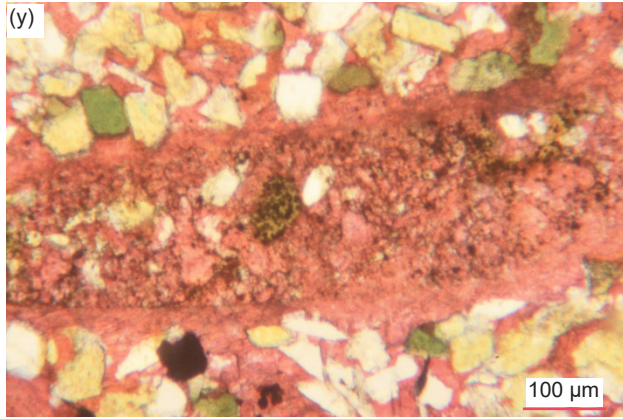
Occasionally within the calcite matrix where it is less iron-oxides-stained some scattered or clumped together tiny-very small (0.03–0.18mm,  $\phi=+5.01$  -  $+2.48$ ) calcite crystals are evident and elsewhere there are small, medium and large blotches, some irregularly-shaped, and thick linear patches of very small to small-medium (0.04–0.30mm,  $\phi=+4.64$  -  $+1.75$ ) bladed tabular calcite crystals with no staining of iron oxides evident, all due to recrystallization. Sometimes these calcite crystals are at various angles grouped together or are medium and large (0.35–0.70mm,  $\phi=+1.50$  -  $+0.52$ ) interlocking platy and sub-euhedral with different extinction angles grouped together, sometimes in unusual patterns enclosing iron-oxides-stained blotches. Elsewhere very small or small recrystallized non-iron-oxides-stained calcite crystals are either thinly scattered or regularly spaced densely through the ultra-fine-grained iron-oxides-stained calcite matrix, with scattered tiny specks and small blotches of iron oxides still present, and sometimes patches of the cleaner recrystallized calcite grains merge with the surrounding iron-oxides-stained dense calcite matrix. And sometimes there is a sharp linear boundary between the densely iron-oxides-stained calcite matrix and the regular “clean” calcite matrix or the smaller-grained recrystallized calcite matrix, and sometimes the boundaries are gradational. In stark contrast, elsewhere some laminae consist of a much coarser-grained mosaic with about equally dominant very small to small (0.07–0.14mm,  $\phi=+3.77$  -  $+2.84$ ) interstitial calcite, and some tiny to very small (0.02–0.07mm,  $\phi=+5.71$  -  $+3.77$ ) dolomite, grains as cement and variably iron-oxides-stained with scattered specks of iron oxides, although adjoining areas are dominated either by interstitial carbonate cement (including some large patches of it) or by other mosaic grains (quartz and K-feldspar).

In some cases, what is likely recrystallized calcite matrix occurs as long and thick, ragged-edged, or round irregular-edged (framboid-like with possible sieve-like texture), micro-crystalline masses that are also iron-oxides-stained, particularly around their edges. Some calcite grains have tiny spots of dolomite replacement around some of their edges, while sometimes the calcite and particularly dolomite cement appears to encroach on mosaic grains such as quartz. Large irregularly-shaped patches of recrystallized calcite engulf several mosaic quartz and K-feldspar grains as well as including some “clean” dolomite grains, so perhaps this recrystallization happened after dolomitization of some of the calcite. Some iron-oxides-stained very small to small (0.04–0.20mm,  $\phi=+4.64$  -  $+2.33$ ), irregular sub-rounded









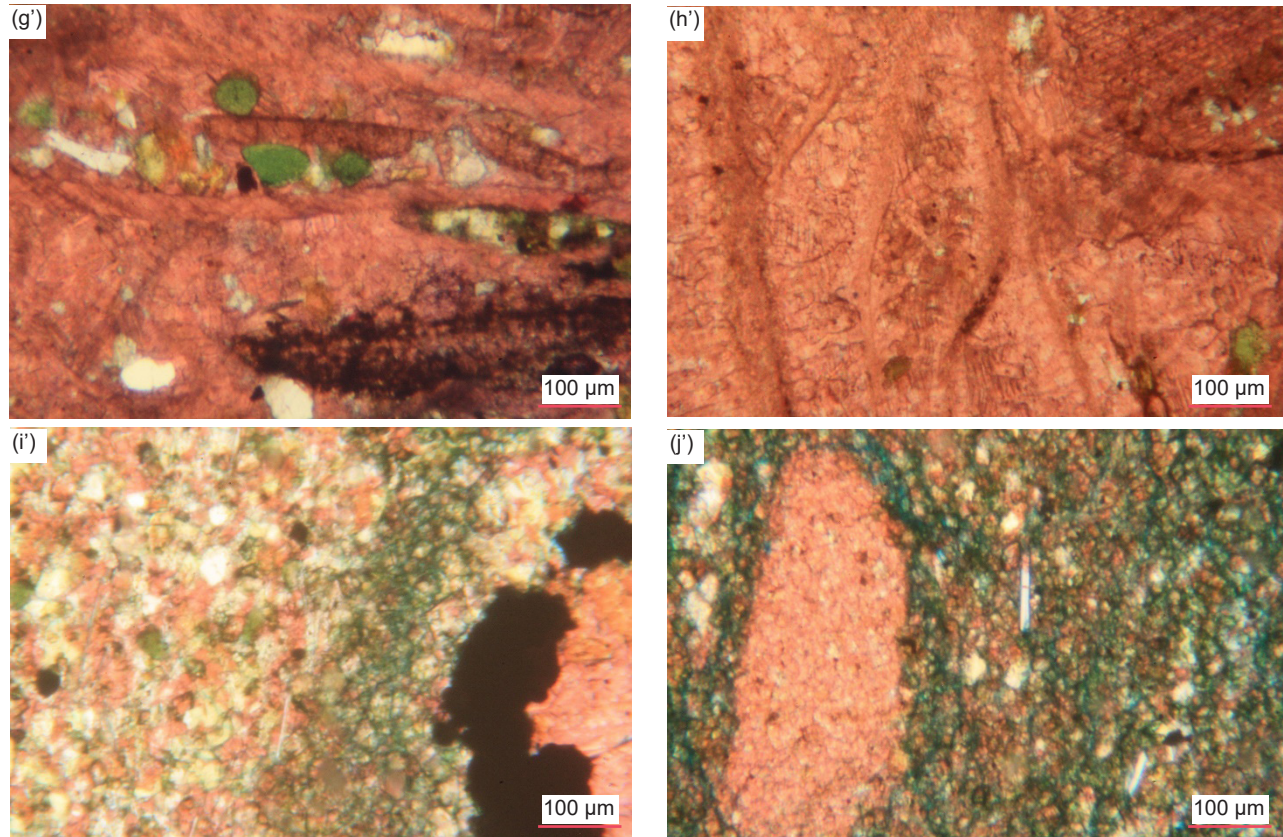


**Fig. 31 (pages 198–202).** A representative set of photomicrographs at various scales (as indicated) showing the calcite grains and crystals in the Muav Formation samples. (a), (b) MLS-01, (c), (d) MLS-02, (e), (f) MLS-03, (g)–(i) MFML-01, (j)–(l) MFML-02, (m), (n) MFML-03, (o)–(q) MFML-04, (r), (s) MFML-05, (t), (u) MFML-06, (v)–(x) MFTB-01, (y)–(a) MFTB-02, (b), (c) MFTB-03, (d)–(f) MFTB-04, (g), (h) MFTB-05, (i), (j) MFTB-06

calcite grains which look like framboids have their perimeters surrounded by dolomite replacing the calcite. Another area consists of a very large platy calcite crystal with very few K-feldspar and quartz grains embedded in it, but with remnants of the regular ultra-fine-grained calcite matrix (with more K-feldspar and quartz grains set in it) from which it recrystallized. Several sharply defined areas of the densely iron-oxides-stained ultra to fine-grained calcite matrix are ovoid in shape, surrounded by relatively “clean” recrystallized matrix. Sometimes the calcite matrix has been recrystallized into various shapes from thin and thick linear to irregular ovoids to micro-crystalline large patches, relatively free of iron oxides, consisting of very small (0.15–0.23mm,  $\phi=+2.75 - +2.13$ ) to small-medium (0.30–0.62mm,  $\phi=+1.75 - +0.69$ ), platy calcite crystals and rhombs at different extinction angles (sometimes with quartz and K-feldspar grains still embedded in them). Alternately, the large-huge patches of calcite matrix have been recrystallized into one or several larger calcite crystals (as evident from the distinctive single “rhomboidal” cleavage and each being at different extinction angles) that fully or only peripherally include quartz and K-feldspar grains and fragments.

Several medium and large recrystallized calcite crystals appear to be sub-angular to sub-rounded clasts that are surrounded by a matrix consisting of small and very small calcite crystals (some of which also look like clasts) with K-feldspar and quartz grains included. Two larger rounded and ovoid patches of calcite matrix, one spattered heavily with iron oxides and both consisting of recrystallized calcite, are outlined by heavy iron-oxides-staining and also appear to be like “pellets” or rounded clasts.

Calcite replaces or coats several small or long, thick, bent or broken edge-on muscovite flakes with frayed ends. In other places, calcite appears to replace or coat some K-feldspar mosaic grains, either wholly, partially or along internal cracks. And in another sample, some glauconite grains are partially altered and/or replaced by calcite stained with iron oxides especially heavily along internal cleavage cracks.

In one sample, two thick veins consisting of small calcite crystals of various shapes at different extinction angles cross-cut the rock fabric almost perpendicular to the bedding, meandering around glauconite grains but cutting through quartz and K-feldspar grains and separating their pieces. Elsewhere, a thick double small-medium-sized crystal width calcite vein

cross-cuts the regular fine-grained calcite matrix at an angle almost perpendicular to the bedding. And in another sample, thin parallel stringers and veins of calcite, sometimes accompanied by elongated blotches and stringers of iron oxides, cross-cut the rock fabric approximately perpendicular to the bedding and appear to fill fracture zones, sometimes close together or even anastomosing. In one instance, one of these thin veins of calcite cross-cuts the rock fabric at a lower oblique angle to the bedding with the calcite generally iron-oxides-stained at the vein edges which are at a fairly consistent width apart. In all these instances, there does not appear to have been any fracturing, crushing or dislocation of mosaic grains during the introduction of the veins along the fracture planes and zones. Elsewhere along another possible fracture, at an oblique angle almost perpendicular to the bedding, the calcite matrix has been recrystallized to adjoining, very small, almost non-iron-oxides-stained calcite crystals (similar to those scattered through the matrix).

In the sample containing large glauconite grains or pellets there are several very large, elongated and flattened pores (or they could be dissolution holes as they are much larger than any of the mosaic grains) that are lined thickly with calcite heavily stained by iron oxides, with the calcite crystals grown inwards to infill the remaining spaces.

#### *Shell Fragments*

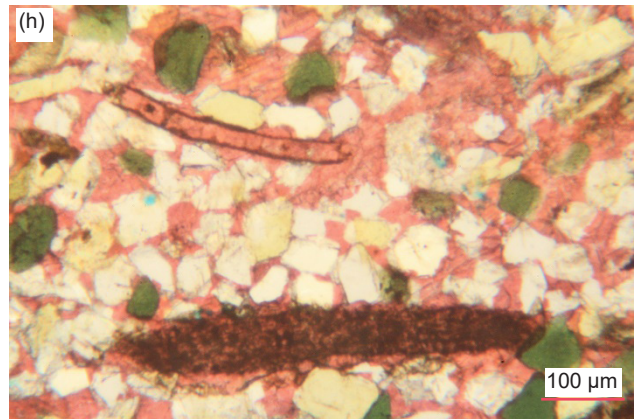
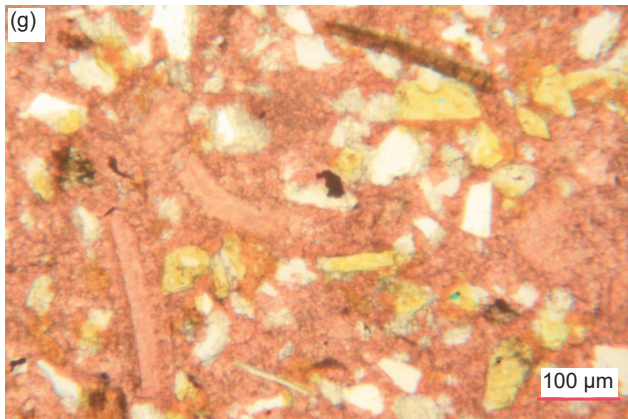
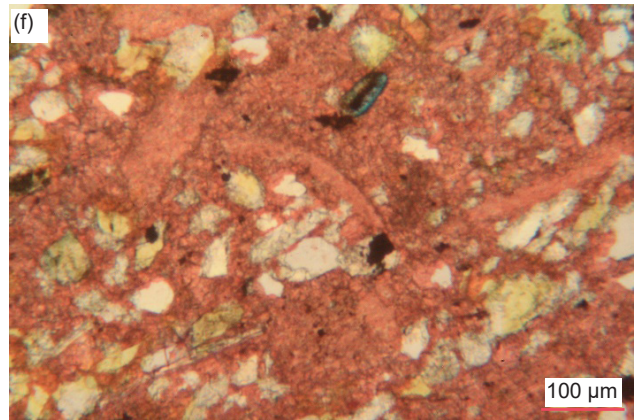
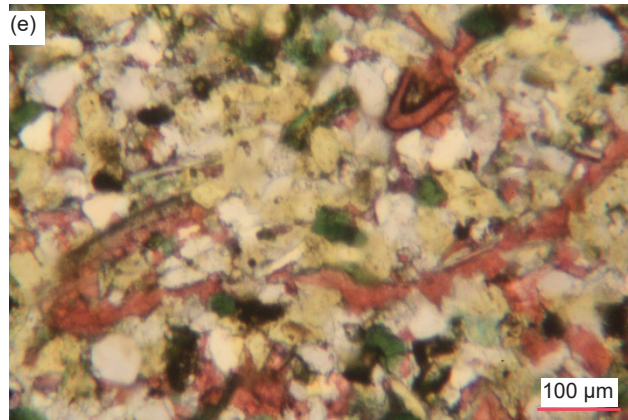
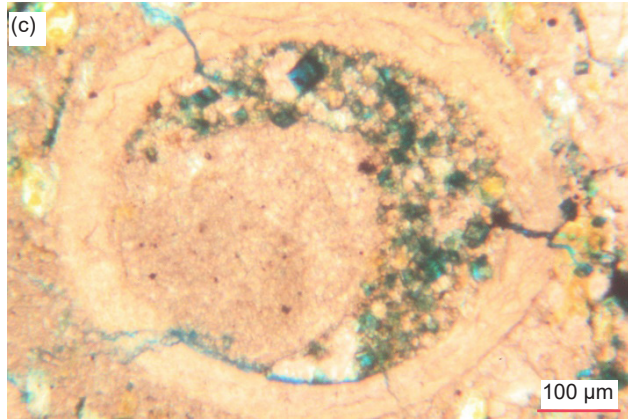
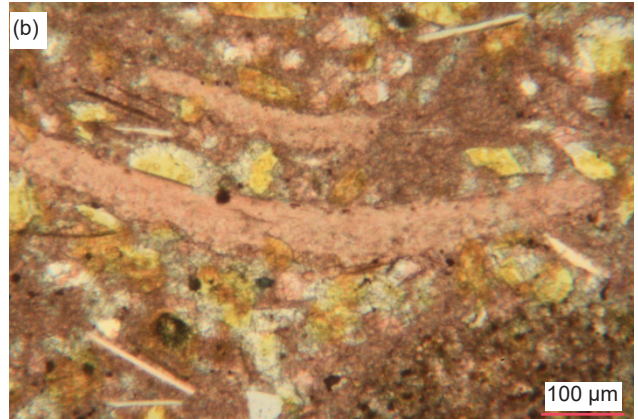
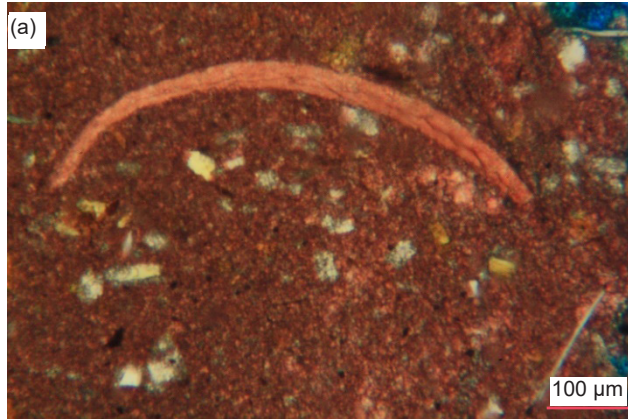
Scattered through some samples are relatively long, thin/narrow, sometimes thicker, curvilinear, linear, ovoid or “worm-like” patches of tiny to very small, recrystallized calcite grains similar to the calcite matrix that are very clearly the edge-on cross-sections of fossilized shells of mostly brachiopods but sometimes probably bivalves (fig. 32). Sometimes the calcite within these fossil shell cross-sections is stained or speckled by iron oxides. Sometimes they have apparent internal divisions suggestive of internal chambers, as well as the internal calcite matrix hosting tiny quartz and K-feldspar grains and even edge-on muscovite flakes. Additionally, some curved, linear, V-shaped and flattened ovoid zones of similar recrystallized calcite grains to those within the calcite matrix, that are iron-oxides-free but often outlined by iron oxides, are likely also edge-on slices through brachiopod, bivalve or even gastropod or some other fossil shells. In one sample some of these apparent cross-sections though fossil shells consist of iron-oxides-stained micro-crystalline dolomite, which must have replaced the original micro-crystalline calcite. In another sample, these curvilinear cross-sections are sometimes bent, some completely bent over, while one fossil shell cross-section is so thick it appears to be rectangular. And in yet another sample,

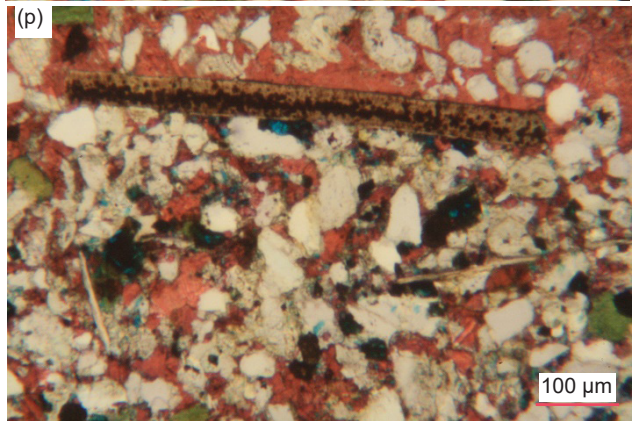
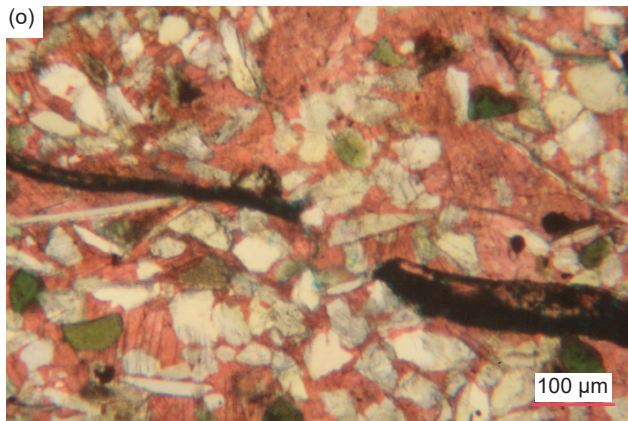
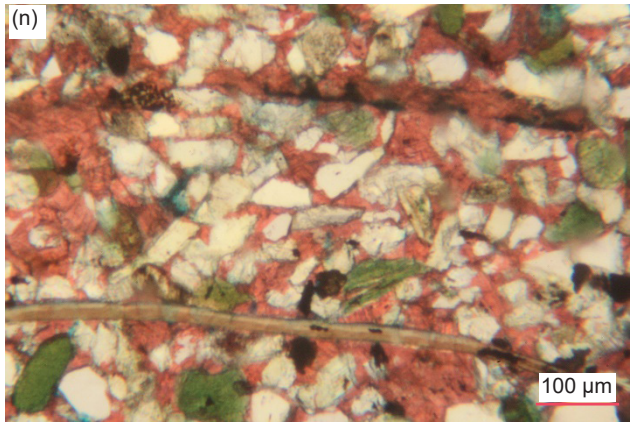
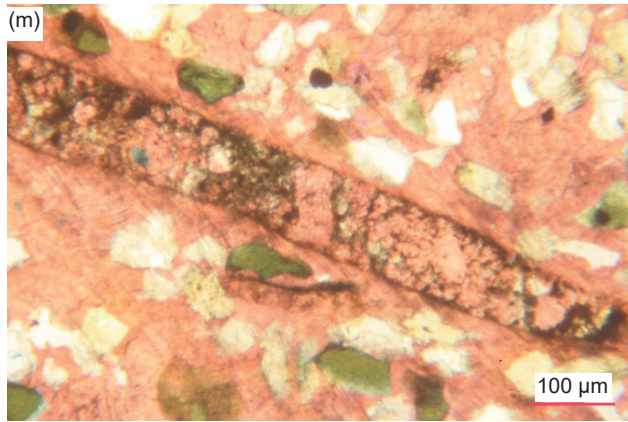
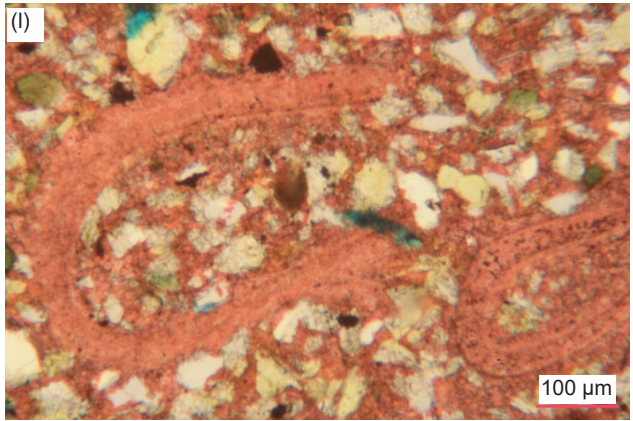
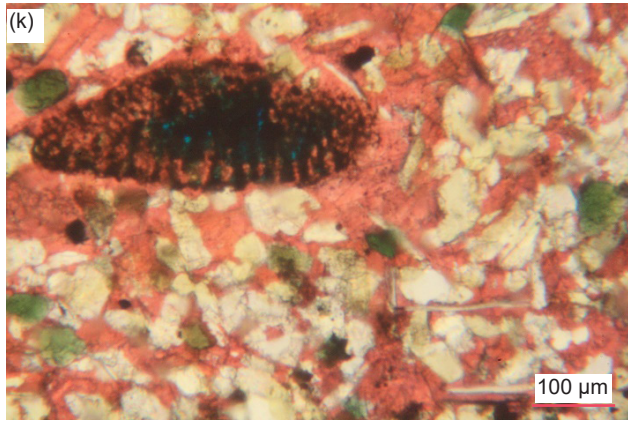
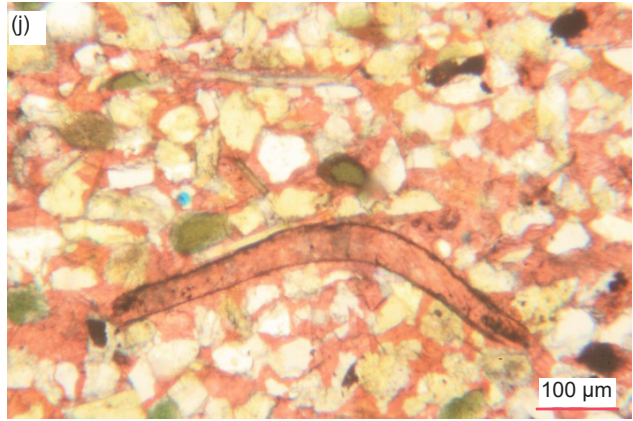
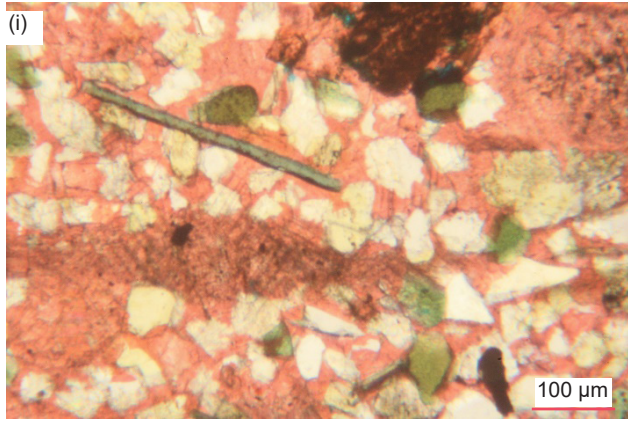
thin or thick, variably elongated rectangular grains, sometimes bent, or elongated curvilinear patches are present. They consist of iron-oxides-stained calcite (giving these grains a brownish tinge), or calcite outlined by iron oxides, or illite replacing calcite, and possibly also represent the cross-sections through fossil shells that have sometimes been broken into segments. In some places the calcite grains between the other mosaic grains are more numerous and become the dominant, though still minor, matrix/cement.

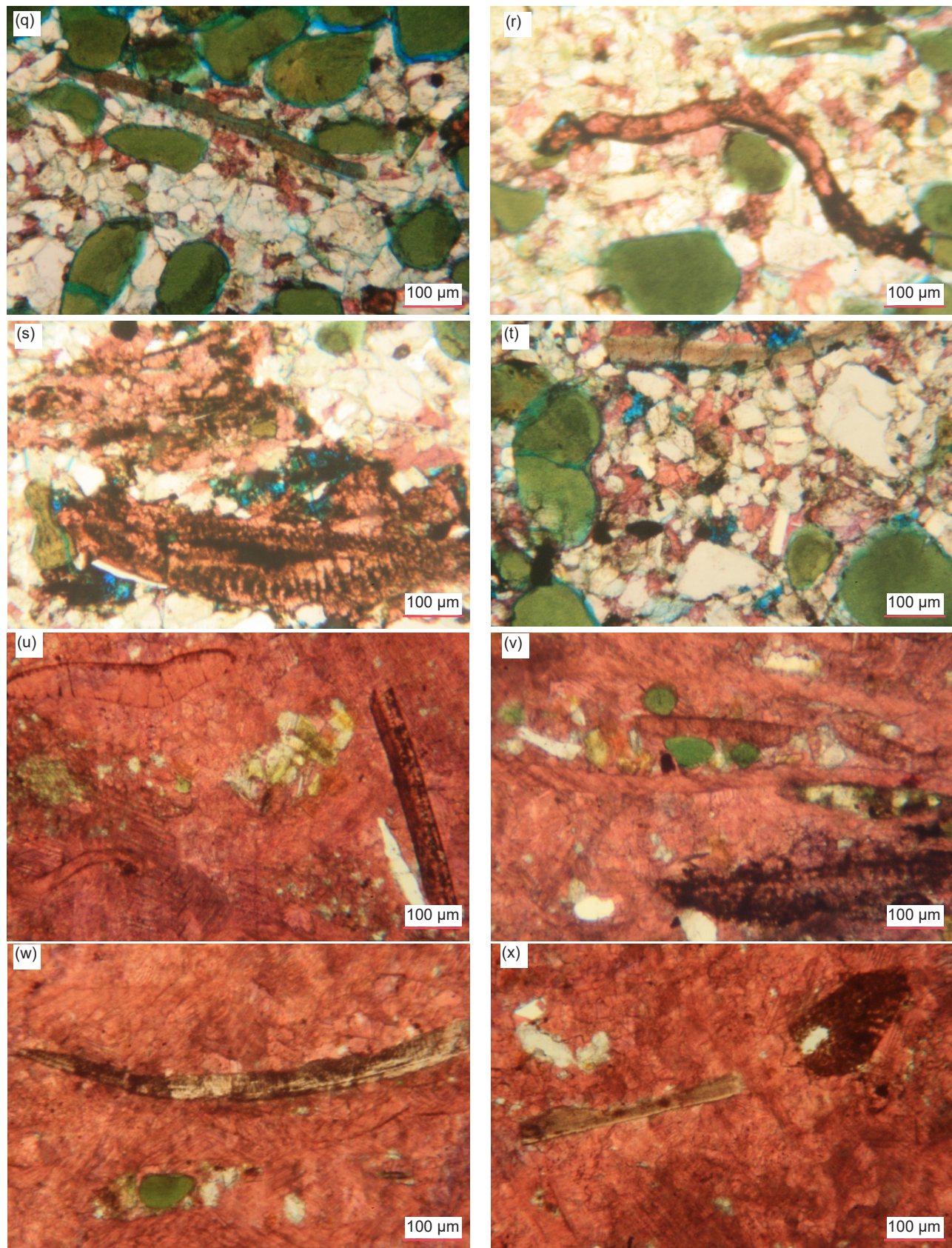
#### *Dolomite*

Dolomite is present in all but one of the 15 samples, usually subordinate to calcite varying from 1.5% to 31.1%, but in one sample dolomite predominates at 81.9% (MFTB-06). In contrast to the calcite grains which are usually pink-stained, the dolomite grains are often easy to identify because they frequently occur as internally clean rhomboidal crystals, though some of the larger crystals have internal “skeletal” growth zones marked by iron oxides, with heavily iron-oxides-stained cores and “clean” outer rims, likely the result of their growth from altering the predominant very-fine-grained (0.01–0.04 mm,  $\phi = +6.72 - +4.64$ ) calcite (micrite) matrix in which they are solidly wedged in continuum with it (fig. 33). The subordinate scattered sub-angular to rounded dolomite grains and fragments, and rhombs in most samples range in size from tiny to very small (0.02–0.06 mm,  $\phi = +5.71 - +4.05$ ), to very small (0.07–0.12 mm,  $\phi = +3.77 - +3.06$ ), small (0.14–0.24 mm,  $\phi = +2.84 - +2.06$ ), medium (0.26–0.36 mm,  $\phi = +1.95 - +1.46$ ) and medium–large (0.39–0.63 mm,  $\phi = +1.36 - +0.67$ ). They are usually randomly distributed in the calcite matrix which they are replacing, though in places the tiny, very small and small dolomite sub-euhedral grains, fragments and rhombs replacing the calcite matrix are clumped together separately with tiny patches of the calcite matrix between them and are outlined by iron oxides and dusted with streaks of light iron oxides, or in some samples are heavily iron-oxides-stained.

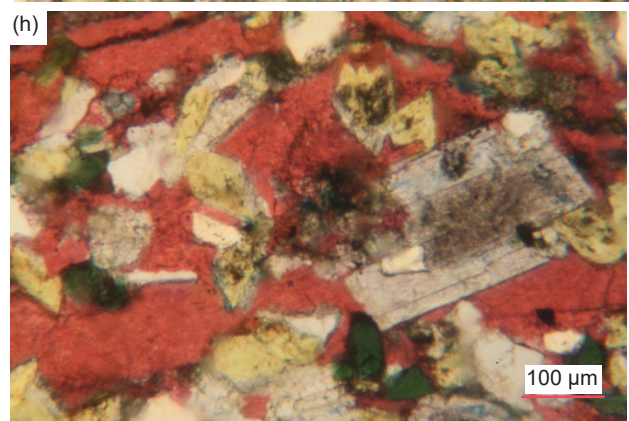
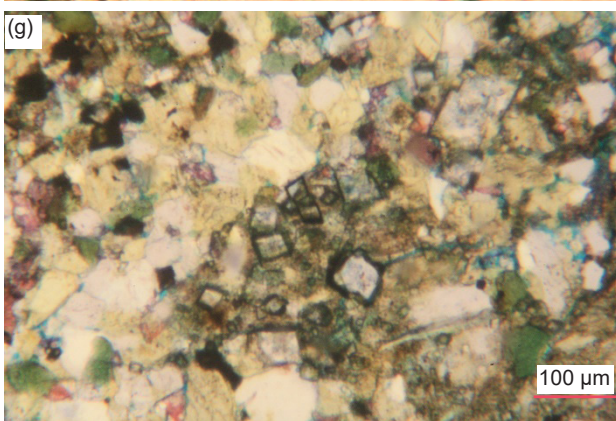
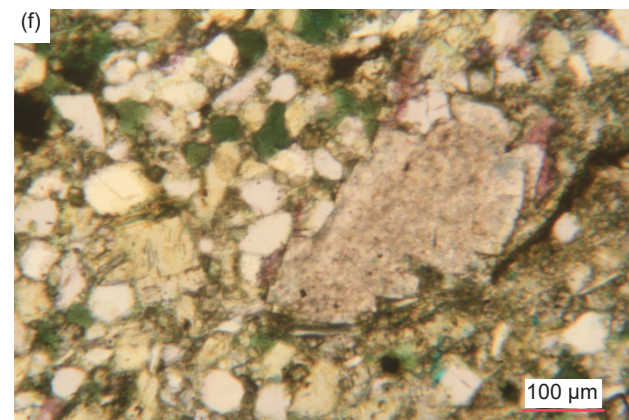
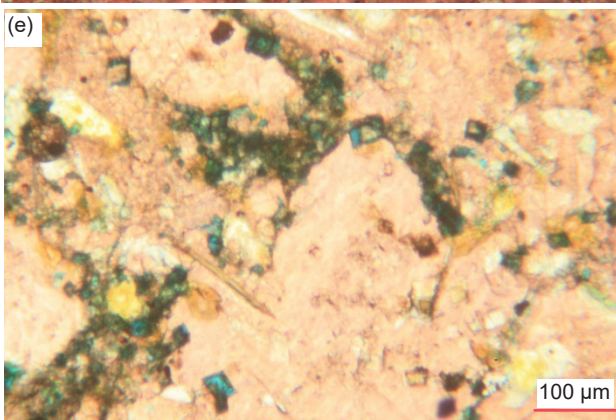
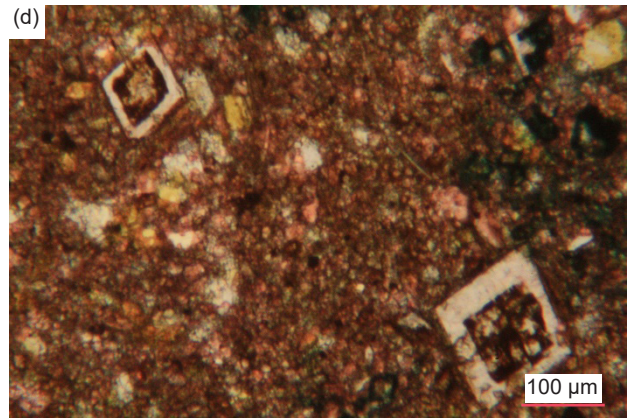
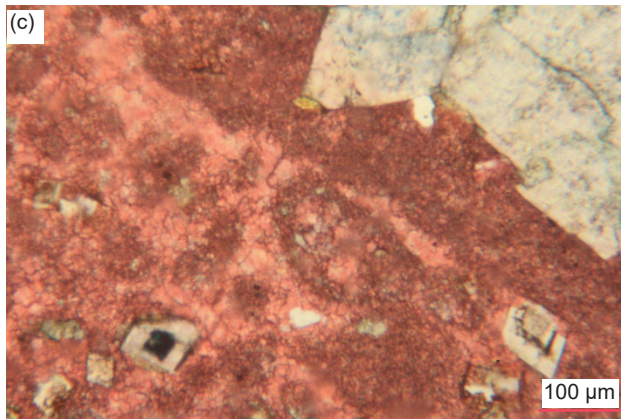
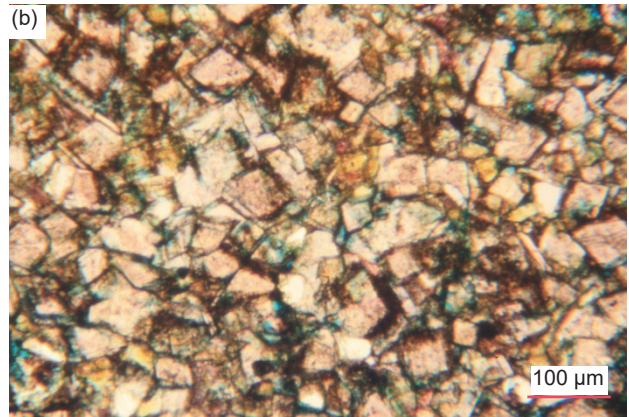
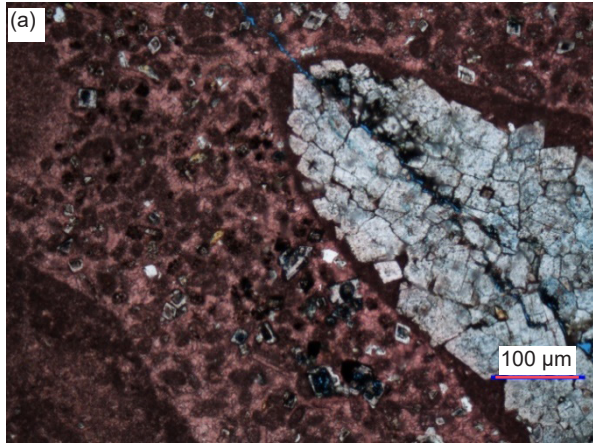
Some sub-euhedral to irregular patches of recrystallized dolomite have mosaic quartz and K-feldspar grains embedded in them, and sometimes also some iron-oxides-stained very small to small (0.04–0.20 mm,  $\phi = +4.64 - +2.33$ ), irregular sub-round calcite grains, some of which look like frambooids or “rosettes” and have their perimeters surrounded by dolomite suggesting dolomite replacement of calcite. Indeed, some of the dolomite patches also have pink-stained calcite cores. In some places, medium to large clumps of the very small densely-packed dolomite matrix grains have cores with the pink stain indicative of calcite, so this is also evidence

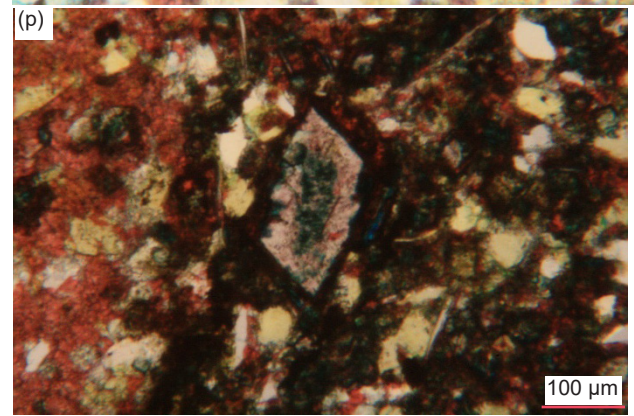
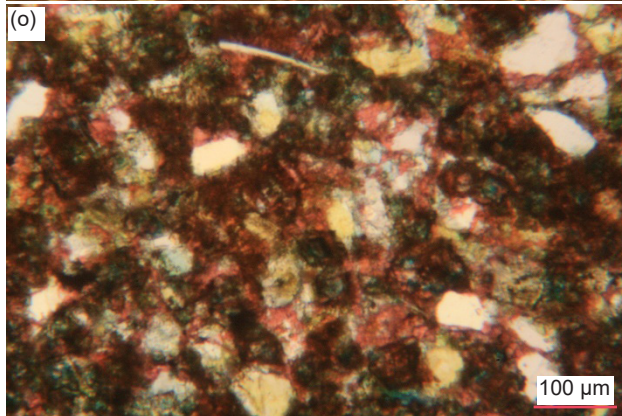
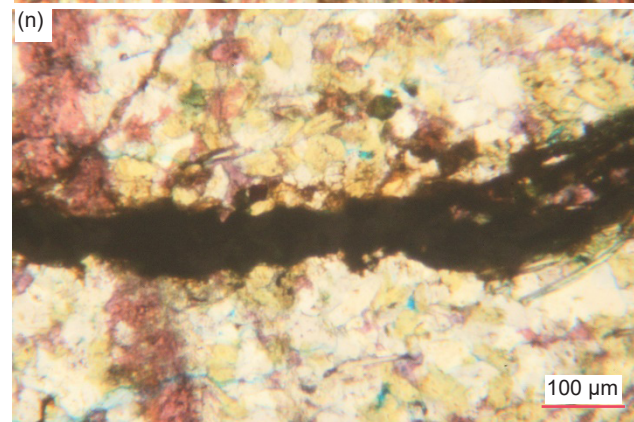
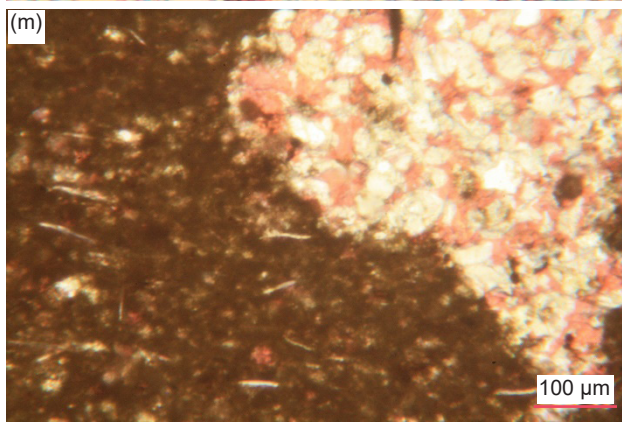
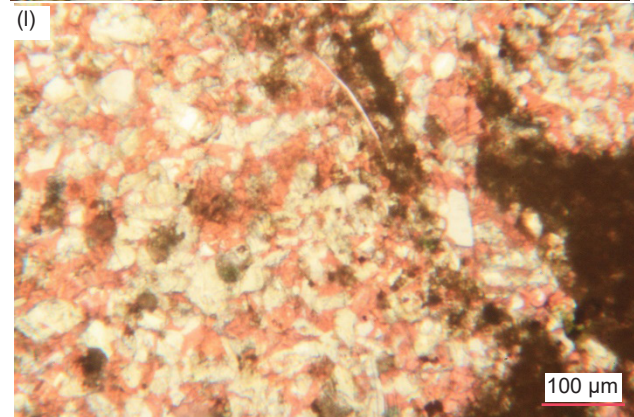
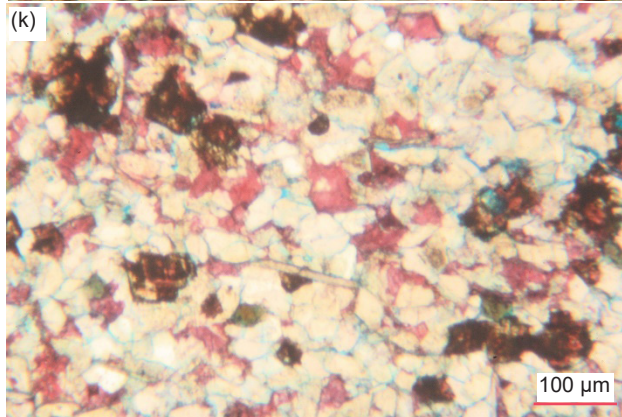
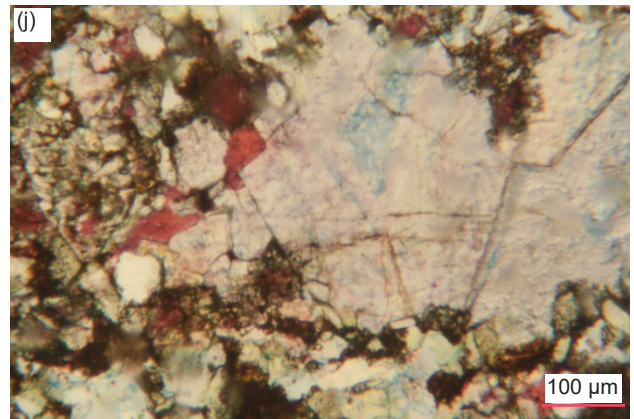
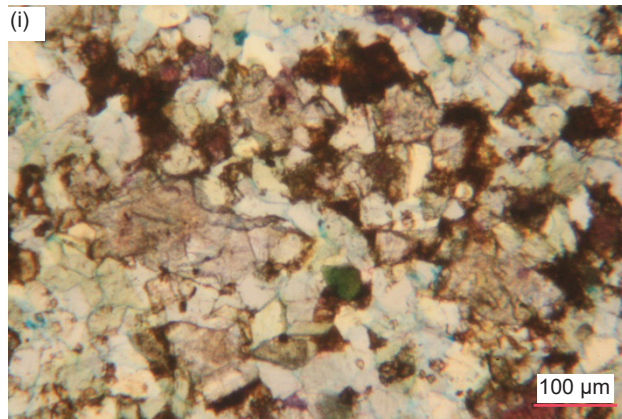






**Fig. 32 (pages 204–206).** A representative set of photomicrographs at various scales (as indicated) showing the shell fragments in cross-section in the Muav Formation samples. (a) MLS-02, (b), (c) MLS-03, (d), (e) MFML-01, (f), (g) MFML-06, (h)–(l) MFTB-02, (m)–(p) MFTB-03, (q)–(t) MFTB-04, (u)–(x) MFTB-05





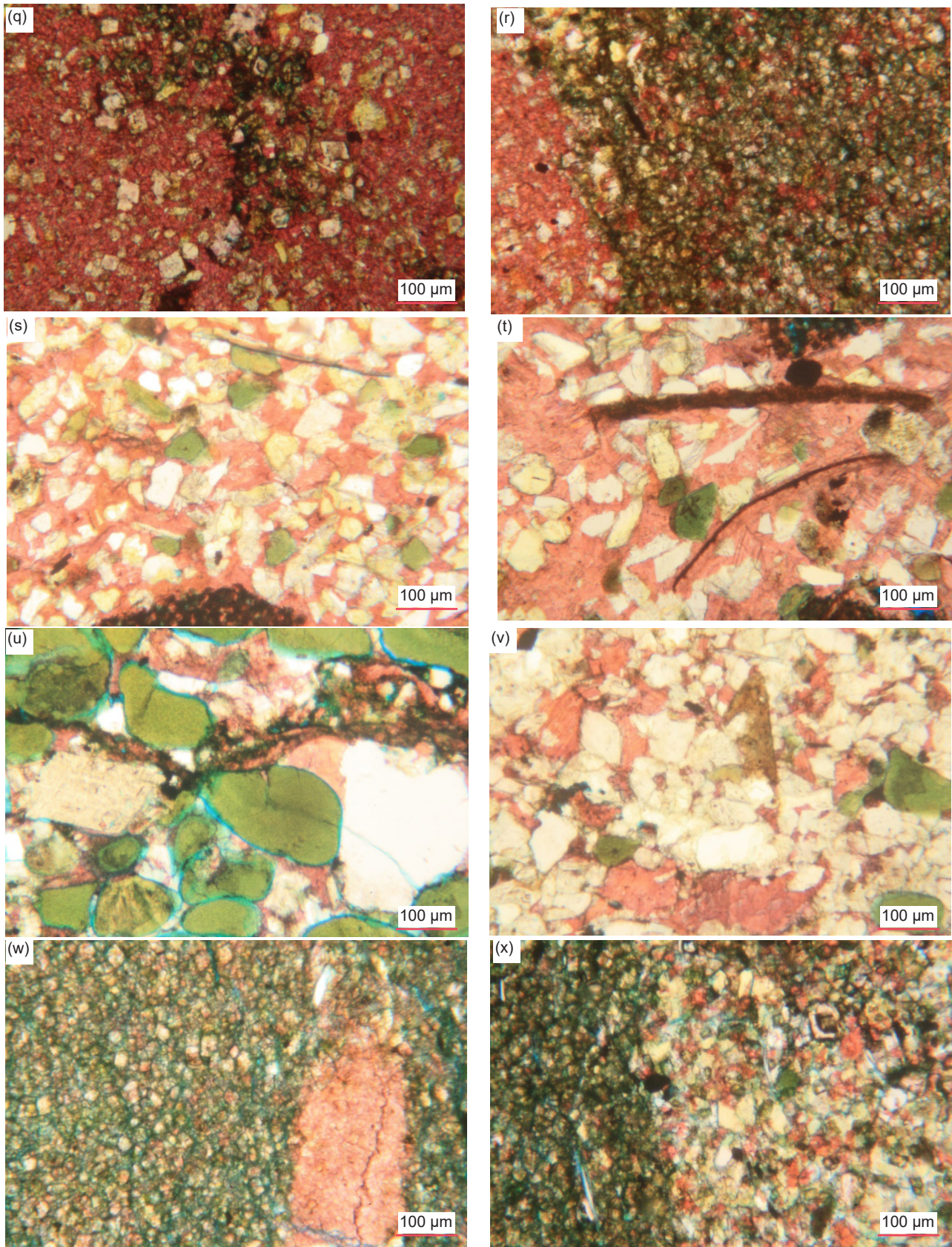


**Fig. 33 (pages 207–209).** A representative set of photomicrographs at various scales (as indicated) showing the dolomite grains and crystals in the Muav Formation samples. (a)–(c) MLS-01, (d) MLS-02, (e) MLS-03, (f) - (h) MFML-01, (i), (j) MFML-02, (k) MFML-03, (l), (m) MFML-04, (n) MFML-05, (o), (p) MFML-06, (q), (r) MFTB-01, (s) MFTB-02, (t) MFTB-03, (u), (v) MFTB-04, (w), (x) MFTB-06.

that dolomite has replaced calcite. In contrast, in another sample several huge patches or bands of recrystallized dolomite consist of large, minimally iron-oxides-stained, sub-euhedral “platy” crystals adjoining one another and generally meeting at triple points with minimal inclusion of other mosaic grains.

In one sample, in one huge circular area, there are numerous medium-large (0.39–0.56 mm,  $\phi=+1.36 - +0.83$ ) (and smaller near the curved edge) dolomite rhombs packed tightly together and set in the calcite matrix with nearby scattered tiny and small dolomite rhombs with internal growth zones marked by iron oxides. In places some of the dolomite rhombs, particularly the larger rhombs, are broken with offset fragments still together. In another place, there is a large, rounded clump of tightly interlocking small to small-medium dolomite rhombs dusted with, and cleavages marked by, iron oxides, and with a touch of pink staining in spots perhaps indicative of some partial calcite substitution. And some clumps of dolomite rhombs appear to have been somewhat broken apart with, or due to, some calcite substitution or replacement.

In a few samples, dolomite forms the matrix with tiny to very small (0.02–0.12 mm,  $\phi=+5.71 - +3.06$ ) densely-packed grains and rhombs that are stained with iron oxides, which is minor in some areas but is a major part of the rock fabric in other areas. Any interstitial calcite grains likely represent remnants of the original limestone. Occasionally the dolomite matrix has been recrystallized into very small to large (0.11–0.76 mm,  $\phi=+3.19 - +0.40$ ) irregularly-shaped and raggedly-shaped or sub-euhedral to sub-angular crystalline patches (or sometimes micro-crystalline patches that have included other mosaic grains in them) or crystals that still cement some of the mosaic, or has been recrystallized into tiny, very small and small (0.03–0.23 mm,  $\phi=+5.01 - +2.13$ ) rhombs outlined by iron oxides. In one sample, there are often sharp lines of demarcation between bands of dolomite-dominated-matrix that predominates the rock’s fabric and of calcite-dominated-matrix. But even in the latter, dolomite grains and rhombs are scattered in the calcite matrix interstitial to the K-feldspar and quartz grains, suggesting variable incomplete dolomitization. Sometimes there are a few very small “clean” (iron-oxides-“free”) and “skeletal” structured dolomite rhombs scattered within both the calcite and dolomite dominated matrixes, which suggests some recrystallization of dolomite has occurred.

In several samples, some scattered minor tiny to small (0.02–0.20 mm,  $\phi=+5.71 - +2.33$ ) dolomite grains appear to partially replace similar-sized K-feldspar grains and even some edge-on muscovite flakes.

In some areas the mosaic quartz and K-feldspar grains are much smaller (tiny) and are accompanied by likely dolomite alteration compared to the general mosaic of very small grains. Occasional very small (0.04–0.14 mm,  $\phi=+4.64 - +2.84$ ), sub-euhedral and sub-angular to sub-rounded dolomite grains are wedged within the mosaic between quartz and K-feldspar grains, possibly replacing the interstitial calcite cement and sometimes possibly mosaic K-feldspar grains.

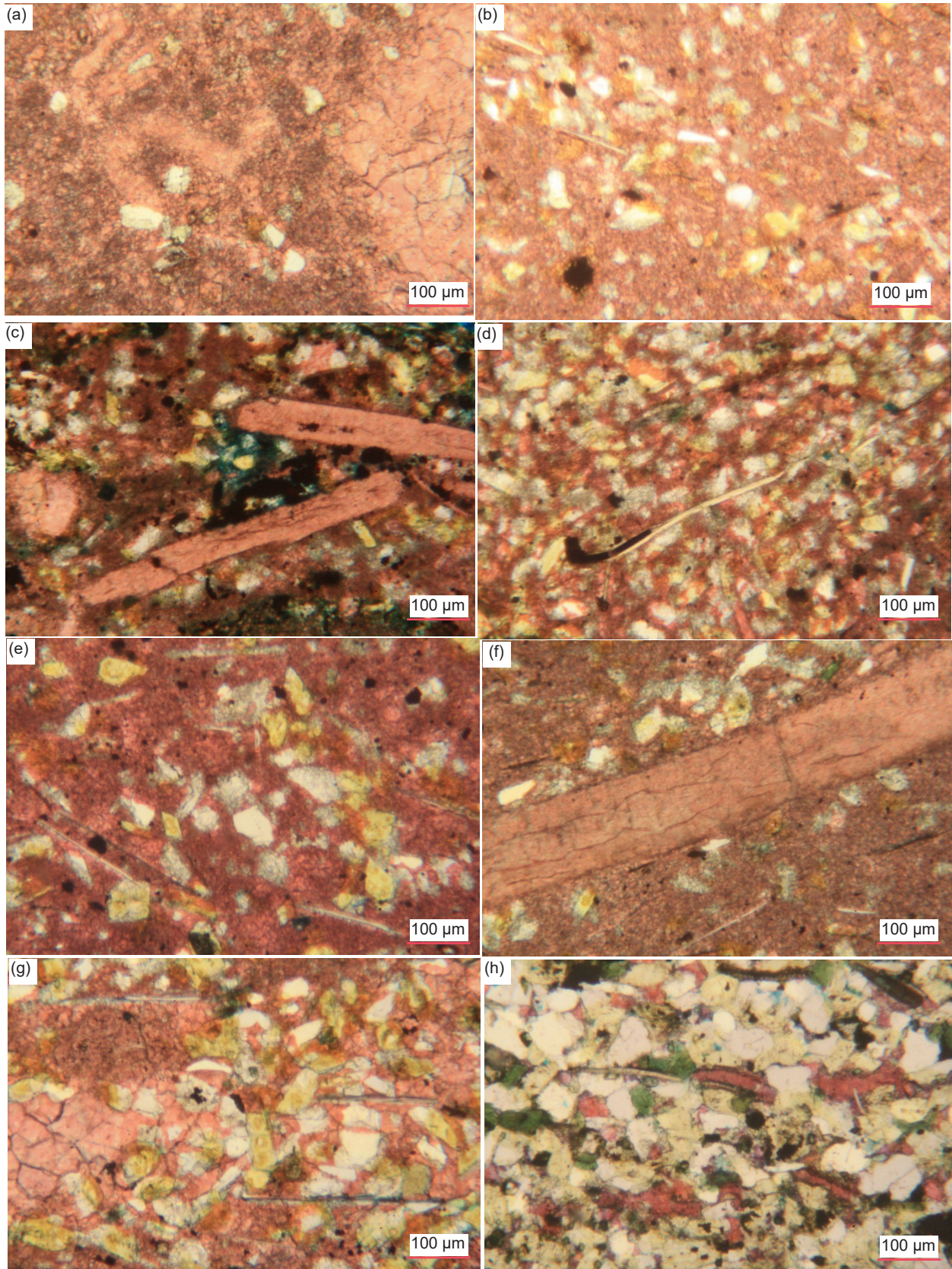
The calcite veins in some samples are sometimes accompanied within them or as a separate veinlet by what appear to be very small sub-euhedral grains of dolomite that may either be replacing the calcite or mosaic K-feldspar grains. Sometimes this dolomite alteration accompanying a calcite vein network also spreads into the adjoining mosaic, having altered the mosaic grains and particularly replaced the calcite cement. In one sample, what appears to be fractures cross-cutting the rock fabric roughly perpendicular to the bedding are filled either with several adjoining elongated, medium-sized “clean” dolomite crystals or with strings of tiny heavily iron-oxides-stained dolomite rhombs, accompanied by elongated patches and streaks of heavy iron oxides.

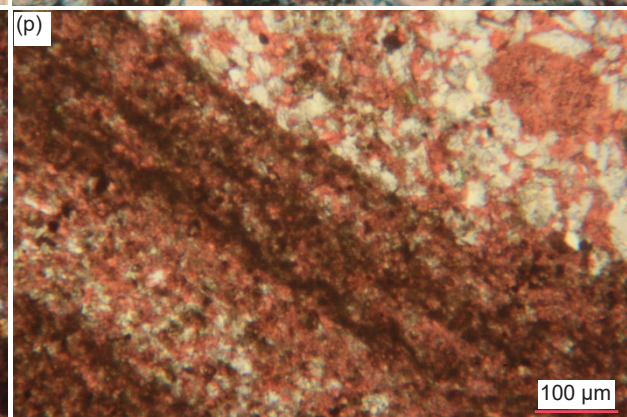
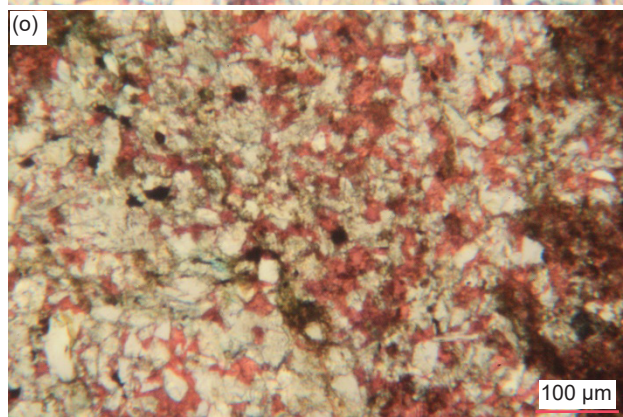
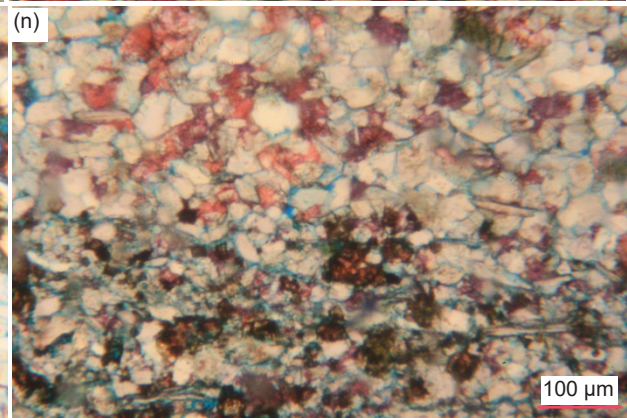
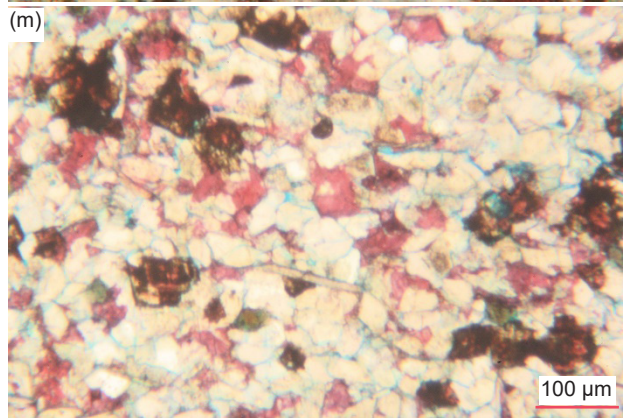
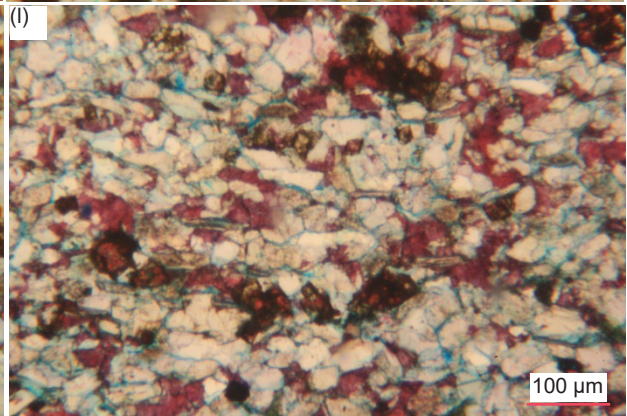
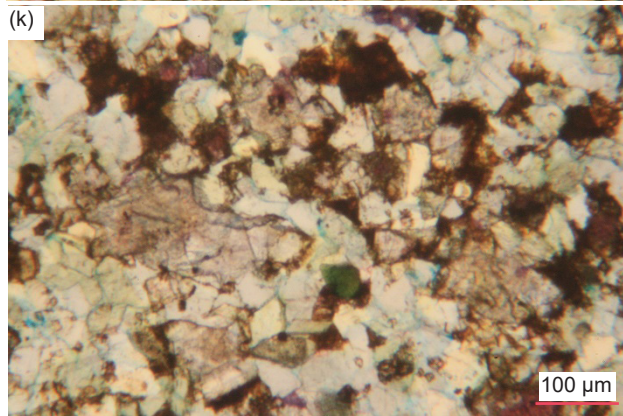
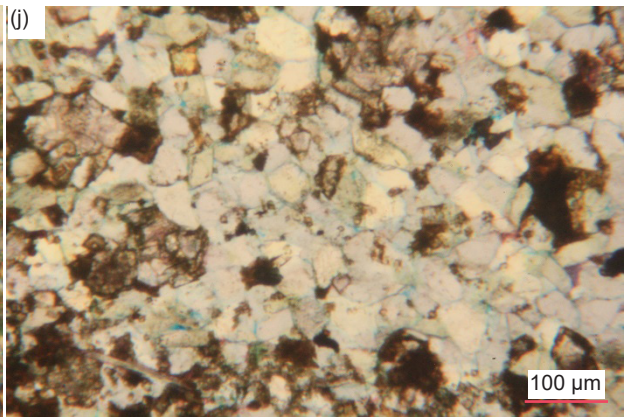
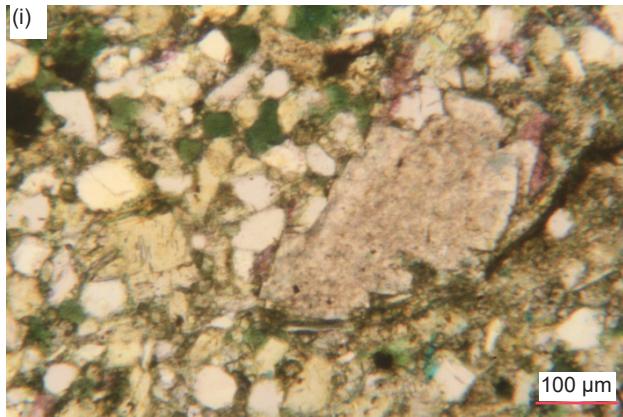
#### *Siderite*

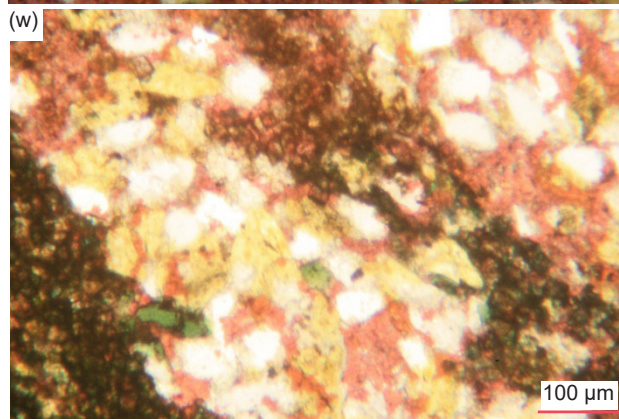
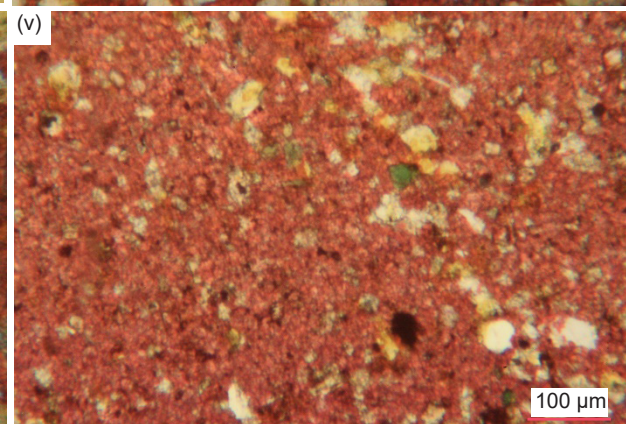
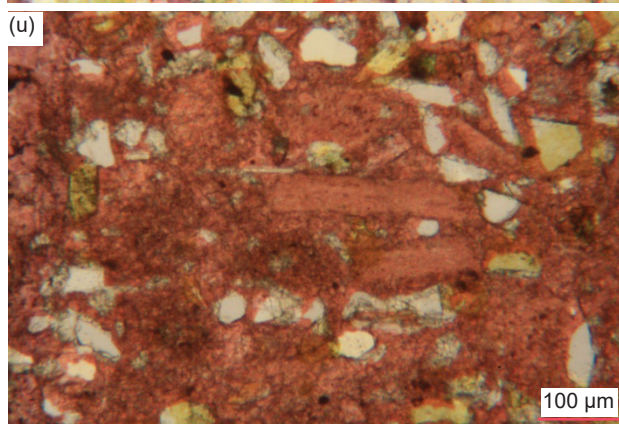
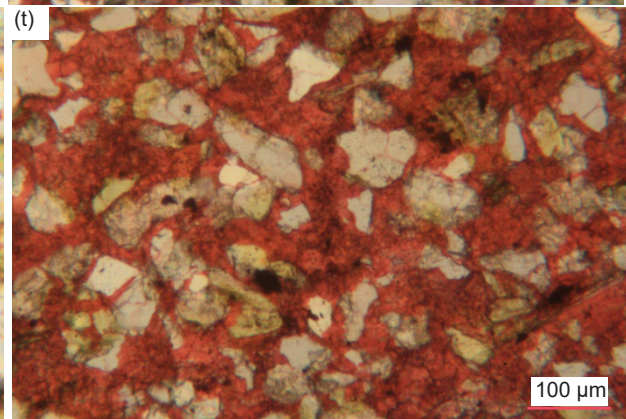
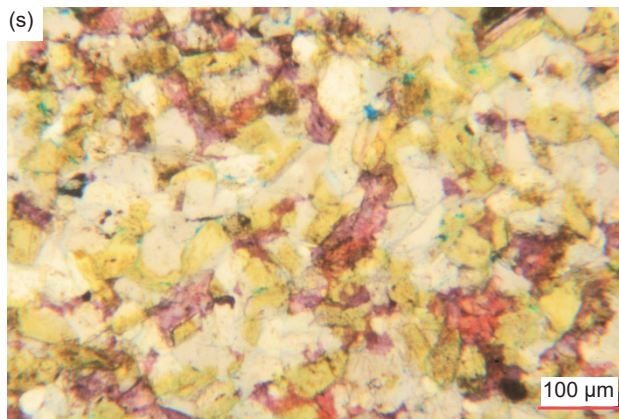
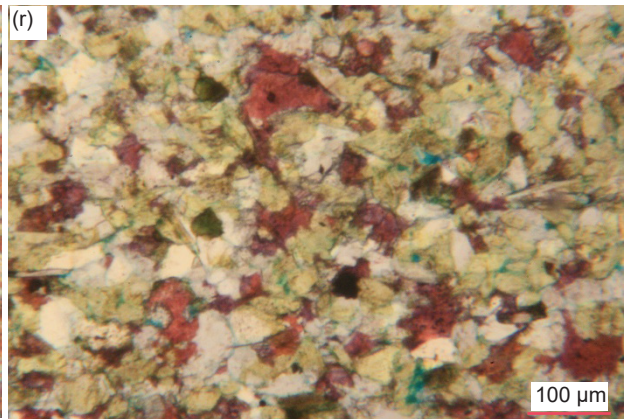
Siderite is only present at 0.8% in one sample (MFTB-03), but it is difficult to distinguish, although in this sample it appears that some siderite replaced a few very small (0.09 mm,  $\phi=+3.47$ ) K-feldspar grains.

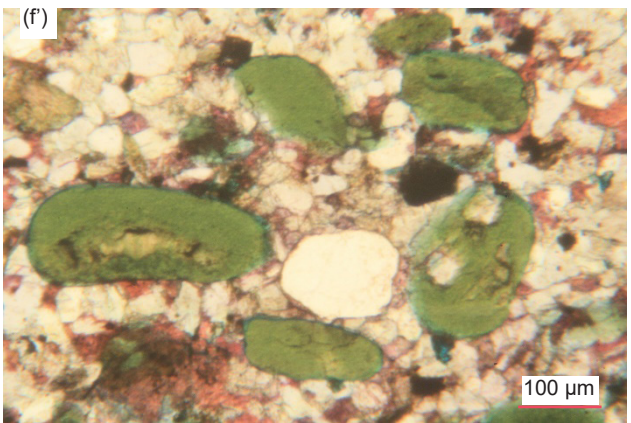
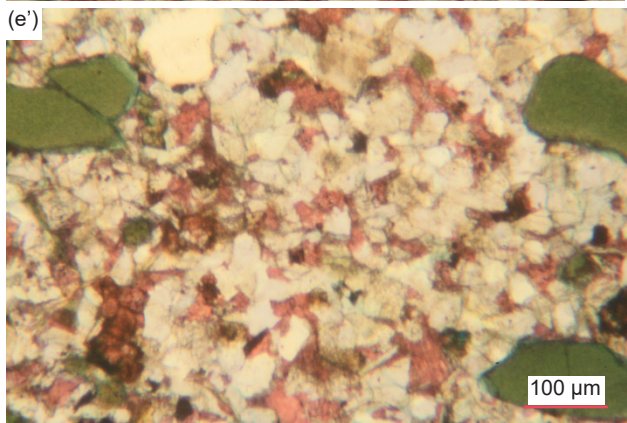
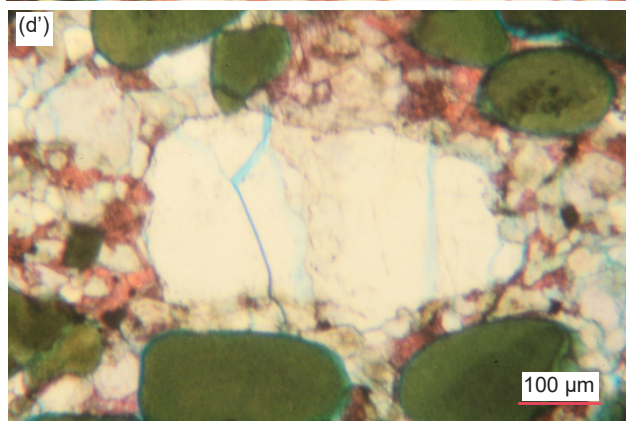
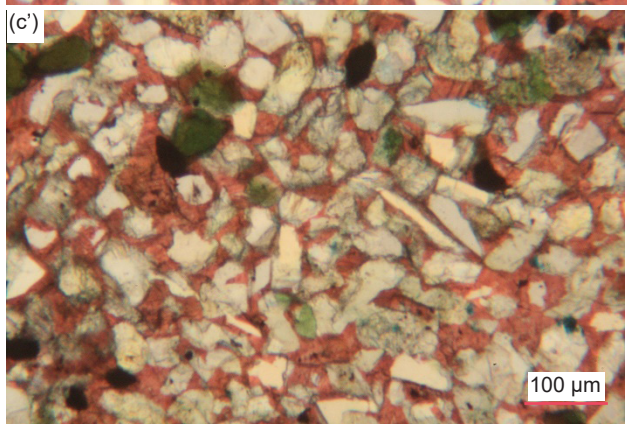
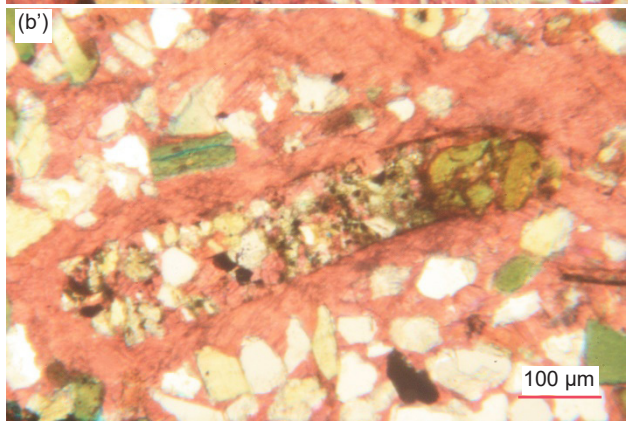
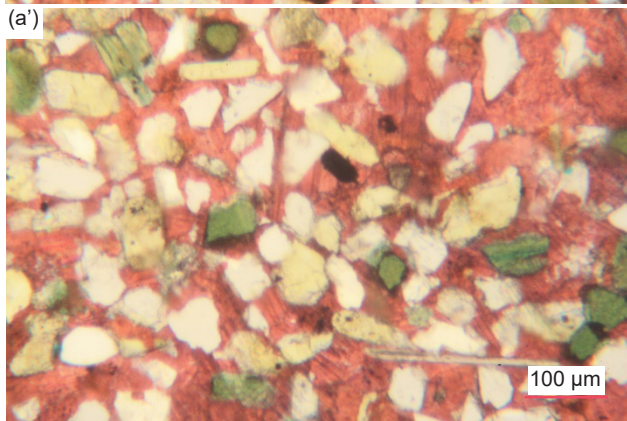
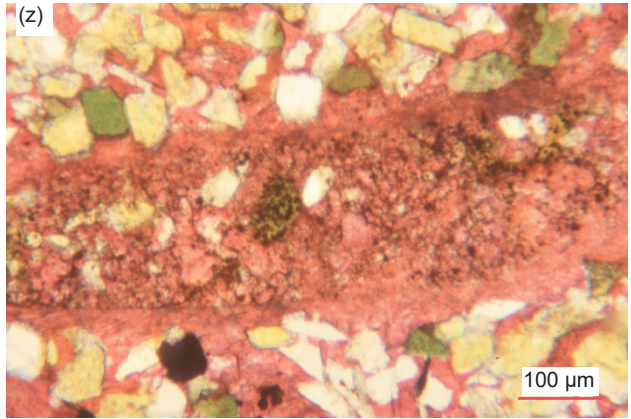
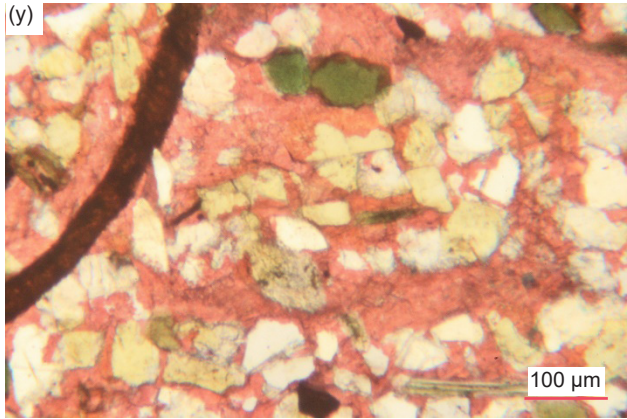
#### *Quartz*

Quartz grains are present in the thin sections of all the samples, ranging from 2.7% to 55.8%, with the content of nine of the fifteen samples being >10% quartz. Invariably the quartz grains are tiny to very small (0.02–0.15 mm,  $\phi=+5.71 - +2.75$ , medium silt to fine sand size), although in some samples there are also a few scattered small to medium grains (0.16–0.50 mm,  $\phi=+2.66 - +1.00$ , fine to medium sand size) (fig. 34). They are mostly sub-angular to sub-rounded, though some are angular and even irregularly-shaped fragments and slivers (some quite elongated and long), and a few are rounded. Some quartz grains have fuzzy/obscured and/or jagged edges, some have internal cracks, and some have been cracked into sub-grains. These variously sized and shaped quartz grains are usually mixed and interspersed with one another, indicative of poor sorting, and are usually scattered (in some samples sparsely) and “floating” in the micrite (fine-grained calcite mud) matrix, though occasionally the density of quartz grains is locally higher.









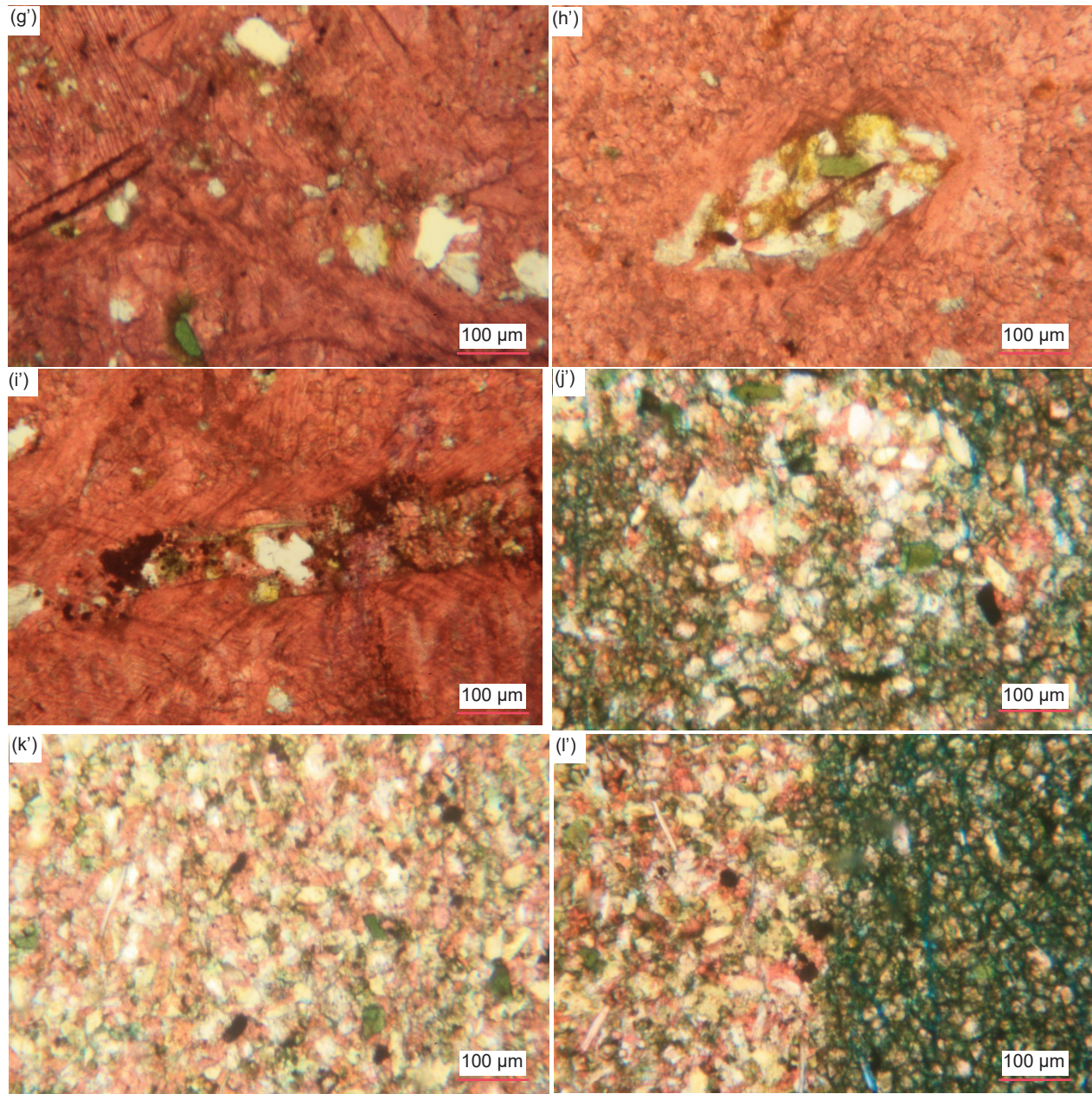


**Fig. 34 (pages 211–215).** A representative set of photomicrographs at various scales (as indicated) showing the quartz grains in the Muav Formation samples. (a) MLS-01, (b)–(d) MLS-02, (e)–(g) MLS-03, (h), (i) MFML-01, (j), (k) MFML-02, (l)–(n) MFML-03, (o)–(q) MFML-04, (r), (s) MFML-05, (t), (u) MFML-06, (v), (w) MFTB-01, (x)–(z) MFTB-02, (a')–(c') MFTB-03, (d')–(f') MFTB-04, (g')–(i') MFTB-05, (j')–(l') MFTB-06.

However, sometimes the variously sized quartz grains are concentrated or more densely packed with accompanying K-feldspar grains in thin laminae (still with some calcite matrix) and occasionally are clumped together, with some or many of the grains in such “aggregates” meeting at triple points. Sometimes the tightly-clumped quartz grains have faint edges, so they look like single very large grains. In one sample, the quartz (and K-feldspar) grains are clustered together in lensoid and ovoid shapes, sometimes clearly outlined as distinctive features, perhaps representing former clasts. The thin laminae

in some samples appear to have slightly larger quartz grains compared to those scattered elsewhere through the calcite matrix or to those in alternating calcite-matrix-dominated laminae. These laminae are clearly depositional, whereas the clumps of grains meeting at triple points could either indicate post-depositional silica cementing of adjoining, in-contact detrital quartz grains, or the clumps are themselves detrital, the triple point cementing have occurred in the source rock prior to its erosion. The former option is clearly evident in some samples where some of the clumped quartz grains have internal “ghost” outlines of faint iron oxides

that suggests original detrital grains were overgrown by silica in optical continuity cementing adjoining quartz and K-feldspar grains into those clumps before or at the same time as calcite cementation occurred. And sometimes where the edge-on muscovite flakes are parallel to the bedding the mosaic quartz (and K-feldspar) grains and the interstitial calcite cement also appear elongated parallel to the bedding, likely being a depositional feature.

In several instances, tiny quartz fragments have been included in medium-sized dolomite rhombs and/or sub-euhedral to irregular dolomite patches, which is consistent with the dolomite being post-depositional replacement of the calcite matrix in which the quartz grains were originally deposited. Similarly, there are in some samples some much larger platy calcite crystals and/or larger irregularly-shaped calcite patches with a few very small quartz grains embedded in them, as well as remnants of the micrite matrix with more very small quartz grains from which the larger platy calcite crystals were obviously recrystallized. And some of the quartz grains even have their edges coated with, or obscured by, calcite, which further suggests there was some post-depositional calcite recrystallization. Furthermore, in one sample (MFTB-04) some of the glauconite peloids have internal/central inclusions of tiny quartz grains around which the glauconite was deposited. Finally, in one sample (MFML-05), in some parts of the rock fabric, the interlocking mosaic of quartz (and K-feldspar) grains appears to be fractured without displacement at an oblique angle to the bedding by a network zone of fractures, making the quartz grains smaller, angular and even elongated aligned parallel to the fracturing. And in another sample, a small-medium-sized subrounded quartz grain is fractured but not displaced, with recrystallization healing through the fracture zone which parallels at the same angle a nearby edge-on muscovite flake and the fractures elsewhere through the rock fabric.

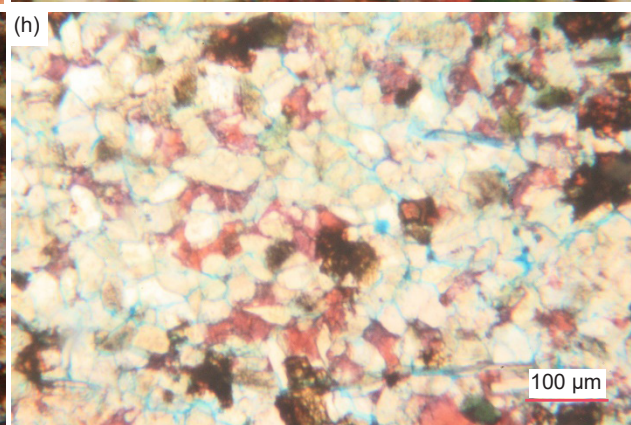
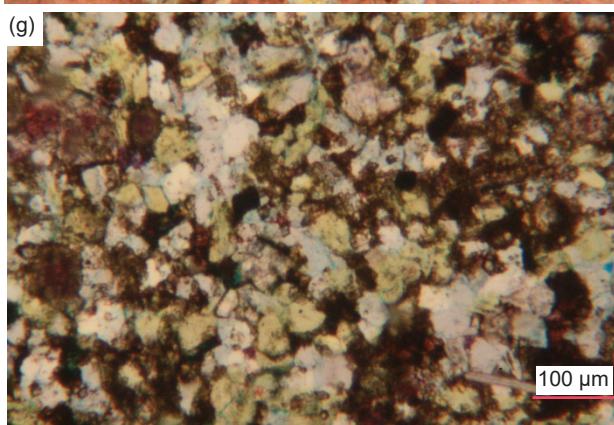
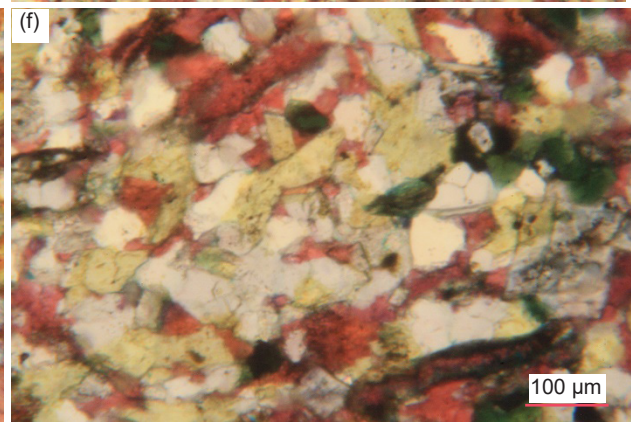
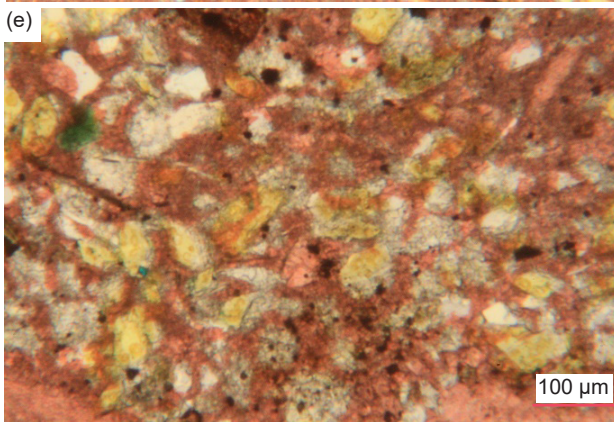
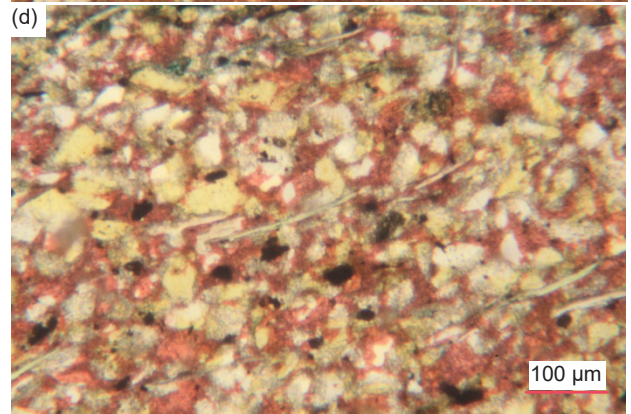
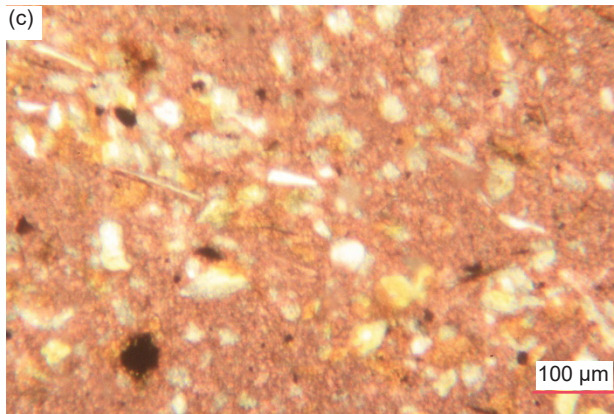
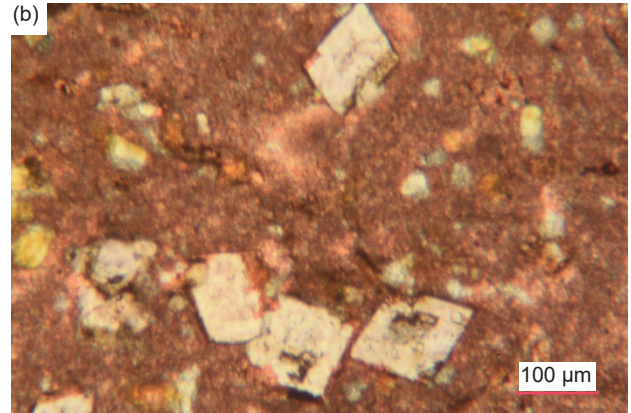
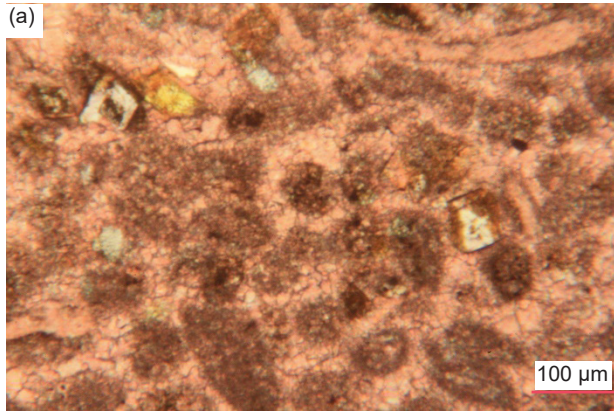
### *K-Feldspar*

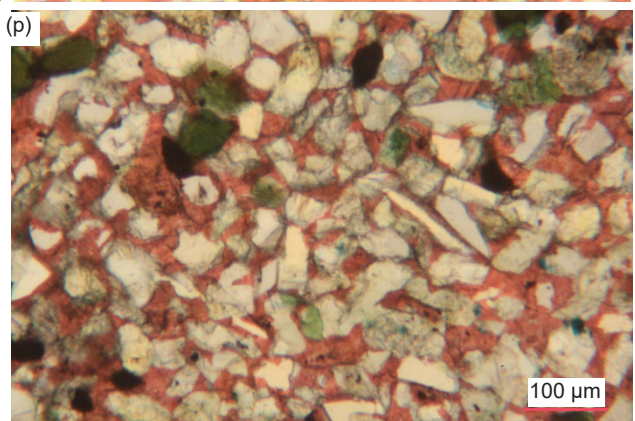
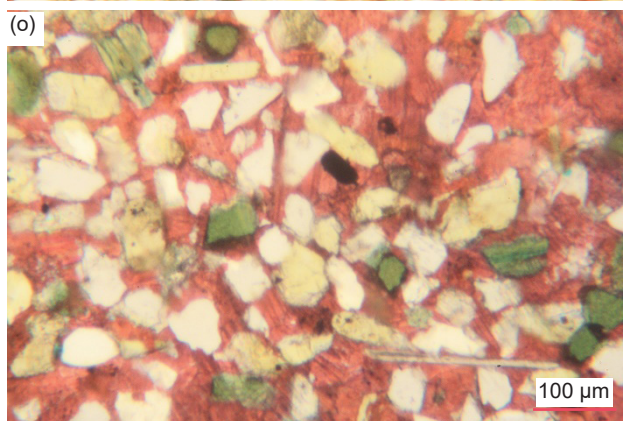
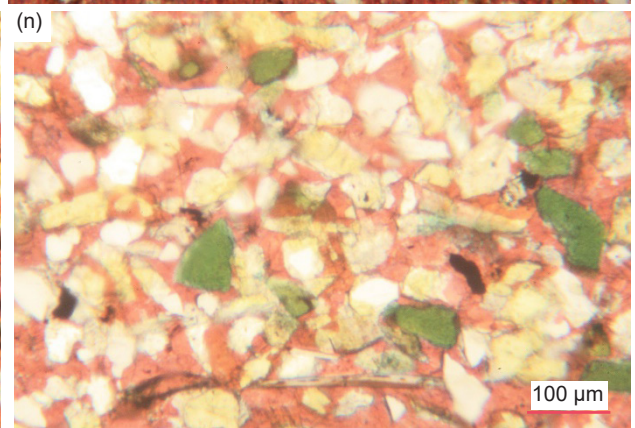
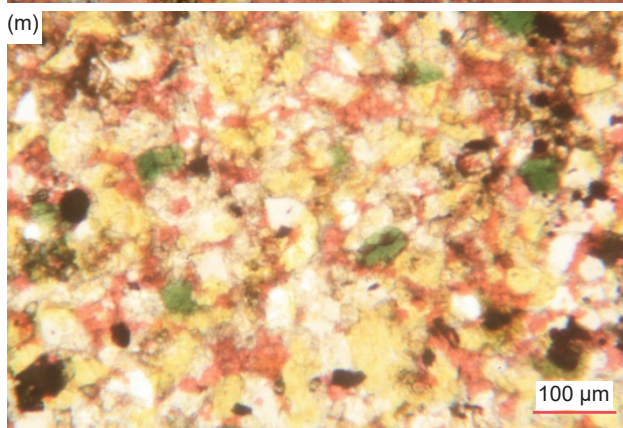
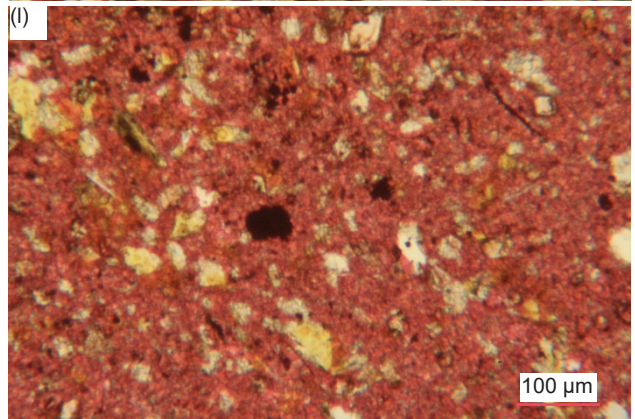
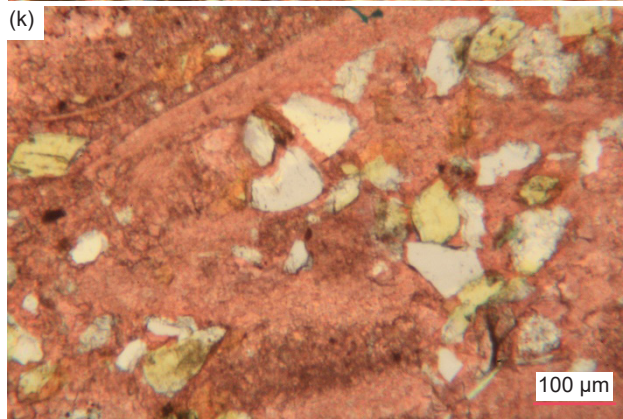
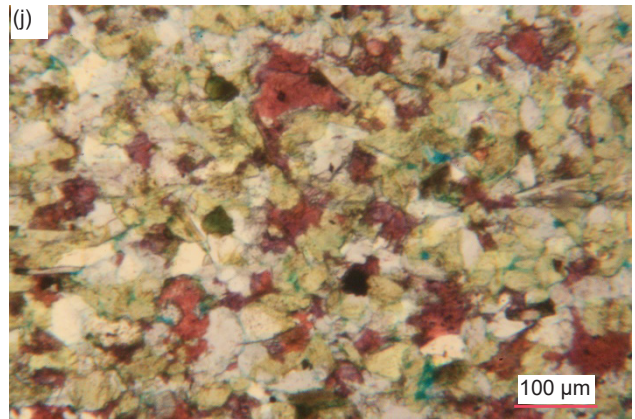
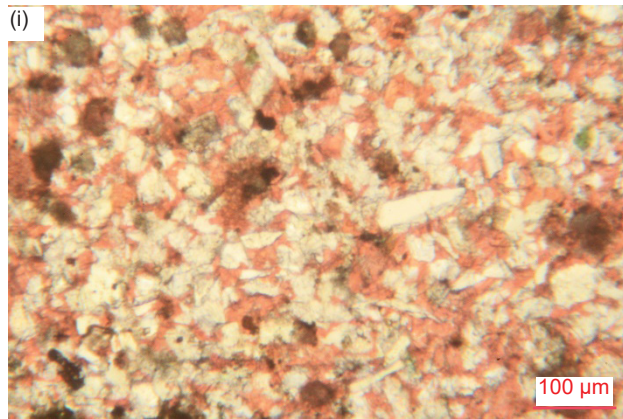
K-feldspar grains are also present in the thin sections of all the samples, ranging from 0.9% to 26.3%, that maximum amount being in two samples (MFML-01 and -03, table 2). In nine of the 15 samples, K-feldspar is the dominant silicate mineral, though often the amounts are not much greater than the quartz contents (table 2). The K-feldspar grains are generally tiny to very small (0.01–0.18mm,  $\phi$ =+6.72 - +2.48, medium silt to fine sand size), though in some samples there are also some small grains (0.19–0.29mm,  $\phi$ =+2.40 - +1.80, fine to medium sand size) (fig. 35). They are mostly sub-angular to sub-rounded, though a few are rounded, and some are angular fragments or sub-euhedral former laths,

while other grains have irregular shapes and ragged edges, sometimes obscured by the calcite matrix encroaching on them. Sometimes the K-feldspar grains exhibit cross-hatched twinning under crossed polars that is characteristic of microcline, while the others exhibit either striped simple-twinning or a uniform appearance that is characteristic of orthoclase.

These variously sized and shaped K-feldspar grains are usually mixed and interspersed with one another and with quartz grains, indicative of poor sorting, and are usually scattered (in some samples sparsely) and “floating” in the micrite (fine-grained calcite mud) matrix, though occasionally the density of K-feldspar (and quartz) grains is locally higher. In some places, rare very tiny K-feldspar grains are wedged with quartz grains between tightly-packed dolomite rhombs. Sometimes the variously-sized K-feldspar grains are concentrated or more densely-packed with accompanying quartz grains in thin bands and laminae (still with some calcite matrix grains) and occasionally are similarly clumped together. Some of these thin laminae appear to have slightly larger K-feldspar (and quartz) grains compared to those scattered elsewhere through the calcite matrix or to those in alternating calcite-matrix-dominated laminae. Where K-feldspar and quartz grains are interlocking in these “aggregates,” the K-feldspar grains are irregularly-shaped and sometimes form triple point junctions with the quartz grains or other K-feldspar grains, likely due to overgrown silica forming a cement in optical continuity with the quartz grains. In one sample, the K-feldspar (and quartz) grains are clustered together in lensoid and ovoid shapes, sometimes clearly outlined as distinctive features, perhaps representing former clasts. And sometimes where the edge-on muscovite flakes are parallel to the bedding the mosaic K-feldspar (and quartz) grains and the interstitial calcite cement also appear elongated parallel to the bedding, likely being a depositional feature.

Some K-feldspar grains have diffuse edges due either to encroaching calcite or illite alteration, while in other samples a few of the tiny and very small sub-angular to sub-rounded K-feldspar grains and sub-euhedral former laths (0.02–0.22mm,  $\phi$ =+5.71 - +2.19, medium silt to fine sand size) appear to be altered by illite to greenish glauconite. There are some samples in which much larger platy calcite crystals and/or larger irregularly-shaped calcite patches have a few very small K-feldspar (and quartz) grains embedded in them. Similarly, in several instances tiny angular K-feldspar grains and tabular laths have been included (with quartz grains) in medium-sized dolomite rhombs and/or sub-euhedral to irregular dolomite patches, which is





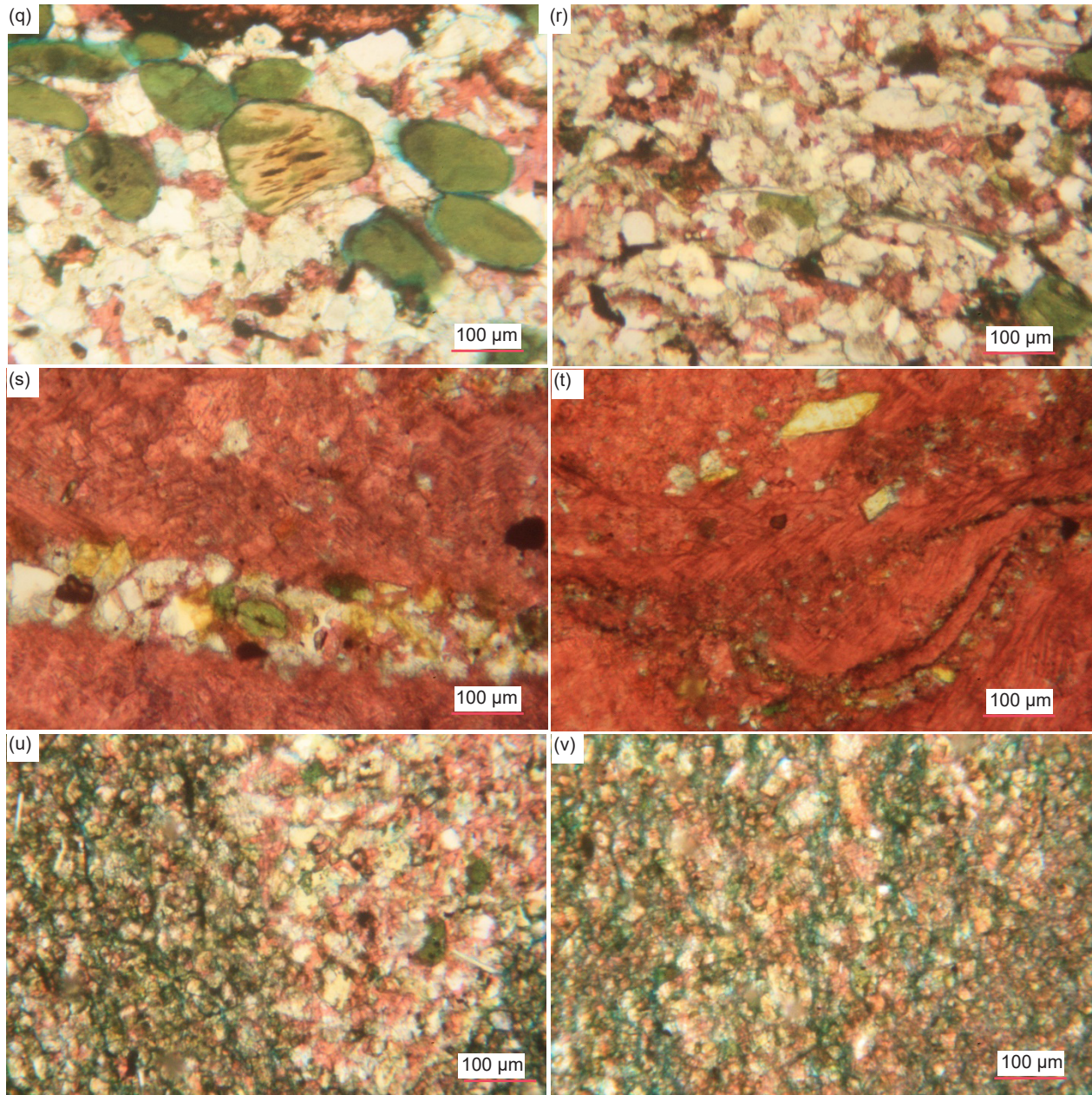


**Fig. 35 (pages 217–219).** A representative set of photomicrographs all at the same scale (as indicated) showing the K-feldspar grains of various sizes, shapes and states of alteration in the Muav Formation samples. (a), (b) MLS-01, (c), (d) MLS-02, (e) MLS-03, (f) MFML-01, (g) MFML-02, (h) MFML-03, (i) MFML-04, (j) MFML-05, (k) MFML-06, (l), (m) MFTB-01, (n) MFTB-02, (o), (p) MFTB-03, (q), (r) MFTB-04, (s), (t) MFTB-05, and (u), (v) MFTB-06.

consistent with the dolomite being post-depositional replacement of the calcite matrix in which the K-feldspar (and quartz) grains were originally deposited. Sometimes the dolomite or calcite, and in one sample even siderite, may even be partially or fully replacing K-feldspar grains. Furthermore, in one sample (MFTB-04) some of the glauconite peloids have internal/central inclusions of tiny K-feldspar grains around which the glauconite was deposited. Finally, in one sample (MFML-05), in some parts of the rock fabric, the interlocking mosaic of K-feldspar (and quartz) grains appears to be fractured without

displacement at an oblique angle to the bedding by a network zone of fractures, making the K-feldspar grains smaller, angular and even elongated aligned parallel to the fracturing.

#### *Plagioclase*

Plagioclase grains occur at 1.9% in one sample (MLS-02) from the Gateway Canyon Member but are also very sparsely present in five other samples (MFML-01 and -06, topmost Gateway Canyon Member, and MFTB-02, -03 and -04, basal Havasu Member) (fig. 36). They are readily identified by their

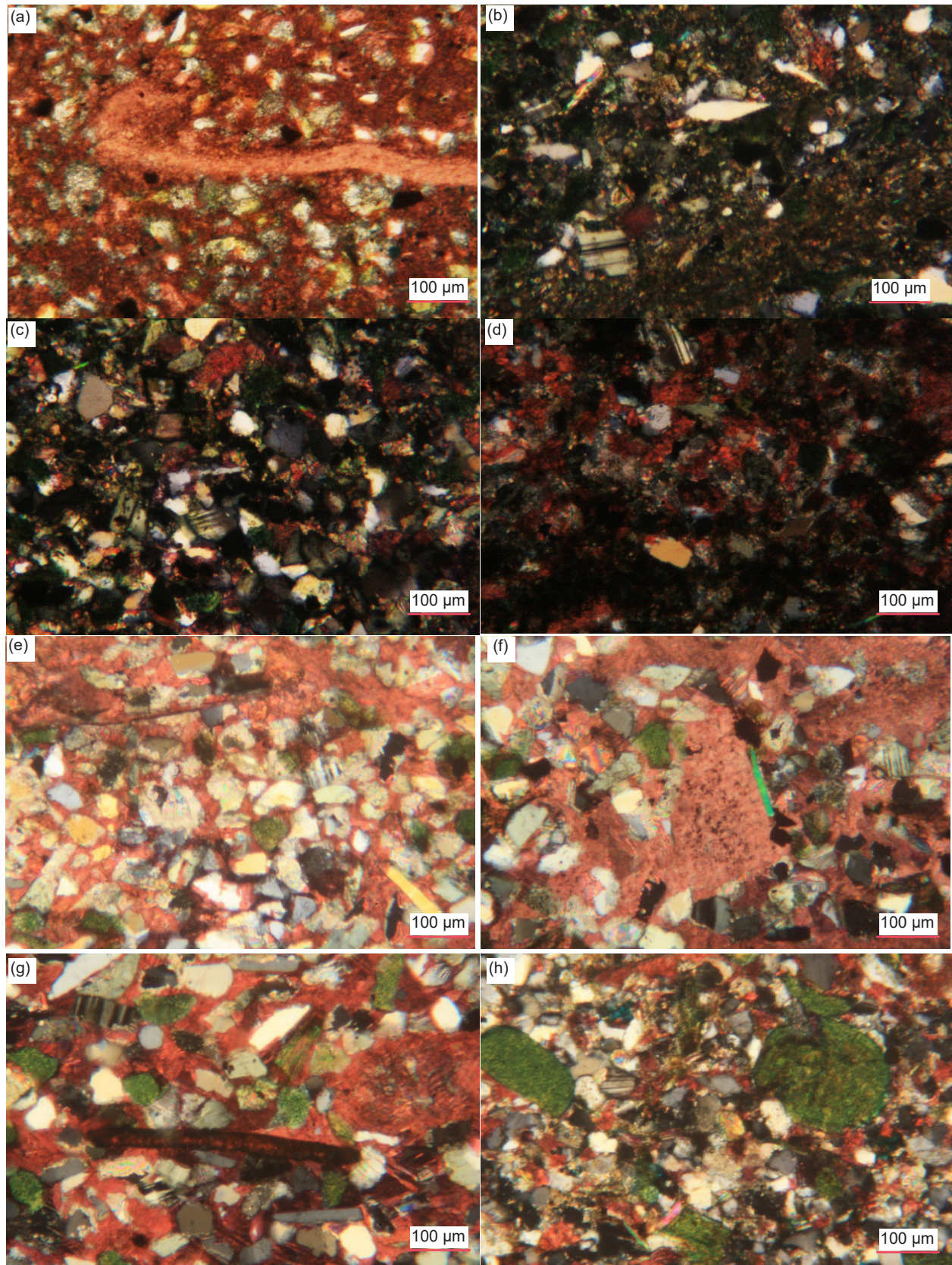


**Fig. 36.** A representative set of photomicrographs at various scales (as indicated) showing the plagioclase grains in the Muav Formation samples. (a) MLS-02, (b), (c) MFML-01 crossed polars (d) MFML-06 crossed polars (e) MFTB-02 crossed polars, (f), (g) MFTB-03 crossed polars, (h) MFTB-04 crossed polars

tell-tale multiple twinning under crossed polars. They are similar in size (very small) and shape (sub-angular to sub-rounded, and occasionally lath-like) to the accompanying K-feldspar and quartz grains.

### *Muscovite*

Muscovite flakes are present in the thin sections of all samples but in varying quantities which are difficult to specify because in the XRD analyses muscovite also registered as illite (table 2). Under the microscope they are always seen edge-on as thin or thicker cross-sections of books of thin sheets (fig. 37). The abundance of these edge-on muscovite flakes varies from rare and a few in some samples to occasional or many and numerous in other samples. In size they vary from tiny and very small (0.03–0.19 mm long,  $\phi = +5.01 - +2.40$ ) in length to small (0.20–0.26 mm,  $\phi = +2.33 - +1.95$ ), medium (0.30–0.42 mm,  $\phi = +1.75 - +1.25$ ), long/large and very long (0.76–1.23 mm,  $\phi = +0.40 - -0.30$ ) (fig. 37). They are usually scattered through the rock fabric at various angles wedged tightly between the other grains in the calcite (or dolomite) matrix, but often parallel to the bedding and to laminations, even when several are in proximity to one another. Sometimes, several flakes are stacked on top of one another (for example, fig. 37f, k, x, and y). Some longer flakes are bent or broken wedged between and around quartz and K-feldspar grains (and in two samples also glauconite grains), occasionally with split and/or frayed ends (for example, fig. 37d, e, g, h, k–m, p, r, t, w, y, a'–d' and h'–j'). These features, namely, wedged between other detrital grains, and bent round them occasionally with split or frayed ends, as well as often being generally parallel to the bedding and to laminations, are consistent with these muscovite flakes also being detrital grains.

Some muscovite flakes appear to be degraded. In some samples, the streaks of iron oxides appear to be where iron oxides have stained, covered or even replaced some of the smaller edge-on muscovite flakes. In some instances, where the edges of the K-feldspar grains have possibly been altered to illite, a few muscovite flakes may have been replaced by illite or glauconite (evident from the greenish stain), or some muscovite flakes have been replaced by illite accompanied by iron oxides. In contrast, in other samples some small thin edge-on muscovite flakes transverse areas of recrystallized clean (non-iron-oxides-stained) interlocking small to medium-large calcite crystals and are even included in some of the larger calcite crystals, which indicates the muscovite was not altered or impacted by the calcite recrystallization process.

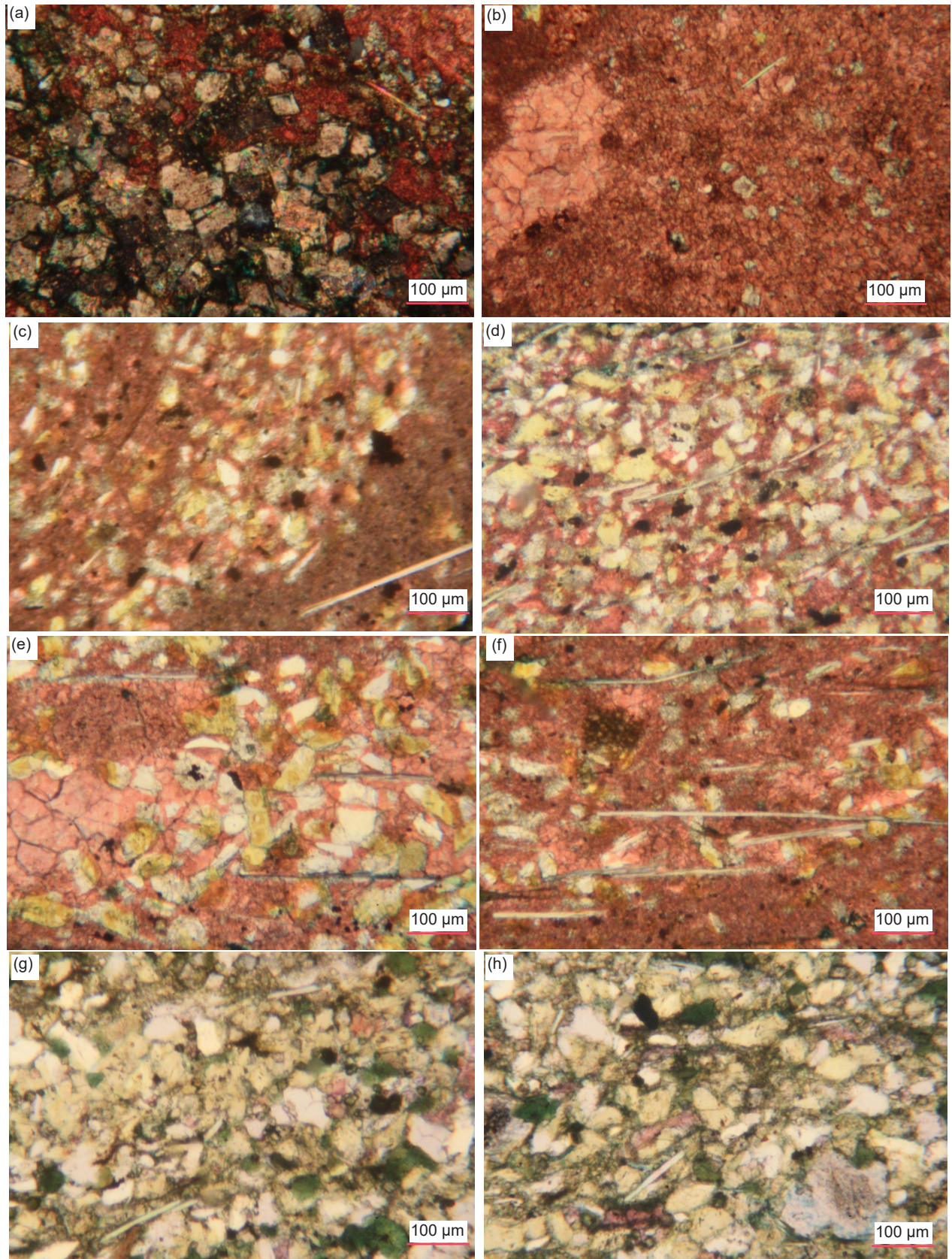
In some samples, there are areas where the long thin edge-on muscovite flakes are at the same

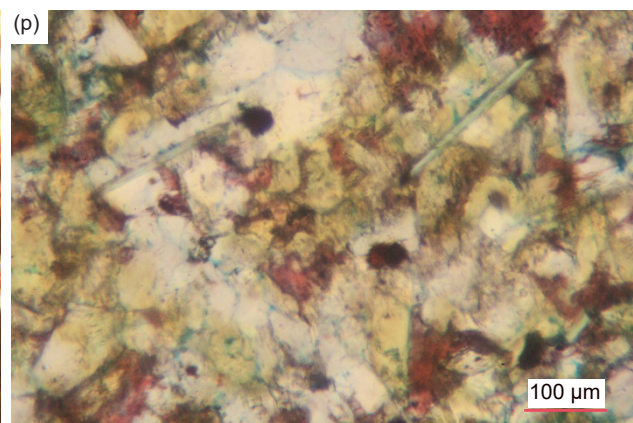
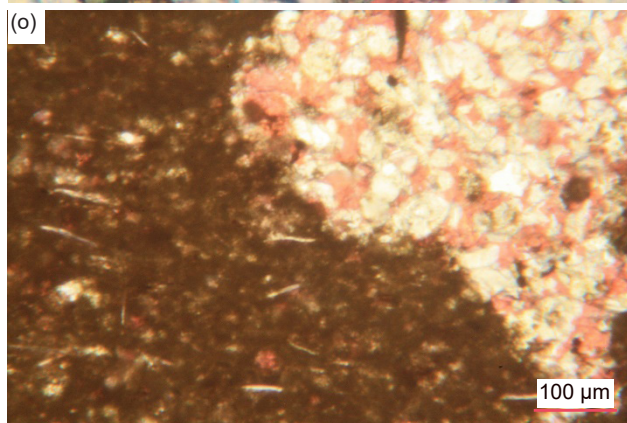
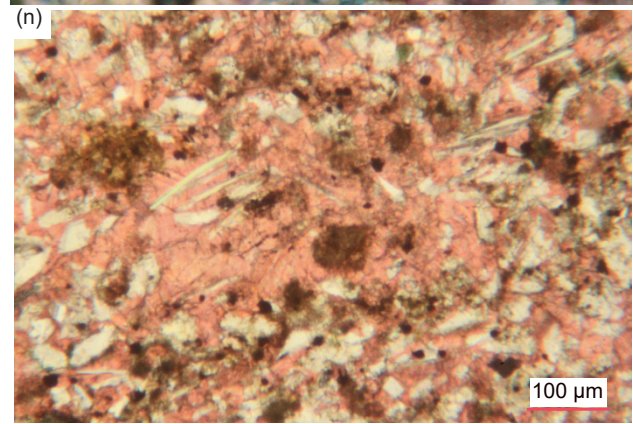
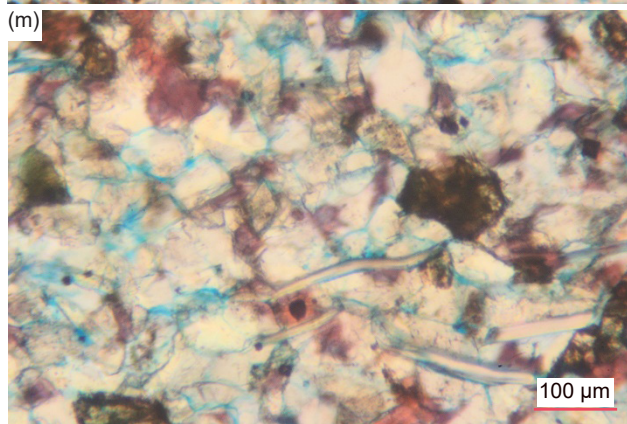
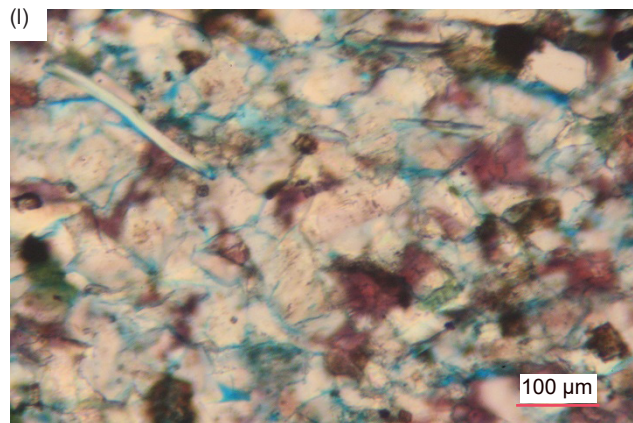
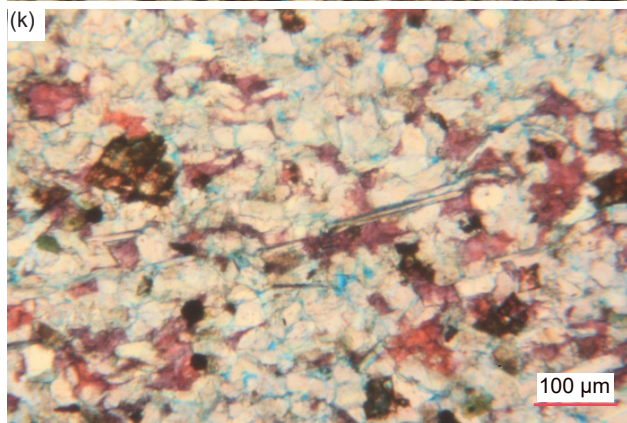
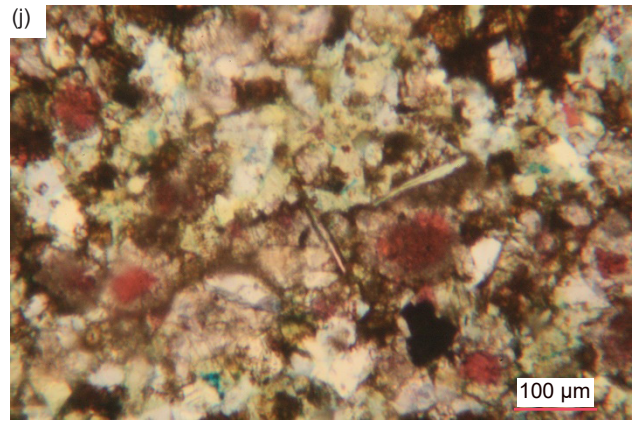
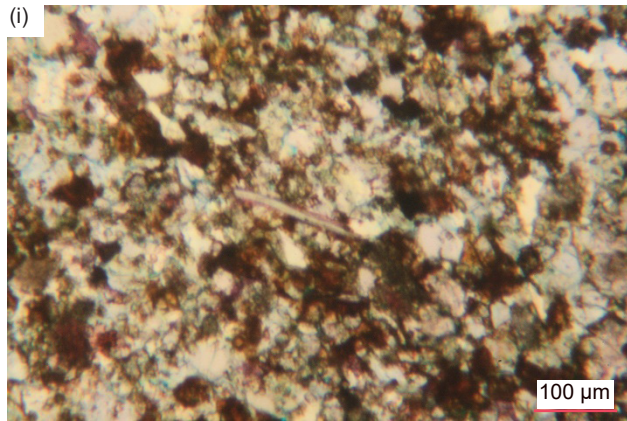
oblique angle with elongated quartz and K-feldspar grains, all aligned parallel at the same oblique angle to the bedding within the calcite matrix, which would be a primary depositional feature. In other samples, occasional long, iron-oxides-stained or fresh thin edge-on muscovite flakes are parallel to the axes of apparent lensoids of clumped grains or are bent around them. Some edge-on muscovite flakes lie along and within fractures, probably having facilitated the location of the fractures which are often at the same low angle to the bedding as are other fractures in those samples (fig. 37e'). Bedding planes can also be accompanied by thin edge-on muscovite flakes paralleling them. In contrast, in one sample, even though the muscovite flakes are usually parallel to one another, they are also parallel to apparent fractures and other lineations which are all perpendicular to the denoted bedding.

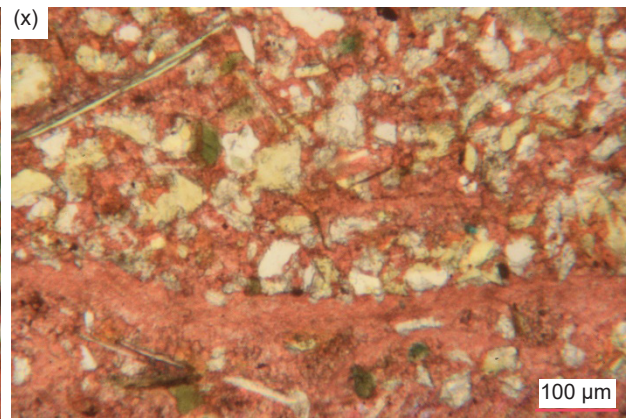
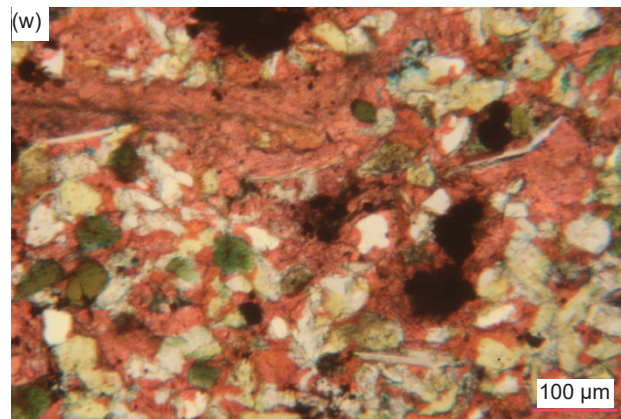
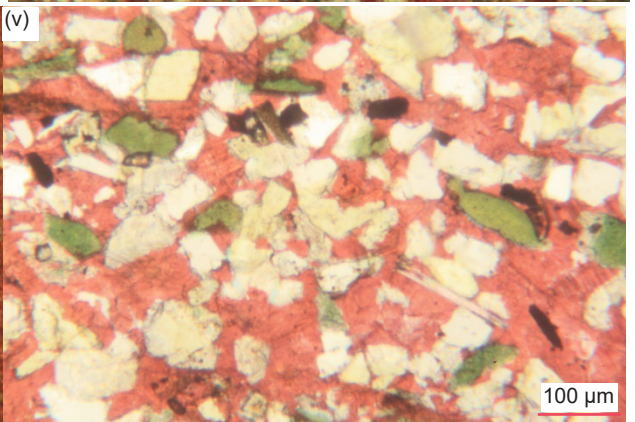
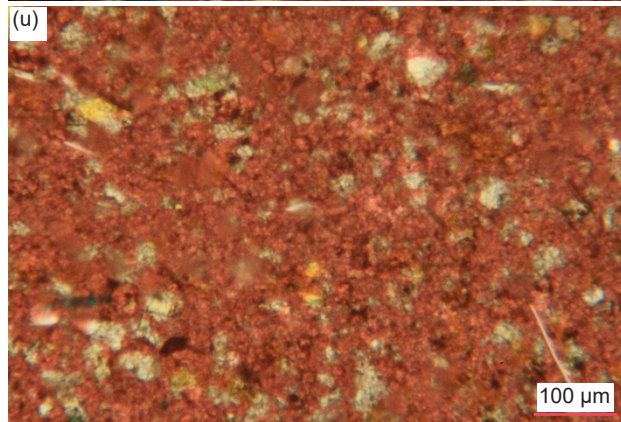
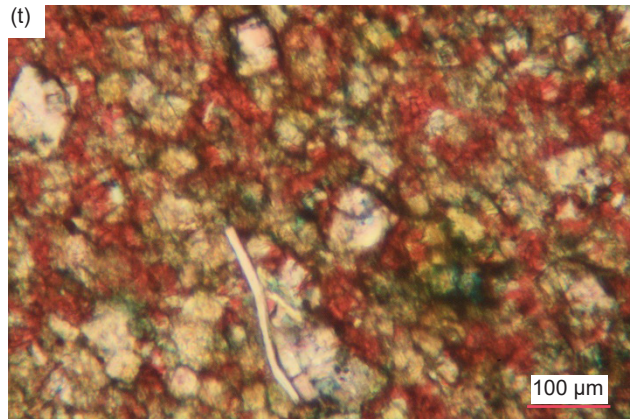
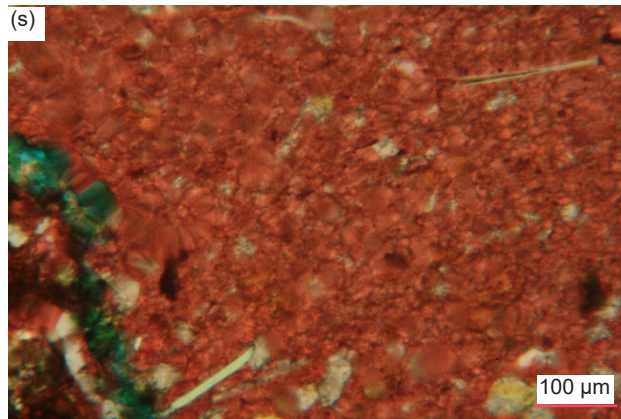
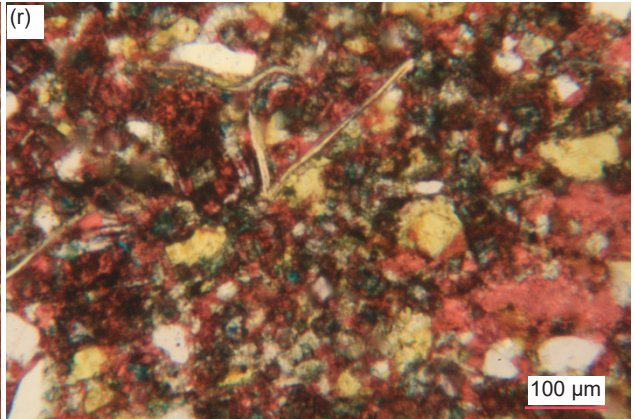
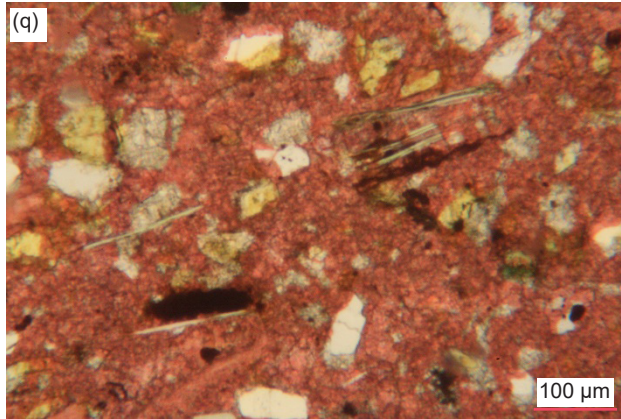
### *Glauconite*

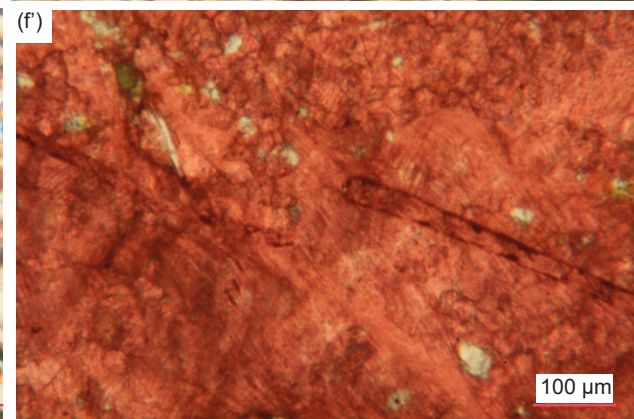
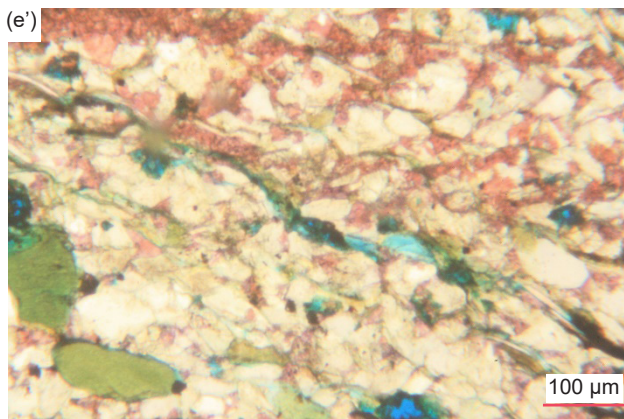
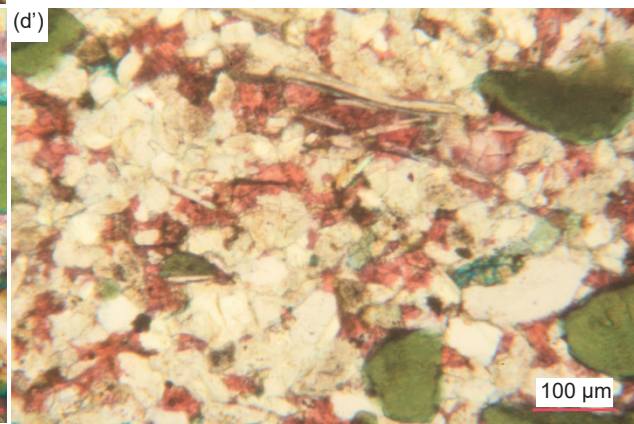
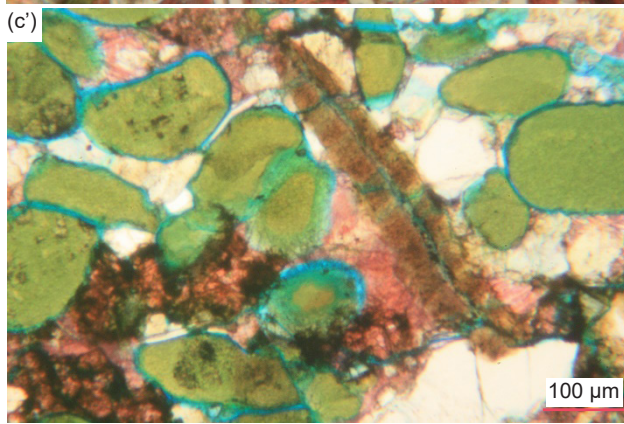
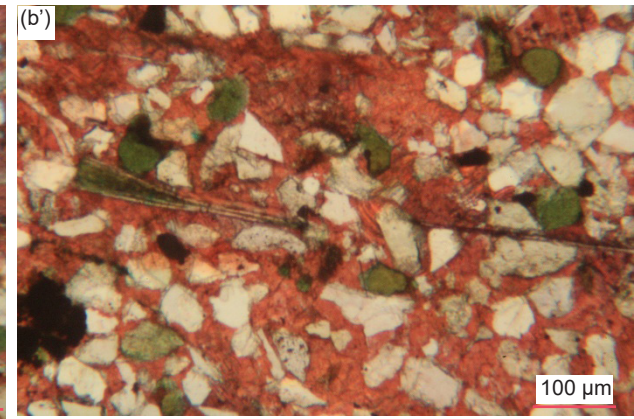
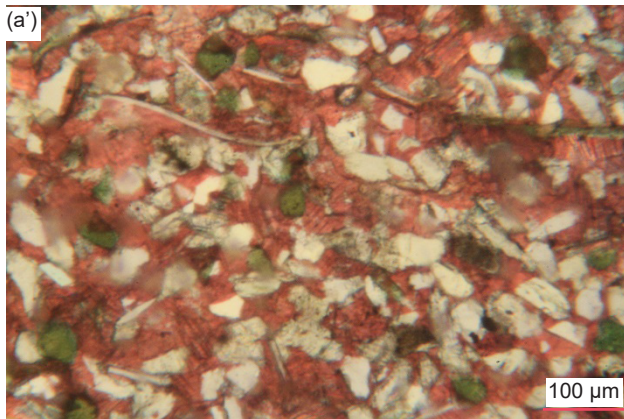
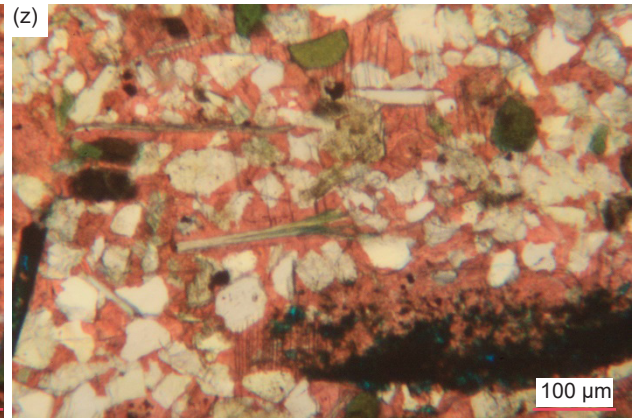
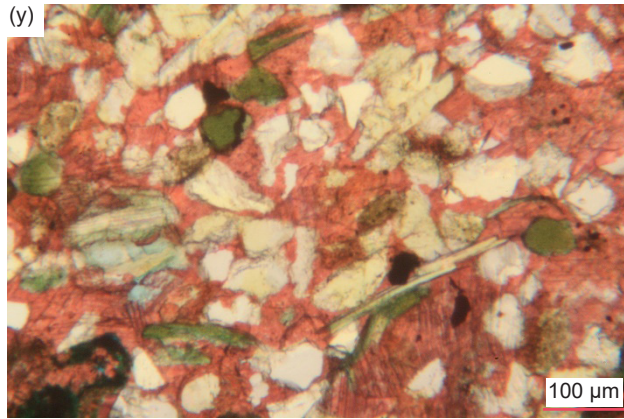
In many of these samples some tiny, very small to small (0.02–0.22 mm,  $\phi = +5.71 - +2.19$ ), sub-angular, sub-rounded and rounded K-feldspar grains and fragments are stained green, likely indicating partial illite alteration to glauconite, are occasionally scattered among the other grains in the matrix (fig. 38). Some are speckled with iron oxides staining and a few sometimes have iron-oxides-lined internal cracks. In one sample, the larger (0.19–0.20 mm,  $\phi = +2.40 - +2.33$ ) former sub-euhedral K-feldspar grains and laths that has been altered to greenish glauconite (illite) are seen broken apart into some very small and small angular and sub-angular fragments that are dislocated but not disconnected within the surrounding matrix. In a few instances, only the edges of some K-feldspar grains appear to be altered to illite (greenish glauconite). A few small (0.18–0.21 mm,  $\phi = +2.48 - +2.25$ ) muscovite flakes in at least two samples may also have been replaced by illite or glauconite (evident from the greenish stain), sometimes accompanied by iron oxides.

Sample MFTB-04 is very different from all the other samples as the rock fabric's appearance is dominated by glauconite grains (~6%) that give it an overall greenish tinge. Under the microscope the rock consists of a tightly-fitting interlocking mosaic dominated by scattered very small to small (0.06–0.18 mm,  $\phi = +4.05 - +2.48$ ) and small-medium (0.20–0.45 mm,  $\phi = +2.33 - +1.15$ ), rounded and often elongated, greenish grains of glauconite (illite) finely speckled and streaked with iron-oxides-staining (some with embayed edges) (figs. 30p and 38l-p). Some have broken off ends suggesting they are detrital clasts, while others are cracked, and others have internal inclusions of tiny quartz and/or K-feldspar. Two also have an internal ribbed









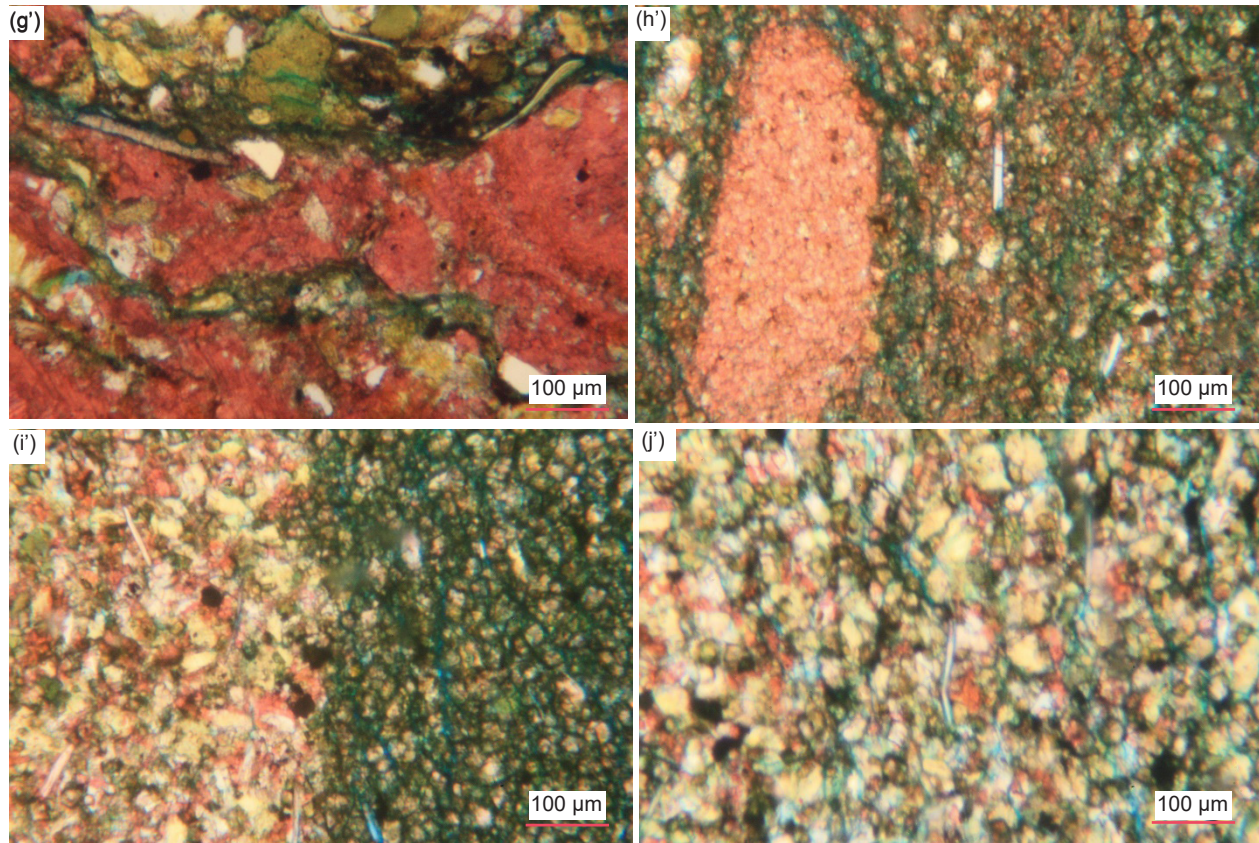


**Fig. 37 (pages 222–226).** A representative set of photomicrographs at various scales (as indicated) showing typical edge-on muscovite flakes in the Muav Formation samples with features such as frayed or flayed ends and/or bent around quartz and K-feldspar grains indicating they are detrital grains, while some have expanded due to alteration. (a), (b) MLS-01, (c), (d) MLS-02, (e), (f) MLS-03, (g), (h) MFML-01, (i), (j) MFML-02, (k)–(m) MFML-03, (n), (o) MFML-04, (p) MFML-05, (q)–(s) MFML-06, (t), (u) MFTB-01 (v)–(x) MFTB-02, (y)–(b') MFTB-03, (c')–(e') MFTB-04, (f'), (g') MFTB-05, (h')–(j') MFTB-06.

scaffolding structure which suggests the glauconite (illite) grew around those grains as pellets. Some glauconite grains are grossly elongated, yet still rounded, so they likely are primary deposited grains. Other glauconite grains are partially altered and/or replaced by calcite stained with iron oxides especially heavily along internal cleavage cracks, giving the grains a variable brownish tinge. In other places the glauconite grains are clumped together.

#### *Iron Oxides*

Though only present in trace amounts, iron oxides are ubiquitous in all samples, often as scattered specks and tiny patches between grains and through the matrix (fig. 39). Most dolomite grains and rhombs are outlined by iron oxides, which also delineate internal growth zones within many of the rhombs. Similarly, some calcite grains and rhombs are outlined by iron oxides and dusted lightly with them, sometimes in streaks. In some samples there are long thin streaks of iron oxides that appear to be altered edge-on muscovite flakes. In others there are occasional very tiny-tiny, very small and small

irregular heavy iron-oxides blotches are scattered within the rock fabric between and encroaching on various mosaic grains. And in several samples where laminae are evident in the rock fabric, the main difference between some adjoining laminae appears to be the intensity of the staining by iron oxides.

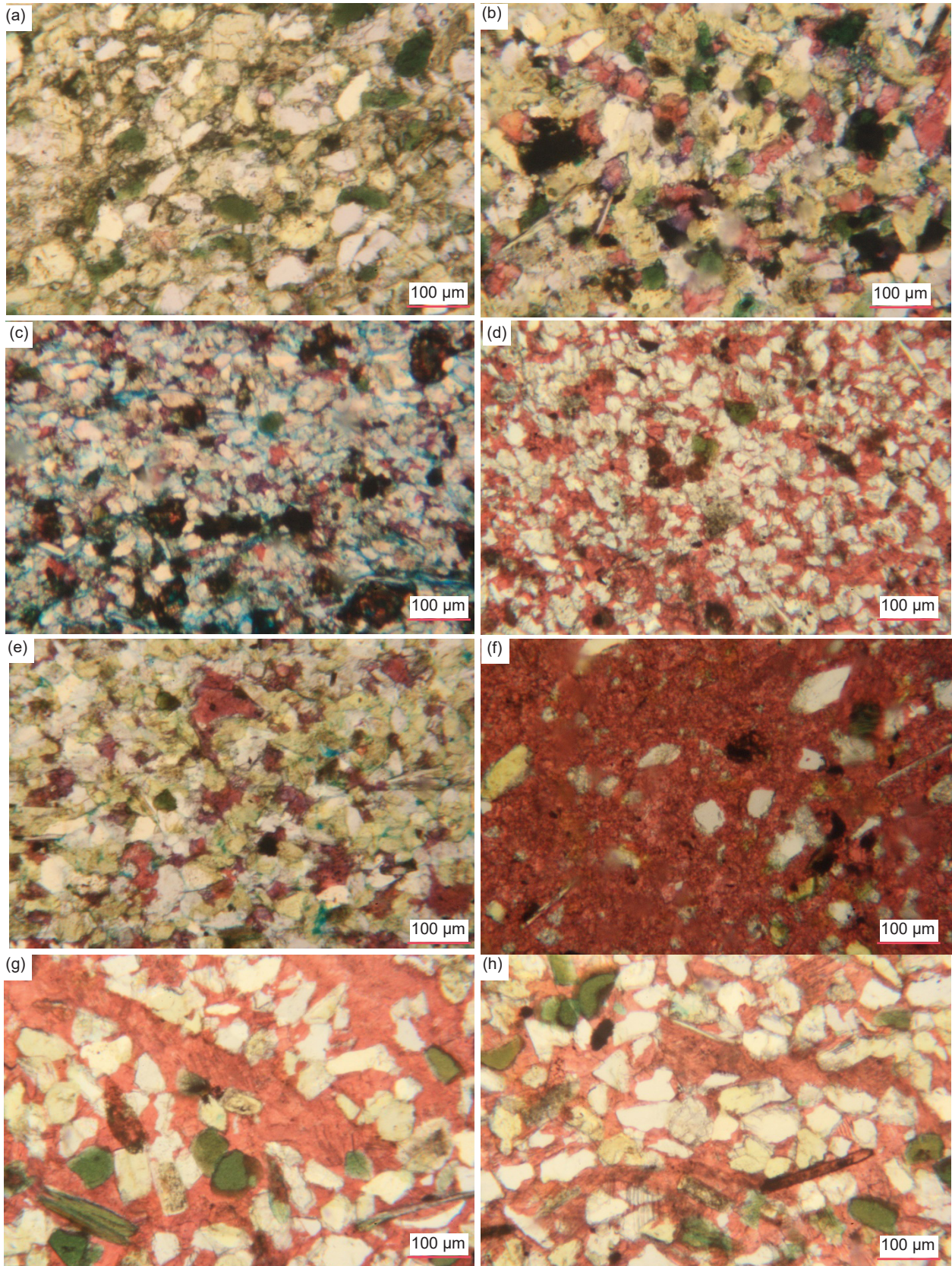
Occasional very long anastomosing and branching iron oxide streaks wind across the rock fabric similarly to hairline fractures generally and approximately perpendicular to the denoted bedding. A thick border of iron oxides surrounds a huge ovoid patch of recrystallized calcite (fig. 39v).

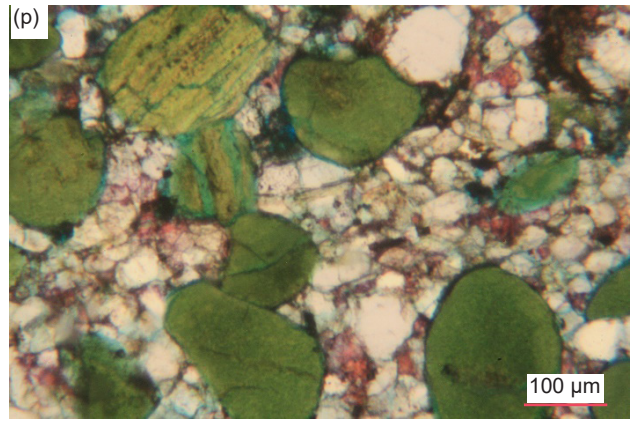
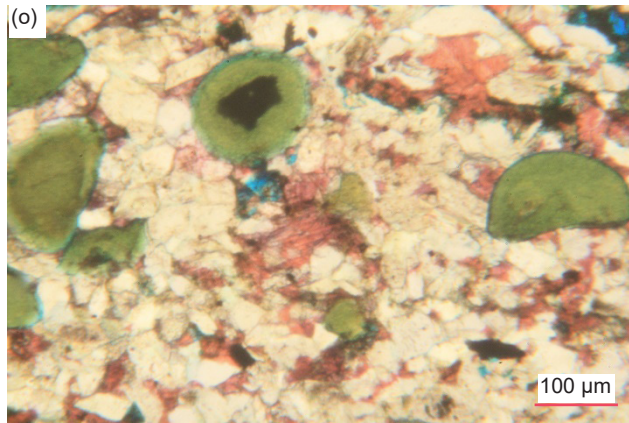
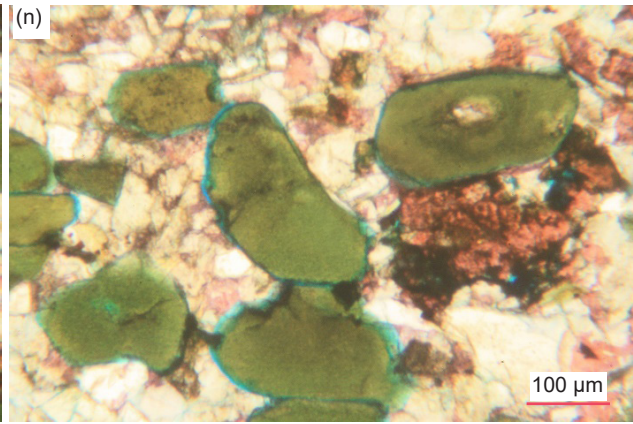
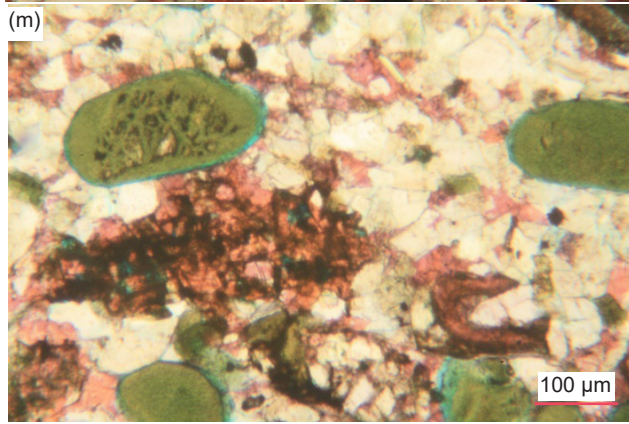
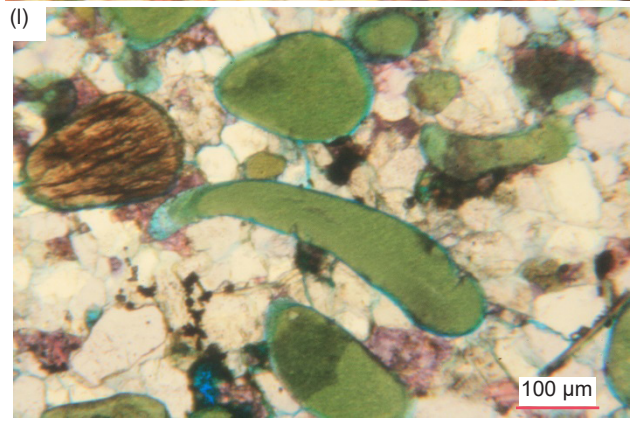
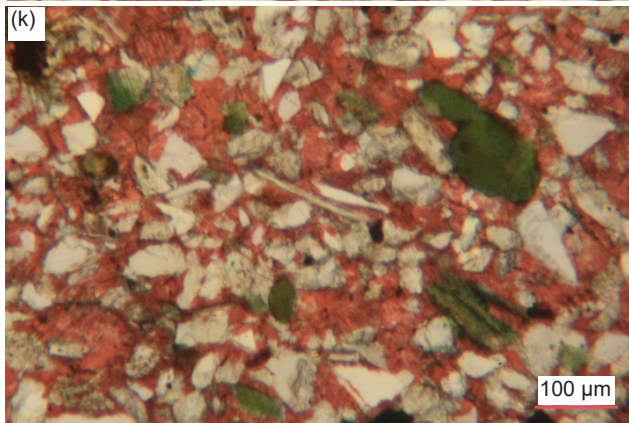
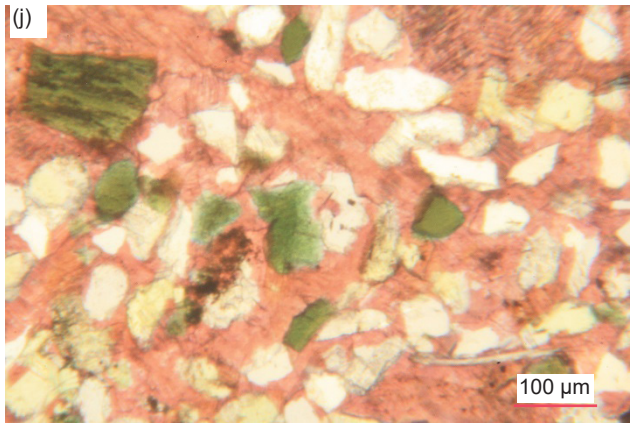
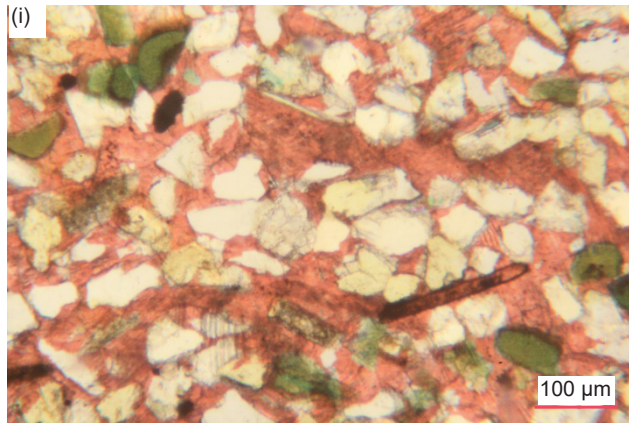
#### *Zircon*

In two samples (MFML-01 and MFTB-02) several very small (0.04 mm,  $\phi=+4.64$ , coarse silt sized) rounded or tabular and heavily iron-oxide-stained grains with high relief and high birefringence are scattered among the quartz and K-feldspar grains in the calcite matrix and are likely zircon.

#### *Pores*

In most samples there are virtually no pores





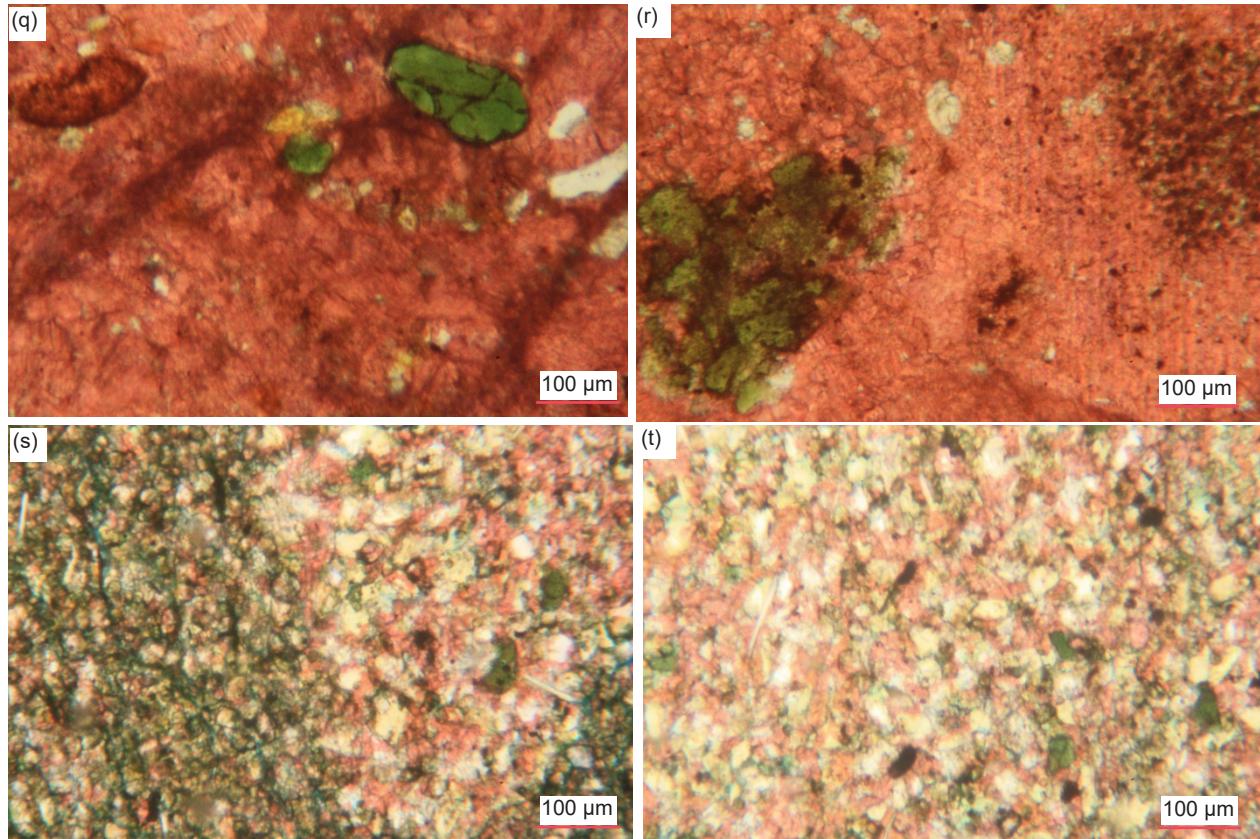


**Fig. 38 (pages 227–229).** A representative set of photomicrographs at various scales (as indicated) showing the glauconite grains in the Muav Formation samples. (a), (b) MFML-01, (c) MFML-03, (d) MFML-04, (e) MFML-05, (f) MFML-06, (g) MFTB-01, (h) MFTB-02, (i) - (k) MFTB-03, (l)–(p) MFTB-04, (q), (r) MFTB-05, (s), (t) MFTB-06.

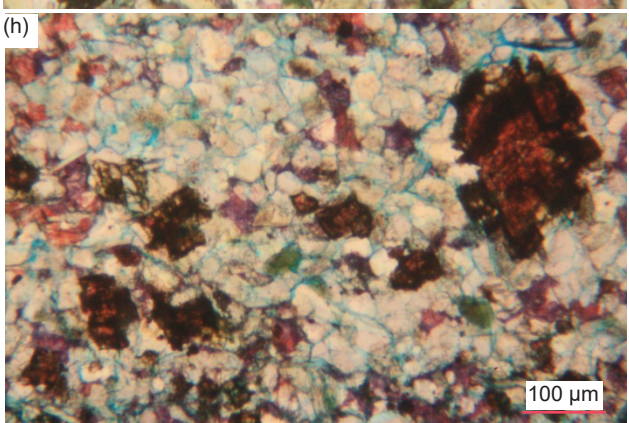
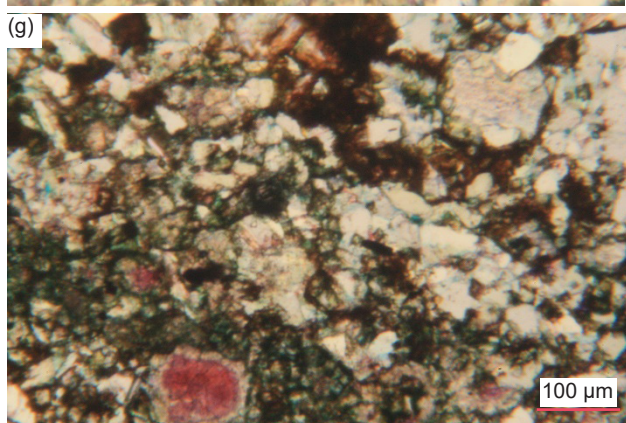
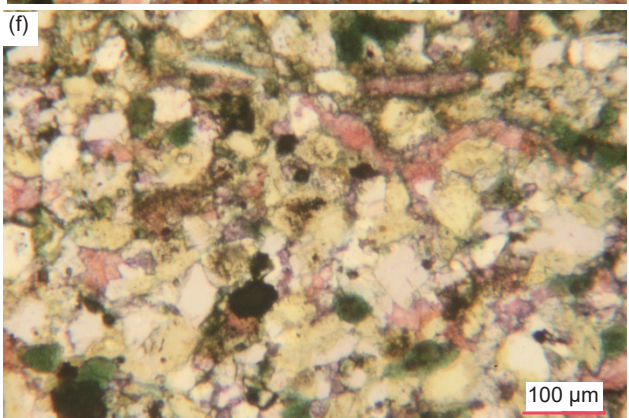
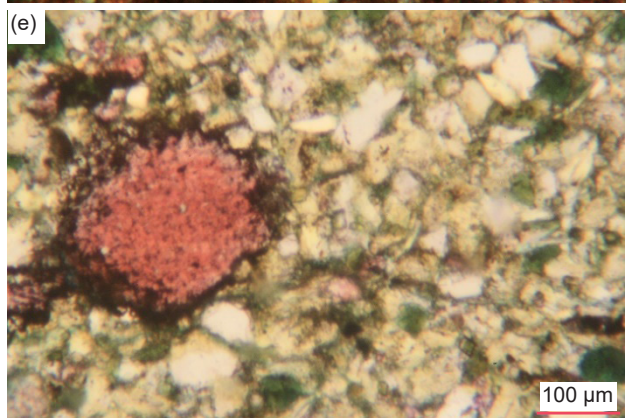
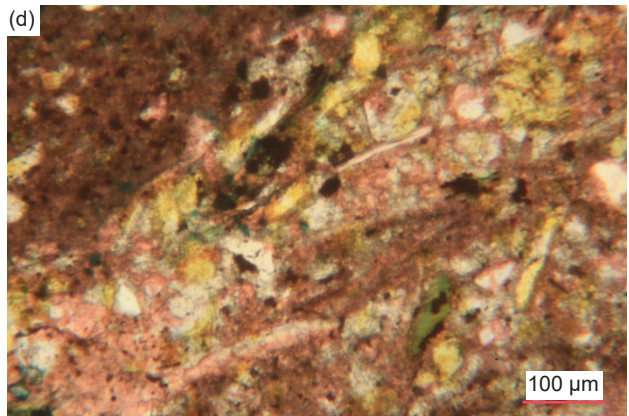
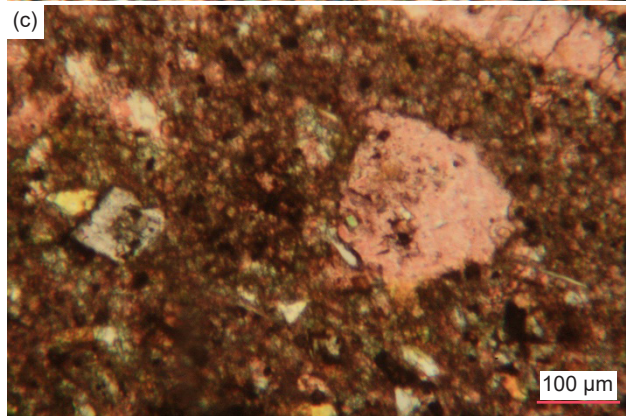
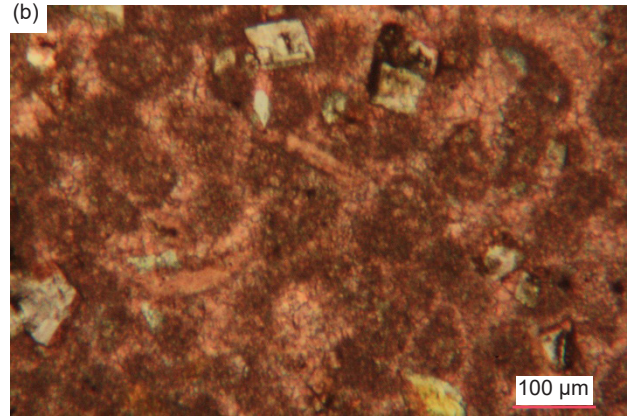
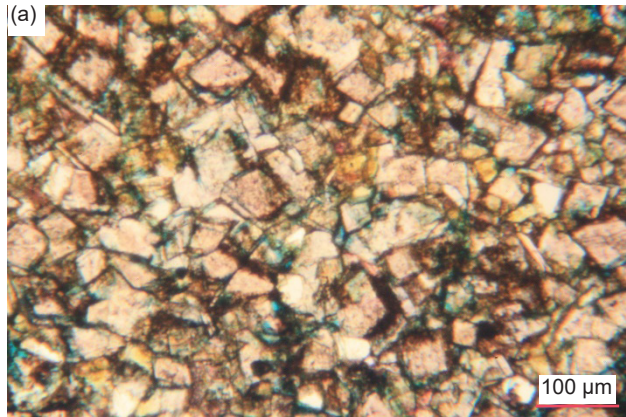
remaining in the rock fabric, just some hairline cracking between grains and rare tiny and very small pores, some likely due to the forced impregnation with blue dye-stained epoxy prior to the thin sections being cut (fig. 30). The blue dye that accompanied the resin used under pressure to impregnate the samples before the thin sections were cut has stained between the grains and encroached on some of them, sometimes covering grains and thus distorting their colors, which can make some look like small pore spaces. It should be noted that in these fine-grained rocks the very small grain radii are smaller than the microscope slide thickness and thus the tight stacking of the grains may obscure any residual tiny pores. However, sample MFTB-04 contains several very large, elongated and flattened pores (or they could be dissolution holes as they are much larger than any of the mosaic grains) that are lined thickly with calcite heavily stained by iron oxides, with the calcite crystals grown inwards to infill the remaining spaces.

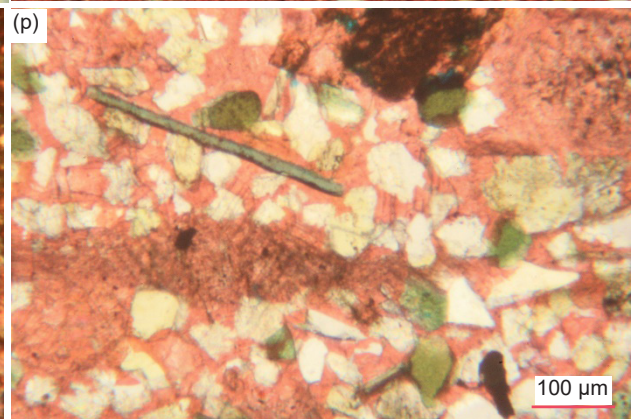
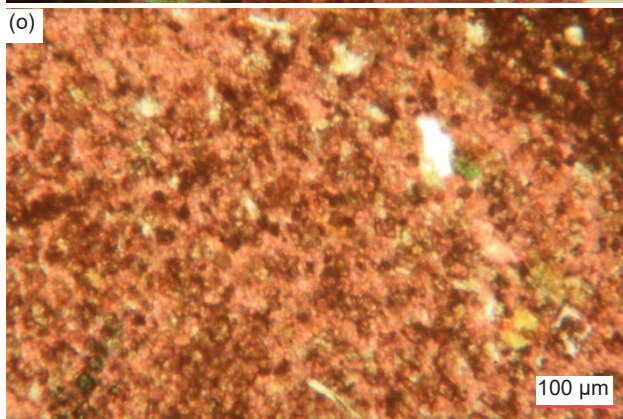
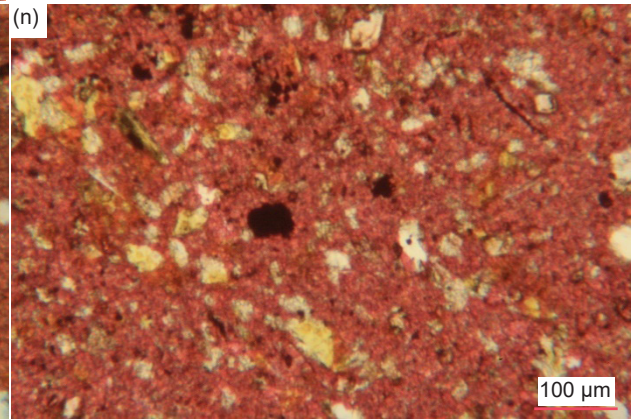
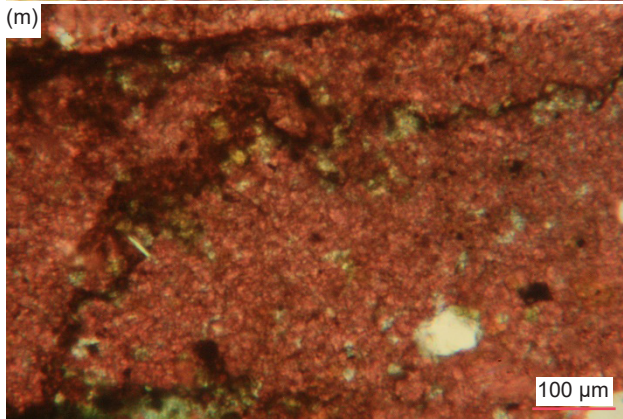
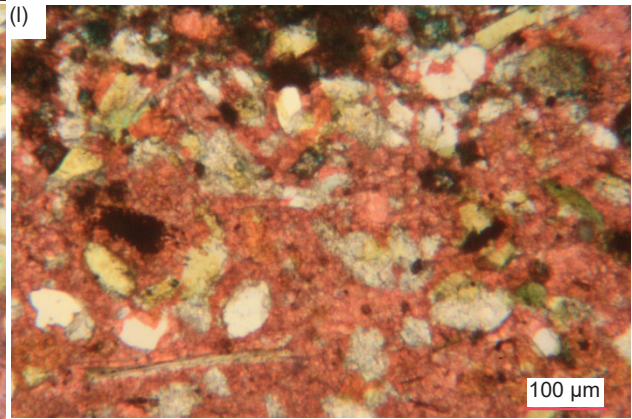
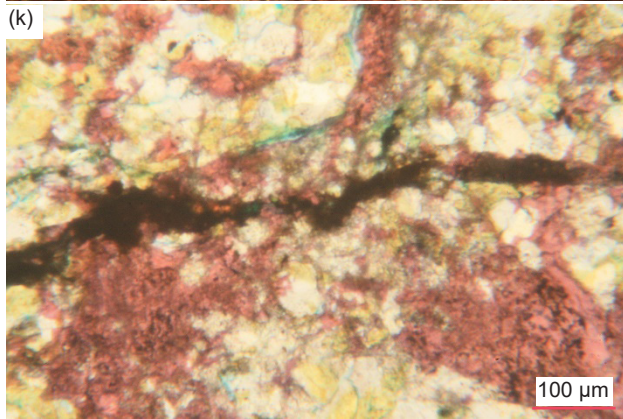
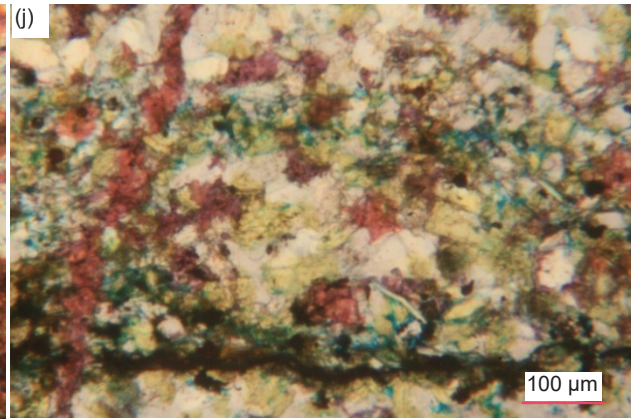
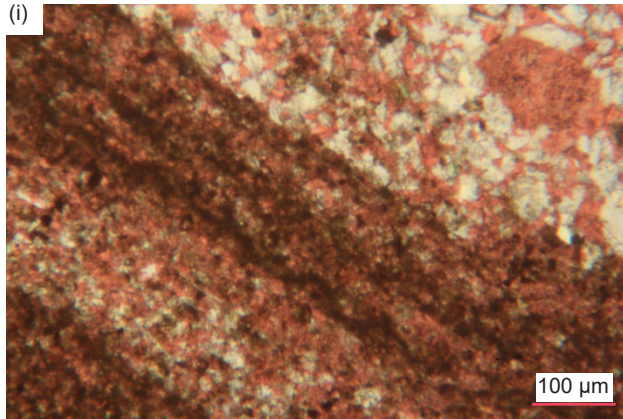
Finally, during extensive petrographic examination of these 15 samples of the Muav Formation, no macroscopic or microscopic evidence was found of any metamorphic effects on the limestones, or their constituent mineral grains. This includes the

12 samples from the Matkatamiba fold, as well as the three samples distant from that fold selected for comparison. Not only have the quartz grains maintained their detrital characteristics, but the ubiquitous K-feldspar grains and the muscovite flakes have also, some of the latter having been bent around the quartz and K-feldspar grains they are wedged between, and some having frayed, or split ends caused by abrasion during deposition. Even slightly elevated temperatures from low-grade metamorphism would have substantially affected the quartz and K-feldspar grains, which usually dominate in these rocks, as well as affecting the muscovite flakes and the textures in the rock fabric. Clay minerals are only present in trace amounts and would not have survived post-depositional diagenesis or metamorphism but would have been transformed into other minerals, such as metamorphic muscovite. Yet the muscovite flakes have survived in these limestones as original detrital clasts. Thus, it is likewise concluded that the Muav Formation is unmetamorphosed in all places where it was examined in Grand Canyon.

### Discussion

Details gleaned from this intensive petrographic examination of these Muav Formation samples in





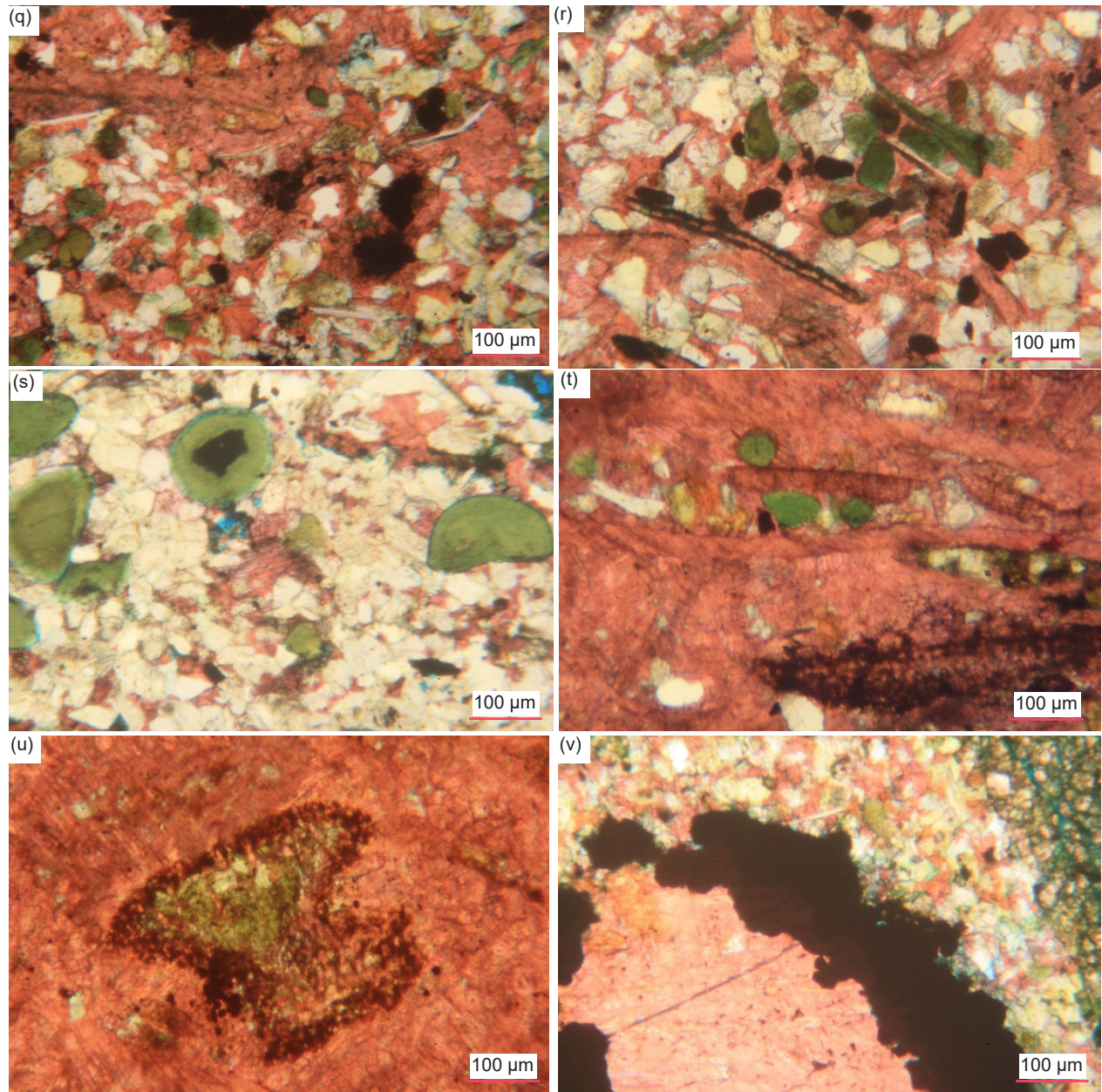


**Fig. 39 (pages 230–232).** A representative set of photomicrographs at various scales (as indicated) showing the occurrences of iron oxides in the Muav Formation samples. (a), (b) MLS-01, (c) MLS-02, (d) MLS-03, (e), (f) MFML-01, (g) MFML-02, (h) MFML-03, (i) MFML-04, (j), (k) MFML-05, (l), (m) MFML-06, (n), (o) MFTB-01, (p), (q) MFTB-02, (r) MFTB-03, (s) MFTB-04, (t), (u) MFTB-05, (v) MFTB-06.

conjunction with previous field and other studies enable various relevant conclusions to be drawn.

#### **Mineralogical Composition Indicates Nearby Sediment Provenance**

Megascopically these Muav Formation rocks are limestones, so it is rather surprising that detrital quartz and K-feldspar grains and detrital muscovite flakes are all routinely visible microscopically in these wackestones (mud-supported) and packstones (grain-supported), ranging from 3.9% to 78.6%

(table 2, last column). In their much-cited and well-illustrated textbook on the petrography of carbonate rocks, Scholle and Ulmer-Scholle (2003) do not list or even mention these minerals as potential detrital grains within such carbonate rocks. Thus, in the Muav Formation the ubiquitous presence of these silicate minerals must be significant with respect to the provenance of these carbonate sediments.

Quartz is the most abundant mineral in terrigenous sedimentary rocks, such as in the sandstones, siltstones and shales of the underlying

Bright Angel Formation, because it is exceedingly durable due to often surviving multiple generations of weathering and deposition (Ulmer-Scholle et al. 2015). Thus, its abundance in the overlying Muav Formation limestones strongly suggests that the source of these carbonate sediments may be the same or related to the provenance of the underlying Bright Angel Formation and Tapeats Sandstone clastic sediments. In clastic sediments, quartz can occur as single crystals or polycrystalline aggregates that may provide clues to the provenance of the grains, but quartz is common to most rock types, though rare in some igneous rocks. Semi-composite and polycrystalline quartz is found in metamorphic and plutonic rocks as well as hydrothermal vein deposits and fractures. In metamorphic rocks, the size of the quartz crystals may represent increasing metamorphic grade, larger crystals forming under higher temperatures and pressures.

Grain size can make provenance determination more difficult (Ulmer-Scholle et al. 2015). With the smaller grain sizes in siltstones and especially shales and limestones, the ability to see undulatory quartz or polycrystalline/composite grains becomes more difficult. Since crystal sizes within polycrystalline grains may be large, grains formed from their breakdown may not exhibit polycrystallinity or undulatory extinction. According to Krynine (1946) and Folk (1980), straight to slightly undulose extinction in quartz is characteristic of plutonic igneous and schistose metamorphic rocks. They also noted that whereas plutonic igneous rocks generally have sub-equant to xenomorphic quartz grains (that is, they did not develop their otherwise typical external form because of late crystallization as the matrix between earlier formed crystals), schistose metamorphic rocks generally have elongated composite quartz grains with straight borders and commonly have mica inclusions.

Feldspars are far less resistant than quartz to chemical and physical destruction, although they can survive some aqueous transport with only a relatively small reduction in grain size, but not angularity (Garzanti et al. 2012, 2015). However, they are altered or removed by weathering, transport and diagenesis yielding secondary pores or alteration products such as illite, white mica/sericite, albite or kaolinite (Ulmer-Scholle et al. 2015). Almost all detrital feldspars are igneous or metamorphic in origin, with the K-feldspars orthoclase and microcline being the most common. Na-rich plagioclase, the next most common feldspar, is usually from volcanic rocks. Sanidine, from high-temperature felsic volcanic rocks, and Ca-rich plagioclase, from mafic to intermediate igneous rocks, are relatively uncommon.

Detrital micas are rarely mentioned or discussed as being present in any sandstones, siltstones and especially shales, except when they are present in rock fragments (Ulmer-Scholle et al. 2015), and they are not generally identified in limestones (Scholle and Ulmer-Scholle 2003). However, standard petrography textbooks suggest that detrital micas should be found in subaqueous sediments, but not eolian ones (Hallam 1981, 20; Moorhouse 1959, 343; Tucker 1981, 45). This notion is so entrenched in the minds of some geologists that they proclaim the absence of mica in certain sandstones based only on their assumption that a particular sandstone is eolian, without even doing any petrographic work, for example, the Permian Coconino Sandstone of Grand Canyon region (Young and Stearley 2008, 305). They claim that the less resistant (softer) mica grains and ultra-fine clay particles all should have been abraded to oblivion and/or wafted off site by the wind. Yet sandstones like the Coconino contain abundant detrital mica flakes (Whitmore et al. 2014), as do the Tapeats Sandstone and the sandstones, siltstones and shales of the Bright Angel Formation as described by Snelling (2021a, b), and now also in the limestones of the Muav Formation as described above, indicating all these sedimentary units are water-deposited, which has always been proposed for the Tapeats Sandstone and the Bright Angel and Muav Formations.

In the Muav Formation, quartz grains are ubiquitous clasts in the limestones where the grain size is generally very small, as observed in every sample in this study, and the grains generally exhibit straight extinction. Subordinate K-feldspar grains and former laths are common, even being dominant in some instances, though occasionally some K-feldspar grains have been partially altered to illite or altered to carbonate around their edges. There are also a few detrital muscovite flakes in every sample, some bent around quartz and other grains and some with frayed ends. The presence of a few possible plagioclase grains and former laths, together with occasional zircon crystals is clearly indicative of an apparent primary sediment source area(s) consisting of granitic plutons and metamorphic rocks, which are of course locally present, exposed in the inner gorges of Grand Canyon (Karlstrom et al. 2003). Usually, the Tapeats Sandstone directly overlies those granites and schists, separated by the Great Unconformity erosion surface, but where resistant "hills" or monadnocks of Shinumo Quartzite occur in the paleotopography of the Great Unconformity surface, the Bright Angel Formation directly sits unconformably on the tilted Grand Canyon Supergroup sedimentary strata. The Muav Formation always conformably overlies the Bright Angel Formation. It is thus consistent for these

silicate detrital grains within the Muav Formation to also be derived from the same nearby source as the same clastic grains in the two underlying members of the Tonto Group, the Tapeats Sandstone and Bright Angel Formation.

Due to the generally very small sizes of these silicate clasts in the Muav limestones it is difficult to recognize undulose extinction in any of the quartz grains or to find any quartz grains with inclusions of muscovite and/or biotite flakes or any K-feldspar grains and former laths with inclusions of quartz or muscovite. However, it is the repeated combination of detrital quartz, K-feldspar, and muscovite clasts with occasional plagioclase and zircon grains in these Muav limestones that is consistent with the conclusion that the source of silicate clasts within the Muav Formation was the granites and schists now exposed in the inner gorges of Grand Canyon, often underlying the Tonto Group formations the length of the Canyon.

Strong confirmation of this conclusion about the provenance of many of the silicate grains within the Muav Formation comes from the U-Pb ages of the detrital zircon grains extracted from the underlying Bright Angel Formation in the study by Gehrels et al. (2011), discussed above. Their Bright Angel Formation sandstone samples yielded detrital zircons overwhelmingly dominated by U-Pb ages of 1.60–1.72 Ga and 1.68–1.80 Ga, consistent with the Mazatzal and Yavapai provinces respectively whose granites and schists crop out in Grand Canyon's inner gorges locally underneath the Muav and Bright Angel Formations and Tapeats Sandstone (Karlstrom et al. 2003). There were secondary and very minor clusters of detrital zircon U-Pb ages around 1.45 Ga and 1.03 Ga respectively that might reflect a contribution from local Grand Canyon Supergroup strata and/or from the more distant Grenville orogen to the south or far east. Perhaps indicative of a very minor contribution of eroded sediment from the Grand Canyon Supergroup are the clasts composed of calcite-cemented clusters of quartz and K-feldspar grains and possible calcite clasts occasionally found in Muav Formation limestone samples. Thus, while not definitive, this combined evidence is certainly consistent with the provenance of the silicate grains within the Muav Formation limestones being local and quite close to where they were deposited, just as in the Bright Angel Formation and Tapeats Sandstone (Snelling 2021a, b).

The other silicate grains within several of the Muav Formation limestone samples that are sometimes detrital is glauconite. While the glauconite usually appears to be due to illite alteration of detrital K-feldspar grains, it also occurs as peloids (pellets), apparently grown around nuclei of tiny quartz and/

or K-feldspar grains, and fragments of them. Such glauconite peloids are common in the Bright Angel Formation where Rose (2003) maintained that they were detrital because in places they were concentrated in cross-bedded greensand horizons often associated with bioturbated green crumbly siltstones (after Amorosi 1997). Glauconite was long accepted as a necessary indicator of low oxygen conditions in a deep marine depositional environment, but that is no longer the case (McRae 1972). However, as a technical term, glauconite cannot be considered a distinct mineral species. As pointed out by Thompson and Hower (1975), the dominant or exclusive mineral in most glauconite pellets is iron-rich interlayered illite-smectite. The term glauconite should thus be strictly used only to denote the morphological occurrence of these clay minerals. Martin (1985) found that the glauconite in the Bright Angel Formation consisted of a disordered mixed layer phase consisting of an illite mixture with ~10% expandable smectite layers (after Hower 1961). Indeed, from a crystallographic perspective, glauconite shares commonality with mixed-layer illite-smectite and micas (which are closely related to illite, with the main differences being the amounts of  $\text{Fe}^{3+}$ ,  $\text{Al}^{3+}$ , and  $\text{K}^+$  substitutions in the crystal structures). From a practical standpoint, the illite or illite-smectite found in glauconite pellets is indistinguishable from other iron-rich illite or illite-smectite found in other morphologies. That is why in the XRD analyses reported in this study (tables 2 and 3) the glauconite was included in the illite reported at a  $2\theta$  angle of  $8.9^\circ$ .

The relevant question now is where was the source of these glauconite peloids? There is petrographic evidence in the thin sections that at least some of the illite forming the glauconite was due to illite alteration of K-feldspar grains. In fig. 38 some of the greenish glauconite grains retain the shapes of original K-feldspar grains and appear to be due to illite alteration of them. Even some of the peloids (pellets) have grown around tiny K-feldspar fragments. It is conceivable that the glauconite peloids formed around tiny K-feldspar (and quartz) fragments eroded from the Precambrian basement granites (and/or metamorphic schists) and washed around in the shallow marine waters that possibly covered Grand Canyon area in the pre-Flood era prior to Flood deposition of the Tonto Group, as evidenced by the stromatolites and in situ stromatolite reefs found in the Kwagunt Formation of the Grand Canyon Supergroup (Wise and Snelling 2005). Additionally, the many glauconite grains that appear to have formed from K-feldspar grains could be the result of the illite alteration during diagenesis after deposition of the Muav Formation (fig. 38). This suggests that those K-feldspar grains were originally detrital along with the quartz grains and muscovite

flakes and were altered to illite during diagenesis subsequent to their deposition. Some muscovite flakes were likewise altered to illite. If the glauconite peloids and the glauconite are a result of illite alteration during diagenesis of detrital K-feldspar grains, then these scenarios are also consistent with the provenance of the silicate clasts within the Muav Formation being local and quite close to where the limestones were deposited.

#### *Mineralogical and Textural Indicators of Rapid Short-Distance Transport and Deposition*

Petrographic examination of the Muav Formation samples in this study revealed unexpectedly that the limestones contained poorly sorted ubiquitous medium silt-sized to fine sand-sized, angular to sub-rounded quartz grains and subordinate ubiquitous medium silt-sized to fine sand-sized, angular to sub-rounded K-feldspar grains and former laths, with rounded grains being rare. The quartz and K-feldspar grains in these limestones are very similar to those in the fine-grained siltstones of the Bright Angel Formation (Snelling 2021b) except that they are less abundant and usually subordinate to the predominant carbonate grains. And occasionally K-feldspar grains are more abundant than quartz grains.

There have been several explanations for how sand grains, especially more resistant quartz grains, become rounded (Chandler 1988; Dott 2003; Goudie and Watson 1981):

- (1) abrasion of sand grains by wind,
- (2) selective transport of better-rounded grains (to the dune) with the more angular ones being left behind in aqueous environments,
- (3) recycling of older deposits containing rounded grains, and
- (4) intense chemical activity causing sharp corners of grains to be removed.

Of these four suggested mechanisms for how sand grains become rounded, the current consensus appears to be *only* eolian transport, especially for the more mechanically and chemically resistant quartz grains, even though there have been the several other explanations for how quartz grains become rounded (Chandler 1988; Dott 2003). Additionally, it should be noted that rounding of sand grains also depends on grain size. Even in eolian settings, silt and fine sand-sized grains never get rounded, only the larger grains. Thus, the mass of the grains in collisions seems to be the major factor in rounding, especially in deserts. Nevertheless, it is inferred that textural and compositional maturity is inherited and usually the result of several sedimentary cycles, with eolian abrasion having happened in at least one of the cycles in the history of the sand grains (Dott 2003; Folk 1978).

In stark contrast, it has been well-known for some time that aqueous transport does not appreciably round quartz or K-feldspar sand grains (Kuenen 1960; Russell and Taylor 1937; Twenhofel 1945). Indeed, it is now undisputed that even energetic aqueous conditions (such as longshore currents and daily tidal currents) are insufficient to round any minerals. It is believed that this is because the differences in rounding between eolian and aqueous environments are due to the ability of water to cushion impacts between grains. Garzanti et al. (2012; 2015) investigated sand from the Orange River that empties into the Atlantic Ocean in southwestern Africa and the Orange River Delta. Sand from these locations is carried northward along the African coast by continuous longshore currents and tidal activity, some of it for over 1,400 km (870 mi). After this great distance of transport and mechanical activity, all sand grains are still angular. The angular beach sand grains are then blown inland by southwesterly winds where they are deposited in the dunes of the Namibian Erg. They found that aqueous transport of beach sand grains, along the entire transport distance, fails to make them appreciably rounded compared to the original river and delta sand grains. It is not until the wind picks up the sand grains and blows them into the erg does any appreciable rounding take place. Thus, from that study it can be concluded that rounding appears to happen *only* by eolian transport and not by any other mechanisms. This has been confirmed by Whitmore and Strom (2017a, b; 2018), whose studies demonstrated that feldspar grains can show rounding with as little as a few 100 m (~1,000 ft) of eolian transport from a beach to a nearby eolian setting.

Thus far, this discussion on rounding has mainly focused on quartz, which is the most common silicate component within the Muav Formation limestones. However, Pye and Tsoar (2009, 72) claim that K-feldspar rounds faster than quartz because of its lower hardness (6.0 on Mohs scale of hardness, compared to 7.0 for quartz). Therefore, it is to be expected that during erosion and transport the softer K-feldspar grains would deteriorate more quickly and, depending on the distance of transport, would likely be eliminated by the abrasive action on them by the harder quartz grains. Some theoretical, experimental, and observational rounding data has been collected on K-feldspar grains. Marsland and Woodruff (1937) demonstrated experimentally that K-feldspar rounds slightly faster than quartz. Yet the lack of consensus is probably because the movement of various shapes, sphericities and sizes of grains is a complex process and is highly dependent on various velocity conditions (Morris 1957).

Despite these studies, some have suggested K-feldspar grains can be successfully abraded in aqueous environments. Odom (1975) and Odom, Doe, and Dott (1976) studied a variety of quartz arenites. They observed that K-feldspar content increases with decreasing grain size. They suggested that this trend occurs because K-feldspar grains are abraded more easily in aqueous high energy environments (forming larger-grained quartz arenites) and conserved in lower energy aqueous environments (forming smaller-grained feldspathic arenites). This trending relationship does not appear to apply to the limestones of the Muav Formation, even in those samples where K-feldspar is slightly more abundant than quartz. The K-feldspar and quartz grains are always similarly medium silt to fine sand size, similarly angular to sub-rounded, poorly sorted and generally scattered within the carbonate matrix. Snelling (2021a) found this inverse relationship between K-feldspar grain size and the K-feldspar percentage also did not apply to the underlying and related Tapeats Sandstone, as some of its largest K-feldspar clasts (2.00–4.00 mm,  $\phi = -1.00$  –  $-2.00$ , granule size) occur in samples with K-feldspar amounting to 22–33% of the rock volume. He concluded that this is consistent with rapid transport and deposition of the Tapeats Sandstone over a short distance, which thus also applies to the Muav Formation as representing the finest sediments in these Tonto Group formations which thus came from the same source with the same rapid transport and deposition processes (see below).

As already noted, Garzanti et al. (2015) found that angular sand grains of all mineral species changed little from fluvial and marine transport but were only significantly rounded by eolian abrasion. Most detrital mineral grains were still angular to sub-angular after ~2,000 km (~1,240 mi) of transport along the Orange River, confirming that fluvial environments are ineffective in rounding sand grains. Roundness changed little in the marine environment even after 300 to 350 km of high-energy littoral transport along the Atlantic shores of the Sperrgebiet. This condition demonstrated that beach action, as any transport in aqueous media, does not have much influence either (Pettijohn 1957) and disproves the long-held idea that beach sand grains are rounded faster than river sand grains because the former grains are rolled back and forth repeatedly on beaches (Folk 1980). This misunderstanding likely occurred because beach pebbles are usually round and flat, so this observation was probably extended to sand grains too.

From their observations Garzanti et al. (2015) also determined the “relative toughness” or susceptibility of various minerals to rounding. Based on the observed compositional trends and differential rates

of increased roundness with transport distance, Garzanti et al. (2015) established the following sequence of relative toughness and mechanical durability (from “toughest” to “weakest”):

garnet > quartz > epidote ≥ volcanic rock fragments  
 ≥ feldspars > opaques ≥ pyroxene > amphibole >  
 sedimentary/metasedimentary rock fragments.

However, K-feldspar also cleaves relatively easily compared to the conchoidal fracture of quartz. This perhaps explains why angular and sub-angular K-feldspar grains were found in most Muav Formation limestone thin sections examined (see Appendix E in the Supplementary material). Similarly, Whitmore et al. (2014), Whitmore and Garner (2018), and Whitmore and Strom (2018) found angular K-feldspar grains in virtually every sample they examined of the Permian Coconino Sandstone and many other related or correlated sandstones in the western USA, England, and Scotland. Indeed, they reported that the angular K-feldspar sand grains were sometimes more angular than the similar-sized quartz grains that surrounded them. Yet many of those same sandstones that have angular K-feldspars also contain angular grains of quartz, and mica flakes (mostly muscovite), and are moderately to poorly sorted (Borsch et al. 2018; Maithel, Garner, and Whitmore 2015; Whitmore et al. 2014). They thus concluded that the presence of angular K-feldspar grains in ancient sandstones should be a reliable indicator of

- (1) a first-order cycle of at least some of the sediment, and
- (2) aqueous transport and depositional processes of the sandstone.

Their conclusions are equally relevant to the angular K-feldspar grains in the Muav Formation limestones. They are consistent with the claim of Wanless (1973a, b; 1981) that water transported sands remained sub-arkosic throughout the entire Tonto Group section (defined at that time as just the Tapeats, Bright Angel, and Muav). This is also consistent with the petrographic observations of Rose (2003) and Snelling (2021a, b) of the Tapeats Sandstone and the sandstones, siltstones and shales of the Bright Angel Formation. These observations imply the rapid transport and depositional dispersal of the Tonto Group’s constituent sandy, silty, muddy, and carbonate units. Indeed, the observation in every Muav Formation limestone sample of the quartz and K-feldspar grains “floating” in the calcite (micrite) matrix suggests that the quartz and K-feldspar clasts were transported rapidly in a thick slurry of carbonate mud and deposited so rapidly that the scattered “floating” quartz and K-feldspar grains “froze” in place within the carbonate mud as it was rapidly deposited (discussed below).

Furthermore, micas are much softer on the Mohs scale of hardness (muscovite 2.0–2.5 and biotite 2.5–3.0) and consist of fragile sheets that easily cleave. Therefore, in a sediment dominated by quartz and K-feldspar grains with hardnesses of 7.0 and 6.0 respectively, the micas should be rapidly abraded. Standard petrography textbooks thus suggest micas should only be found in subaqueously transported and deposited sediments (Hallam 1981, 20; Moorhouse 1959, 343; Tucker 1981, 45).

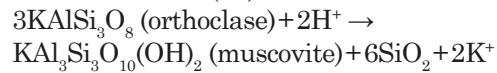
In their studies of sand transport along the southwestern coast of Africa, Garzanti et al. (2012, 2015) found no appreciable change in the composition of the sand (which contained micas) transported for hundreds of kilometers along the coastline. However, when the beach sand was picked up by wind and transported to the Namib dunes, all mineral grains became quickly rounded and the mica flakes either disappeared or possibly were never transported to the dunes.

Similarly, Whitmore (2017) and Whitmore and Strom (2017a, b) collected sand samples from beaches along the California and Oregon coastline and compared those samples with coastal dune samples from the same locations. They found that mica flakes were conspicuously absent from dune samples, unless those dunes were in close proximity (less than tens of kilometers) from mica-bearing bedrock, stream (fluvial) sediments or beach sands.

Anderson et al. (2013) and Anderson, Struble, and Whitmore (2017) devised a series of experiments to test the durability of mica flakes in eolian and subaqueous environments. A small amount of muscovite-rich sand was placed in a one-gallon glass jar with an RC airplane propeller attached on the inside of the lid and laid on a rock tumbler assembly, so that the rotation of the jar sustained a lateral dune. The velocity of the propeller was adjusted so that a small “dune” slowly migrated around the bottom of the jar. Surprisingly, after one year of spinning in this water-saturated tumbler (roughly equivalent to transport of 7,500 km or 4,660 mi), not only did the sand still contain an appreciable number of muscovite grains, but they were still large enough to be seen with the naked eye. This is potentially explained by the cushioning effect of the water, which has a much higher viscosity than air and reduces the kinetic energy of grain-grain collisions, thereby preventing the rapid degradation of mica flakes and other softer minerals. The experiments of Marsland and Woodruff (1937) further confirm these observations. Despite the simplicity of these experiments, they confirm field and experimental observations that mica flakes are rare in modern eolian deposits and commonly present in subaqueously deposited sands. And these observations are equally relevant to the

muscovite-containing Muav Formation limestones, which in outcrop display sedimentary structures consistent with rapid water transport of its constituent carbonate and silicate silt and fine sand grains (discussed below).

Borsch et al. (2018) emphasized it is important to note that the mica flakes they found in cross-bedded sandstones are detrital (transported) rather than diagenetic (altered from other minerals post-deposition) in character, which also applies to the mica flakes found in the Muav Formation limestones. For example, muscovite can be formed via the following chemical alteration of K-feldspar (orthoclase) in the presence of an acid ( $H^+$ ):



The mica produced in this conversion is sericite, which most often occurs entirely within the host grain, and is visible in thin section as fibrous bundles. Consequently, sericite is generally much smaller than the host grain and randomly oriented. By contrast, many of the mica flakes observed in their study were longer than the matrix grains (size inversion), and the characteristic fibrous textures were not present. Furthermore, in their samples Borsch et al. (2018) observed:

- (1) thin books of mica bent around other grains (often quartz),
- (2) thin contorted mica books with splayed ends,
- (3) the mica flakes did not often occupy the fairly common empty spaces of dissolved K-feldspar grains, and
- (4) significant amounts of orthoclase (as much as ~8–15%) were often found in the thin sections along with the mica flakes (that is, orthoclase had not been diagenetically altered).

Together, these clearly indicated that the mica flakes they observed are detrital, and thus are part of the original depositional fabric.

The micas observed in every thin section of the Muav Formation limestones in this study are muscovite flakes, even though the underlying Precambrian granites and schists also contain biotite which is slightly harder than muscovite. These muscovite flakes in the Muav Formation limestones have the same characteristics as listed by Borsch et al. (2018). Most of them are visible as edge-on stacked sheets in thin books. Because the thin sections were cut perpendicular to the bedding this means those muscovite flakes are parallel, and when at an angle are sub-parallel, to the bedding, a pattern consistent with aqueous deposition of detrital flakes. Furthermore, while the lengths of the flakes are variable, they are often longer than the widths of the surrounding quartz and K-feldspar grains and thus wedged between the quartz and K-feldspar grains

(fig. 37). Sometimes, they are also bent around the quartz and K-feldspar grains, and occasionally with their ends frayed, split, splayed, and even bent back. In other instances, the long thin books of muscovite have been altered after deposition, probably to illite or illite/smectite, the sheets sometimes expanding to be thicker, but still disposed in the positions in which they were originally deposited as detrital flakes. Furthermore, the muscovite flakes do not occupy empty spaces due to dissolved K-feldspar grains. To the contrary, all fifteen samples contain significant amounts of K-feldspar (0.9–26.3%), which is mostly orthoclase, along with the muscovite flakes (table 2). Some K-feldspar grains and former laths still display cross-hatched twinning under crossed polars characteristic of microcline and any diagenetic alteration of them is partial and in situ. Therefore, there can be little doubt these muscovite flakes are detrital and were transported and deposited subaqueously.

In conclusion, the collective evidence suggests a short-distance rapid transport of the fine sandy, silty and muddy silicate-containing carbonate sediments during rapid deposition of the Muav Formation. The transport distance had to be very short, since the source of the sediment has been clearly identified as the underlying Precambrian granitic plutons and schists of the Granite Gorge Metamorphic Suite, with probably little or no apparent contributions from the stratigraphically intervening Grand Canyon Supergroup sedimentary strata. Thus, erosion of the Great Unconformity was most likely catastrophic to supply so much sediment locally. And transport and deposition, likewise, was very possibly rapid and over only a very short distance for detrital muscovite flakes to have survived, and for K-feldspar grains and former laths to be so widely distributed within the full thickness of the Tonto Group, including the Muav Formation. The fact that the Muav Formation limestones contain so many angular to sub-angular quartz and K-feldspar (as well as plagioclase) grains also suggests rapid transport and deposition.

#### *Sedimentary Structures and the Depositional Environment*

The above observations and conclusions clearly seem to conflict with the uniformitarian interpretation of the Muav Formation being the product of a comparatively tranquil marine transgression lasting several million years involving shallow open shelf distal offshore to subtidal, intertidal and even tidal flats sedimentary environments (McKee 1945; Middleton and Elliott 2003; Rose 2003; 2006; 2011; Wanless 1973a, b; 1975; 1981). Indeed, Kennedy, Kablanow and Chadwick (1997) and Chadwick and Kennedy (1998) provided compelling evidence

of more catastrophic deep-water deposition of at least some of the underlying Tapeats Sandstone, which implies that both the overlying Bright Angel and Muav Formations were similarly deposited more catastrophically in deeper water. Thus, the sedimentary structures used to identify the Muav Formation as a shallow marine subtidal to tidal flats facies need to be re-evaluated.

If the Muav Formation was instead deposited under the catastrophic conditions of the global Flood cataclysm in which the sea level rose rapidly and the resulting “dramatic global marine transgression” (Karlstrom et al. 2018) was exceedingly rapid, then there are no similar processes operating today. The slavish commitment to the uniformitarian dogma that “the present is the key to the past” by most past workers researching the Muav Formation is unwarranted. Such researchers have tried to interpret the sedimentary structures in the Muav Formation on the basis of those produced in today’s relatively slow-and-tranquil shallow marine, intertidal and even tidal flats sedimentary environments. Garzanti (2017) has commented that sedimentologists “often resort to mythical thinking in the face of natural phenomena that we hardly understand” and that myths are ideas that owe their popularity to plausible reasoning rather than to observational evidence. It is no wonder that no unified consensus has been reached after over 150 years of investigations. The very potential of a global catastrophic Flood event is not even considered. Indeed, since the focus of uniformitarian-thinking investigators has been only on the Muav Formation primarily in Grand Canyon region, they have ignored the global context of this “dramatic global marine transgression” which catastrophically eroded the underlying Precambrian basement rocks and rapidly deposited the Muav Formation as a component of the Sauk megasequence on a global scale (Clarey 2019; 2020).

Therefore, in reevaluating the sedimentary structures in the Muav Formation, the only sedimentary environment today that might be used as a guide to the more catastrophic environmental conditions under which it was deposited would be that produced by severe storms and hurricanes, identical to the depositional conditions for the Tapeats Sandstone and Bright Angel Formation (Snelling 2021a, b). Yet, even that comparison would be deficient, as today severe storms and hurricanes are seasonally intermittent, whereas under the likely catastrophic flooding conditions of a dramatic global marine transgression severe storms and hurricane-like conditions would be happening continuously. The sedimentary structures within the Muav Formation that need re-evaluation include the thin laminated

bedding with siltstone partings between carbonate laminae, the wavy and undulating thicknesses and pinching out of carbonate laminae, planar and trough cross-laminations/stratification and small-scale cross-bedding, current and interference ripple marks, megaripples, and intraformational flat-bed conglomerates with imbricated clasts and cross-laminations, as well as the claimed desiccation cracks. These structures confirm high-energy, depositional conditions for the Muav Formation.

Furthermore, thin-section petrographic examination reveals that the Muav Formation limestones contain some occasional shell fragments that are sometimes broken (fig. 32). Added to those are large quantities of silicate mineral clasts (quartz and K-feldspar particularly) within the matrix of carbonate grains (usually calcite). Both the silicate clasts and the carbonate matrix grains are medium silt to fine sand-sized and yet the rock fabric is generally poorly sorted (figs. 34 and 35). However, at the outcrop scale, most of the limestones consist of thinly-laminated beds with alternating siltstone partings (fig. 20). Uniformitarians have traditionally envisaged such laminated beds being deposited one lamina at a time, the grain sizes deposited according to the variability in the energy of the sedimentation processes. Furthermore, the finer-grained muds are envisaged as settling very slowly out of suspension in the water column in the slackest energy conditions. Such slow-and-gradual depositional processes punctuated by occasional high-energy storms across a shallow shelf marine environment and its intertidal reach is essentially what has been envisaged for deposition of the underlying Bright Angel Formation by uniformitarians (Snelling 2021b), but quieter conditions have been suggested for the fine-grained Muav Formation limestones. However, observations of sedimentation in laboratory experiments in flumes substantiated by observations of the sedimentation resulting from real-world depositional events has resoundingly demonstrated that whole sequences of laminated sediment layers are deposited rapidly, virtually all-at-once, from heterogranular sediment mixtures, and muds (including lime muds) are also deposited rapidly (Schieber, Southard, and Thaisen 2007).

Berthault (1988, 1990), Julien, Lan, and Berthault (1994), and Julien, Lan, and Raslan (1998) reported numerous laboratory experiments in which heterogranular mixtures of sediments transported in water or air rapidly deposited in multiple laminae consisting of alternating fine and coarse grains. From each surging slurry of mixed grain sizes, the motion of the grains plus gravity sorted and separated them during the depositional process so that the resulting alternating fine- and coarse-grained laminae were

identical to shales and other laminated sedimentary layers found in the geologic record. Subsequently, Fineberg (1997) and Makse et al. (1997) confirmed those findings from further experiments and referred to this grain-size separation process as spontaneous stratification, substantiating their experimental outcomes with many papers in the literature on the physics involved, including when there are vibrations added to the transport of the heterogranular mixture. Furthermore, that this same spontaneous stratification process does occur in real-world depositional events to produce laminated sedimentary layers has been confirmed by Austin (1986; 2009) and Rowley, Kuntz, and MacLeod (1981). On June 12, 1980, pyroclastic flows generated by the collapse of the eruption plume of heterogranular debris and steam over the Mount St. Helens volcano and travelling at a hurricane velocity of 90 mph (150 kph) deposited stratified layers in total up to ~7.6 m (~25 ft) thick and up to ~2 km (~1.25 mi) wide on the pumice plain to the north of the volcano within three hours. These layers deposited from the slurries consisted of alternating fine- and coarse-grained thin laminae and included graded bedding and cross-bedding.

Uniformitarians have assumed that most mud accumulates directly from suspension in the water column, that mud deposition requires quiet bottom-water conditions, and that hence it takes long periods of time to deposit the great thicknesses of mudstones and shales that make up the majority of the geologic record (Macquaker and Bohacs 2007; Schieber, Southard, and Thaisen 2007). These assumptions are even more firmly adhered to by uniformitarians with the deposition of the lime muds that produced most limestones. Moshier, Helble, and Hill (2016, 59–62) specifically state that limestones formed from accumulations of calcium-carbonate shell fragments and/or limey muds that take a long time to be deposited, much longer than the time span of a flood, so by implication the Muav Formation could not have accumulated in Noah's Flood. They also claimed that in a violent flood lots of clay and quartz sand should be mixed together with the lime material, which is precisely what petrographic examination demonstrates, something they and other critics have not done. The Muav Formation limestones contain large amounts of medium silt to fine sand sized quartz and K-feldspar grains in the alternating thin limestone laminae, as well as in the siltstone partings.

However, while Schieber, Southard, and Thaisen (2007) admitted it is difficult to reconstruct the complex processes of mud deposition in the laboratory, such as the clumping of particles into flocules, they successfully used flume experiments

to investigate the bedload transport and deposition of clay floccules. In fact, they demonstrated that the clumping of clay particles into floccules occurs at flow velocities that transport and deposit sand. First, they found that deposition-prone floccules form over a wide range of experimental conditions, which suggests an underlying universal process. And second, at a critical flow velocity of only 20–25 cm/sec (0.66–0.82 ft/sec) or 0.72–0.90 kph (0.45–0.56 mph) floccule ripples develop into low-angle foresets and mud beds that appear laminated after post-depositional compaction. But the layers retain signs of floccule ripple bedding that would be detectable in the rock record. Schieber, Southard, and Thaisen (2007) concluded that because mudstones were long thought to record low-energy conditions of offshore and deeper water environments, their experimental results call for re-evaluation of published interpretations of ancient mudstone successions and derived paleo-oceanographic conditions.

In commenting on these experimental findings, Macquaker and Bohacs (2007) agreed this mechanism for depositing mud is at odds with the perceived (uniformitarian) wisdom that most mud accumulates directly from suspension in the water column requiring quiet bottom-water conditions, and that mudstones containing closely-spaced, parallel laminae represent continuous deposition. They affirmed that, in contrast, Schieber, Southard, and Thaisen (2007) had shown that mud can accumulate as current ripples composed of grain aggregates under currents that can transport very fine sand. Furthermore, their laboratory investigations have now provided direct evidence of advective sediment transport of mud-sized material in floccules, those clay aggregates forming migrating ripples with low crests (2–20 mm) and very long spacings (300–400 mm) that deposited the sediment in non-parallel inclined laminae that could be easily misinterpreted as parallel-laminated under much higher current velocities than previously assumed.

Macquaker and Bohacs (2007) asserted that the results call for critical reappraisal of all mudstones previously interpreted as having been continuously deposited under still waters. Instead, substantial volumes of mud can accumulate in higher-energy conditions than most researchers had assumed. Furthermore, these experimental results came at a time when mudstone science was poised for a paradigm shift.

Schieber and Southard (2009) performed additional flume experiments to demonstrate that muds can be transported in bedload as floccule ripples and deposited at current velocities that would suffice to transport and deposit sand. Their further experiments provided firsthand observations of the

processes that shape and propagate mud ripples, whose geometries are very similar to those produced in sandy sediments.

Lest it be thought their experimental results did not apply to lime muds, Schieber et al. (2013) did further flume experiments using carbonate muds with particle sizes less than 0.06 mm ( $\phi = +4.0$ , coarse silt), which is exactly in the lower-range of the silicate and carbonate particle sizes in the Muav Formation limestones. They found that those suspensions of lime muds also form floccules that travel in bedload, form ripples, and deposits laminated sediments at the same range of velocities at which sand grains start to move and form ripples, just as observed in their previous experiments with clay-mineral suspensions. Furthermore, the ripples formed during this floccule deposition of lime muds were found to be in essence identical to those formed by clay-mineral floccules or sand grains under similar conditions. The resulting carbonate mud deposits showed internal laminae and in plan view a pattern of ripple foresets identical to those in sandstones. They concluded that the key controls on lime mud deposition are flocculation and suspended-sediment concentration, which are more important than particle mineralogy and water chemistry. Yet, just as it has been assumed the deposition of terrigenous (silicate) muds required quiescent conditions (Potter 2003), so too there has been a long-standing notion that the accumulation of abundant carbonate muds reflects low depositional energy in quiescent conditions in offshore and deeper-water environments (Boggs 1995). Schieber et al. (2013) thus insisted their experiments demonstrate unequivocally that carbonate muds can also accumulate in energetic conditions, and that carbonate rocks in the sedimentary record may therefore not necessarily reflect shifts in depositional energy (or water depth), but alternatively, may only imply a shift in supplied sediment type.

Thus, there is no excuse for Moshier, Helble, and Hill (2016) ignoring these well-established experimental conclusions (published in 2013) in their claims about the slow-and-gradual deposition of limestones in Grand Canyon strata, such as in the Muav Formation. The Muav Formation limestones contain a poorly-sorted mixture of medium silt to fine sand sized silicate and carbonate grains which they admit would be expected if deposited by catastrophic flood conditions. And these limestones have been deposited in laminae with ripples just as reproduced in the experiments by Schieber et al. (2013) at velocities in which sand grains are similarly deposited. They have also been deposited in laminae alternating with siltstone partings that match the alternating fine- and coarser-grained laminae produced by the spontaneous stratification

of heterogranular sediment mixtures in both experiments and field observations. Furthermore, as Schieber et al. (2013) demonstrated, such deposition of lime muds may not necessarily reflect shifts in depositional energy or water depth, but alternatively may only imply a shift in supplied sediment type. Thus, all this evidence is consistent with the Muav Formation limestones being deposited under the same storm and hurricane-like conditions as the underlying Bright Angel Formation and Tapeats Sandstone as concluded by Snelling (2021a, b).

Furthermore, the other sedimentary structures within the Muav Formation are entirely compatible with its rapid deposition by high-energy, storm-driven water currents in a relatively shallow marine environment. A key hallmark of such storm deposition is hummocky cross-stratification (Boggs 1995; Harms et al. 1975; Seilacher and Aigner 1991; Walker and Plint 1992), which has been identified in both the Tapeats Sandstone and Bright Angel Formation (Snelling 2021a, b). Dott and Bourgeois (1982) calculated the formation of hummocky beds (storm beds or tempestites) occurred in the upper sheet flow regime with water flow velocities at 80–200 cm/sec (0.8–2 m/sec), with intense oscillatory flow in shallow water depths. After examining the paleogeographic distribution of 107 occurrences of hummocky cross-stratification in the geologic record spanning the Proterozoic to the Recent, Duke (1985) concluded that most occurrences were generated by hurricanes and that hurricane-generated bottom flows tend to be oscillatory- or multi-directionally-dominant. Furthermore, Duke (1985) and Duke, Arnott and Cheel (1991) proposed a depositional model for hummocky cross-stratification formation as due to storm transport of coastal sand to the inner shelf under dominantly oscillatory flow controlled by a very minor component of unidirectional flow, based in part on controlled laboratory experiments by Arnott and Southard (1990) and Southard et al. (1990). Also, Swift et al. (1983) concluded that hummocky cross-strata sets are due to the action of strong storm-wave surges involving combined-flow currents with sediment deposition throughout much of the storm's duration, while Swift and Thorne (1991) argued that the depositional hydraulic conditions during storms meant sediment accumulation only occurred below storm wave base, which Walker and Plint (1992) estimated was at greater than ~25 m (~82 ft) water depth.

While hummocky cross-stratification as defined is not readily evident in the Muav Formation, wavy and undulating, thickening, thinning, and pinching out of laminae, the planar and trough cross-laminations, small-scale cross-stratification, current and interference ripple marks, megaripples with internal cross-stratification, and intraformational flat-bed conglomerates with imbricated clasts and cross-laminations are all consistent with high-energy water deposition. Such wavy and undulating, thickening and thinning and pinching out of laminae has been well-established as occurring under high current flow power when the sediment particles are fine-grained as they are in the Muav Formation (fig. 40) (Allen 1970). Ripple marks with cross-lamination are produced at lesser water current power (fig. 40), and these have also been produced in the flume experiments by Schieber, Southard, and Thaisen (2007) and Schieber et al. (2013), although non-parallel laminae also resulted. Such changes in water current power depositing the alternating thickening and thinning lime mud and silt laminae are consistent with oscillations due to hurricane-generated bottom flows. Likewise, planar and trough cross-laminations, small-scale cross-stratification,

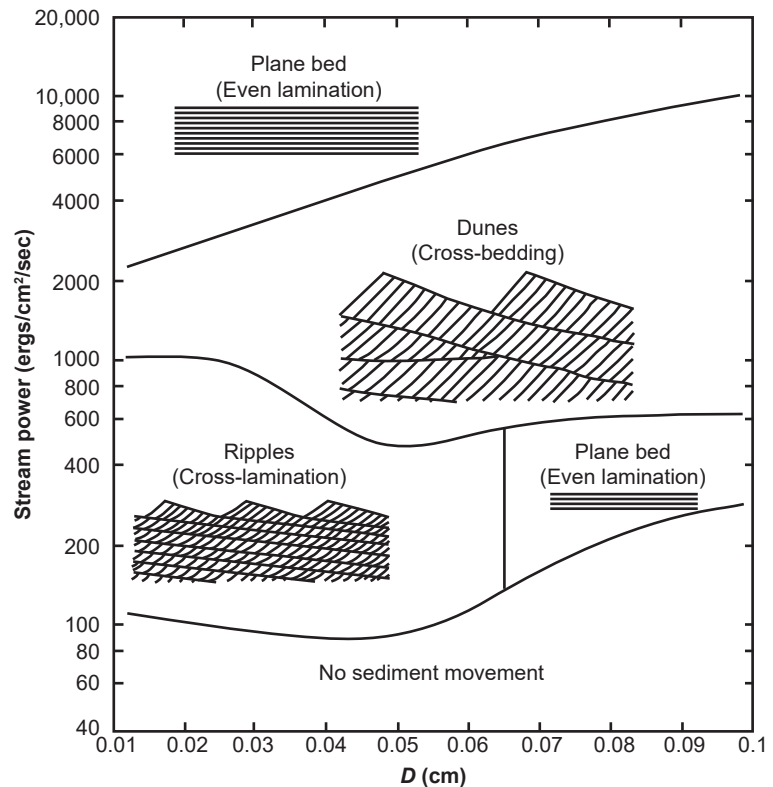


**Fig. 40.** Bedforms in relation to stream (or water current power) and caliber of bed-material load (after Allen 1970, 79, fig. 2.6). Note that plane bed even lamination can occur at extremely high stream flow power, especially when the sediment particles are fine-grained, as in the Muav Formation. Ripples with cross-lamination form at lower stream flow power.

and megaripples with internal cross-stratification are consistent with high-energy water flows under storm conditions. Indeed, megaripples with amplitudes of ~10cm (~4in.) and wavelengths of ~65cm (~26in.) are never produced in tranquil slow-and-gradual deposition of lime muds. All these sedimentary structures require swift horizontal water flows rather than the slow vertical settling of lime muds.

Additional testimony to the high-energy water flow responsible for depositing the Muav Formation are the laterally-persistent intraformational flat-pebble conglomerates consisting of thin and flat limestone pebbles, generally rounded on their edges and relatively small, and tending to be oriented in a horizontal attitude parallel to the bedding planes, although some pebbles rest on end or dip at steep angles (McKee 1945). Rose (2003) described them as in 5–25cm (~2.0–9.8in.) thick beds interbedded with thin-bedded limestone with the pebbles sometimes imbricated in bi-directional co-sets within cross-lamination patterns. And sometimes these conglomerates occur in apparent lens-shaped channels. Rose (2003; 2006; 2001) admitted that these flat-pebble conglomerate beds indicated strong bottom agitation and bedload transport of rounded limestone pebbles in medium quartz sand, which was consistent with high-energy storm deposition, as suggested for similar conglomerates by Kazmierczak and Goldring (1978), Sepkoski et al. (1991), and Wu (1982). He tried to side-step the obvious conclusion by claiming the apparent lens-shaped channels indicated storm-enhanced deposition in tidal channels, but such a model cannot explain the predominant laterally extensive flat-pebble conglomerate beds that McKee (1945) found extended up to 45mi (~73km). These widespread conglomerate layers interbedded with laminated limestone beds are only consistent with high-energy, hurricane-like-induced, storm deposition over a huge area.

Both Wanless (1975) and Rose (2003) described what they interpreted as desiccation cracks or features. For comparison, Hill and Moshier (2009, 2016) provided a photograph of recently formed mud cracks in wet mud along the Little Colorado River. They argued that such mud cracks in the Tapeats Sandstone indicate dry subaerial conditions at that bounding surface. Similarly, Wanless (1975) and Rose (2003) argued such interpreted desiccation cracks and features were evidence of a tidal flats model for deposition of some of the Muav Formation, which is incompatible with the deeper water storm-driven water current deposition during catastrophic flood conditions as proposed here, and as suggested by Baumgardner (2013; 2018a, b). However, these cannot possibly be desiccation cracks because these features are in clay-poor limestone and dolostone, not

silicate mud. When silicate mud dries and cracks the polygonal shapes become concavely arched, whereas the claimed fossilized desiccation features are not adequately described for potential comparison. For any sediment to crack by desiccation, it must be dominated by clay-sized particles and must have certain clay minerals. In the XRD analyses of the Muav Formation (table 2) there is illite in only 11 of the 15 samples, ranging between 0.5% and 6.7%, which is largely muscovite and also some illite alteration of K-feldspar, as observed under the microscope. In the clay fraction XRD analyses (table 3), the clay contents are dominated by illite and illite/smectite, with only one sample containing any kaolinite (8.8%). So, the most common clay mineral in the Muav Formation is illite, but in insignificant amounts. By comparison, modern soils that crack due to desiccation have significant amounts of clay minerals. Basma et al. (1996), Harianto et al. (2008), Yassoglou et al. (1994), and Yesiller et al. (2000) report cracking in soils with clay contents ranging from 13 to 58.3%. The Muav Formation limestones simply do not have the clay minerals necessary for any kind of desiccation to occur. Instead, these apparent shrinkage features in the Muav Formation are more likely to be due to subaqueous shrinkage known as syneresis, which occurs when a liquid such as pore water is expelled from a gel-like substance such as water-saturated silicate and lime muds containing smectite in response to changes in salinity and possibly triggered by ground motion during earthquakes (Boggs 1995; Burst 1965; Plummer and Gostin 1981; Pratt 1998). Whitmore (2009) has also proposed other feasible possibilities for such apparent mud crack features, such as diastasis cracks and clastic dikes. Thus, the apparent shrinkage features within the Muav Formation (which contains minor smectite, see table 3) are not evidence contrary to deposition by high-energy, storm-driven water currents in a relatively shallow marine environment during catastrophic flood conditions.

Finally, the body and trace fossils found in the Muav Formation are consistent with such rapid deposition of the lime muds and silts. Indeed, in order to produce body fossils rapid deposition is required to bury creatures whole before they decayed or were scavenged. Furthermore, the shell fragments found in the Muav Formation are consistent with transport and deposition by high-energy water flows. In contrast, Hill and Moshier (2009, 2016) claimed erroneously that delicate trace fossils require relatively gentle conditions for their preservation. However, once trails and burrows are made, they need to be buried rapidly before being obliterated by stormy conditions and/or by continuing burrowing activity of the trail-makers. Furthermore, whereas Pemberton, MacEachern,

and Frey (1992) argued that such trails would only be preserved below the minimum wave base, that is, in deeper water, Bromley and Asgaard (1991) warned that trace fossils could be preservational (where they are buried) rather than behavioral (where they lived). Even the pervasive mottling in some of the Muav Formation limestones that has been attributed by Noble (1914), Schuchert (1918), and Rose (2003) to intense repetitive burrowing is consistent with rapid accumulation of the limestones while the worms frantically burrowed through the lime muds that were actively burying them. Resser (1945) also claimed that there were algal structures in portions of the Muav Formation limestones but never checked to demonstrate that they were visibly present. Similarly, Wanless (1975) claimed he had found small stromatolite domes that were marked simply by crinkly disrupted laminations but never provided evidence of these being true stromatolitic mats. Thus, overall, there is no definitive evidence that precludes the Muav Formation having been rapidly deposited by high-energy, hurricane-driven water currents during catastrophic flood conditions.

#### *Post-Depositional Dolomite Alteration*

While dolomite has been reported as present in the Muav Formation by McKee (1945), Wanless (1973a; 1975), and Rose (2003), both in mineral content in limestones or as dolostone layers, none of these investigators has discussed how the dolomite formed, either as a primary depositional product or as post-depositional alteration of the limestones. Given the very minor scale of dolomite formation today in the very specialized warm-to-hot saline environments needed for dolomite precipitation, uniformitarianism have struggled to explain dolomite alteration of limestones and the deposition of dolostone beds. Thus, most uniformitarian investigators like those who have studied the Muav Formation usually sidestep this so called “dolomite problem” and simply postulate a warm saline tidal flats depositional environment for both limestones and dolostones despite the clear indications in the Muav Formation of its rapid deposition in deeper waters. Furthermore, it is very clear from the petrographic evidence already presented here that post-depositional dolomite alteration of the originally-deposited limestones has occurred, confirmed at outcrop scale where adjoining samples only 6 m (19.5 ft) apart at the same stratigraphic level at the base of the Havasu Member in the Matkatamiba fold are dominated by calcite (92.8%) (MFTB-05) and dolomite (81.9%) (MFTB-06).

Both Warren (2000) and Ning et al. (2020) provide excellent overviews of this “dolomite problem.” Dolomite is regarded as one of the most enigmatic minerals, being abundant in pre-Cenozoic strata

but rare in Cenozoic and modern sediments. It is hypothesized conventionally that such sharp contrast of dolomite distribution might be linked to the changes of uniformitarian-interpreted environmental conditions, although factors controlling dolomite precipitation on a global scale remain elusive (Burns, McKenzie, and Vasconcelos 2000). The “dolomite problem” (Fairbridge 1957) refers to the sharp distinctions between ancient dolostone strata and dolomite in modern sediments in the spatial distribution, stratigraphic thickness and degree of crystal ordering (Kaczmarek and Sibley 2011; Lumsden and Caudle 2001; Mresah 1998), and has puzzled geologists for more than 200 years (Warren 2000). Most modern dolomite occurrences are penecontemporaneous, patchy, and micritic, with dolomite (the mineral) only making up less than 50% of the resultant dolostone. In contrast, most ancient dolostones entrain dolomite (the mineral) as more than 90% of the dolostone volume, are secondary, extensive and often sparry. Furthermore, the dolomite has apparently overprinted whole limestone platforms as diagenetic units that are typically some hundreds of meters thick and extend across areas that may be hundreds of kilometers wide (Warren 2000).

The “dolomite problem” includes one key aspect, namely, how dolomite could precipitate from the natural aqueous environment, since  $Mg^{2+}$  hydration inhibits dolomite precipitation (Lippmann 1982). Land (1998) concluded after a 32-year experiment with a thousand-fold oversaturated solution at room temperature which failed to precipitate dolomite that the “dolomite problem” results from the kinetic inhibition of dolomite crystallization. However, the energy barrier of  $Mg^{2+}$  hydration could be overcome by, for example, an increase of Mg/Ca ratio of solution (Shinn, Ginsburg, and Lloyd 1965), dilution of solution (Badiozamani 1973), microbial or organic compound mediation (Roberts et al. 2013, Vasconcelos et al. 1995), or increase of ionic strength of fluid and with zinc complexation (Vandeginste et al. 2019). Therefore, although the exact pathways of dolomitization remain unclear, precipitation of dolomite at earth’s surface temperatures and pressures is entirely possible. On the other hand, various models, including the sabkha distillation (Shinn, Ginsburg, and Lloyd 1965), brine re-flux (Adams and Rhodes 1960), burial diagenesis (Mattes and Mountjoy 1980), thermogenesis (Davies and Smith, 2006) and organogenesis (Vasconcelos et al. 1995) models, have been proposed to interpret the formation of modern dolomite. However, the application of these models individually or sequentially to interpret ancient massive dolostone is difficult (Kaczmarek et al. 2017; Land 1985;

Machel 2004). For example, it remains unclear whether massive dolostone formation involves a single or multiple dolomitization events or how to recognize/sequence the dolomitization events in the stratigraphic record. Little is known about the Mg source or the mechanism that effectively pumps Mg into thick carbonate deposits over the platform scale.

Therefore, the origin of ancient massive dolostone is an important yet unresolved part of the “dolomite problem” (Land 1985; Machel 2004; Warren 2000). It is typically a consensus that ancient massive dolostone was generated by the replacement of Ca-carbonate precursors (Kaczmarek et al. 2017; Land 1985; Machel 2004). Massive dolostone formation not only needs to overcome the kinetic barrier imposed by  $\text{Mg}^{2+}$  hydration, but also requires sufficient Mg-bearing fluids and a long-term Mg pumping mechanism. Obviously, a single dolomitization event is hard to envision for the extensive dolomite formation over a large carbonate platform. Lumsden and Caudle (2001) proposed that massive dolostone could be generated by stacking of multiple episodes of dolomitization events that are linked to sea-level fluctuation. This model seems reasonable, because most ancient massive dolostones are composed of cyclic depositions of shoaling upward sequences, for example, massive dolostone in the Alpine Triassic (Meister et al. 2013). In addition, Kah, Grotzinger, and James (2000) reported progressive enrichment of  $^{18}\text{O}$  from subtidal to supratidal (exposed) dolostone of the Mesoproterozoic Social Cliff Formation, reflecting the supposed sea-level driven environmental changes. Yet, dolomitization in massive dolostone has not been unambiguously sequenced by sedimentological or geochemical approaches. Ning et al. (2020) concluded that none of the existing dolomitization models can explain the origin of ancient massive dolostones hundreds-meter thick with platform-wide distribution.

In a new approach to this “dolomite problem,” Fang and Xu (2022) presented the experimental case for an abiotic mechanism by which dissolved silica can catalyze dolomite precipitation. They demonstrated that the presence of only 1–2 mM of aqueous  $\text{Si}(\text{OH})_4$  in high Mg:Ca ratio solutions at room temperature will promote disordered dolomite precipitation, with up to 48.7 mol%  $\text{MgCO}_3$ . Dissolved silica in solution also promotes incorporation of Mg into the Ca-Mg carbonates. They found that this was because dissolved silica possesses a low-dipole moment and a dielectric constant similar to hydrogen sulfide, dioxane and polysaccharide, and to exopolymeric substances (EPS) produced by microbial mats, all of which are catalysts in previously established room-temperature dolomite synthesis. These low-dipole-moment molecules adsorbed on the dolomite surface

evidently can lower the dehydration energy barrier of a surface  $\text{Mg}^{2+}$ -water complex and promote dolomite nucleation and growth. They concluded their new model for abiotic dolomite formation might explain the significant amount of primary dolomite in the geologic record.

In summary, Warren (2000) stated that the possible reason for the “dolomite problem” in the disparity between modern and ancient modes of occurrence is related to dolomite’s unique mineralogy and chemistry. The most important control on distribution is possibly kinetics. Then, there is the problem of parity, namely, do variations in seawater chemistry influence dolomite volumes in carbonate platforms, or are changes in the volume of dolomite influencing seawater chemistry? Proposed dolomitizing solutions include marine brines (Behrens and Land 1972; Mackenzie 1981), continental brines (Clayton et al. 1968; Von der Borch, Lock, and Schwebel 1975), essentially normal seawater (Carballo, Land and Miser 1987; Mazzullo, Bischoff and Teal 1995; Saller 1984), seawater modified by extensive sulfate reduction (Baker and Kastner 1981; Kelts and Mackenzie 1982) seawater mixed with meteoric water (Cander 1994; Land 1973; Magaritz et al. 1980), seawater mixed with hypersaline brines (Meyers, Lu, and Zachariah 1997), and dissolved silica in carbonate-rich fluids (Fang and Xu 2022). Burns, McKenzie, and Vasconcelos (2000) argued that the relative level of Mg/Ca and  $p\text{CO}$  in the dolomite precipitating fluid is far less important in precipitating the varying volumes of dolomite than the levels of oceanic oxygen. In conclusion, Warren (2000) admitted that at the current state of our understanding we simply do not know why there is so little modern dolomite, why there is so much ancient dolomite, and how the chemistry of ancient dolomite forming settings has evolved over time. In other words, we do not know the relative importance of kinetics versus parity in dolomite precipitation, and we do not yet have a good understanding of how the volume of dolomite precipitation has varied through time. Is it controlled by seawater chemistry, or does it control seawater chemistry?

However, in contrast to the uniformitarians’ failure to solve this “dolomite problem,” the model of the catastrophic global Flood during which catastrophic plate tectonics occurred (discussed below) can explain both primary deposition of dolostone layers in the Muav Formation and the post-depositional dolomite alteration of Muav Formation limestones. As described by Austin et al. (1994) and Baumgardner (2003) the Flood event was initiated by the breaking up of the fountains of the great deep (Genesis 7:11) which triggered catastrophic plate tectonics. Those fountains likely consisted of superheated steam

released from rapidly upwelling mantle-derived magmas along ocean ridges and continental rifts and would have been laden with dissolved salts and gases, including CO<sub>2</sub>, resulting in a rapid rise in local seawater salinity and temperature, initiating a dramatic change in seawater chemistry (Austin and Humphreys 1990). Increased seawater salinity could have included abundant Ca and Mg ions as well as dissolved silica from the breakdown of mantle minerals by cavitation due to the out-bursting of superheated steam (Baumgardner 2018a). Together with CO<sub>2</sub> from the steam, this combination could have facilitated the precipitation of prodigious calcite and secondary dolomite grains on the seafloor as the hot superheated steam mingled with the colder seawater. The catastrophic plate tectonics model (Austin et al. 1994) predicted that seawater temperatures would have risen dramatically during the Flood event, raising them steadily to the temperatures at which dolomite is known to more readily form. Early in the Flood the precipitation of carbonate sediments would have been adjacent to the ocean ridges where the silica- and carbonate-laden, superheated steam jets were erupting into the cooler ocean waters. High-energy, tsunami-driven water flows generated during the Flood (discussed below) would have then transported the carbonate muds and silts to eventually deposit them in limestone and dolostone beds across the continents. Given the significantly different densities or specific gravities of calcite and dolomite (2.71 and 2.85 respectively), mixtures of calcite and dolomite grains in sediment slurries would as they were deposited spontaneously stratify (Makse et al. 1997), which explains the alternating limestone and dolostone layers, sometimes with this chert beds, within parts of the Redwall Limestone in Grand Canyon (Austin 1994). Furthermore, even when limestones were the primarily deposited layers, not only would some dolomite grains potentially have been included in them, as seen in the Muav Formation limestones, but the warm fluids trapped in the pores between the deposited calcite grains would likely have retained significant enough quantities of Mg ions to have resulted in post-depositional dolomite alteration of calcite and some of the susceptible inter-mixed silicate grains such as K-feldspar, as also seen in the Muav Formation limestones.

#### “Age” Indicators

The conventional age of the Muav Formation was initially established based on the formation’s stratigraphic position overlying the Bright Angel Formation and relative to trilobite fossil assemblage zones. In western and central Grand Canyon the *Solenopleurella* fossil assemblage zone lies within the topmost Havasu Member of the formation and in

western Grand Canyon the *Alokistocare-Glossopleura* fossil assemblage zone lies just below the base of the formation and its basal Rampart Cave Member (fig. 5). Thus, the Muav Formation was designated as Middle Cambrian.

Claimed absolute numerical ages of these trilobite zones have subsequently been determined by precisely U-Pb dated zircon grains in regional and global sections (Schmitz 2012; Sundberg et al. 2016; 2020), tied to U-Pb zircon dated Cambrian marker beds elsewhere (Landing et al. 2015; Peng, Babcock, and Cooper 2012) (fig. 28). Note that the Muav Formation is now regarded as lying between the *Glossopleura* fossil assemblage zone at its base in western Grand Canyon and the *Spencerella* fossil assemblage zone within the topmost Havasu Member (fig. 28). Karlstrom et al. (2018, 2020) have thus established the conventional age of the Muav Formation at ~499–502Ma based on U-Pb dating of detrital zircons in the underlying Tapeats Sandstone and the now established U-Pb zircon dates of these trilobite fossil zones. But the methodology they all used raises numerous issues and questions, including how reliable is the U-Pb dating method?

In their supplemental data, Karlstrom et al. (2018) tabulated all the U-Pb dating results of every detrital zircon grain from the Tapeats Sandstone that they, Gehrels et al. (2011) and Matthews, Guest, and Madronich (2018) analyzed. They obtained a wide spectrum of U-Pb ages with peaks corresponding to the published ages of the source rocks from which they concluded the zircon grains had been eroded. Together with Karlstrom et al. (2020), they established the age of the Tapeats Sandstone by statistically determining from the spectrum of the lowest detrital zircon U-Pb ages the peak of the “bell-shaped” curve, which at 507–508Ma they called the maximum depositional age. Yet, the supplemental data tables listed that many of the detrital zircons yielded U-Pb ages less than that 507–508Ma age for the Tapeats Sandstone—at least 59 spot analyses of zircons from their Hermit Creek sample with the lowest U-Pb age of 407.2Ma, at least 45 spot analyses of zircons from their Frenchman Mountain sample with the lowest U-Pb age of 481.8Ma, and at least 51 spot analyses of zircons from their East Verde River sample with the lowest U-Pb age of 468.0Ma. Karlstrom et al. (2018) do not explain how the supposedly 507–508 million years old Tapeats Sandstone can have included within it so many detrital zircons with U-Pb ages less than its supposed depositional age, including one as “young” as only 407.2 million years old. Nor do they explain where these “younger” detrital zircons originated from within the Tapeats Sandstone. Indeed, how could the 507–508Ma detrital zircons be incorporated in the Tapeats Sandstone if the

underlying rocks that were eroded to provide the sand grains, including the zircon grains, are older than 507–508Ma? This question alone raises serious doubts as to the applicability and reliability of this technique for supposedly quantifying the apparent depositional ages of sedimentary rock units.

Not only is their methodology questionable, so must be the U-Pb dating method they used if it produced such illogical ages. The latter problem alone raises questions as to the accuracy of the zircon U-Pb method for dating the Cambrian marker beds elsewhere and thus the fossil assemblage zones that are within the Muav Formation.

Snelling (2000; 2009) has already provided details of numerous problems with the U-Pb dating method that are well-documented in the scientific literature. Furthermore, Snelling (2017a) reviewed all the determinations of the U-Pb decay rates (half-lives) and demonstrated that these crucial parameters are not yet precisely known, while Snelling (2017b; 2018; 2019) highlighted in detail the problems of common Pb, U, and Pb mobility, and mass fractionation respectively that plague all efforts to obtain accurate U-Pb age determinations. Nevertheless, Karlstrom et al. (2018; 2020) championed the tandem U-Pb dating procedure they used, that is, LA-ICP-MS (laser-ablation–inductively coupled plasma–mass spectrometry) analyses followed by CA-ID-TIMS (chemical abrasion–isotope dilution–thermal ionization mass spectrometry) analyses. And even though it often produced apparently concordant U-Pb dates (essentially matching  $^{206}\text{Pb}$ - $^{207}\text{Pb}$ ,  $^{238}\text{U}$ - $^{206}\text{Pb}$  and  $^{235}\text{U}$ - $^{207}\text{Pb}$  ages), there were still many detrital zircon grains that yielded illogically younger ages than the supposed depositional age of the Tapeats Sandstone. Furthermore, Snelling (2005b) reported CA-ID-TIMS analyses of six zircon grains recovered from a thin tuff bed in the Muav Formation in western Grand Canyon, only two of which yielded concordant U-Pb ages of 74.8Ma and 169.0Ma (fig. 26). Otherwise, the individual grain model ages ranged from a  $^{206}\text{Pb}/^{238}\text{U}$  age of 68.2Ma to a  $^{207}\text{Pb}/^{206}\text{Pb}$  age of 1621.2Ma. And Snelling (2005b) also obtained single zircon grain fission track ages of 75Ma, 158Ma, and 408Ma that are very much younger than the Karlstrom et al. (2018, 2020) tandem U-Pb ages for deposition of the Muav Formation. Fission tracks are the physical evidence of the quantity of nuclear decay that has actually occurred. How then could zircon grains U-Pb dated as 74.8Ma and 169Ma be included in a tuff bed deposited within the supposedly 499–502Ma Muav Formation? These considerations and highly inconsistent U-Pb results from what is touted as a superior analytical procedure only highlight the unreliability and fallibility of the U-Pb dating method.

However, it could be argued that the accepted radiometric ages of various Grand Canyon strata, including the basement granites and schists, date those rocks and strata in the correct relative order, and consistently in hundreds of millions to almost two billion years, except for the recent lava flows in western Grand Canyon (Wiens 2016). Vardiman, Snelling, and Chaffin (2005) have demonstrated, from six lines of evidence supported by experimental results, that the reason for this systematic consistency of radiometric ages in the Grand Canyon stratigraphic sequence is because during a past catastrophic event there was a systematic acceleration of nuclear decay rates, potentially by six orders of magnitude. Three of those six lines of evidence involved experimental results obtained on Grand Canyon samples, namely, discordant radiometric ages obtained from four Precambrian units (the Cardenas Basalt, the Bass Rapids diabase sill, the Elves Chasm Granodiorite and the Brahma Schist amphibolites) (Snelling 2005c), coexisting uranium and polonium radiohalos (Snelling 2005a) and fission tracks in zircons (Snelling 2005b). Critics have pointed to the enormous quantities of heat that apparently would be released by such accelerated nuclear decay (Wiens 2016), yet Vardiman, Snelling, and Chaffin (2005) had already anticipated this criticism and provided plausible possible explanations, including the experimental fact that the radiohalos (which only form below 150°C) would have been annealed if such an enormous heat release had occurred (Snelling 2005a).

In conclusion, there is sufficient overwhelming evidence, also documented in the scientific literature, to question the reliability, and even the validity, of the U-Pb dating method. This is highly evident from so many U-Pb dates for zircons within the Tapeats Sandstone that are markedly younger than the claimed depositional age of that sandstone which directly underlies the Bright Angel and Muav Formations. Thus, the U-Pb dating of detrital zircons from the Tapeats Sandstone that was used to obtain a ~499–502Ma age for the Muav Formation (Karlstrom et al. 2018, 2020), coupled with the claimed biostratigraphic age of the Muav Formation linked to U-Pb ages of marker beds elsewhere (Karlstrom et al. 2020; Sundberg et al. 2020), is not an impediment to explaining the deposition of the Muav Formation in a much more recent catastrophic event, namely, the global Genesis Flood cataclysm. That would be more consistent with the textural and mineralogical evidence for the rapid local erosion and short-distance rapid transport and deposition of its constituent silicate and carbonate silt and mud.

#### *Initial Flood Catastrophic Erosion and Deposition*

Austin (1994) provided a detailed comprehensive

description and account of the geological development of Grand Canyon strata in the context of the global Genesis Flood cataclysm and the Canyon's erosion in the Flood's aftermath. In particular, he described the Tonto Group as being deposited by the Flood waters advancing eastwards onto the western edge of the North American portion of the pre-Flood supercontinent at the initiation of the Flood event with the breaking up of the fountains of the great deep (Genesis 7:11) and the triggering of catastrophic plate tectonics (Austin et al. 1994; Baumgardner 2003). However, before the Tonto Group was deposited, there was likely a prolonged period (possibly days or more) in which there was a significant amount of continental-scale erosion to bevel the Precambrian (pre-Flood) land surface to produce the Great Unconformity. In Grand Canyon region, this involved intensive catastrophic erosion removing several thousand meters of Grand Canyon Supergroup strata (which appear to only have survived in several down-faulted blocks) and then beveling of the underlying metamorphic schists and granite plutons. After this period of destructive erosion, and subsequent to the localized deposition of the Sixtymile Formation, the Tapeats Sandstone, and the overlying Bright Angel Formation and then Muav Formation were deposited as the first widespread (continental-scale) deposits of the Tonto Group. That initial brief period of catastrophic erosion may have coincided with the initial rifting ("breaking up") that occurred until significant plate motion began to generate the tsunamis in surges of waves that deposited the Tonto Group strata (Baumgardner 2013; 2018a, b).

Austin (1994) diagrammatically envisaged a fining upwards model for the time transgressive rapid deposition of the Tonto Group strata as the powerful westward back under-flow of the advancing Flood waters, moving at a water flow speed of  $>2\text{m/sec}$ , intensely scoured and catastrophically eroded pre-Flood rocks to produce the Great Unconformity before sequentially depositing their load of sediments as horizontally segregated facies in the vertically stacked Tonto Group strata (fig. 41). In the adjacent shallow-water area, the westwards-flowing, intense bottom-surging current deposited coarse pebbles and sand with lag boulders up to 9m (30ft) diameter in flat beds or cross beds to form the base of the Tapeats Sandstone at a water flow speed of  $1.5\text{m/sec}$ . Further westwards in deeper water the central portion (cliff-forming unit) of the Tapeats Sandstone composed of sand waves of coarse sand in thin cross-beds with westerly and south-westerly dips was deposited in a water velocity of about  $1\text{m/sec}$ . Simultaneously, and even further westward, the top of the formation composed of thinner, fine-grained sand and silt beds

dominated by plane beds with ripples was deposited by deeper and slower moving waters at  $0.5\text{m/sec}$ , forming a gradational transition into the overlying shales and siltstones of the Bright Angel Formation. In these deeper and slower-moving waters, the silicate clay- and silt-sized particles accumulated as the graded siltstone and shale beds of the Bright Angel Formation. These deposits were the residue winnowed from the sands in the more energetic shoreward zones where the Tapeats Sandstone was deposited.

Finally, farthest to the west in the deepest and slow-moving water, where there were fewer silicate clay- and silt-sized particles left in the sediment load and the water current velocity was  $<0.5\text{m/sec}$ , the carbonate mud and silt, potentially the dominant type of pre-Flood sediment to the west on the pre-Flood ocean floor, accumulated on top of the Bright Angel Formation as the rhythmically laminated and bedded flat strata of the Muav Formation. Thus, as the Flood waters advanced continuously across Arizona deeper-water, slower-velocity sediment facies were stacked above the shallower-water, faster-velocity sediment facies. The result was the vertical sequence consisting of the Great Unconformity, the Tapeats Sandstone, the Bright Angel Formation and the Muav Formation comprising the Tonto Group, with each having an enormous horizontal extent measured in hundreds of kilometers. That these three stacked formations are depositionally related as the Tonto Group is very evident from the petrographic observation in this study that the same quartz and K-feldspar grains and muscovite flakes from the same source are present in all three formations (Snelling 2021a, b), the quantities and grain sizes of these silicate clasts diminishing upwards in accordance with the general fining upwards sequence.

This sedimentation model is consistent with the conventional, classical time-transgressive deepening seas model first advocated by McKee (1945) and the deep-water deposition of the Tapeats Sandstone proposed by Kennedy, Kablanow, and Chadwick (1997), except that the timeframe for simultaneous deposition of the Tapeats Sandstone, the Bright Angel Formation and the Muav Formation is a mere few days as part of the initial catastrophic erosion and deposition of the global Genesis Flood cataclysm, about 4,350 years ago. This is in stark contrast to the conventional 3 million years of slow deposition of the Muav Formation claimed to have occurred about 499–502 million years ago following equally slow prior sequential deposition of the Tapeats Sandstone (507–508Ma) and the Bright Angel Formation (502–507Ma) (Karlstrom et al. 2020). Karlstrom et al. (2018) admitted that the Sauk transgression represented by the Tonto Group "was one of the

New Mexico

Arizona

Nevada

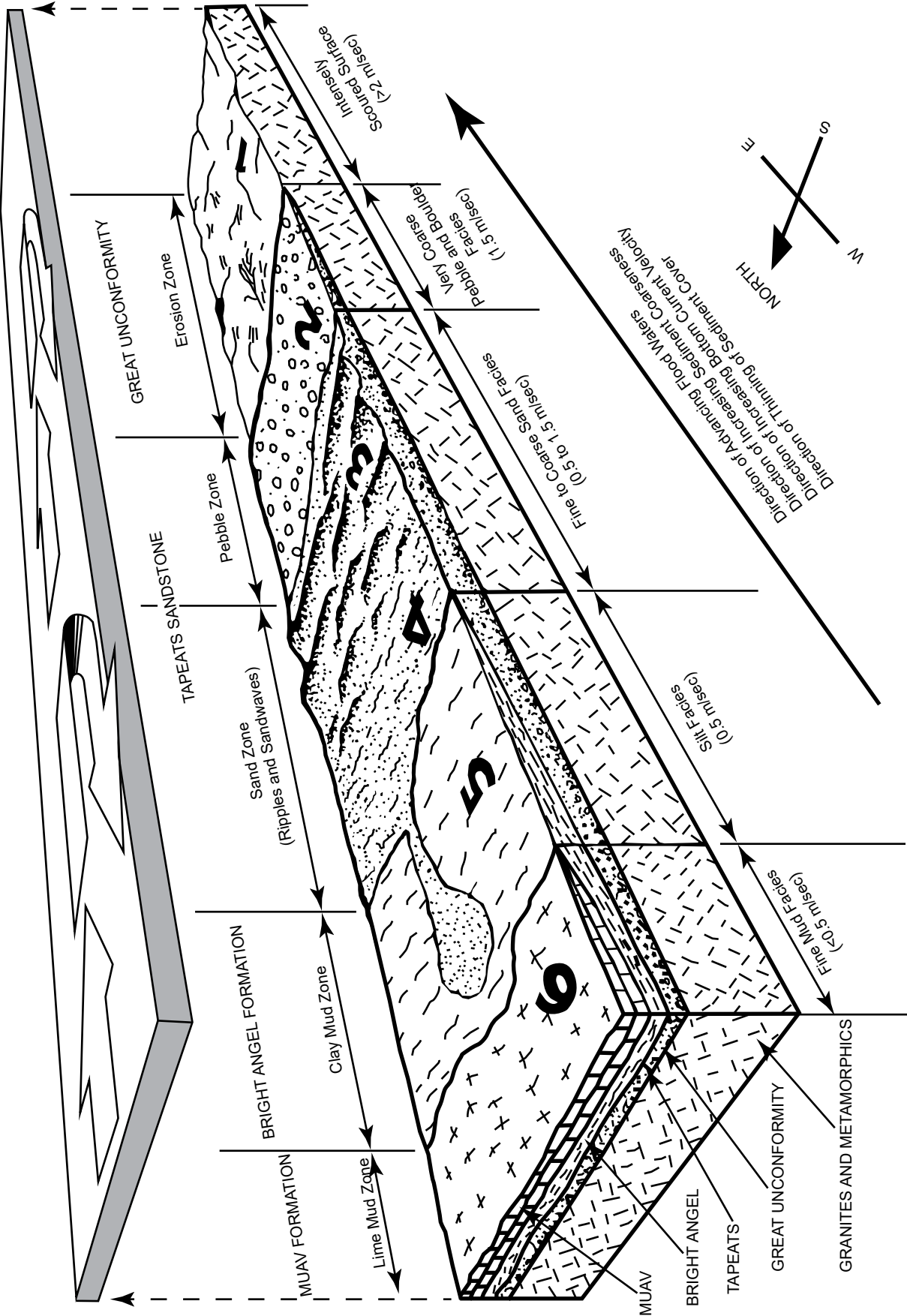


**Fig. 41 (page 248).** A model for the formation of the Tonto Group sedimentary deposits beneath advancing floodwaters across Nevada, Arizona, and New Mexico (after Austin 1994, 69. fig.4.12). This likely occurred well after the onset of the Flood, as much of the Grand Canyon Supergroup had to be first planed off down to the crystalline basement granites and metamorphics. The water mass advancing eastward over Arizona has been “lifted” off the surface of the earth to reveal, underneath, the erosion and sedimentation that was occurring. The Flood model explains the erosion of the Great Unconformity, and simultaneous deposition of the Tapeats Sandstone, Bright Angel Formation (mostly shale and siltstone), and Muav Formation (mostly limestone). The waters of the Flood have advanced eastward through Nevada (lower left of diagram), finally reaching the more elevated area in Arizona and New Mexico (upper right of diagram). As the Flood advances eastward, the deep westward-flowing, strong under-current produced horizontally segregated deposits (facies) and vertically stacked sediments (strata).

**Zone 1** is the highest elevation area of the continent, where shallow, fast floodwaters are causing intense scouring and erosion of the pre-Flood rocks.

**Zone 2** is the adjacent shallow-water area, where coarse pebbles and lag boulders are accumulating at the base of the Tapeats Sandstone. All the finer sand, silt, and mud are being winnowed from Zone 2, and moved westward into Zones 3 and 4 by the intense bottom-surfing current (velocity about 1.5 meters per second).

**Zone 3** is composed of sand waves forming thinly cross-bedded sands, which compose the middle section of the Tapeats Sandstone (the cliff-forming unit). Here, the water velocity is about 1.0 meters per second.

**Zone 4** is plane beds of sand and some silt, with ripples representing the deepest and lowest-velocity waters depositing the uppermost Tapeats Sandstone (the “transitional” unit).

**Zone 5** is located in still deeper and slower-moving waters. The silicate clay- and silt-sized particles are accumulating as graded silt and clay beds. These deposits are the residue winnowed from Zones 1 through 4 and compose the Bright Angel Formation (principally shale and siltstone). Here, the water velocity is about 0.5 meters per second.

**Zone 6** is farthest to the west, in the deepest and slowest-moving water, where there is a deficiency of silicate clay and silt-sized particles. Carbonate mud, apparently the dominant type of pre-Flood sediment to the west, is accumulating in Zone 6 as rhythmically laminated and bedded flat strata, where the water current velocity is less than 0.5 meters per second.

The continuous advance of the Flood over Arizona caused deeper-water, slower-velocity sediment facies to be stacked above the shallower-water, faster-velocity sediment facies. The result is the vertical sequence, consisting of the Great Unconformity, and the Tapeats Sandstone, Bright Angel Formation, and Muav Formation comprising the Tonto Group. Each has enormous horizontal extent, which can be measured in hundreds of kilometers.

most dramatic global marine transgressions in Earth history.” And even Rose (2003) admitted that these lower Paleozoic strata were deposited during higher rates of tectonism and accompanying inertial true polar wander (plate motion) which generated an historic high sea-level rise and abnormally high-frequency sea-level fluctuations. The fact is that the Great Unconformity is well-recognized and documented as a global stratigraphic surface (Peters and Gaines 2012). And in many regions across the globe, it bounds continental crystalline basement rocks from the overlying Sauk megasequence shallow marine sedimentary deposits, including the basal Tapeats Sandstone and its equivalents and the overlying Muav Formation. Furthermore, this is totally consistent with initial catastrophic erosion of local underlying basement rocks and rapid, short-distance transport and deposition at the onset of the global Genesis Flood cataclysm, which would have been accompanied by continuous intensive high-energy storm-like conditions and surging tsunamis generated by plate motion and earthquakes during the breaking up of the fountains of the great deep and the release of the saline superheated steam jets.

Furthermore, the westward transport of the detritus, depicted by Austin (1994) in fig. 41 as due to the deep counter-current, has been confirmed by the documentation of continental-wide paleocurrent

direction indicators by Brand, Wang, and Chadwick (2015), who have demonstrated this was a global phenomenon consistent with the direction of the global tidal movements in the global Flood cataclysm. Baumgardner (2013; 2018a, b) has made considerable progress with numerical simulations of the catastrophic erosion of bedrock via cavitation to produce the sediments that were rapidly deposited on the continental plates as shallow waters moved rapidly around the surface of the rotating globe. His modeling posits that the dominant means for sediment transport during the Flood was by rapidly-flowing turbulent water, and that water motion was driven by large-amplitude tsunamis that were generated along subduction zone segments by powerful earthquakes as the subducting plate and overriding plate, in a cyclic manner, locked and then suddenly released and slipped rapidly past one another. His calculations show that with plausible parameter choices average erosion and sedimentation rates on the order of 9m/day (~30ft/day) at 0.38m/hr (~1.25ft/hr) occurred with tsunami-driven pulses of turbulent water that transported the generated sediments vast distances across the continental plate surfaces, sufficient to simultaneously deposit the Tonto Group including the Muav Formation within 3–10 days, early during the 150-day rising and prevailing waters phase of

the Flood (Genesis 7:18–24), and to thus account for the vast majority of the Phanerozoic sediments that blanket the earth's continental surfaces today.

Austin and Wise (1994) described in detail five robust criteria for defining the pre-Flood/Flood boundary and then applied them to Grand Canyon region. They concluded that the Great Unconformity under the Tapeats Sandstone and occasionally under the locally underlying Sixtymile Formation in eastern Grand Canyon matched all five criteria. Thus, they included the Sixtymile Formation in the Sauk megasequence, which has recently been confirmed by Karlstrom et al (2018; 2020), who have proposed the formation be added to the base of the Tonto Group. Within the Sixtymile Formation, Wise and Snelling (2005) reported large megaclasts of the underlying Kwagunt Formation of the Chuar Group piled up at least three deep and separated by meter-thick pebble to boulder breccia layers, which were first recognized by Elston (1979) and subsequently documented by Karlstrom et al. (2018). Elston (1979) and Elston and McKee (1982) argued that these megaclasts were emplaced by sliding as the Sixtymile Formation was rapidly deposited as a result of more than 2 km (>6,500ft) of displacement of the adjacent Butte Fault in a sudden tectonic disturbance. Austin and Wise (1994) also likened these megaclasts and breccias in the Sixtymile Formation with the gigantic breccia clasts, some more than a mile wide, in the Kingston Peak Formation in the eastern Mohave Desert of California, with the tectonic upheaval that marked the initiation of the Flood cataclysm (the breaking up of the fountains of the great deep). They suggested those gigantic breccia clasts in the Kingston Peak Formation resulted from the collapse of the continental margin westward towards what was the pre-Flood ocean basin.

This overall scenario and model for the tectonic upheaval at pre-Flood/Flood boundary and the initial catastrophic Flood deposition of the Tapeats Sandstone and the overlying Bright Angel and Muav Formations has also been summarized by Snelling (2009). However, critics have countered with the claimed evidence for slow-and-gradual deposition of the Muav Formation in shallow marine to subtidal and tidal flats environments as suggested by McKee (1945), Middleton and Elliott (2003), Rose (2003, 2006), and Wanless (1973a, 1975). Hill and Moshier (2016) have pointed to supposed mud cracks found in the Muav Formation, suggesting such delicate features require subaerial exposure of sediment surfaces and relatively gentle conditions for preservation. However, as already discussed above, the interpretation that they are mud cracks is very uncertain and not established by careful investigation. Rather, in the context of other evidence

for deeper water deposition of the Muav Formation they are more likely to be subaqueous shrinkage or syneresis cracks, which may possibly have been triggered by ground motion during earthquakes, or they may even be diastasis cracks (Boggs 1995; Burst 1965; Plummer and Gostin 1981; Pratt 1998; Whitmore 2009). That possibility is consistent with the earthquakes generated by the catastrophic rifting and rapid movement of plates in the early stages of the global Flood cataclysm.

Furthermore, both the fossil content and sedimentary structures within the Muav Formation are entirely compatible with its catastrophically rapid deposition by hurricane-like storm surges and very frequent tsunamis. Indeed, the invertebrate fossils found in the Muav Formation required rapid burial in storm events for their preservation before decay or scavenging. This required burial below storm wave base, yet the presence of broken shell fragments in the Muav Formation limestones indicates how destructive the stormy conditions must have also been. And the trace fossils, mainly trails and burrows, within the Muav Formation seem to have been buried in high-energy stormy depositional conditions as worms feverishly avoided being rapidly buried. These considerations totally debunk the claim of Hill and Moshier (2009, 2016) that these delicate trace fossils required relatively gentle conditions for preservation. Rather, once the trails and burrows had been made, they needed to be buried rapidly to be preserved before any bioturbation occurred. And all this was happening on a global scale (Clarey 2019, 2020). Thus, the trace fossils in the Muav Formation instead indicate that these invertebrate trail and burrow makers were highly active as they tried to survive during the rapid deposition of the Muav Formation soon after the beginning of the global Flood cataclysm, and not in the postulated slow-and gradual, gentle conditions of the supposed uniformitarian sedimentary environments.

Hill and Moshier (2016) make mention of the fossilized ripple marks in the Muav Formation and provide a photograph for comparison of ripple marks on a sandy sea bottom under about 20ft (6m) of water and formed by a current of about 0.5–1.0 mph (0.2–0.4m/sec), thus again implying those fossilized in the Muav Formation are incompatible with hurricane-and tsunami-driven, rapid sediment transport and deposition during the global Flood cataclysm. However, their photograph of the modern ripple marks still clearly acknowledges that the Muav ripple marks were formed subaqueously. Furthermore, the small-scale cross-bedding and megaripples within beds of the Muav Formation have resulted from small subaqueous dunes in the fine-grained sediments, even though Hill and Moshier (2016)

do not specifically acknowledge that. Yet, these are precisely the sedimentary structures observed to form in carbonate mud and silt sediments in flume experiments conducted by Schieber, Southard, and Thaisen (2007), Schieber and Southard (2009), and Schieber et al. (2013) with water velocities the same as those which deposit cross-bedded sands. Furthermore, the limestone laminae alternating with siltstone partings in the Muav Formation match the alternating fine- and coarser-grained laminae produced by the spontaneous stratification of heterogranular sediment mixtures from high-energy water flows in both experiments and field observations (Austin 1986, 2009; Julien, Lan, and Berthault 1994; Julien, Lan, and Raslan 1998; Makse et al. 1997; Rowley, Kuntz, and MacLeod 1981). And the extensive intraformational flat-pebble conglomerate layers interbedded with thin laminated limestone beds in the Muav Formation are only consistent with high-energy, hurricane-induced, storm deposition over a huge area.

Thus, none of the apparent objections counter the rock evidence. All such features can be reconciled with the rapid transport of silt and mud particles of carbonate and silicate minerals and their rapid deposition as the Muav Formation very soon after the initiation of the global Flood cataclysm. The fact that the Muav Formation was deposited virtually on top of the very source rocks some of its sediment grains were eroded from indicates a very short transport distance. And the ubiquitous presence of K-feldspar grains, as well as soft and fragile detrital muscovite flakes, throughout the thickness of the formation, is indicative of rapid transport and deposition. The sedimentary structures within the Muav Formation, particularly the alternating laminae and partings, cross-bedding, megaripples, and conglomerate beds, are consistent with this rapid transport and deposition. The invertebrates likely caught up in the eroded silt and mud left their trails and burrows within some beds immediately after their deposition as they tried to survive before eventually being overwhelmed. Robust simulations of the catastrophic erosion of the underlying basement rocks and rapid deposition of the Muav Formation is consistent with this occurring within the early days of the global Flood cataclysm being initiated. Once deposited, carbonates dissolved in the connate water trapped between the sediment grains subsequently precipitated to lithify the formation's limestone layers and produce post-depositional dolomite alteration as they dewatered under burial pressures.

### Summary and Conclusions

The Cambrian Muav Formation is the 42–252 m (136–827 ft) thick cliff-forming formation that

outcrops towards the top of the Tonto Group across ~500 km in the walls of Grand Canyon, Arizona, and beyond. It is an integral component of the fining upwards lithologies of the Cambrian Tonto Group, which has been touted conventionally as the classic example of the time-transgressive “deepening seas” sedimentation model. Originally described as the Muav Limestone, it has been recently designated to formation status due to it consisting of minor dolostone beds and laminae, and some extensive intraformational flat-pebble conglomerate layers, within the dominant thick and thin beds and laminae of limestones, sometimes with alternating siltstone partings. The Muav Formation immediately overlies a gradational and intertonguing boundary with the Bright Angel Formation, which in turn overlies the Tapeats Sandstone that mostly sits directly on a pronounced erosion surface known as the Great Unconformity. The underlying rocks eroded at the Great Unconformity include granitic plutons intruded into the Granite Gorge Metamorphic Suite schists unconformably overlain by the tilted sedimentary strata and basalt layers of the Grand Canyon Supergroup, all dated as Precambrian. Both the correlated equivalents of the Muav Formation and the Great Unconformity have been traced across several continents and around the globe, respectively (Clarey 2019; 2020; Peters and Gaines 2012).

Within the Muav Formation a few trilobites and some brachiopods and gastropods are sparsely scattered within some members. Difficult-to-recognize trace fossils are present in the formation, primarily burrows and trails likely left by various worms and other invertebrates. Some limestone beds are mottled due to apparent ubiquitous worm burrows. The formation itself is well-bedded with thick and thin limestone laminae, in some sections with alternating siltstone partings. Cross-laminations are common but difficult to observe, and sometimes are also associated with current ripples and megaripples. Some intraformational flat-pebble conglomerate layers are extensive. Detrital zircon grains extracted from the Tapeats Sandstone have been U-Pb dated to determine the maximum depositional age of that formation and coupled with biostratigraphic trilobite faunal zones correlated globally have constrained the conventional age of the overlying Muav Formation to 499–502 Ma (early Middle Cambrian). Additionally, U-Pb dates obtained from detrital zircon grains extracted from the underlying Bright Angel Formation potentially identify the provenance of its sediment grains. U-Pb age peaks among its detrital zircons matched the nearby Paleoproterozoic Yavapai and Mazatzal provinces, indicating the primary source of its sediment grains was the locally underlying granitic

plutons and schists, plus a very small portion from the underlying Grand Canyon Supergroup strata (though a long-distance transport of some grains cannot be entirely ruled out). Given that the smaller quantities of finer-grained clasts scattered through the poorly-sorted limestones of the Muav Formation are of the same silicates, it is reasonable to conclude those grains came from the same sources. The consensus uniformitarian interpreted depositional environments for accumulation of the Muav Formation are shallow-marine distal offshore to subtidal, intertidal and even tidal flats sedimentary environments, yet it has been described as part of “one of the most dramatic global marine transgressions in Earth history” (Karlstrom et al. 2018).

Calcite grains are the dominant component of the Muav Formation with subordinate dolomite. However, bulk rock XRD analyses of the 15 samples studied demonstrated that quartz and K-feldspar feature prominently in many samples, ranging from 2.7% to 55.9% and 0.9% to 26.3% respectively. Illite is also present, indicative mostly of muscovite, but likely some from glauconite and minor illite alteration also. In thin section, the limestones are fine-grained and generally poorly sorted, with angular to sub-rounded, medium silt to fine sand-sized quartz and K-feldspar grains scattered through the tiny-grained calcite matrix (micrite) that has in places been recrystallized into larger grains and patches. Occasional thin edge-on detrital muscovite flakes are wedged between the quartz and K-feldspar grains. A few samples contain small glauconite pellets and grains, and a few contain small shell fragments. There are virtually no original pores remaining, the rock fabric being cemented mostly by recrystallized calcite. In many samples, post-depositional dolomite alteration of calcite has occurred. There is no evidence, macroscopic or microscopic, of any metamorphic changes to the detrital mineral grains or textures.

The silicate grains within the Muav Formation are consistent with their provenance being the underlying local basement rocks, as indicated by the detrital zircon U-Pb ages, while the carbonate mud was likely derived from the ocean floor to the west. Indeed, due to the very short-distance transport of the sediment and rapid deposition of the limestones, quartz and K-feldspar grains are scattered randomly through the entire formation and are often angular or sub-angular, while the extremely soft detrital muscovite flakes have survived, sometimes bent with frayed ends. The dominant thickening, thinning and pinching out of laminae in the limestones (with some alternating siltstone partings), the occasional cross-laminations, ripples, and megaripples, and the extensive intraformational flat-pebble conglomerate layers are consistent with rapid deposition by

high-energy storm-like surges. Furthermore, they are consistent with observational evidence of spontaneous stratification and continuous rapid deposition of heterogranular sediment mixtures including carbonate mud floccules. Numerous detrital zircon grains in the underlying Tapeats Sandstone yield U-Pb ages that are considerably younger than its designated depositional age. These coupled with the well-documented problems with the many assumptions undergirding the U-Pb dating method, and the evidence of past grossly accelerated nuclear decay rates, totally undermine the validity of the conventional age for the Muav Formation. Instead, when summing up the mineralogical content, textural features, sedimentary structures, the continental-scale deposition, the invertebrate fossils and fragments, and even the trails and burrows of transitory invertebrates that had to be buried and fossilized rapidly, these results are all consistent with the catastrophic erosion of the Great Unconformity near the onset of the global Genesis Flood cataclysm about 4,350 years ago, and with the hurricane- and tsunami-driven rapid short-distance transport and deposition of the Muav Formation within the fining upwards Sauk megasequence in the first few days or week of that year-long event.

### Future Work

As indicated at the outset, the purpose of this study on the petrology of the Muav Formation was to thoroughly describe this rock unit in preparation for detailed studies to determine the nature and timing of the folding of this unit in the Matkatamiba fold in Grand Canyon. Future work will thus involve closer attention to comparing the petrography of the 12 samples from the fold with the three samples distant from the fold, especially with respect to grain boundary relationships and textures, the frequency of remaining pores, the compaction of the limestone and dolostone, and the nature and timing of the cement between the detrital grains that produced the lithification of those layers. This will require scanning electron microscope (SEM) imaging of selected samples to closely examine the cement crystals which would show evidence of brittle fracturing and healing if the folding occurred after lithification but would be still pristine if cementation occurred after soft-sediment deformation and before lithification.

### Acknowledgements

All the Muav Formation samples were collected under the authority of National Park Service Scientific Research and Sampling Permit # GRCA-2017-SCI-0052 dated June 23, 2017, issued by Grand Canyon National Park's Research Office. The

Alliance Defending Freedom (ADF) team led by then Senior Counsel Gary McCaleb is especially thanked for their legal work that resulted in a successful lawsuit against viewpoint discrimination in the permit application and granting process. Tom Vail, founder of Canyon Ministries who encouraged this research from its start, is also thanked for organizing with Terry Vallely, and assisted by their wives Paula and Kathy, respectively, the August 6–12, 2017, research raft trip down the Colorado River through Grand Canyon to collect the samples, facilitated by Grand Canyon National Park Special Use Permit #GRCA-3701 issued June 26, 2017. Special thanks go to Tom Vail and Dr. John H. Whitmore, Senior Professor of Geology at Cedarville University, Ohio for their invaluable field assistance, without which the samples would not have been collected, especially after I was injured early in the trip. Ray Strom of Calgary Rock and Materials Services, Inc. is thanked for the thin sections he prepared, and for the XRD analyses, as well as for the use of their research microscope for photography. Cedarville University is also thanked for use of its research microscope and Dr. John H. Whitmore for his advice, support, and encouragement. The helpful comments and edits from the kind reviewers were much appreciated. This research was fully funded by many generous donors to Answers in Genesis and has had the full support of the Answers in Genesis leadership team under Ken Ham. Our production assistant Laurel Hemmings is also thanked for her work in preparing this paper for publication. Nevertheless, I take full the responsibility for the content of this paper.

## References

- Adams, John Emery, and Mary Louise Rhodes. 1960. "Dolomitization by Seepage Refluxion." *American Association of Petroleum Geologists Bulletin* 44, no.12 (December): 1912–1920.
- Adams, Roy D., and John P. Grotzinger. 1996. "Lateral Continuity of Facies and Parasequences in Middle Cambrian Platform Carbonates, Carrara Formation, Southeastern California, U.S.A." *Journal of Sedimentary Research* 66, no.6 (1 November): 1079–1090.
- Aitken, J.D. 1967. "Classification and Environmental Significance of Cryptalgal Limestones and Dolomites, with Illustrations from the Cambrian and Ordovician of Southwestern Alberta." *Journal of Sedimentary Petrology* 37, no.4 (December): 1163–1178.
- Allen, John R.L. 1970. *Physical Processes of Sedimentation: An Introduction*. London, United Kingdom: George Allen & Unwin Publishers Ltd.
- Alpert, Stephen P. 1974. "Systematic Review of the Genus *Skolithos*." *Journal of Paleontology* 48, no.4 (July): 661–669.
- Amorosi, Alessandro. 1997. "Detecting Compositional, Spatial, and Temporal Attributes of Glaucony: A Tool for Provenance Research." *Sedimentary Geology* 109, nos.1–2 (March): 135–153.
- Anderson, Calvin J., Matthew S. Cheney, Alex Struble, and John H. Whitmore. 2013. "Muscovite Survival in Simulated (Turbulent) Eolian and Subaqueous Conditions." *Journal of Creation Theology and Science Series C: Earth Sciences* 3: 1.
- Anderson, Calvin J., Alexander Struble, and John H. Whitmore. 2017. "Abrasion Resistance of Muscovite in Aeolian and Subaqueous Transport Experiments." *Aeolian Research* 24 (February): 33–37.
- Arnott, R. William, and John B. Southard. 1990. "Exploratory Flow-Duct Experiments on Combined-Flow Bed Configurations, and Some Implications for Interpreting Storm-Event Stratification." *Journal of Sedimentary Petrology* 60, no.2 (1 March): 211–219.
- Austin, Steven A. 1986. "Mount St. Helens and Catastrophism." In *Proceedings of the First International Conference on Creationism*, edited by Robert E. Walsh, Christopher L. Brooks, and Richard S. Crowell, Vol.1, 3–10. Pittsburgh, Pennsylvania: Creation Science Fellowship.
- Austin, Steven A. ed. 1994. *Grand Canyon: Monument to Catastrophe*. Santee, California: Institute for Creation Research.
- Austin, Steven A., and D. Russell Humphreys. 1990. "The Sea's Missing Salt: A Dilemma for Evolutionists." In *Proceedings of the Second International Conference on Creationism*, edited by Robert E. Walsh, and Christopher L. Brooks, Vol. 1, 17–34. Pittsburgh, Pennsylvania: Creation Science Fellowship.
- Austin, Steven A., and Kurt P. Wise. 1994. "The Pre-Flood / Flood Boundary: As Defined in Grand Canyon and East Mojave Desert, California." In *Proceedings of the Third International Conference on Creationism*, edited by Robert E. Walsh, 37–47. Pittsburgh, Pennsylvania: Creation Science Fellowship.
- Austin, Steven A., John R. Baumgardner, D. Russell Humphreys, Andrew A. Snelling, Larry Vardiman, and Kurt P. Wise. 1994. "Catastrophic Plate Tectonics: A Global Flood Model of Earth History." In *Proceedings of the Third International Conference on Creationism*, edited by Robert E. Walsh, 609–621. Pittsburgh, Pennsylvania: Creation Science Fellowship.
- Austin, Steven A. 2009. "The Dynamic Landscape on the North Flank of Mount St. Helens." In *Volcanoes to Vineyards: Geologic Field Trips through the Dynamic Landscape of the Pacific Northwest*, edited by Jim E. O'Connor, Rebecca J., Dorsey, and Ian P. Madin, 337–344. Boulder, Colorado: Geological Society of America, *Field Guide* 15.
- Badiozamani, Khosrow, 1973. "The Dorag Dolomitization Model, Application to the Middle Ordovician of Wisconsin." *Journal of Sedimentary Petrology* 43, no.4 (1 December): 965–984.
- Baker, Paul A., and Miriam Kastner. 1981. "Constraints on the Formation of Sedimentary Dolomite." *Science* 213, no.4504 (10 July): 214–216.
- Basma, Adnan A., Azm S. Al-Homoud, Abdallah I.Husein Malkawi, and Mohamed A. Al-Bashabsheh. 1996. "Swelling-Shrinkage Behavior of Natural Expansive Clays." *Applied Clay Science* 11, nos.2–4 (December): 211–227.
- Basu, Abhijit. 1981 "Weathering Before the Advent of Land Plants: Evidence from Unaltered Detrital K-Feldspars in Cambrian-Ordovician Arenites." *Geology* 9, no.3 (March): 132–133.

- Bathurst, Robin G.C. 1991. "Pressure-Dissolution and Limestone Bedding: The Influence of Stratified Cementation." In *Cycles and Events in Stratification*, edited by Gerhard Einsele, Werner Ricken, and Adolf Seilacher, 450–463. New York, New York: Springer-Verlag.
- Baumgardner, John R. 2003. "Catastrophic Plate Tectonics: The Physics Behind the Genesis Flood." In *Proceedings of the Fifth International Conference on Creationism*, edited by Robert L. Ivey Jr., 113–126. Pittsburgh, Pennsylvania: Creation Science Fellowship.
- Baumgardner, John R. 2013. "Explaining the Continental Fossil-Bearing Sediment Record in Terms of the Genesis Flood: Insights from Numerical Modeling of Erosion, Sediment Transport, and Deposition Processes on a Global Scale." In *Proceedings of the Seventh International Conference on Creationism*, edited by Mark Horstemeyer. Pittsburgh, Pennsylvania: Creation Science Fellowship.
- Baumgardner, John R. 2018a. "Numerical Modeling of the Large-Scale Erosion, Sediment Transport, and Deposition Processes of the Genesis Flood." *Answers Research Journal* 11 (June 27): 149–170. <https://answersresearchjournal.org/numerical-modeling-genesis-flood-2/>.
- Baumgardner, John R. 2018b. "Understanding How the Flood Sediment Record was Formed: The Role of Large Tsunamis." In *Proceedings of the Eighth International Conference on Creationism*, edited by John H. Whitmore, 287–305. Pittsburgh, Pennsylvania: Creation Science Fellowship.
- Behrens, E. William, and Lynton S. Land. 1972. "Subtidal Holocene Dolomite, Baffin Bay, Texas." *Journal of Sedimentary Petrology* 42, no. 1 (1 March): 155–161.
- Berthault, Guy. 1988. "Experiments on Lamination of Sediments." *Ex Nihilo Technical Journal* 3, no. 1 (April): 25–29.
- Berthault, Guy. 1990. "Sedimentation of a Heterogranular Mixture: Experimental Lamination in Still and Running Water." *Ex Nihilo Technical Journal* 4, no. 1 (April): 95–102.
- Billingsley, George H. 1970. "General Geology of Tuckup Canyon, Central Grand Canyon, Mohave County, Arizona." M.S. Thesis (unpublished). Northern Arizona University.
- Billingsley, George H., John D. Hendricks, and Ivo Lucchitta. 1987. "Field Guide to the Lower Grand Canyon, from Peach Springs to Pierce Ferry, Arizona." In *Geologic Diversity of Arizona and its Margins: Excursions to Choice Areas*, edited by George H. Davis and Evelyn M. VandenDolder, 20–38. Tucson, Arizona: Arizona Bureau of Geology and Mineral Technology, *Special Paper* 5.
- Billingsley, George H., and Donald P. Elston. 1989. "Geologic Log of the Colorado River from Lees Ferry to Temple Bar, Lake Mead, Arizona." In: *Geology of Grand Canyon, Northern Arizona (with Colorado River Guides)*, edited by Donald P. Elston, George H. Billingsley, and Richard A. Young, 1–36. Washington, D.C.: American Geophysical Union.
- Blakey, Ronald C., and Larry T. Middleton. 2012. "Geologic History and Paleogeography of Paleozoic and Early Mesozoic Sedimentary Rocks, Eastern Grand Canyon, Arizona." In *Grand Canyon Geology: Two Billion Years of Earth's History*, edited by J. Michael Timmons and Karl E. Karlstrom, 81–92. Boulder, Colorado: Geological Society of America, *Special Paper* 489.
- Boggs, Samuel, Jr. 1995. *Principles of Sedimentology and Stratigraphy*, 2nd ed., 79–107. Upper Saddle River, New Jersey: Prentice-Hall.
- Borsch, K., John H. Whitmore, Raymond Strom, and George Hartree. 2018. "The Significance of Micaceous in Ancient Cross-Bedded Sandstones." In *Proceedings of the Eighth International Conference on Creationism*, edited by John H. Whitmore, 306–326. Pittsburgh, Pennsylvania: Creation Science Fellowship.
- Brand, Leonard R., Mingmin Wang, and Arthur V. Chadwick. 2015. "Global Database of Paleocurrent Trends Through the Phanerozoic and Precambrian." *Scientific Data* 2: 150025. doi:10.1038/sdata.2015.25.
- Bromley, Richard G., and Ulla Asgaard. 1991. "Ichnofacies: A Mixture of Taphofacies and Biofacies." *Lethaia* 24, no. 2 (April): 153–163.
- Burns, Stephen J., Judith A. McKenzie, and Crisogono Vasconcelos. 2000. "Dolomite Formation and Biogeochemical Cycles in the Phanerozoic." *Sedimentology* 47, no. 1 (February): 49–61.
- Burst, J.F. 1965. "Subaqueously Formed Shrinkage Cracks in Clay." *Journal of Sedimentary Petrology* 35, no. 2 (June): 348–353.
- Cander, Harris S. 1994. "An Example of Mixing-Zone Dolomite, Middle Eocene Avon Park Formation, Floridan Aquifer System." *Journal of Sedimentary Research* 64, no. 3a (1 July): 615–629.
- Carballo, José D., Lynton S. Land, and Donald E. Miser. 1987. "Holocene Dolomitization of Supratidal Sediments by Active Tidal Pumping, Sugarloaf Key, Florida." *Journal of Sedimentary Petrology* 57, no. 1 (1 January): 153–165.
- Chadwick, Arthur V., and Elaine G. Kennedy. 1998. "Depositional Environment of the Tapeats Sandstone in the Region of Grand Canyon, Arizona, USA." In *15th International Sedimentological Congress* 15: 247–248. Ghent, Belgium: International Association of Sedimentologists.
- Chandler, Francis W. 1988. "Quartz Arenites: Review and Interpretation." *Sedimentary Geology* 58, nos. 2–4 (August): 105–126.
- Clarey, Timothy L., and Davis J. Werner. 2018. "Global Stratigraphy and the Fossil Record Validate a Flood Origin for the Geologic Column." In *Proceedings of the Eighth International Conference on Creationism*, edited by John H. Whitmore, 327–350. Pittsburgh, Pennsylvania: Creation Science Fellowship.
- Clarey, Timothy L. 2019. "European Stratigraphy Supports a Global Flood." *Acts & Facts* 48, no. 12 (November 27): 10–12.
- Clarey, Timothy L. 2020. *Carved in Stone: Geological Evidence of the Worldwide Flood*. Dallas, Texas: Institute for Creation Research.
- Clayton, R. N., H. C. W. Skinner, R. A. Berner, and M. Rubinson. 1968. "Isotopic Compositions of Recent South Australian Lagoonal Carbonates." *Geochimica et Cosmochimica Acta* 32, no. 9 (September): 983–988.
- Cloyd, Kelly C., Robert V. Demicco, and Ronald J. Spencer. 1990. "Tidal Channel, Levee, and Crevasse-Splay Deposits from a Cambrian Tidal Channel System: A New Mechanism to Produce Shallowing-Upward Sequences." *Journal of Sedimentary Petrology* 60, no. 1 (January 1): 73–83.

- Davies, Graham R., and Langhorne B. Smith. 2006. "Structurally Controlled Hydrothermal Dolomite Reservoir Facies: An Overview." *American Association of Petroleum Geologists Bulletin* 90, no. 11 (November): 1641–1690.
- Dehler, Carol M., George E. Gehrels, Susannah M. Porter, Matt Heizler, Karl E. Karlstrom, Grant Cox, Laura J. Crossey, and J. Michael Timmons. 2017. "Synthesis of the 780–740Ma Chuar, Uinta Mountain, and Pahrump (ChUMP) Groups, Western USA: Implications for Laurentia-wide Cratonic Marine Basins." *Geological Society of America Bulletin* 129, nos. 5–6 (1 May): 607–624.
- Demico, Robert V., and Lawrence A. Hardie 1994. *Sedimentary Structures and Early Diagenetic Features of Shallow Marine Carbonate Deposits*. Tulsa, Oklahoma: Society of Economic Paleontologists and Mineralogists, *Atlas Series No. 1*.
- Dew, E.A. 1985. "Sedimentology and Petrology of the DuNoir Limestone (Upper Cambrian) South Wind River Range, Wyoming." M.S. Thesis (unpublished). Flagstaff, Arizona: Northern Arizona University.
- Dott, Robert H. Jr., and Joanne Bourgeois. 1982. "Hummocky Stratification: Significance of its Variable Bedding Sequences." *Geological Society of America Bulletin* 93, no. 8 (August 1): 663–680.
- Dott, Robert H. Jr. 2003. "The Importance of Eolian Abrasion in Supermature Quartz Sandstones and the Paradox of Weathering on Vegetation-Free Landscapes." *The Journal of Geology* 111, no. 4 (July): 387–405.
- Droser, Mary L., and David J. Bottjer. 1986. "A Semiquantitative Field Classification of Ichnofabric." *Journal of Sedimentary Petrology* 56, no. 4 (July 1): 558–559.
- Duke, William L. 1985. "Hummocky Cross-Stratification, Tropical Hurricanes, and Intense Winter Storms." *Sedimentology* 32, no. 2 (April): 167–194.
- Duke, William L., R. William C. Arnott, and Richard J. Cheel. 1991. "Shelf Sandstones and Hummocky Cross-Stratification: New Insights on a Stormy Debate." *Geology* 19: 625–628.
- Dunham, Robert J. 1962. "Classification of Carbonate Rocks According to Depositional Textures." In *Classification of Carbonate Rocks*, edited by William E. Ham, 108–121. Tulsa, Oklahoma: The American Association of Petroleum Geologists, *Memoir 1*.
- Elston, Donald P. 1979. "Late Precambrian Sixtymile Formation and Orogeny at Top of the Grand Canyon Supergroup, Northern Arizona." *Professional Paper 1092*, 1–17. Washington, D.C.: U.S. Geological Survey.
- Elston, Donald P., and Edwin H. McKee. 1982. "Age and Correlation of the Late Proterozoic Grand Canyon Disturbance, Northern Arizona." *Geological Society of America Bulletin* 93, no. 8 (August): 681–699.
- Elston, Donald P. 1989. "Correlations and Facies Changes in Lower and Middle Cambrian Tonto Group, Grand Canyon, Arizona." In *Geology of Grand Canyon, Northern Arizona (with Colorado River Guides)*, edited by Donald P. Elston, George H. Billingsley, and Richard A. Young, 131–136. Washington, D.C.: American Geophysical Union.
- Fairbridge, Rhodes W. 1957. "The Dolomite Question." In *Regional Aspects of Carbonate Deposition*, edited by Rufus J. LeBlanc, and Julia G. Breeding, 125–178. Tulsa, Oklahoma: Society of Economic Paleontologists and Mineralogists, *Special Publication 5*.
- Fang, Yihang, and Huifang Xu. 2022. "Dissolved Silica-Catalyzed Disordered Dolomite Precipitation." *American Mineralogist* 107, no. 3 (March): 443–452.
- Fein, J.B. 2000. "Experimental and Field Constraints on the Role of Silica-Organic Complexation and Silica-Microbial Interactions During Sediment Diagenesis." In *Quartz Cementation in Sandstones*, edited by Richard H. Worden, and Sadoon Morad, 119–127. Oxford, United Kingdom: Blackwell Scientific Publications, *International Association of Sedimentologists Special Publication 29*.
- Fineberg, Jay. 1997. "From Cinderella's Dilemma to Rock Slides." *Nature* 386, no. 6623 (27 March): 323–324.
- Folk, Robert Louis. 1955. "Student Operator Error in Determination of Roundness, Sphericity, and Grain Size." *Journal of Sedimentary Petrology* 25, no. 4 (December 1): 297–301.
- Folk, Robert L. 1959. "Practical Petrographic Classification of Limestones." *American Association of Petroleum Geologists Bulletin* 43, no. 1 (January 1): 1–38.
- Folk, Robert L. 1962. "Spectral Subdivision of Limestone Types." In *Classification of Carbonate Rocks*, edited by William E. Ham, 62–84. Tulsa, Oklahoma: The American Association of Petroleum Geologists, *Memoir 1*.
- Folk, Robert L. 1966. "A Review of Grain-Size Parameters." *Sedimentology* 6, no. 2 (March): 73–93.
- Folk, Robert L. 1978. "Angularity and Silica Coatings of Simpson Desert Sand Grains, Northern Territory, Australia." *Journal of Sedimentary Petrology* 48, no. 2 (June 1): 611–624.
- Folk, Robert L. 1980. *Petrology of Sedimentary Rocks*, 2nd ed. Austin, Texas: Hemphill Publishing Co.
- Garzanti, Eduardo. 2017. "The Maturity Myth in Sedimentology and Provenance Analysis." *Journal of Sedimentary Research* 87, no. 4 (April): 353–365.
- Garzanti, Eduardo, Sergio Andò, Giovanni Vezzoli, Michele Lustrino, Maria Boni, and Pieter Vermeesch. 2012. "Petrology of the Namib Sand Sea: Long-Distance Transport and Compositional Variability in the Wind-Displaced Orange Delta." *Earth-Science Reviews* 112, nos. 3–4 (May): 173–189.
- Garzanti, Eduardo, Alberto Resentini, Sergio Andò, Giovanni Vezzoli, Alcides Pereira, and Pieter Vermeesch. 2015. "Physical Controls on Sand Composition and Relative Durability of Detrital Minerals during Ultra-Long Distance Littoral and Aeolian Transport (Namibia and Southern Angola)." *Sedimentology* 62, no. 4 (June): 971–996.
- Gehrels, George E., Ronald C. Blakey, Karl E. Karlstrom, J. Michael Timmons, William Dickinson, and Mark Pecha. 2011. "Detrital Zircon U-Pb Geochronology of Paleozoic Strata in the Grand Canyon, Arizona." *Lithosphere* 3, no. 3 (May): 183–200.
- Gilbert, George K. 1874. "On the Age of the Tonto Sandstone." *Philosophical Society of Washington Bulletin* 1: 109.
- Gilbert, George K. 1875. "Report Upon the Geology of Portions of Nevada, Utah, California, and Arizona. Examined in the Years 1871 and 1872." *U.S. Geographic and Geologic Surveys West of the 100th Meridian*. Vol. 3, pt. 1, 17–187.
- Goudie, Andrew S., and A. Watson. 1981. "The Shape of Desert Sand Dune Grains." *Journal of Arid Environments* 4, no. 3 (September): 185–190.
- Hagadorn, James W., Joseph L. Kirschvink, Timothy D. Raub, and Eben C. Rose. 2011. "Above the Great Unconformity:

- A Fresh Look at the Tapeats Sandstone, Arizona-Nevada, U.S.A." In *Cambrian Stratigraphy and Paleontology of Northern Arizona and Southern Nevada, The 16th Field Conference of the Cambrian Stage Subdivision Working Group, International Subcommittee on Cambrian Stratigraphy*, edited by J. Stewart Hollingsworth, Frederick A. Sundberg, and John R. Foster, 63–76. Flagstaff, Arizona: Museum of Northern Arizona, *Bulletin* 67.
- Hallam, Anthony. 1981. *Facies Interpretation and the Stratigraphic Record*. Oxford, United Kingdom: W.H. Freeman and Company.
- Hariato, Tri, Shigenori Hayashi, Yan Jun Du, and Daisuke Suetsugu. 2008. "Effects of Fiber Additives on the Desiccation Crack Behavior of the Compacted Akaboku Soil as a Material for Landfill Cover Barrier." *Water, Air, and Soil Pollution* 194, no. 1 (October): 141–149.
- Harms, John C., John B. Southard, D.R. Spearing, and Roger G. Walker. 1975. "Depositional Environments as Interpreted from Primary Sedimentary Structures and Stratification Sequences." *Society of Economic Paleontologists and Mineralogists, Short Course 2*. Broken Arrow, Oklahoma: Society of Economic Paleontologists and Mineralogists.
- Hayes, Philip T., and George C. Cone. 1975. "Cambrian and Ordovician Rocks of Southern Arizona and New Mexico and Westernmost Texas." *Professional Paper 873*. Washington, D.C.: U.S. Geological Survey.
- Hereford, Richard. 1975. "Chino Valley Formation (Cambrian?) in Northwestern Arizona." *Geological Society of America Bulletin* 86, no. 5 (May): 677–682.
- Hereford, Richard. 1977. "Deposition of the Tapeats Sandstone (Cambrian) in Central Arizona." *Geological Society of America Bulletin* 88, no. 2 (February): 199–211.
- Hill, Carol A., and Stephen O. Moshier. 2009. "Flood Geology and the Grand Canyon: A Critique." *Perspectives in Science and Christian Faith* 61, no. 2 (June): 99–115.
- Hill, Carol A. and Stephen O. Moshier. 2016. "Sedimentary Structures: Clues from the Scene of the Crime." In *The Grand Canyon, Monument to an Ancient Earth: Can Noah's Flood Explain the Grand Canyon?* edited by Carol A. Hill, Gregg Davidson, Tim Helble, and Wayne Ranney. Chapter 6, 66–71. Grand Rapids, Michigan: Kregel Publications.
- Hower, John. 1961. "Some Factors Concerning the Nature and Origin of Glauconite." *American Mineralogist* 46, nos. 3–4, part 1 (April): 313–334.
- Huntoon, Peter W. 1989. "Cambrian Stratigraphic Nomenclature, Grand Canyon, Arizona—Mappers Nightmare." In: *Geology of Grand Canyon, Northern Arizona (with Colorado River Guides)*, edited by Donald P. Elston, George H. Billingsley, and Richard A. Young, 128–129. Washington, D.C.: American Geophysical Union.
- Huntoon, Peter W. 2003. "Post-Precambrian Tectonism in the Grand Canyon Region. In *Grand Canyon Geology*, edited by Stanley S. Beus, and Michael Morales, 222–259. New York: Oxford University Press.
- International Commission on Stratigraphy. 2022. *International Chronostratigraphic Chart v.2022/02*. ChronostratChart2022-02 (stratigraphy.org).
- Jade 2010. "Software for X-Ray Diffraction Analyses." JADE for XRD (materialsdata.com). Livermore, California: Materials Data, Inc.
- Julien, Pierre Y., Yongqiang Lan, and Guy Berthault. 1994. "Experiments on Stratification of Heterogeneous Sand Mixtures." *Creation Ex Nihilo Technical Journal* 8, no. 1 (April): 37–50.
- Julien, Pierre Y., Yongqiang Lan, and Y. Raslan. 1998. "Experimental Mechanics of Sand Stratification." *Creation Ex Nihilo Technical Journal* 12, no. 2 (August): 218–221.
- Kaczmarek, Stephen E., Jay M. Gregg, David L. Bish, Hans G. Machel, and Bruce W. Fouke. 2017. "Dolomite, Very High-Magnesium Calcite, and Microbes—Implications for the Microbial Model of Dolomitization." In *Characterization and Modeling of Carbonates—Mountjoy Symposium 1*, edited by Alex J. Macneil, Jeff Lonnee, and Rachel Wood, 7–20. Tulsa, Oklahoma: Society of Economic Paleontologists and Mineralogists, *Special Publication* 109.
- Kaczmarek, Stephen E., and Duncan F. Sibley. 2011. "On the Evolution of Dolomite Stoichiometry and Cation Order during High-Temperature Synthesis Experiments: An Alternative Model for the Geochemical Evolution of Natural Dolomites." *Sedimentary Geology* 240, nos. 1–2 (15 August): 30–40.
- Kah, Linda C., John P. Grotzinger, and Noel P. James. 2000. "Depositional  $\delta^{18}\text{O}$  Signatures in Proterozoic Dolostones: Constraints on Seawater Chemistry and Early Diagenesis." In *Carbonate Sedimentation and Diagenesis in the Evolving Precambrian World*, edited by John P. Grotzinger, and Noel P. James, 345–360. Tulsa, Oklahoma: Society of Economic Paleontologists and Mineralogists, *Special Publication* 67.
- Karlstrom, Karl E., Bradley R. Ilg, Michael L. Williams, David P. Hawkins, Samuel A. Bowring, and S.J. Seaman. 2003. "Paleoproterozoic Rocks of the Granite Gorges." In *Grand Canyon Geology*, 2nd ed., edited by Stanley S. Beus, and Michael Morales, 9–38. New York: Oxford University Press.
- Karlstrom, Karl E., and J. Michael Timmons. 2012. "Faulting and Uplift in the Grand Canyon Region." In *Grand Canyon Geology: Two Billion Years of Earth's History*, edited by J. Michael Timmons and Karl E. Karlstrom, 93–107. Boulder, Colorado: Geological Society of America, *Special Paper* 489.
- Karlstrom, Karl E., Samuel A. Bowring, Carol M. Dehler, Andrew H. Kroll, Susannah M. Porter, David J. Des Marais, et al. 2000. "Chuar Group of the Grand Canyon: Record of Breakup of Rodinia, Associated Change in the Global Carbon Cycle, and Ecosystem Expansion by 740Ma." *Geology* 28, no. 7 (July): 619–622.
- Karlstrom, Karl E., James W. Hagadorn, George E. Gehrels, William Matthews, Mark D. Schmitz, Lauren Madronich, Jacob Mulder, Mark Pecha, Dominique Giesler, and Laura J. Crossey. 2018. "Cambrian Sauk Transgression in the Grand Canyon Region Redefined by Detrital Zircons." *Nature Geoscience* 11, no. 6 (28 May): 438–443.
- Karlstrom, Karl E., Mike T. Mohr, Mark D. Schmitz, Frederick A. Sundberg, Stephen M. Rowland, Ronald C. Blakey, John R. Foster, Laura J. Crossey, Carol M. Dehler and James W. Hagadorn. 2020. "Redefining the Tonto Group of Grand Canyon and Recalibrating the Cambrian Time Scale." *Geology* 48, no. 5 (1 May): 425–430.
- Kaźmierczak, J., and R. Goldring. 1978. "Subtidal Flat-Pebble Conglomerate from the Upper Devonian of Poland: A Multiprovenant High-Energy Product." *Geological Magazine* 115, no. 5 (September): 359–366.
- Kelling, Gilbert, and Peter R. Mullin. 1975. "Graded Limestones and Limestone-Quartzite Couplets: Possible

- Storm Deposits from the Moroccan Carboniferous." *Sedimentary Geology* 13, no. 3 (June): 161–190.
- Kelts, Kerry R., and Judith A. Mackenzie. 1982. "Diagenetic Dolomite Formation in Quaternary Anoxic Diatomaceous Muds of Deep Sea Drilling Project Leg 64, Gulf of California." *Initial Reports of the Deep Sea Drilling Project* 64: 553–569.
- Kennedy, Elaine G. Ray Kablanow, and Arthur V. Chadwick. 1997. "Evidence for Deep Water Deposition of the Tapeats Sandstone, Grand Canyon, Arizona." In *Proceedings of the Third Biennial Conference of Research on the Colorado Plateau*, edited by Charles van Riper, III, and Elana T. Deschler, 215–228. Washington, D.C.: U.S. Department of the Interior, National Park Service, Transactions and Proceedings Series NPS/NRNAU/NRTP-97/12.
- Kozub, P. 1997. "The Origin of Flat-Pebble Conglomerates in the Upper Cambrian of the Clark Forks Region, Park County, Wyoming." In *Proceedings of the Tenth Keck Research Symposium in Geology*, compiled by C.V. Middleton, and C.M. Maniewicz, 126–129. South Beloit, Illinois: Department of Geology, Beloit College.
- Krynine, Paul D. 1946. "Microscopic Morphology of Quartz Types." *Annals of 2nd Pan-American Congress of Mining and Geological Engineers*, 35–49.
- Kuenen, Philip H. 1960. "Experimental Abrasion 4: Eolian Action." *The Journal of Geology* 68, no. 4 (July): 427–449.
- Land, Lynton S. 1973. "Holocene Meteoric Dolomitization of Pleistocene Limestones, North Jamaica." *Sedimentology* 20, no. 3 (August): 411–424.
- Land, Lynton S. 1985. "The Origin of Massive Dolomite." *Journal of Geological Education* 33, no. 2: 112–125.
- Land, Lynton S. 1998. "Failure to Precipitate Dolomite at 25°C from Dilute Solution Despite 1000-Fold Oversaturation after 32 Years." *Aquatic Geochemistry* 4, nos. 3–4 (September): 361–368.
- Landing, Ed, Gerd Geyer, Robert Buchwaldt, and Samuel A. Bowring. 2015. "Geochronology of the Cambrian: A Precise Middle Cambrian U-Pb Zircon Date from the German Margin of West Gondwana." *Geological Magazine* 152, no. 1 (January): 28–40.
- Larson, Edwin E., Penny E. Patterson, and Felix E. Mutschler. 1994. "Lithology, Chemistry, Age, and Origin of the Proterozoic Cardenas Basalt, Grand Canyon, Arizona." *Precambrian Research* 65, nos. 1–4 (January): 255–276.
- Lehmann, Christoph, David A. Osleger, Isabel P. Montañez, Jeff Jaech, Erik Stokstad, and Milt Kwong. 1996. "Lateral Continuity of Middle Cambrian Peritidal Cycles, Southern Nevada: Implications for Their Origin." In *Field Conference Guide 1996*, edited by Patrick L. Abbott, and John D. Cooper, 85–90. Pacific Section American Association of Petroleum Geologists, *Guidebook 73*, and Pacific Section Society of Economic Paleontologists and Mineralogists, *Book 80*.
- Lippman, Friedrich. 1982. "Stable and Metastable Solubility Diagrams for the System CaCO<sub>3</sub>-MgCO<sub>3</sub>-H<sub>2</sub>O at Ordinary Temperatures." *Bulletin of Mineralogy* 105: 273–279.
- Lochman-Balk, Christina. 1970. "Upper Cambrian Faunal Patterns on the Craton." *Geological Society of America Bulletin* 81, no. 11 (November 1): 3197–3224.
- Lochman-Balk, Christina. 1971. "The Cambrian of the Craton of the United States." In *Cambrian of the New World*, edited by Charles Hepworth Holland, 79–169. New York: John Wiley and Sons.
- Lumsden, David N., and G. Clifford Caudle. 2001. "Origin of Massive Dolomite: The Upper Knox Model." *Journal of Sedimentary Research* 71, no. 3 (May): 400–409.
- Machel, Hans G. 2004. "Concepts and Models of Dolomitization: A Critical Appraisal." In *The Geometry and Petrogenesis of Dolomite Hydrocarbon Reservoirs*. Edited by C.J.R. Braithwaite, G. Rizzl, and G. Drake, 7–63. London, United Kingdom: The Geological Society, *Special Publication 235*.
- Mackenzie, J. 1981. "Holocene Dolomitization of Calcium Carbonate Sediments from the Coastal Sabkhas of Abu Dhabi, U.A.E.: A Stable Isotope Study." *The Journal of Geology* 89, no. 2 (March): 185–198.
- Macquaker, Joe H.S., and Kevin M. Bohacs. 2007. "On the Accumulation of Mud." *Science* 318, no. 5857 (14 December): 1734–1735.
- Magaritz, M., L. Goldenberg, U., Kafri, and A. Arad. 1980. "Dolomite Formation in the Seawater-Freshwater Interface." *Nature* 287, no. 5783 (16 October): 622–624.
- Maithel, Sarah A., Paul A. Garner, and John H. Whitmore. 2015. "Preliminary Assessment of the Petrology of the Hopeman Sandstone (Permo-Triassic), Moray Firth Basin, Scotland." *Scottish Journal of Geology* 51, no. 2 (23 September): 177–184.
- Makse, Hernán A., Shlomo Havlin, Peter R. King, and H. Eugene Stanley. 1997. "Spontaneous Stratification in Granular Mixtures." *Nature* 386, no. 6623 (27 March): 379–382.
- Marsland, Paul S., and John G. Woodruff. 1937. "A Study of the Effects of Wind Transportation on Grains of Several Minerals." *Journal of Sedimentary Petrology* 7, no. 1 (April 1): 18–30.
- Martin, Daryl L. 1985. "Depositional Systems and Ichnology of the Bright Angel Shale (Cambrian), Eastern Grand Canyon, Arizona." M.S. Thesis (unpublished). Northern Arizona University.
- Martin, Daryl L., Larry T. Middleton, and David K. Elliott. 1986. "Depositional Systems of the Middle Cambrian Bright Angel Shale (Cambrian), Grand Canyon, Arizona." *Geological Society of America Abstracts with Programs* 18: 394.
- Mattes, Bret W., and Eric W. Mountjoy. 1980. "Burial Dolomitization of the Upper Devonian Miette Buildup, Jasper National Park, Alberta." In *Concepts and Models of Dolomitization*, edited by Donald H. Zenger, John B. Dunham, and Raymond L. Ethington. Tulsa, Oklahoma: Society of Economic Paleontologists and Mineralogists, *Special Publication 28*.
- Matthews, William, Bernard Guest, and Lauren Madronich. 2018. "Latest Neoproterozoic to Cambrian Detrital Zircon Facies of Western Laurentia." *Geosphere* 14, no. 1 (December 20): 243–264.
- Mazzullo, S.J., William D. Bischoff, and C.S. Teal. 1995. "Holocene Shallow-Subtidal Dolomitization by Near-Normal Seawater, Northern Belize." *Geology* 23, no. 4 (April 1): 341–344.
- McKee, Edwin D. 1932. "Some Fucoids from the Grand Canyon." *Grand Canyon Study Notes* 7, no. 8 (November): 58–161.
- McKee, Edwin D. 1945. "Stratigraphy and Ecology of the Grand Canyon Cambrian: Part 1. Cambrian History of the Grand Canyon Region." *Carnegie Institute of Washington Publication* 563, 1–168. Washington, D.C.: Carnegie Institute of Washington.

- McRae, Stuart G. 1972. "Glauconite." *Earth-Science Reviews* 8, no. 4 (December): 397–440.
- Meglitsch, Paul A. 1972. "The Lophophorate Coelomates." In *Invertebrate Zoology*, 2nd ed., edited by Paul A. Meglitsch, 671–697. Toronto, Canada: Oxford University Press.
- Meister, Patrick, Judith A. McKenzie, Stefano M. Bernasconi, and Peter Brack. 2013. "Dolomite Formation in the Shallow Seas of the Alpine Triassic." *Sedimentology* 60, no. 1 (January): 270–291.
- Meyers, William J., Feng H. Lu, and John K. Zachariah. 1997. "Dolomitization by Mixed Evaporative Brines and Freshwater, Upper Miocene Carbonates, Nijar, Spain." *Journal of Sedimentary Research* 67, no. 5 (1 September): 898–912.
- Middleton, Larry T. 1989. "Cambrian and Ordovician Depositional Systems in Arizona." In *Geologic Evolution of Arizona*, Vol. 17, edited by J.P. Jenney, and S.J. Reynolds, 273–286. *Arizona Geological Society Digest*.
- Middleton, Larry T., and David K. Elliott. 2003. "Tonto Group." In *Grand Canyon Geology*, 2nd ed., edited by Stanley S. Beus, and Michael Morales, 90–106. New York: Oxford University Press.
- Middleton, Larry T., James R. Steidtmann, and Daniel A. DeBour. 1980. "Stratigraphy and Depositional Setting of Some Middle and Upper Cambrian Rocks, Wyoming." *Wyoming Geological Association, 32nd Annual Field Conference*, 23–35.
- Moorhouse, Walter W. 1959. *The Study of Rocks in Thin Section*. New York: Harper & Row.
- Morris, William Joseph. 1957. "Effects of Sphericity, Roundness, and Velocity on Traction Transportation of Sand Grains." *Journal of Sedimentary Petrology* 27, no. 1 (1 March): 27–31.
- Moshier, Stephen O., Tim Helble, and Carol A. Hill. 2016. "Sedimentary Rock Types and How They Form." In *The Grand Canyon, Monument to an Ancient Earth: Can Noah's Flood Explain the Grand Canyon?* edited by Carol A. Hill, Gregg Davidson, Tim Helble, and Wayne Ranney, chapter 5, 54–65. Grand Rapids, Michigan: Kregel Publications.
- Mresah, Mohamed H. 1998. "The Massive Dolomitization of Platformal and Basinal Sequences: Proposed Models from the Paleocene, Northeast Sirte Basin, Libya." *Sedimentary Geology* 116, nos. 3–4 (March): 199–226.
- Naeser, Chris W., Ian R. Duddy, Donald P. Elston, Terry A. Dumitru and Paul F. Green. 1989. "Fission-Track Dating: Ages for Cambrian Strata and Laramide and Post-Middle Eocene Cooling Events from the Grand Canyon, Arizona." In *Geology of Grand Canyon, Northern Arizona (with Colorado River Guides)*, edited by Donald P. Elston, George H. Billingsley, and Richard A. Young, 139–144. Washington, D.C.: American Geophysical Union.
- Ning, Meng, Xianguo Lang, Kanguun Huang, Chao Li, Tianzheng Huang, Honglin Yuan, Chaochao Xing, Runyu Yang, and Bing Shen. 2020. "Towards Understanding the Origin of Massive Dolostones." *Earth and Planetary Science Letters* 545 (1 September): 116403.
- Noble, Levi F. 1914. "The Shinumo Quadrangle, Grand Canyon District, Arizona." *Bulletin* 549. Washington, D.C.: U.S. Geological Survey.
- Noble, Levi F. 1922. "A Section of the Paleozoic Formations of the Grand Canyon at the Bass Trail." *Professional Paper 131-B*, 23–73. Washington, D.C.: U.S. Geological Survey.
- Nummedal, Dag. 1991. "Shallow Marine Storm Sedimentation—The Oceanographic Perspective." In *Cycles and Events in Stratigraphy*, edited by Gerhard Einsele, Werner Ricken, and Adolf Seilacher, 227–248. Berlin, Germany: Springer-Verlag.
- Odom, I. Edgar. 1975. "Feldspar-Grain Size Relations in Cambrian Arenites, Upper Mississippi Valley." *Journal of Sedimentary Research* 45, no. 3 (1 September): 636–650.
- Odom, I. Edgar, Thomas W. Doe, and Robert H. Dott. 1976. "Nature of Feldspar-Grain Size Relations in Some Quartz-Rich Sandstones." *Journal of Sedimentary Petrology* 46, no. 4 (1 December): 862–870.
- Osleger, David A., Isabel P. Montañez, Javier Martín-Chivelet, and Christoph Lehmann. 1996. "Cycle and Sequence Stratigraphy of Middle to Upper Cambrian Carbonates, Bonanza King Formation, Southern Great Basin." In *Field Conference Guide 1996*, edited by Patrick L. Abbott, and John D. Cooper, 55–84. Pacific Section American Association of Petroleum Geologists, *Guidebook* 73, and Pacific Section Society of Economic Paleontologists and Mineralogists, *Book* 80.
- Owens, S.M. 1985. "Stratigraphy and Sedimentology of Flat-Pebble Conglomerates of the Upper Lone Rock (Upper Cambrian), Western Wisconsin." M.S. Thesis (unpublished). University of Wisconsin-Madison.
- Pemberton, S. George, James A. MacEachern, and Robert W. Frey. 1992. "Trace Fossil Facies Models: Environmental and Allostratigraphic Significance." In *Facies Models: Response to Sea Level Change*, edited by Roger G. Walker, and Noel P. James, 47–72. St. John's, Newfoundland, Canada: Geological Association of Canada.
- Peng, Shanchi, Loren E. Babcock, and Roger A. Cooper. 2012. "The Cambrian Period." In *The Geologic Time Scale 2012*, Vol. 2, edited by Felix M. Gradstein, James G. Ogg, Mark D. Schmitz, and Gabi M. Ogg, 437–488. Amsterdam, The Netherlands: Elsevier.
- Peters, Shanan E., and Robert R. Gaines. 2012. "Formation of the 'Great Unconformity' as a Trigger for the Cambrian Explosion." *Nature* 484, no. 7394 (April 18): 363–366.
- Pettijohn, Francis J. 1957. *Sedimentary Rocks*. New York: Harper.
- Pettijohn, Francis J., Paul E. Potter, and Raymond Siever. 1973. *Sand and Sandstone*. Berlin, Germany: Springer.
- Plummer, Phillip S, and Victor A. Gostin. 1981. "Shrinkage Cracks: Desiccation or Synaeresis?" *Journal of Sedimentary Petrology* 51, no. 4 (December): 1147–1156.
- Potter, Paul E. 2003. "Mudrocks." In *Encyclopedia of Sediments and Sedimentary Rocks*, edited by Gerard V. Middleton, Michael J. Church, Mario Coniglio, Lawrence A. Hardie, and Frederick J. Longstaffe, 451–459. Dordrecht, The Netherlands: Kluwer Scientific Publishers.
- Powell, John W. 1876. *Report on the Geology of the Eastern Portion of the Uinta Mountains and a Region of Country Adjacent Thereto*. Washington, D.C.: U.S. Geologic and Geographic Survey of the Territories.
- Powell, John W. 1891. *Grand Canyon of the Colorado*. New York: Flood and Vincent.
- Powers, Maurice C. 1953. "A New Roundness Scale for Sedimentary Particles." *Journal of Sedimentary Petrology* 23, no. 2 (June 1): 117–119.
- Pratt, Brian R. 1998. "Syneresis Cracks: Subaqueous Shrinkage in Argillaceous Sediments Caused by Earthquake-Induced

- Dewatering." *Sedimentary Geology* 117, nos.1–2 (April): 1–10.
- Pratt, Brian R., and Noel P. James. 1986. "The St. George Group (Lower Ordovician) of Western Newfoundland: Tidal Flat Island Model for Carbonate Sedimentation in Shallow Epeiric Seas." *Sedimentology* 33, no. 3 (June): 313–343.
- Pye, Kenneth, and Haim Tsoar. 2009. *Aeolian Sand and Sand Dunes*. Berlin, Germany: Springer-Verlag.
- Ramsay, John G. 1967. *Folding and Fracturing of Rocks*. New York: McGraw-Hill.
- Resser, Charles E., 1945. "Cambrian Fossils of the Grand Canyon: Part II. Cambrian History of the Grand Canyon Region." *Carnegie Institute of Washington Publication* 563, 168–232. Washington, D.C.: Carnegie Institute of Washington.
- Ricken, Werner, and F. Wolfgang Eder. 1991. "Diagenetic Modification of Calcareous Beds—An Overview." In *Cycles and Events in Stratification*, edited by Gerhard Einsele, Werner Ricken, and Adolf Seilacher, 430–449. New York: Springer-Verlag.
- Roberts, Jennifer A., Paul A. Kenward, David A. Fowle, Robert H. Goldstein, Luis A. González, and David S. Moore. 2013. "Surface Chemistry Allows for Abiotic Precipitation of Dolomite at Low Temperature." *Proceedings of the National Academy of Sciences* 110, no. 36 (August 20): 14540–14545.
- Rooney, Alan D., Jacqueline Austermann, Emily F. Smith, Yang Li, David Selby, Carol M. Dehler, Mark D. Schmitz, Karl E. Karlstrom, and Francis A. Macdonald. 2018. "Coupled Re-Os and U-Pb Geochronology of the Tonian Chuar Group, Grand Canyon." *Geological Society of America Bulletin* 130, nos. 7–8 (1 July): 1085–1098.
- Rose, Eben C. 2003. "Depositional Environment and History of the Cambrian Tonto Group, Grand Canyon, Arizona." M.S. Thesis (unpublished). Northern Arizona University.
- Rose, Eben C. 2006. "Nonmarine Aspects of the Cambrian Tonto Group of the Grand Canyon, USA, and Broader Implications." *Palaeoworld* 15, nos.3–4 (August–November): 223–241.
- Rose, Eben C. 2011. "Proposed Modification of the Nomenclature and Revised Depositional Model for the Cambrian Tonto Group of the Grand Canyon, Arizona." In *Cambrian Stratigraphy and Paleontology of Northern Arizona and Southern Nevada, The 16th Field Conference of the Cambrian Stage Subdivision Working Group, International Subcommission on Cambrian Stratigraphy*, edited by J. Stewart Hollingsworth, Frederick A. Sundberg, and John R. Foster, 77–98. Flagstaff, Arizona: Museum of Northern Arizona, *Bulletin* 67.
- Rose, Eben C., Larry T. Middleton, and David K. Elliott. 1998. "Storm- and Fair-Weather Controls of Deposition of the Middle Cambrian Bright Angel Shale, Grand Canyon, Arizona: Sedimentologic and Ichnologic Evidence." *Geological Society of America Abstracts with Programs* 30: 35.
- Rowland, Stephen M., Gerald D. Osborn, and David J. Graber. 1995. "Lower Paleozoic Stratigraphy of Fern Glen Canyon, Central Grand Canyon, Arizona." *Journal of the Arizona-Nevada Academy of Science* 28, no. 1–2: 1–11.
- Rowley, Peter D., Mel A. Kuntz, and Norman S. MacLeod. 1981. "Pyroclastic-Flow Deposits." In *The 1980 Eruptions of Mount St. Helens*, edited by Peter W. Lipman, and Donal R. Mullineaux, 489–512. Washington, D.C.: U.S. Geological Survey, *Professional Paper* 1250.
- Russell, R. Dana, and Ralph E. Taylor. 1937. "Roundness and Shape of Mississippi River Sands." *The Journal of Geology* 45, no.3 (April–May): 225–267.
- Saller, Arthur H. 1984. "Petrologic and Geochemical Constraints on the Origin of Subsurface Dolomite, Enewetak Atoll: An Example of Dolomitization by Normal Seawater." *Geology* 12, no. 4 (April): 217–220.
- Schieber, Juergen. 1999. "Microbial Mats in Terrigenous Clastics: The Challenge of Identification in the Rock Record." *Palaios* 14, no.1 (February): 3–12.
- Schieber, Juergen, and John B. Southard. 2009. "Bedload Transport of Mud by Floccule Ripples—Direct Observation of Ripple Migration Processes and Their Implications." *Geology* 37, no. 6 (June): 483–486.
- Schieber, Juergen, John B. Southard, and Kevin Thaisen. 2007. "Accretion of Mudstone Beds from Migrating Floccule Ripples." *Science* 318, no.5857 (14 December): 1760–1763.
- Schieber, Juergen, John B. Southard, Patrick Kissling, Britt Rossman, and Robert Ginsburg. 2013. "Experimental Deposition of Carbonate Mud from Moving Suspensions: Importance of Flocculation and Implications for Modern and Ancient Carbonate Mud Deposition." *Journal of Sedimentary Research* 83, no. 11 (November): 1025–1031.
- Schmitz, Mark D. 2012. "Radiometric Ages Used in GTS2012." In *The Geologic Time Scale 2012*, Vol. 2, edited by Felix M. Gradstein, James G. Ogg, Mark D. Schmitz, and Gabi M. Ogg, 1045–1082. Amsterdam, The Netherlands: Elsevier.
- Scholle, Peter A., and Dana S. Ulmer-Scholle. 2003. *A Color Guide to the Petrography of Carbonate Rocks: Grains, Textures, Porosity, Diagenesis*. Tulsa, Oklahoma: The American Association of Petroleum Geologists, *Memoir* 77.
- Schuchert, Charles. 1918. "The Cambrian of the Grand Canyon of Arizona." *American Journal of Science, 4th Series* 45, no. 269 (1 May): 362–369.
- Seilacher, Adolf, and Thomas Aigner. 1991. "Storm Deposition at the Bed, Facies, and Basin Scale: The Geologic Perspective." In *Cycles and Events in Stratigraphy*, edited by Gerhard Einsele, Werner Ricken, and Adolf Seilacher, 249–267. Berlin, Germany: Springer-Verlag.
- Sepkoski, J. John Jr. 1982. "Flat-Pebble Conglomerates, Storm Deposits, and the Cambrian Bottom Fauna." In *Cycles and Event Stratification*, edited by Gerhard Einsele, Werner Ricken, and Adolf Seilacher, 371–385. New York: Springer-Verlag.
- Sepkoski, J. John Jr., Richard K. Bambach, and Mary L. Dorser. 1991. "Secular Changes in Phanerozoic Event Bedding and the Biological Overprint." In *Cycles and Events in Stratification*, edited by Gerhard Einsele, Werner Ricken, and Adolf Seilacher, 298–312. New York: Springer-Verlag.
- Seward, A.C. 1931. *Plant Life Through the Ages: A Geological and Botanical Retrospect*. New York: Macmillan Co.
- Sharp, Robert P. 1940. "Ep-Archean and Ep-Algonkian Erosion Surfaces, Grand Canyon, Arizona." *Geological Society of America Bulletin* 51, no.8 (1 August): 1235–1270.
- Shinn, Eugene A., R.N. Ginsburg, and R. Michael Lloyd. 1965. "Recent Supratidal Dolomite from Andros Island, Bahamas." In *Dolomitization and Limestone Diagenesis*, edited by Lloyd C. Pray, and Raymond C. Murray, 112–123. Tulsa, Oklahoma: Society of Economic Paleontologists and Mineralogists, *Special Publication* 13.

- Sloss, Laurence L. 1963. "Sequences in the Cratonic Interior of North America." *Geological Society of America Bulletin* 74, no.2 (February): 93–114.
- Snelling, Andrew A. 2000. "Geochemical Processes in the Mantle and Crust." In *Radioisotopes and the Age of the Earth: A Young-Earth Creationist Research Initiative*, edited by Larry Vardiman, Andrew A. Snelling, and Eugene F. Chaffin, 123–304. El Cajon, California: Institute for Creation Research, and St. Joseph, Missouri: Creation Research Society.
- Snelling, Andrew A. 2005a. "Radiohalos in Granites: Evidence of Accelerated Nuclear Decay." In *Radioisotopes and the Age of the Earth: Results of a Young-Earth Creationist Research Initiative*, edited by Larry Vardiman, Andrew A. Snelling, and Eugene F. Chaffin, 101–207. El Cajon, California: Institute for Creation Research, and Chino Valley, Arizona: Creation Research Society.
- Snelling, Andrew A. 2005b. "Fission Tracks in Zircons: Evidence for Abundant Nuclear Decay." In *Radioisotopes and the Age of the Earth: Results of a Young-Earth Creationist Research Initiative*, edited by Larry Vardiman, Andrew A. Snelling, and Eugene F. Chaffin, 209–324. El Cajon, California: Institute for Creation Research, and Chino Valley, Arizona: Creation Research Society.
- Snelling, Andrew A. 2005c. "Isochron Discordances and the Role of Mixing and Inheritance of Radioisotopes in the Mantle and Crust." In *Radioisotopes and the Age of the Earth: Results of a Young-Earth Creationist Research Initiative*, edited by Larry Vardiman, Andrew A. Snelling, and Eugene F. Chaffin, 393–524. El Cajon, California: Institute for Creation Research, and Chino Valley, Arizona: Creation Research Society.
- Snelling, Andrew A. 2009. *Earth's Catastrophic Past: Geology, Creation and the Flood*. Dallas, Texas: Institute for Creation Research.
- Snelling, Andrew A. 2017a. "Determination of the Decay Constants and Half-Lives of Uranium-238 ( $^{238}\text{U}$ ) and Uranium-235 ( $^{235}\text{U}$ ), and the Implications for U-Pb and Pb-Pb Radioisotope Dating Methodologies." *Answers Research Journal* 10 (January 18): 1–38. <https://answersresearchjournal.org/radioisotope-decay-uranium/>.
- Snelling, Andrew A. 2017b. "Problems with the U-Pb Radioisotope Dating Methods—1. Common Pb." *Answers Research Journal* 10 (July 26): 121–167. <https://answersresearchjournal.org/problems-radioisotope-dating-u-pb-1/>.
- Snelling, Andrew A. 2018. "Problems with the U-Pb Radioisotope Dating Methods—2. U and Pb Mobility." *Answers Research Journal* 11 (June 13): 85–140. <https://answersresearchjournal.org/problems-radioisotope-dating-u-pb-2/>.
- Snelling, Andrew A. 2019. "Problems with the U-Pb Radioisotope Dating Methods—3. Mass Fractionation." *Answers Research Journal* 12 (November 13): 355–392. <https://answersresearchjournal.org/problems-radioisotope-dating-u-pb-3/>.
- Snelling, Andrew A. 2021a. "The Petrology of the Tapeats Sandstone, Tonto Group, Grand Canyon, Arizona." *Answers Research Journal* 14 (June 23): 159–254. <https://answersresearchjournal.org/petrology-tapeats-sandstone-tonto-group/>.
- Snelling, Andrew A. 2021b. "The Petrology of the Bright Angel Formation, Tonto Group, Grand Canyon, Arizona." *Answers Research Journal* 14 (September 8): 303–415. <https://answersresearchjournal.org/petrology-bright-angel-tonto-group/>.
- Southard, John B., John M. Lambie, Dennis C. Federico, Harold T. Pile, and Christopher R. Weidman. 1990. "Experiments on Bed Configurations in Fine Sands Under Bidirectional Purely Oscillatory Flow, and the Origin of Hummocky Cross-Stratification." *Journal of Sedimentary Petrology* 60, no.1 (January 1): 1–17.
- Stewart, John H. 1972. "Initial Deposits in the Cordilleran Geosyncline: Evidence of a Late Precambrian (<850 m.y.) Continental Separation." *Geological Society of America Bulletin* 83, no.5 (May): 1345–1360.
- Stewart, John H., and Christopher A. Suczek. 1977. "Cambrian and Latest Precambrian Paleogeography and Tectonics in the Western United States." In *Paleozoic-Paleogeography of the Western United States*, edited by John H. Stewart, Calvin H. Stevens, and A. Eugene Fritsche, 1–18. Society of Economic Paleontologists and Mineralogists, Pacific Section, *Paleogeography Symposium* 1.
- Sundberg, Frederick A. 1999. "Redescription of *Alokistocare subcoronatum* (Hall and Whitfield, 1877), the Type Species of *Alokistocare*, and the Status of *Alokistocaridae* Resser, 1939B (Ptychopariida: Trilobita, Middle Cambrian)." *Journal of Paleontology* 73, no.6 (November): 1126–1143.
- Sundberg, Frederick A. 2011. "Cambrian of Peach Springs Canyon, Hualapai Indian Reservation, Arizona." In *Cambrian Stratigraphy and Paleontology of Northern Arizona and Southern Nevada, The 16th Field Conference of the Cambrian Stage Subdivision Working Group, International Subcommission on Cambrian Stratigraphy*, edited by J. Stewart Hollingsworth, Frederick A. Sundberg, and John R. Foster, 186–190. Flagstaff, Arizona: Museum of Northern Arizona, *Bulletin* 67.
- Sundberg, Frederick A., Gerd Geyer, Peter D. Kruse, Linda B. McCollum, Tatyana V. Pegel, Anna Żylińska, and Andrey Y. Zhuravlev. 2016. "International Correlation of the Cambrian Series 2–3, Stages 4–5 Boundary Interval." *Australasian Palaeontological Memoirs* 49 (June): 83–124.
- Sundberg, Frederick A., Karl E. Karlstrom, Gerd Geyer, John R. Foster, James W. Hagadorn, M.T. Mohr, Mark D. Schmitz, Carol M. Dehler, and Laura J. Crossey. 2020. "Asynchronous Trilobite Extinctions at the Early to Middle Cambrian Transition." *Geology* 48, no.5 (February 14): 441–445.
- Swift, Donald J.P., Albert G. Figueiredo, Jr., G.L. Freeland, and George F. Oertel. 1983. "Hummocky Cross-Stratification and Megaripples: A Geological Double Standard?" *Journal of Sedimentary Petrology* 53, no.4 (1 December): 1295–1317.
- Swift, Donald J.P., and Julian A. Thorne. 1991. "Sedimentation on Continental Margins, I: A General Model for Shelf Sedimentation." In *Shelf Sand and Sandstone Bodies: Geometry, Facies, and Sequence Stratigraphy*, edited by Donald J.P. Swift, George F. Oertel, Roderick W. Tillman, and Julian A. Thorne, *International Association of Sedimentologists, Special Publication Number 14*, 3–31. Oxford, United Kingdom: Blackwell Scientific Publications.
- Tapp, Bryan, and Ken Wolgemuth. 2016. "Broken and Bent Rock: Fractures, Faults, and Folds". In *The Grand Canyon*,

- Monument to an Ancient Earth: Can Noah's Flood Explain the Grand Canyon?* edited by Carol A. Hill, Gregg Davidson, Tim Helble, and Wayne Ranney, chapter 12, 116–127. Grand Rapids, Michigan: Kregel Publications.
- Thompson, Graham R., and John Hower. 1975. "The Mineralogy of Glauconite." *Clays and Clay Minerals* 23, no. 4 (1 August): 289–300.
- Tucker, Maurice E., 1981. *Sedimentary Petrology: An Introduction*. Oxford, United Kingdom: Blackwell Scientific Publications.
- Twenhofel, William H. 1945. "The Rounding of Sand Grains." *Journal of Sedimentary Petrology* 15, no. 2 (1 August): 59–71.
- Udden, Johan A. 1914 "Mechanical Composition of Clastic Sediments." *Bulletin of the Geological Society of America* 25, no. 1 (January): 655–744.
- Ulmer-Scholle, Dana S., Peter A. Scholle, Juergen Schieber, and Robert J. Raine. 2015. *A Color Guide to the Petrography of Sandstones, Siltstones, Shales and Associated Rocks*. Tulsa, Oklahoma: The American Association of Petroleum Geologists, *Memoir 109*.
- Vandeginste, Veerle, Oliver Snell, Matthew R. Hall, Elizabeth Steer, and Arne Vandeginste. 2019. "Acceleration of Dolomitization by Zinc in Saline Waters." *Nature Communications* 10 (23 April): 1851. <https://doi.org/10.1038/s41467-019-09870-y>.
- Vannier, Jean, Ivan Calandra, Christian Gaillard, and Anna Żylińska. 2010. "Priapulid Worms: Pioneer Horizontal Burrowers at the Precambrian-Cambrian Boundary." *Geology* 38, no. 8 (August): 711–714.
- Vardiman, Larry, Andrew A. Snelling, and Eugene F. Chaffin, Editors. 2005. *Radioisotopes and the Age of the Earth: Results of a Young-Earth Creationist Research Initiative*. El Cajon, California: Institute for Creation Research, and Chino Valley, Arizona: Creation Research Society.
- Vasconcelos, Crisogono, Judith A. McKenzie, Stefano Bernasconi, Djordje Grujic, and Albert J. Tiens. 1995. "Microbial Mediation as a Possible Mechanism for Natural Dolomite Formation at Low Temperatures." *Nature* 377, no. 6546 (21 September): 220–222.
- Von der Borch, Chris C., David E. Lock, and Douglas Schwebel. 1975. "Ground-water Formation of Dolomite in the Coorong Region of South Australia." *Geology* 3, no. 5 (May): 283–285.
- Walcott, Charles D. 1880. "The Permian and Other Paleozoic Groups of the Kanab Valley, Arizona." *American Journal of Science, 3rd Series* 20, no. 117 (September): 221–225.
- Walcott, Charles D. 1890. "The Fauna of the Lower Cambrian or *Olenellus* Zone." *10th Annual Report*, 509–760. Washington, D.C.: US Geological Survey
- Walcott, Charles D. 1895. "Algonkian Rocks of the Grand Canyon of the Colorado." *The Journal of Geology* 3, no. 3 (April–May): 312–330.
- Walcott, Charles D. 1910. "Cambrian Geology and Paleontology II: Abrupt Appearance of the Cambrian Fauna on the North American Continent." *Smithsonian Miscellaneous Collections* 57, no. 6: 1–16.
- Walcott, Charles D. 1920. "Cambrian Geology and Paleontology IV: Middle Cambrian Spongiae." *Smithsonian Miscellaneous Collections* 67, no. 6: 261–364.
- Walker, Roger G., and A. Guy Plint. 1992. "Wave- and Storm-Dominated Shallow Marine Systems." In *Facies Models: Response to Sea Level Change*, edited by Roger G. Walker, and Noel P. James, 219–238. St. John's, Newfoundland, Canada: Geological Association of Canada.
- Wanless, Harold R. Jr. 1973a. "Cambrian of the Grand Canyon—A Reevaluation of the Depositional Environment." Ph.D. Thesis (unpublished). Johns Hopkins University.
- Wanless, Harold R., Jr. 1973b. "Cambrian of the Grand Canyon—A Reevaluation." *American Association of Petroleum Geologists Bulletin* 57, no. 4 (April): 810–811.
- Wanless, Harold R., Jr. 1975. "Carbonate Tidal Flats of the Grand Canyon Cambrian." In *Tidal Flats: A Casebook of Recent Examples and Fossil Counterparts*, edited by Robert N. Ginsburg, 269–277. New York: Springer-Verlag.
- Wanless, Harold R., Jr. 1981. "Environments and Dynamics of Clastic Sediment Dispersal across Cambrian of Grand Canyon." *American Association of Petroleum Geologists Bulletin* 65, no. 5 (May): 1004–1005.
- Warren, John. 2000. "Dolomite: Occurrence, Evolution and Economically Important Associations." *Earth-Science Reviews* 52, nos. 1–3 (November): 1–81.
- Wentworth, Chester K. 1922. "A Scale of Grade and Class Terms for Clastic Sediments." *The Journal of Geology* 30, no. 5 (July–August): 377–392.
- Wheeler, Russell B., and Albert R. Kerr. 1936. "Preliminary Report on the Tonto Group of the Grand Canyon, Arizona." *Grand Canyon Natural History Association Bulletin* 5: 1–16.
- Whitmore, John H. 2009. "Do Mud Cracks Indicate Multiple Droughts During the Flood?" In *Rock Solid Answers: The Biblical Truth Behind 14 Geologic Questions*, edited by Michael J. Oard and John K. Reed, 167–184. Green Forest, Arkansas: Master Books.
- Whitmore, John H., Raymond Strom, Stephen Cheung, and Paul A. Garner. 2014. "The Petrology of the Coconino Sandstone (Permian), Arizona, USA." *Answers Research Journal* 7 (December 10): 499–532. <https://answersresearchjournal.org/petrology-of-the-coconino-sandstone/>.
- Whitmore, John H., 2017. "Rapid Rounding of K-Feldspar Sand Grains from Beach to Dune Environments and its Significance for Ancient Sandstones." *Journal of Creation Theology and Science Series C: Earth Sciences* 7 (25 October): 2–3.
- Whitmore, John H., and Raymond Strom. 2017a. "Rounding of K-Feldspar and Quartz Sand Grains from Beach to Dune Environments: Implications for Ancient Sandstones." *Geological Society of America Abstracts with Programs* 49, no. 6 (January): 295-5.
- Whitmore, John H., and Raymond Strom. 2017b. "Rounding of Quartz and K-Feldspar Sand from Beach to Dune Settings Along the California and Oregon Coastlines: Implications for Ancient Sandstones." *Answers Research Journal* 10 (November 15): 259–270. <https://answersresearchjournal.org/rounding-quartz-and-k-feldspar-sand/>.
- Whitmore, John H., and Paul A. Garner. 2018. "The Coconino Sandstone (Permian, Arizona, USA): Implications for the Origin of Ancient Cross-bedded Sandstones." In *Proceedings of the Eighth International Conference on Creationism*, edited by John H. Whitmore, 581–627. Pittsburgh, Pennsylvania: Creation Science Fellowship.
- Whitmore, John H., and Raymond Strom. 2018. "The Significance of Angular K-Feldspar Grains in Ancient Sandstones." In *Proceedings of the Eighth International Conference on Creationism*, edited by John H. Whitmore, 628–651. Pittsburgh, Pennsylvania: Creation Science Fellowship.

- Wiens, Roger. 2016. "So Just How Old is That Rock?" In *The Grand Canyon, Monument to an Ancient Earth: Can Noah's Flood Explain the Grand Canyon?* edited by Carol A. Hill, Gregg Davidson, Tim Helble, and Wayne Ranney, chapter 9, 88–97. Grand Rapids, Michigan: Kregel Publications.
- Wise, Kurt P., and Andrew A. Snelling. 2005. "A Note on the Pre-Flood/Flood Boundary in the Grand Canyon." *Origins* 58: 7–29.
- Wright, V.P. 1992. "A Revised Classification of Limestones." *Sedimentary Geology* 76, nos. 3–4 (March): 177–185.
- Wu, Xian-tao. 1982. "Storm-Generated Depositional Types and Associated Trace Fossils in the Lower Carboniferous Shallow-Marine Carbonates of Three Cliffs Bay and Ogmores-by-Sea, South Wales." *Palaeogeography, Palaeoclimatology, Palaeoecology* 39, nos. 3–4 (October): 187–202.
- Yassoglou, N., Costas S. Kosmas, Nikolaos Moustakas, E. Tzianis, and Nikolaos G. Danalatos. 1994. "Cracking in Recent Alluvial Soils as Related to Easily Determined Soil Properties." *Geoderma* 63, nos. 3–4 (November): 289–298.
- Yesiller, Nazli, C.J. Miller, G. Inci, and K. Yaldo. 2000. "Desiccation and Cracking Behavior of Three Compacted Landfill Liner Soils." *Engineering Geology* 57, nos. 1–2 (June): 105–121.
- Young, Davis A., and Ralph F. Stearley. 2008. *The Bible, Rocks and Time: Geological Evidence for the Age of the Earth*. Downers Grove, Illinois: InterVarsity Press.

#### Supplementary Material

**Appendix A**—Graphic Stratigraphic Log of the Tonto Group in the Unkar Creek Area (River Mile 73)

**Appendix B**—Graphic Stratigraphic Log of the Tonto Group in the Blacktail Canyon Area (River Mile 120.5)

**Appendix C**—Graphic Stratigraphic Log of the Tonto Group in the Olo Canyon Area (River Mile 146)

**Appendix D**—Graphic Stratigraphic Log of the Tonto Group in the Diamond Creek Area (River Mile 226)

**Appendix E**—Locations and Petrographic Descriptions of Muav Formation Samples

Available in a single pdf file at <https://assets.answersresearchjournal.org/doc/articles/arj/v15/muav-formation-supplement.pdf>